SEEPAGE CRITERIA BASED OPTIMAL DESIGN OF WATER RETAINING STRUCTURES WITH RELIABILITY QUANTIFICATION UTILIZING SURROGATE MODEL LINKED SIMULATION-OPTIMIZATION APPROACH

A thesis submitted by

Muqdad Raoof Kareem Al-Juboori

2018

For the degree of Doctor of Philosophy (Ph.D.)

College of Science and Engineering

James Cook University, QLD, Australia

Statement of Access

I, the undersigned, author of this work, understand that James Cook University will make this thesis available for use within the University Library and, via the Australian Digital Thesis network, for use elsewhere.

I understand that, as an unpublished work, a thesis has significant protection under the Copyright Act and I wish this work to be embargoed until September 2019, after which date I do not wish to place any further restriction on access to this work.

Signature   Date

Statement of Sources Declaration

I herewith declare that I have produced this thesis without the prohibited assistance of third parties and without making use of aids other than those specified; notions taken over directly or indirectly from other sources have been identified as such. This thesis has not previously been presented in identical or similar form to any other Australian or foreign examination board.

Signature   Date

Electronic Copy

I, the undersigned, the author of this work, declare that the electronic copy of this thesis provided to James Cook University Library is an accurate copy of the print thesis submitted.

Signature   Date

Statement of Contribution of Others

All the prescribed methods, results and conclusions in the thesis were developed and written by Muqdad Al-Juboori under complete supervision from my supervisor Dr. Bithin Datta. He proficiently guided me for the entire PhD project, and provided me valuable recommendations to overcome difficult challenges in my research. The material in the published articles in journals, conference proceedings and the thesis was fulfilled by Muqdad Al-Juboori with important feedback provided by Dr. Bithin Datta.

To My Mother (Alia Al-Ramahi)

To My Father (Raoof Al-Juboori)

To My Wife (Nawres Al-Yasiri)

To My Sons (Ali & Hussein)

To My Sisters (Nahid & Nabba)

To My Brothers (Ammar, Ahmed & Khalid)

I sincerely dedicate this thesis

Muqdad Al-Juboori

Acknowledgements

Publications Produced During Ph.D. Candidature

Peer-reviewed papers:

1. Al-Juboori, M & Datta, B. 2018 .*Performance evaluation of a Genetic Algorithm based linked simulation-optimization model for optimal hydraulic seepage related design of concrete gravity dams.* Journal of Applied Water Engineering and Research, Doi:10.1080/23249676.2018.1497558

2. Al-Juboori, M & Datta, B. 2018. *Effects ofthe of the soil permeability on the optimum design of hydraulic water retaining structures utilizing support vector machine based linked simulation optimization models.* KSCE Journal of Civil Engineer/ accepted

3. Al-Juboori, M & Datta, B. 2018. *Linked simulation-optimization model for optimum hydraulic design of water retaining structures constructed on permeable soils.* International Journal of GEOMATE, Doi: 10.21660/2018.44.7229

4. Al-Juboori, M & Datta, B. 2018.*optimum hydraulic design of concreter gravity dams founded on anisotropic soils utilizing interior point algorithm based hybrid genetic algorithm.* ISH Journal of Hydraulic Engineering, under review

5. Al-Juboori, M & Datta, B. 2018.*Reliability based optimum design of hydraulic water retaining structure constructed on heterogeneous porous media: utilizing stochastic.* Life Cycle Reliability and Safety Engineering, under review

6. Al-Juboori, M & Datta, B. 2018. *Incorporating uncertainty of heterogeneous hydraulic conductivity: utilizing stochastic ensemble surrogate models in multi-objective multi-realization optimization model for optimum design of hydraulic water retaining structure.* Journal of Computational Design and Engineering, under review.

Conference papers:

1. Al-Juboori, M & Datta, B .2017. *Artificial Neural Network Modelling and Genetic Algorithm Based Optimization of Hydraulic Design Related to Seepage under Concrete Gravity Dams on Permeable Soils.* The 19th International Conference on Environmental and Water Resources Engineering, Melbourne- Australia.

2. Al-Juboori, M & Datta, B .2017. *Influence of hydraulic conductivity and its anisotropic ratio on the optimum hydraulic design of water retaining structures founded on permeable soils.* The 13th Hydraulics in Water Engineering Conference, Sydney – Australia.

3. Al-Juboori, M & Datta, B .2018. *Linked Simulation-Optimization model for optimum hydraulic design of water retaining structures constructed on permeable soils.* Seventh

International Conference on Geo-technique, Construction Materials and Environment, Mie, Japan, Nov. 21-24, 2017, Mie- Japan.

4. Al-Juboori, M & Datta, B .2018. *Predicting Exit Gradient of Water Retaining Structures: A Comparative Study of Five Machine Learning Techniques.* Academicsera 18th International Conference, Sydney –Australia.

Nomenclature and Abbreviations

γ_{sub}	Submerged soil density (kN/m^3)
γ_w	Unite weight of water (kN/m^3)
G_S	Specific gravity of soil (kN/m^3)
ANN	Artificial neural network
b	Width of HWRS (m)
B	Total width of structures (m)
b*	Part of the floor on upstream side of HWRS (m)
b$_i$	Width of the floor between cut-off (i) and (i+1), $\forall$ i, (m)
COV	Coefficient of variation
CV	Cross validation
DOE	Design of experiment
d$_1$	Upstream cut-off depths (m)
d$_2$	Downstream cut-off depths (m)
e	Eccentric load distance (m)
FEM	Finite element method
F$_{ovt}$	Design safety factor against overturning
GA	Genetic algorithm
GPR	Gaussian process regression
H	Total upstream hydraulic head or difference in elevation of water between upstream and downstream (m)
HC	Hydraulic conductivity (m/day)
HHC	Heterogeneous hydraulic conductivity
HS	Halton sequences
HGA	Hybrid genetic algorithm

HWRS	Hydraulic water retaining structure
i_e	Exit gradient
IPA	Interior point algorithm
K_s	Sliding safety factor
k_x	Hydraulic conductivity in horizontal direction
k_y/k_x	Ratio of the hydraulic conductivity in y direction to the value of hydraulic conductivity in x direction
LD	Soil layer depth (m)
LHS	Latin hypercube sampling method
MAE	Mean absolute error
MSE	Mean square error
MOMRO	Multi-objective multi-realization optimization
NSGA-II	Non-dominated sorting genetic algorithm II
Pc_1	Uplift pressure on upstream (kpa)
Pe_2	Uplift pressure on downstream (kpa)
RBOD	Reliability based optimum design
RSQ	Coefficient of determination
S-O	Simulation-optimization
SVM	Support vector machine
t_i	Thickness of HWRS floor near the cut-off (i), $\forall$ i, (m)
β_i	Inclination angle of the cut-off (i), $\forall$ I, (degree)
γ_C	Concrete weight density (kN/m^3)
θC	Uplift pressure at the upstream cut-off (kpa)
θE	Uplift pressure at the downstream cut-off (kpa)
μ	Mean of hydraulic conductivity (m/day)
σ	Standard deviations of the hydraulic conductivity (m/day)

Abstract

The safety of hydraulic water retaining structures (HWRS) is an important issue as many instances of HWRS failure have been reported. Failure of HWRS may lead to catastrophic events, especially those associated with seepage failures. Therefore, seepage safety factors recommended for HWRS design are generally very conservative. These safety factors have been developed based on approximation calculations, unreliable assumptions, and ideal experimental conditions, which are rarely replicated in real field situations. However, with the development of the numerical methods, and high speed processors, more accurate seepage analysis has become possible, even for complex flow domains, different scenarios of boundary conditions, and varied hydraulic conductivity. On the other hand, because construction of HWRS requires a significant amount of construction material and engineering effort, the construction cost efficiency of HWRS is an issue that must be considered in design of HWRS.

This study aims to determine the minimum cost design of HWRS constructed on permeable soils, incorporating numerical solutions of a seepage system related to HWRS, utilizing linked a simulation–optimization (S-O) model. Due to the complexity and inefficacy of directly linking a simulation model to the optimization model, the numerical simulation model was replaced by trained surrogate models. These surrogate models can be trained based on numerically simulated data sets. Therefore, trained surrogate models expeditiously and accurately provide predicted responses relating to seepage characteristics pertaining to HWRS. The optimization model based on the linked S-O technique incorporated different safety factors and hydraulic structure design requirements as constraints. The majority of these constraints and objective function(s) were affected by the responses of predicted seepage characteristics based on the developed surrogate models.

To improve the safety of HWRS design, the effect of non-homogenous and anisotropic hydraulic conductivity were incorporated in the S-O model. Obtained solution results demonstrated that considering stratification of the flow domain due to different hydraulic conductivity values or anisotropic ratios can significantly change the optimum design of HWRS. Low hydraulic conductivity and anisotropic ratios resulted in more critical seepage characteristics. Consequently, the minimum construction cost increased due to an increase of dimensions of involved seepage protection design variables.

Furthermore, uncertainty in estimating hydraulic conductivity is incorporated in the S-O model. The reliability based optimal design (RBOD) framework based on the multi-realization optimization technique was implemented using the S-O model. The uncertainty in seepage quantities

due to uncertainty of hydraulic conductivity was represented using many stochastic ensemble surrogate models. Each ensemble model included many surrogate models trained in utilizing input–output data sets simulated with different scenarios of hydraulic conductivity drawn from diverse random fields based on different log-normal distributions. Obtained results of this approach demonstrated substantial consequences of considering uncertainty in hydraulic conductivity. Also, the deterministic safety factors, especially for those pertaining to the exit gradient, were insufficient to provide prescribed safety in the long term.

Although surrogate models are utilized in S-O approaches, each run of the S-O model takes a long time as developed S-O models are applied to complex and large scale problems. Hence, efficiency of the S-O model was a key factor to successfully implement the methodology. Three main techniques were utilized to increase the efficiency of the S-O technique: using parallel computing, utilizing nested function technique, and using a vectorised formulation system. These strategies substantially boosted efficiency of implementing the S-O model.

The S-O models were implemented for many hypothetical scenarios for different purposes. In general, results demonstrated that optimum design of the seepage protection system relating to HWRS design must include two end cut-offs with an apron between them. The dimensions of these components were augmented with an increase of upstream water head, and reduction of anisotropic ratios or hydraulic conductivity value. The main role of the downstream cut-off was to decrease the actual exit gradient value. This impact is more pronounced if the inclination angle of the cut-off is toward the downstream side (>90 degrees). The role of the upstream cut-off was to decrease uplift pressure values on the HWRS base. Consequently, this partially contributed to decreasing the exit gradient value. The effect of the upstream cut-off in reducing the uplift pressure was more when the inclination angle was toward the upstream side (<90 degrees). Moreover, the apron (floor) width helped to increase the stability of HWRS. This variable provided the required weight to improve HWRS resistance to external hydraulic forces and to uplift pressure. Incorporating the weight of water (hydrostatic pressure) at the upstream side in counterbalancing momentum and hydraulic forces showed improvement in the safety of the HWRS. Also, all conditions and safety factors pertaining to HWRS design were satisfied. The exit gradient safety factor was the most important critical factor affecting optimum design as obtained optimum solutions satisfied the minimum permissible values of the exit gradient safety factor, i.e., at the minimum permissible value. Also, the eccentric load condition played a crucial role in resulting optimum solutions.

Finally, applying the S-O model to obtain reliable and safe design of HWRS at minimum cost was successfully implemented for performance evaluation purposes. This technique may be

extended to incorporate more complex scenarios in HWRS design where the impact of dynamic and seismic load could be incorporated. The effect of unsteady state seepage system could be another interesting direction for future studies. Further, incorporating more sources of the uncertainty associated with design parameters could achieve a more accurate estimation of actual safety for the HWRS design.

Table of Contents

List of Tables

List of Figures

1 Introduction

1.1 General Introduction

Construction of hydraulic water retaining structures (HWRS), such as dams, barrages, regulators and weirs, is essential for stable and safe water management and to generate clean energy. Future projections of water resources indicate that water availability will significantly decrease for several countries around the world (Gerten et al., 2011). This may be attributed to climate change and carbon dioxide (greenhouse gas) emissions due to human activities. Building HWRS is a beneficial and important solution to reduce the impacts of water scarcity. However, significant considerations and hazards must be considered in design of HWRS. The economic cost of building such projects is enormous; additionally, failures of HWRS threaten human life and properties on downstream. Accordingly, the design and analysis of such structures must involve precise estimation and sufficient understanding of the influencing design variables and parameters, especially the seepage quantities and their impacts on safety of HWRS. This study presents coupled simulation-optimization (S-O) approaches to identify the minimum cost HWRS design, incorporating numerical seepage analysis and considering the hydraulic design safety factors in S-O models. Furthermore, the effects of permeability (hydraulic conductivity) and its uncertainty are integrated in S-O models. The numerical seepage simulation is indirectly linked to the optimization model using machine learning techniques based on surrogate models. Artificial neural network (ANN), support vector machine (SVM) and Gaussian process regression (GPR) machine learning techniques were used to develop surrogate models. The genetic algorithm (GA), hybrid genetic algorithm (HGA) and non-dominated sorting genetic algorithm II (NSGA-II) were utilized to solve optimization tasks due to the complexity and the attribute of each S-O model.

Hydraulic structures that impound a considerable amount of water (head) and are constructed on permeable soil foundation are associated with water seepage impacts. Seepage forces threaten hydraulic efficiency and structural stability of hydraulic structures. Seepage failure is classified as the second or third most frequent cause of dam failure after overtopping (ICOLD, 2016; NPODP, 2015). A critical and dangerous seepage consequence is piping failure. This failure is attributed to seepage forces, which move small soil grains and wash them out of the flow domain. Unless sufficient precautions are taken, continuous erosion of the soil constituent inevitably happen, and leads to piping failure. Furthermore, another consequence of seeping water is pore-water

pressure, which applies uplift (upward) pressure on the structure floor (apron) and may result in collapse of the floor.

The hydraulics of seeping water and associated mathematical relationship of seepage variables with flow domain characteristics is complex and nonlinear. The complexity arises from many factors, such as sub-structure geometry, soil properties and hydraulic conductivity variation and uncertainty. An analytical solution may be obtained only for simple and symmetrical cases and is often based on assumptions that are not always correct. However, it is difficult to obtain analytical solutions for more complex scenarios, which occur in most of existing projects. Therefore, many approximation and empirical theories have been proposed to estimate seepage quantities (uplift pressure and exit gradient). These theories include Bligh's creep theory, Lane's weighted creep theory, flow-net method, fragment method and Khosla's theory. Solutions of these approximate theories are acceptable to some extent. Their applications have an associated non-trivial amount of error compared to applications that use analytical solutions or experimental modelling, as shown in Figure1.1. Additionally, these theories apply to ideal general soil conditions (homogeneous and isotropic), which are rarely found in real life cases (Lambe & Whitman, 1969). Also, it is not possible to integrate the effects of hydraulic conductivity and uncertainty when utilizing these methods and theories.
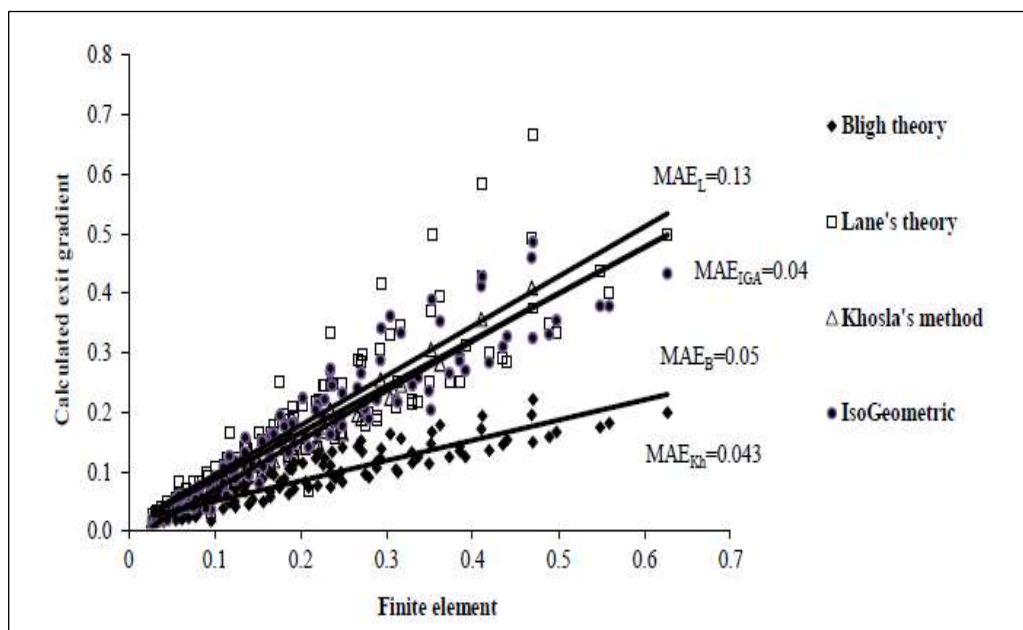
Figure 1.1 Comparing computed exit gradient by different methods and FEM based numerical solutions (Shahrbanozadeh, Barani, & Shojaee, 2015)

Recently, as a result of development of numerical methods and computerized processes, many seepage problems related to HWRS have been accurately simulated and solved by numerical

methods, such as finite element method (FEM) and finite difference method (FDM). The FEM and FDM are the dominant numerical methods in this field. These methods provide accurate and efficient results even for complex problems. Consequently, many software and codes have been developed to facilitate numerical simulation of seepage problems, particularly after development of high-speed computer processors. These codes can be used to analyse complex seepage problems precisely. Furthermore, hydraulic conductivity variation and other soil parameters can be integrated in the numerical model to study consequences of soil parameter variation on HWRS design. However, a source of weakness of using numerical solutions is that the numerical technique only provides a solution for predetermined problems, including pre-defined boundary conditions and geometry of the flow domain of hydraulic structures. This means the numerical model may not provide a generalized performance equation regarding what can be obtained by analytical solution.

Considering the above-mentioned arguments, contradicting goals of safety and cost must be simultaneously integrated in design of HWRS to attain optimum, safe and economic design based on accurate seepage numerical solutions. Hence, the optimization approach can be used to identify optimal design of HWRS. As a result, the minimum cost and safest HWRS can be achieved. Directly integrating the numerical model with the optimization model to attain an optimum HWRS design is computationally inefficient, a computational burden and time consuming task. Also, most evolutionary optimization algorithms (solvers) utilize direct search techniques based on a large population size. These optimization solvers present many random candidate solutions (individuals) and evaluate each single solution based on numerical seepage responses for that solution. This optimization process and others continue for many generations until the stopping criteria is met. Accordingly, directly linking the optimization model to the simulation model is a complex and computationally expensive process. Alternatively, the numerical model could be replaced by an approximate machine learning model (surrogate model) that accurately and expeditiously imitates numerical model responses. The surrogate model may be trained based on numerically simulated data (input and output) sets. There are many machine learning techniques that can be utilized to develop a surrogate mode, such as artificial neural network (ANN), support vector machine and Gaussian process regression (GPR).

The aim of this thesis is to develop a linked S-O methodology to produce a safe, reliable and economic design of HWRS based on adequately trained surrogate models. These models are trained based on numerically simulated data sets. Basically, different scenarios of hydraulic conductivity and geometry of the flow domain (number and attributes of cut-offs and apron length) are incorporated in S-O models to simulate the effects of these design parameters on optimum design

of HWRS. The uncertainty and spatial variation of hydraulic conductivity are considered in optimum design of HWRS. Identifying the most important design variable in optimum design is another goal of this study. Also, computational efficiency of the developed methodology is a significant aspect that must be considered in developing S-O techniques. Induced seepage forces and many safety factors and design requirements related to HWRS, such as overturning, sliding safety factors and preventing the eccentric load condition, are considered in the S-O approaches. For each S-O model, the type of machine learning technique and optimization solver are selected based on prediction accuracy and efficiency.

1.2   Problem Statement

The relationship between seepage design variables related to HWRS is usually categorized as a high degree nonlinearity problem, especially for complex problems (Harr, 1962). Many existing hydraulic structures built with high cost suffered from seepage problems, which may lead to failure of the structure. Such problems may be attributed to the approximation methods and theories by which the seepage related structures were analysed. Furthermore, these theories disregard spatial variation and uncertainties in some parameters, such as hydraulic conductivity, which have a significant effect on seepage characteristics. Providing a safe exit gradient for HWRS based on accurate and reliable analysis reduces actual possibility of piping failure. Also, decrease in the uplift pressure impacts provide a safer HWRS design. Moreover, construction of HWRS requires a considerable amount of construction materials and engineering effort, resulting in higher construction cost. Also, the HWRS safety design requirement must be simultaneously considered in HWRS design. Hence, there is a knowledge gap in obtaining optimum design for HWRS, which is partially filled by this research via developing a linked S-O model to determine minimum cost and safe design of HWRS by integrating numerical responses. These responses are based on trained surrogate models adequately trained and validated using numerically simulated data sets.

1.3   Objectives of the Research

The main objectives of this research are:

1. Develop and evaluate a coupled S-O model to obtain optimum design of HWRS founded on homogenous isotropic permeable soils and including a variable flat apron (floor) with variable length cut-offs.
2. Develop and evaluate a coupled S-O model to find the optimum design of HWRS founded on non-homogenous non-isotopic permeable soil and including variable and multi aprons with many cut-offs having variable length and orientation.

3. Enhancing the performance of the S-O model by hybridizing the genetic algorithm with the interior point algorithm to attain a global optimum solution of multiple cut-offs multi aprons seepage flow domain under HWRS constructed on homogenous anisotropic permeable soil.

4. Develop stochastic ensemble surrogate models to incorporate various uncertainties to develop reliability based optimum design (RBOD) framework to determine the reliable and optimum design of HWRS founded on heterogeneous isotopic permeable soil, and including and a flat apron with end cut-offs.

5. Develop a multi-objective multi-realization optimization model for reliability based optimum design framework to find a reliable and optimum design of HWRS founded on heterogeneous isotopic permeable soils.

1.4 Organization of the Thesis

The thesis contains eight chapters, encompassing the current (Introduction) chapter. The introduction chapter provides a brief description of the main effects of seepage quantities on the HWRS design. The chapter includes an overview of the utilized methodology to find the optimum design and to incorporate the numerical seepage responses based on surrogate models in the S-O model. The problem statement and objective of the study are also presented in this chapter.

Chapter two provides a review of literature starting with earliest methods related to seepage analysis of HWRS. Also, important previous studies utilizing numerical methods for seepage solution are briefly discussed. The chapter cites previous research which incorporates optimization models to improve HWRS design. This chapter also highlights the contribution of machine learning techniques in enhancing understanding of relationships between design variables of HWRS. Additionally, machine learning technique applications in predicting the future behaviour or consequences for a particular design of HWRS are presented.

Chapter three demonstrates the formulation of the linked S-O approach to determine the optimum design of HWRS constructed on homogenous permeable soils, including two end cut-offs with apron. The description of generated and simulated data, training surrogate models based on ANN and the attributed genetic algorithm optimization solver are presented in this chapter. All design requirements of HWRS and related seepage safety factors are considered in formulating the S-O model. Obtained results for implemented cases and performance evaluation of the S-O model are included in this chapter.

Chapter four contains the formulation of the linked S-O model to attain the optimum design of HWRS comprising of many cut-offs and aprons between them. The effects of non-homogenous anisotropic hydraulic conductivity are incorporated in the S-O model. Development of surrogate models was based on the support vector machine (SVM) technique, and the optimization model was based on the hybrid genetic algorithm (HGA). The optimum solution obtained via the S-O model and evaluation of S-O models are also included in this chapter.

Chapter five demonstrates the efficiency of hybridizing the genetic algorithm with the gradient search algorithm to achieve the global optimum solution within the linked S-O technique. Description and formulation of the optimization model are demonstrated in this chapter. The conceptual model of seepage includes many cut-offs, many aprons and homogenous anisotropic permeable flow domain. The SVM technique was utilized to develop the surrogate models. The safety factors and HWRS design requirements are included, with the results and performance evaluation of the S-O model presented in this chapter.

Chapter six encompasses formulation of the reliability based optimum design of HWRS. This was achieved by developing many ensemble surrogate models to incorporate stochastic responses of seepage characteristics due to uncertainties in estimating hydraulic conductivity in the linked S-O model. The surrogate models were developed based on the Gaussian progress recession (GPR) technique and the optimization solver was the genetic algorithm (GA). Hydraulic conductivity was represented as a random field sampled from a log-normal distribution based on different standard deviation values. Solution results and performance evaluation of the developed methodology are included in this chapter.

Chapter seven presents a new formulation of the reliability based optimum design utilizing the multi-objective, multi-realization optimization model based on the ensemble surrogate models. Many ensemble surrogate models were developed to represent the stochastic responses of seepage characteristics due to uncertainty in estimation of hydraulic conductivity. The conceptual model included an apron between two end cut-offs. Hydraulic conductivity was defined as a random field based on log-normal distribution. The results and performance evaluation of the methodology are presented in this chapter.

Chapter eight presents the conclusion of this study and recommendations for future studies.

2 Theoretical Background and Literature Review

This chapter covers seepage theory and related equations of seeping water through porous media, and presents a review of literature related to seepage analysis and HWRS design. This literature review is organized in accordance with techniques utilized in the proposed methodology, starting from earliest methods to analyses of seepage, then numerical seepage analysis methods, previous studies utilizing the FEM method and previously developed surrogate models. Also, the optimization theory and previous studies related to linked simulation optimization approaches are described. Additionally, the inadequacy and difficulties of applying the previous methods and theories to analysis of seepage under HWRS are presented. The complexity of developing an analytical solution for complex seepage models is described in this chapter. Applications of the numerical solutions based on FEM in obtaining accurate seepage analysis are included. Also, utilization of the previous research for the optimization technique in obtaining optimum design of hydraulic structures and for water resource management is discussed. The efficiency of building a linked simulation optimization approach is demonstrated with its application in water resource management and in ground water to find the optimum design integrating numerical responses based on the surrogate models.

2.1 Earlier Empirical Seepage Analysis Methods for Hydraulic Structures

2.1.1 Bligh's and Lane's Theory

Bligh (1910) concluded that the weight of the hydraulic structure is the most significant factor involving in hydraulic structure stability. However, Bligh (1915) adopted the hydraulic gradient and creep theory to explain water movement under a hydraulic structure and compared his theory with experimental results. He found that the seepage stream is the shortest and closer path to the foundation of the hydraulic structure. This path is called the length of creep (L) at which the hydraulic gradient (H.G.) decreases with an increase in (L) according to this equation (H.G. =h/L) (Garg, 1987; Khosla, Bose , & Taylor, 1936).

Where: h= difference between upstream and downstream water level, and

L= total length of water seepage stream near hydraulic structure foundation.

Furthermore, Bligh (1915) assumed empirical exit gradient safety factors relate to different soil classes, and he considered the exit gradient is safe compared with these factors. Additionally, the uplift pressure hazard could be addressed by designing sufficient thickness of the floor. This thickness could be computed by the physical equilibrium of the submerge weight of floor at certain points with uplift pressure value at the same point. The computed thickness can be magnified by a factor of 1.33 to achieve safer situations (Bligh, 1910, 1915; Garg, 1987). Although Bligh's theory has been utilized to design many hydraulic structures, the theory did not distinguish between horizontal and vertical or other directions of seeping water movement. This shortcoming was solved by Lane's weighted creep theory.

Lane (1935) observed, after a precise investigation of 200 dams around the world, that water movement in the horizontal direction was relatively easier than the vertical direction. Consequently, he recommended that horizontal creep length must be shortened by a factor of 1/3, whereas vertical length could be kept without change. He assumed different safe exit gradient factors for different soil types to compare with computed hydraulic exit gradients to obtain safe hydraulic design (Garg, 1987; Khosla et al., 1936).

For comparison purposes, recently many researchers have considered solutions of Bligh's and Lane's methods. They concluded that the obtained values of seepage characteristics based on these methods are inaccurate compared to experimental observations or numerical solutions (Sedghi-Asl, Rahimi, & Khaleghi, 2012; Shahrbanozadeh et al., 2015; Tokaldany & Shayan, 2013)

2.1.2 Khosla's Theory

Khosla et al. (1936) used an independent variable technique to develop a method by which seepage characteristics under weirs including different seepage features, such as aprons, floor slopes and a varied number of cut-offs, could be analysed. Khosla's theory is based on an analytical solution (conformal mapping concept) and experimental data analysis. According to this theory, complex sub-structures related to seepage control variables can be split into three categories: end sheet piles (cut-offs), intermediate cut-offs and depressed floors. By this method, the uplift pressure values could separately be determined at a specific points (key points). Pressure values must be corrected based on the interaction effects between these variables (Garg, 1987; Khosla et al., 1936).

Moreover, Khosla et al. (1936) derived different exit gradient equations considering many design cases, such as flat floor, single cut-off, depressed floor and cut-off at the end of the floor. However, Khosla et al. (1936) supposed that exit gradient is affected by end floor condition (geometry) only and disregarded other components, such as hydraulic conductivity of porous media

(Eq. 2.1). Khosla et al. (1936) recommended that the exit gradient safety factor is: 4 to 5 for gravel, 5 to 6 for coarse sand and 6 to7 for fine sand. The safety factor is the ratio of the critical exit gradient to the computed exit gradient (Delleur, 2006). The exit gradient is computed as given by Eq. (2.1):

$$i_e = \frac{h}{\pi d \sqrt{\lambda}} \tag{2.1}$$

Where i_e is the exit gradient by Khosla et al. (1936) theory, h is total head, d is length of downstream cut-off and λ is computed by equation 2.2

$$\lambda = \frac{\sqrt{1 + \alpha_1^2} + \sqrt{1 + \alpha_2^2}}{2} \tag{2.2}$$

Where $\alpha_1 = \frac{b1}{d}$, $\alpha_2 = \frac{b2}{d}$ as shown in Figure 2.1 and the factor of safety can be computed by $F.S = \frac{i_c}{i_e}$, $i_c = \frac{\gamma_{sub}}{\gamma_w}$ or $i_c = \frac{(G_S - 1)}{(1 + e)}$.

Where G_S is the specific gravity of the soil, e is void ratio, i_c is critical exit gradient, γ_{sub} is the submerged soil density, γ_w is weight water density.
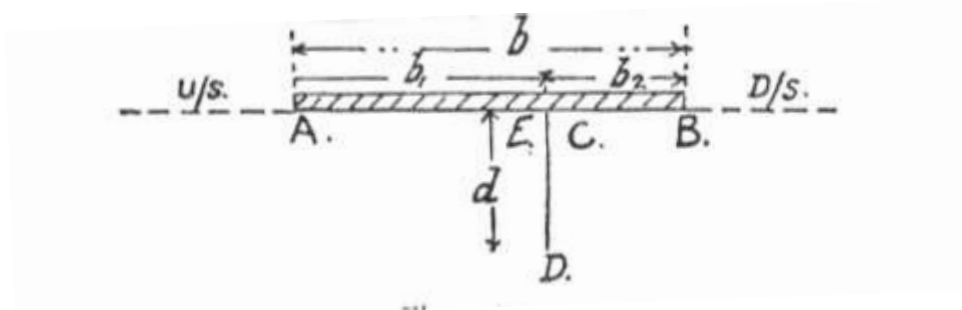
Figure 2.1 One cut-off with apron (Khosla et al., 1936)

Furthermore, Khosla's theory is based on homogenous and isotropic hydraulic conductivity. Khosla et al. (1936) considered that the geometry of flow domain is the dominant factor for seepage quantities. That is clearly seen in Eq. 2.1 (above). The hydraulic conductivity value is disregarded in computing the exit gradient which is illogical to some extent. However, approximation ranges of safety factors have been proposed based on the main types of soil. Few researchers have utilized Khosla's for seepage analysis and employed Khosla's equations in optimization models (Garg, Bhagat, & Asthana, 2002; Singh, 2010).

2.2   Approximate Solutions of Seepage

2.2.1   Fragment Method

Pavlovsky (1935) developed the approximation fragment method to determine seepage characteristics easily and directly under HWRS. In this method, the seepage flow domain was divided into a certain number of fragments. An imaginary section was assumed, where the equipotential line could be considered a vertical line (Harr, 1962). Therefore, flow rate and consequent head could be computed for regular shape regions. The mathematical expression of this theory is expressed below as:

$$Q_m = kh_m/\Phi_m$$	(2.3)

Where: m= 1, 2, 3,…, n, Q_m= discharge passed through fragment

h_m = head loss through fragment

Φ_m = dimensionless shape factor depends on the geometry of the fragment

And when discharge for all fragments is the same

$Q = kh_1/\Phi_1 = kh_2/\Phi_2 = kh_3/\Phi_3$……. Kh_n/Φ_n

$$Q = k\ \Sigma h_m/\Sigma\Phi_m$$	(2.4)
$$Q = K\frac{\Sigma h_m}{\Sigma\Phi} = \frac{kh}{\sum_{m=1}^{n}\Phi_m}$$	(2.5)

Where h without a subscript is total head loss. Therefore, by a similar method:

$$h = \frac{h\,\Phi_m}{\Sigma\Phi}$$	(2.6)

Consequently, the distribution of pressure head and exit gradient can be estimated as head losses have been computed. Also, there are many standards and forms to calculate the shape factor for each fragment easily according to the geometry and location of these fragments.

It could be seen that application of the fragment method is only limited for regular soil properties. It is difficult to implement the fragment method for stratified, anisotropic or heterogeneous soils due to the variation of hydraulic conductivity value. Also, there are limited shape factors and standards, which means that this method cannot cover all expected scenarios of the flow domain.

Recently, many researchers have utilized the fragment method to determine seepage characteristics for the stop during filling in the mining industry (Madanayaka & Sivakugan, 2016; Sivakugan & Rankine, 2011; Sivakugan, Rankine, Lovisa, & Hall, 2013). For these studies, the solutions using fragment method were compared to numerical simulation and the results demonstrated good agreement with the numerical solution.

2.2.2 *Flow Net Method*

Flow net is one of the easiest and most prominent approximation methods used for seepage analysis. It depends on many sketching trials of equipotential lines and streamlines. These lines must be drawn in such a way that each equipotential line intersects the streamline orthogonally. When an imaginary grid of equipotential line and streamline is created, seepage characteristics can be determined at each intersection point using Eq. (2.7) (Das, 2008; Lambe & Whitman, 1969; Terzaghi, Peck, & Mesri, 1996).

$$q = N_f \, \Delta q = \ kh\frac{N_f}{N_d} \tag{2.7}$$

Where: h = total hydraulic head or difference in elevation of water between upstream and downstream, N_d = number of potential drops, N_f = number of flow channel, k = soil conductivity (L/T), q = discharge (L^3/T).

2.3 Analytical Solution/Conformal Mapping by Schwarz-Christoffel Transformation

The Schwarz-Christoffel transformation is one of the most important transformation methods commonly used to derive analytical solutions for groundwater movement or seepage. Conformal mapping constitutes geometric transformation of the complex domain to another simple domain (plan), while retaining the properties of the complex domain in the new domain. In groundwater problems, by using conformal mapping, Laplace's equation can be solved with related boundary conditions and seepage characteristics (Harr, 2012). The basic concept of this mapping consists of opening the boundary polygon of the flow domain from a certain point in z(x, y) plan to extract this polygon in a straight line aligned with a real axis of t(r, s) plan from -∞ to +∞ on the upper half plan. The interior angles of the polygon must be considered in this transformation. The new polygon is described as part of a semicircle with one or more vertices at the infinity on the upper half t-plan. The transformation equation is given by Eq. (2.8).

$$\frac{dz}{dt} = \frac{A}{(a-t)^{\alpha/\pi} * (b-t)^{\beta/\pi} * (c-t)^{\gamma/\pi} * \dots}$$

(2.8)

Where A refers to a complex number in z-plan and a, b and c are the real constants corresponding to the projection location in z-plane and α, β and γ represent the external angles of the polygon.

A substantial amount of research has been conducted based on this technique. Elganainy (1986) determined the exit gradient and seepage flow for a filter constructed between two hydraulic structures and at the downstream, using a conformal mapping technique. Elganainy (1987) utilized the Schwarz–Christoffel method to derive a mathematical solution (for exit gradient and uplift pressure) for new conditions of Nile barrages and the subside weir. Ilyinsky and Kacimov (1991) demonstrated the procedure to compute the ground water flow around cut-off walls and to trench. The adopted conformal mapping concept conjugated with the variation method. Ilyinsky, Kacimov, and Yakimov (1998) reviewed different techniques, inverse method, variation theorems and optimization process, to develop an analytical solution for seepage under hydraulic structures.

Additionally, conformal mapping method has been used by Farouk and Smith (2000) to derive the exit gradient and potential seepage equations for hydraulic structures with two intermediate filters. Jain (2011) derived mathematical models to determine seepage flow parameters underneath a weir with aprons, two cut-offs, finite depth condition and step at down side. Ijam (2011) used the Schwarz–Chrisoffel transformation method to obtain an analytical solution for seepage flow under hydraulic structures to analyze many variables in the seepage equation, such as cut-off wall with variable locations and angles.

Previous discussion of analytical and approximation methods shows that there are many limitations to apply these methods in the S-O model. For example, the analytical solution based on conformal mapping can be applied only for simple and symmetrical cases. Solving the integration of the transformation equation is a demanding task, especially for non-homogenous anisotropic hydraulic conductivity, even for simple geometry. Moreover, the solutions of approximation methods have a noticeable amount of error and are limited to a specified range of simple flow conditions. In the present study, a comprehensive method is required to describe the seepage characteristic for different underground flow conditions, including varied length, number and orientation of cut-offs. These different scenarios provide more alternatives to find optimum design at minimum cost. Incorporating heterogeneous and non-homogeneous hydraulic conductivity of the flow domain must be considered in the utilized seepage analysis technique. Using the traditional

approximation and analytical solution for this study is not possible. Hence, numerical method based on the finite element method (FEM) is adopted in developing the linked S-O approach.

2.4   Numerical Solution

The numerical solution is considered more beneficial than analytical and approximation solutions, as complex seepage problems can be solved precisely. Analytical solutions are based on many simplified assumptions, such as isotropic, homogeneous soil properties, which are not always correct. Moreover, the upstream water level is assumed as horizontal level, and the seepage flow domain is mostly considered in a rectangular shape. These assumptions are not necessary for numerical methods. The numerical model can be utilized to solve complex seepage problems, including different boundary conditions. Hence, several efficient numerical methods such as finite difference method (FDM) and FEM are used to solve and simulate a large number of seepage related problems (Wang & Anderson, 1995).

2.4.1   Finite Element Method (FEM)

The FEM is based on the approximation integration approach to solve differential governing Laplace equations (Jain, 2011). FEM solves complex problems with accurate results that is not possible using the closed form solution. The results are more accurate and precise if more time and effort are spent on the computational process (Rao, 2013).

The small panels resulting from subdivision of the flow domain or continuum are called finite elements. Each element is connected with an adjacent element by nodal points (nodes), which lie on the element boundaries. Variation of any design variable or parameter through the continuum is not easy to be determined. Hence, the interpolation model (approximate simple function) is assumed to identify seepage variable values for each node. By applying the interpolation model, boundary condition and governing equation, the variable value for each node can be calculated accurately (Rao, 2013).

The steps of the FEM process are summarized as:

1. Subdividing the continuum of the problem into finite elements with a certain number, size and shape depending on the problem feature.
2. Finding the best interpolation model describing boundary conditions and variables variation. The interpolation model is mostly derived as a simple polynomial (linear, quadratic or cubic).
3. Deriving the action and deformation element matrix equation.
4. Formulating a control equation (equilibrium) for the general model.

5.   Solving the control equation for each node.

In 1970, FEM was applied for the first time by Neuman and Whiterspoon for steady state seepage problems involving anisotropic heterogeneous soil and different boundary conditions. The efficiency and accuracy of the FEM solution compared to experimental, analytical and published results was demonstrated by Neuman and Whiterspoon (Chen, Huan, & Ma, 2006)

As FEM provides precise solutions, numerous researchers have utilized FEM to solve seepage problems. Lefebvre, Lupien, Pare, and Tournier (1981) used FEM to evaluate different scenarios to control and reduce the exit gradient value for embankment dams. Alsenousi and Mohamed (2008) studied the effect of inclined cut-offs for varying distances and angles. Heterogeneous and anisotropic underlying soil layers with limited depth were assumed for the numerical model. Tatone, Donnelly, Protulipac, and Clark (2009) evaluated the efficiency of $21000m^2$ plastic concrete cut-off in a newly constructed dam in northern Ontario. FEM models were developed to simulate seepage flow of the dam to be compared to drilling investigations and laboratory tests.

Azizi, Salmasi, Abbaspour, and Arvanaghi (2012) utilized hydraulic design data and the structural parameters of a diversion dam to simulate the flow process. SEEP/W based on FEM software was used to evaluate hydraulic design parameters. El-Jumaily and AL-Bakry (2013) utilized the finite volume method to analyze seepage through permeable soil. Furthermore, he studied the effects of anisotropic and non-homogenous soil on uplift pressure and exit gradient.

Mansuri, Salmasi, and Oghati (2014) determined the effects of positions and angles of cut-offs on exit gradient, seepage flow and uplift pressure underneath a diversion dam. Moharrami, Moradi, Bonab, Katebi, and Moharrami (2014) evaluated the effects of cut-off beneath dams to reduce uplift pressure and prevent piping problems. Shahrbanozadeh et al. (2015) adopted a complementary numerical method ISO-geometrical analysis (IGA) and FEM to determine the uplift pressure and exit gradient value for a hydraulic structure model. They compared the experimental results to approximation methods and numerical methods solutions to demonstrate that FEM and IGA provide the most accurate solutions.

This literature review of FEM shows that most researchers focus on evaluating, comparing and studying the effect of seepage parameters and simulate a certain seepage system for a particular case. Most conducted research shows that FEM provides an efficient and accurate solution for complex problems. However, FEM is applicable for pre-defined problems and cannot provide generalized equations representing the relationship between seepage variables as in the closed form

solution. Therefore, the machine learning technique is utilized to develop surrogate models based on many input and output data sets simulated by the FEM numerical method to accurately predict numerical responses within inked S-O models.

2.4.2 SEEP/W numerical seepage modeling and limited validation

The Geo-Studio SEEP/W software (numerical model) based on FEM was used to find the seepage characteristic value for all simulated seepage scenarios in this study. The seepage characteristics obtained by SEEP/W were solely utilized to create training data (input-output data sets) to train surrogate models, or to evaluate the seepage characteristics of the optimum solution obtained by the S-O technique. SEEP/W can efficiently solve different seepage problems, such as saturated/ unsaturated cases, steady/ transient states, multilayer system and isotropic / anisotropic / heterogeneous hydraulic conductivity, etc. Furthermore, the effect of other geotechnical considerations, stresses, loads, boundary conditions and soil parameters can be combined with SEEP/W numerical seepage simulation. This is achieved based on integrating the provided Geo-Studio components, such as SLOP/W, SIGMA/W and QUAKE/W, with the SEEP/W model (Krahn, 2012). However, it should be noted that the linked simulation-optimization methodology being proposed here is not dependent on a particular simulation model. Indeed, it is possible to easily replace SEEP/W by an even more robust or efficient simulation model in the future. In that case, only surrogate models will require fresh training and validation.

Many researchers have applied SEEP/W for different problems. Chenaf and Chapuis (2007) utilized SEEP/W as a numerical model to validate many approximation equations used to describe a seepage system related to a pumping well. Oh and Vanapalli (2010) combined SLOPE/W and SEEP/W to study the effect of water infiltration on the stability of homogenous compacted embankments. White, Beaven, Powrie, and Knox (2011) used SEEP/W numerical solutions to compare with observed depths of drained liquid resulting from field testing of the leachate recirculation model for different periods. Chapuis, Chenaf, Bussière, Aubertin, and Crespo (2001) conducted a precise validation for SEEP/W solution compared to the analytical solution of different seepage problems.

Additionally, in this study, before utilizing SEEP/W as a numerical solution for seepage related to HWRS, the SEEP/W solution is validated with a closed form solution. Many arbitrary selected scenarios of a simple model, including one end cut-off (at downstream) and apron were solved by the closed form method (Harr, 1962; Khosla et al., 1936) and SEEP/W numerical modeling. The evaluation demonstrated that SEEP/W can provide accurate solutions compared to

the closed form solution. The mean absolute error (MAE) for the uplift pressure obtained by SEEP/W was 0.905 (2.5%) and for exit gradient was 0.041 (4.6%), as shown in Figures 2.2 and 2.3.
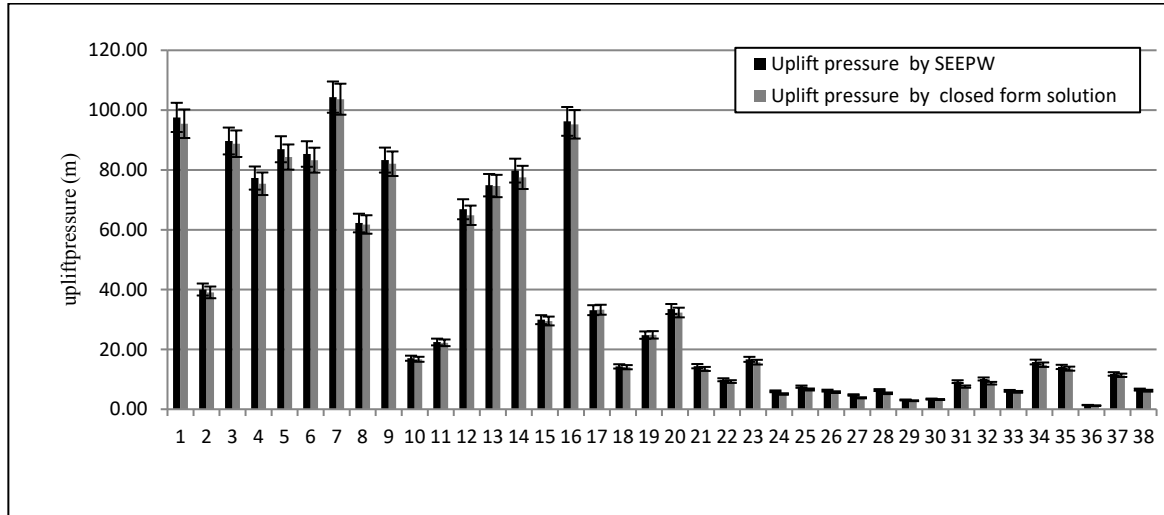
Figure 2.2 Validation of the SEEP/W solutions (uplift pressure)
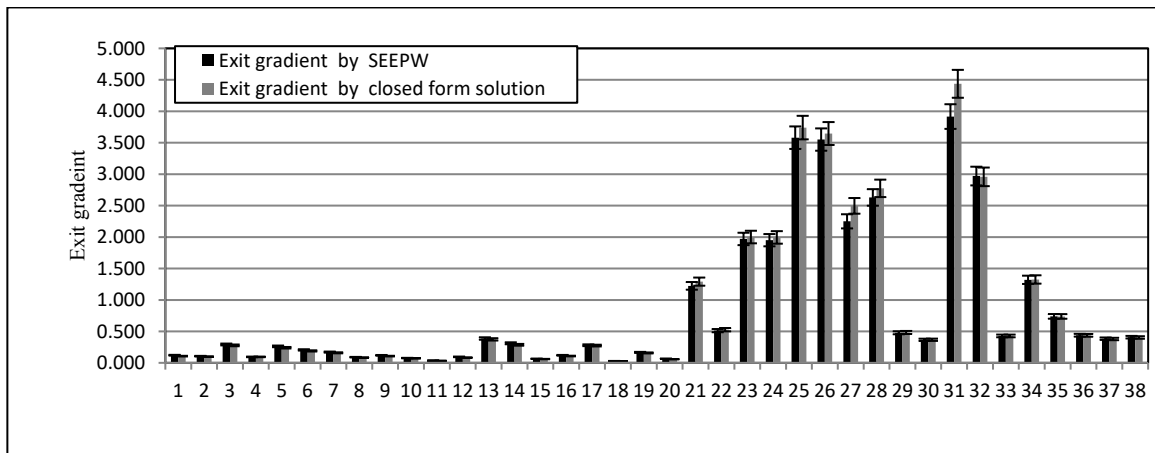
Figure 2.3 Validation of the SEEP/W solutions (Exit gradient)

2.5   Meta Model (Surrogate Model)

The surrogate models in the linked simulation optimization model have been efficiently utilized to imitate the numerical model responses for complex and computationally expensive problems. Furthermore, meta modeling techniques have been implemented to enhance understanding of input design variable effects on the output design variable. Also, meta models are used as predictors for future expectations of some variables in a specified design. Developing an efficient surrogate (meta) model is based on selecting an adequate machine learning technique and

sufficient and uniformly distributed data sets. Many studies have utilized different machine learning techniques to develop efficient surrogate models for hydraulic structures and ground water applications. The most efficient machine learning techniques are artificial neural network (ANN), support vector machine (SVM) and Gaussian process regression (GPR).

2.5.1   Artificial Neural Network (ANN)

ANN imitates human brain neurons, which can change responses according to different environments and / or actions. In the 1940's, McCulloch and Pitts designed the first neural network, and at the end of this year, Donal Hebb designed the first learning law for ANN. In 1972, Kohonen and Anderson developed strength theory between neurons. Between 1958 and 1988 Rosenblatt, Block, Minsky, Widrow and Hoff submitted a complementary concept for ANN, such as input layer perceptron, connection to associated neurons, fixed weights and other learning rules (Ersayın, 2006; Sivanandam, Sumathi, & Deepa, 2006).

For seepage and ground water problems related to hydraulic structures, ANN has been utilized to simulate and identify seepage characteristics. Garcia and Shigidi (2006) utilized ANN as an approximation model to compute aquifer transmissivity and hydraulic head values. Ersayın (2006) developed an ANN model to predict the phreatic line (seepage path) in an earth fill dam (Jeziorsko Dam) in Poland. Szidarovszky, Coppola, Long, Hall, and Poulton (2007) combined numerical models with the ANN model (hybrid-ANN numerical) to improve the simulation of groundwater characteristics. Kim and Kim (2008) used the ANN method to predict relative crest settlement of concrete faced rock fill dams. Predicted results of the utilized methodology showed good agreement with conventional methods.

Joorabchi, Zhang, and Blumenstein (2009) successfully developed ANN models to simulate and predict the ground water fluctuation based on many variables, such as water table, tide elevation, beach slope and hydraulic conductivity, in five locations on the east coast of Australia. Nourani, Sharghi, and Aminfar (2012) used a single ANN model to predict head values for each piezo-metric on upstream and downstream of different sections of the Sattarkhan earth fill dam (Iran). Santillán, Fraile-Ardanuy, and Toledo (2013) developed an ANN model for seepage analysis beneath a hydraulic structure, considering different water head. Al-Suhaili and Karim (2014) presented a methodology based on the ANN model to optimize the cost of cut-off walls and floors for small hydraulic structures constructed on permeable foundation using genetic algorithm (GA).

The main shortcoming of using the ANN model is a tendency to overfit unless a sufficient amount of data is used for validation and test phases. Also, there are many training algorithms, such

as Bayesian regularization and Lievenberg-Marquardt, which can be used to decrease overfitting effects. Also, the early stopping and regularization technique significantly improves performance of the ANN model. The early stopping strategy monitors training error and validation error. The training process is continued while training and validation errors decrease. However, when training error decreases and validation error increases (overfitting phenomena), the training process stops too soon (early stopping) and the optimum value of weight and biases are saved. The regularization technique evaluates performance of the ANN model not only based on the error of predicted data, but it tries to minimize the summation of weights and biases to provide smother responses.

2.5.2 Support Vector Machine

Originally, Vapnik (1999) developed and discussed the advantages of using optimal spreading hyper plane in classification and regression machine learning problems. He showed that the generalization ability of the developed technique with fewer support vectors is better. The SVM has the ability to overcome the over-training (overfitting) phenomena (Raghavendra.N & Deka, 2014; Vapnik, 2013). Recently, SVM has been widely used in research in civil engineering and hydraulic structure disciplines (Fisher, Camp, & Krzhizhanovskaya, 2016; Mahani, Shojaee, Salajegheh, & Khatibinia, 2015; Parsaie, Yonesi, & Najafian, 2015; Ranković, Grujović, Divac, & Milivojević, 2014; Su, Chen, & Wen, 2016). Many other researchers have employed SVM for different purposes related to water resources and hydrology application (Azamathulla, Ghani, Chang, Hasan, & Zakaria, 2010; Bhagwat & Maity, 2012; Cimen, 2008; Eslamian, Gohari, Biabanaki, & Malekian, 2008; Goel & Pal, 2009; Han, Chan, & Zhu, 2007; Hipni et al., 2013; Khan & Coulibaly, 2006; Lin, Cheng, & Chau, 2006; Misra, Oommen, Agarwal, Mishra, & Thompson, 2009; Moghaddamnia, Ghafari, Piri, & Han, 2009; Ranković et al., 2014; Samui, 2011; Yu, Chen, & Chang, 2006).

Specifically for ground water applications, many researchers have used SVM to predict the ground water fluctuation and study the seepage characteristic in a specific system for various conditions (Behzad, Asghari, & Coppola Jr, 2009; Yoon, Jun, Hyun, Bae, & Lee, 2011). Others have utilized SVM to assess the quality of the ground water and quantify the pollution sources (Bashi-Azghadi, Kerachian, Bazargan-Lari, & Solouki, 2010; Liu, Chang, & Zhang, 2009). Most of these studies include comparison of SVM performance to another technique, such as ANN model, and the results revealed that SVM prediction is better than ANN. Also, SVM is more likely to capture the relationship between input and output data and filter out outliers and noise instances.

The majority of previous studies were implemented in predicting/forecasting responses of a certain variable based on training data. Different error measures were used to evaluate performance of SVM prediction. The key conclusion was that SVM can provide an efficient prediction, especially when the proper options of kernel function and box-constraint are setup carefully. For some complex problems, developing a SVM was used to enhance understanding of input variable effects on prediction responses. However, SVM is rarely linked with the optimization model in civil engineering applications. Also, reported studies utilizing SVM as a prediction or a surrogate related to HWRS models are scarce.

2.5.3 *Gaussian Process Regression (GPR)*

Originally, Rasmussen (2004) developed the GPR technique. However, there were many earlier applications of Gaussian distribution in the machine learning technique. The radial basis function network and Gaussian kernel function based on SVM are an initial and simple version of the GPR.

The GPR machine learning technique is a generalization of the probability distribution. The stochastic Gaussian process based on random probability distribution governs the properties of the GPR function ($f(x)$) at a particular point. Hence, the GPR algorithm provides a flexible technique based on Bayesian framework to figure out the relationship between given data sets. Many technical factors, such as hyper-parameter and uncertainty estimation, make the GPR a robust technique (Sun, Wang, & Xu, 2014).

Few studies have been conducted in different disciplines and engineering applications. The GPR technique is utilized for prediction and forecasting purposes (Chen & Ren, 2009; He et al., 2017; Kang, Han, Salgado, & Li, 2015; Kang, Xu, Li, & Zhao, 2017; Kim, Lee, & Essa, 2011; Li et al., 2017; Pal & Deswal, 2010; Samui & Jagan, 2013; Xu & Suzuki, 2011). From these studies, the most important conclusion was that GPR is less impacted by noisy training data, and the generalization ability of GPR is better than other machine learning techniques, such as SVM and ANN. Although, there are many factors which enhance prediction ability and efficiency of the GPR technique compared to other techniques, applications of the GPR technique in ground water and hydraulic structures are scarce. Furthermore, utilization of GPR as a surrogate model replacing the numerical model is extremely limited for different disciplines (Xia, Luo, & Liao, 2011).

2.5.4 *Optimization Theory and the Application in HWRS*

Optimization is a technique utilized to find the best solution, design or maintenance engineering system. The objective of optimization is either searching for a minimum or maximum value of the objective function, which includes design (decision) variables. Basically, in this study,

the optimum solution represents the optimum value for the seepage control design variables. These variables, such as upstream and downstream cut-offs, location and orientation of cut-offs and apron length, provide minimum cost and safe HWRS design. The constraints of the optimization model reflect the design safety factor of HWRS and other design requirements. As the optimization solver is based on surrogate model responses to evaluate the objective function value and constraints, evolutionary optimization algorithms, such as the genetic algorithm (GA), are utilized for such complex problems. Most evolutionary optimization algorithms are based on direct search and natural selection techniques. Recently, evolutionary optimization algorithms have been widely utilized, as compared to traditional optimization methods. Complex engineering optimization problems can be solved using these algorithms, such as GA, simulated annealing, fuzzy optimization and other methods (Rao, 2009). These algorithms imitate biological behavior for some creatures, swarming of insects and neurobiological system as listed below:

1. Genetic algorithm (GA) is based on a direct search technique and natural gene selection. GA is effective in identifying the global minimum or maximum.

2. Simulated annealing (SA) is based on complete thermal annealing of critically heated mutation and is efficient in identifying the global optimum solution.

3. Particle swarm optimization is based on the behavior of a colony of living things, such as birds, insects and fish.

4. Ant colony optimization is based on the behavior of ant colonies.

In this study, GA, hybird genetic algoritim (HGA) and non-dominated sorting genetic algorithm II (NSGA-II) are selected as the optimization algorithms. These algorithms can efficiently locate a global optimal solution, especially for nonlinear optimization problems. In general, Many researchers from different engineering backgrounds have utlized GA. They conclude that GA provies an efficient optimum solution (Al-Suhaili & Karim, 2014; Bornschlegell et al., 2012; Cojocaru, Duca, & Gonta, 2013; Datta, Chakrabarty, & Dhar, 2011; Hassan, 2015; Housh, Ostfeld, & Shamir, 2012; Innal, Dutuit, & Chebila, 2015; Islam, Buijk, Rais-Rohani, & Motoyama, 2015; Rajper & Amin, 2012; Singh, 2010, 2011).

Particularly in hydraulic structures, different optimization algorithms are utilized to find an optimal solution for the design. Yazd, Arabshahi, Tavousi, and Alvani (2015) studied optimum geometry of concrete gravity dams at minimum cost using the particle swarm optimization (PSO) algorithm. Sustainable and seismic loads are considered in the optimization model. Arman and Ghader (2014) studied the optimum shape of concrete gravity dams by applying a new objective

function. This function is the allowable duration under earthquake loads, as this duration gives an indication of a specific tension stress value.

AL-Musawi, Shukur, and Al-Delewy (2006) studied the optimum characteristics for three alternatives, cut-off wall, blanket floor and filter trench, to reduce seepage effects. FEM was used to analyze and simulate each case of the optimization model based on Lagrange multipliers. Optimization results showed that the filter trench attained minimum cost. Singh (2010) used GA to minimize construction cost of barrages. Additionally, Singh (2011) used fuzzy numbers to measure the uncertainty in seepage analysis under a varied hydraulic head. Singh and Duggal (2015) used the hybrid differential evolution multiple particle swarm optimization technique (HDEMPSO) to solve the optimization model of the hydraulic structures. Seyedpoor, Salajegheh, and Salajegheh (2010) studied optimal design of arch dams using soft computing techniques which included dam-water-rock interactions. They used FEM simulation model with earthquake load to estimate the dynamic behavior of an arch dam. Furthermore, optimization models are applied to minimize construction cost.

2.6   Linked Simulation Optimization (S-O) Model for HWRS design

The linked simulation optimization (S-O) approach is considered a useful technique for complex problems to identify the optimum solution based on numerical simulations. The first attempt of this technique in groundwater and water resources was conducted by (Gorelick, 1983) followed (Das & Datta, 1999; Wagner & Gorelick, 1986; Willis & Finney, 1988). These authors applied the S-O model to identify the contaminate source characteristics in specific aquifers and a case study area. Later, as linked S-O provides efficient and accurate solutions, S-O has been applied to many problems related to groundwater management in coastal aquifers and identifying source of contaminants, which are considered complex and computationally expensive tasks (Ayvaz, 2016; Bhattacharjya & Datta, 2009; Bhattacharjya, Datta, & Satish, 2007; Datta et al., 2011; Dhar & Datta, 2009; Hazrati-Yadkoori & Datta, 2017; Heydari, Saghafian, & Delavar, 2016; Jha & Datta, 2011; Shourian, Mousavi, Menhaj, & Jabbari, 2008; Sreekanth & Datta, 2011, 2015a, 2015b).

Specifically in HWRS design involving seepage effects, few studies have utilized S-O techniques. Singh (2010, 2011) formulated an optimization model to find the optimum dimension of barrage at minimum cost. The author used Khosla's theory to obtain seepage characteristics to be processed in the optimization algorithm. The limitation of this study was that Kholsa's theory is only applicable for small hydraulic structures and the solution by Khosla's theory has a noticeable amount of error. Also, incorporating the effects of hydraulic conductivity on seepage analysis is not possible

using Khosla's theory. Moreover, Khosla's theory can be applied for specified components of substructures related to seepage under HWRS with many restrictions.

Hamidian and Seyedpoor (2010); Seyedpoor, Salajegheh, Salajegheh, and Gholizadeh (2009); Seyedpoor, Salajegheh, Salajegheh, and Gholizadeh (2011) developed a new methodology to find the optimum shape of a concrete dam. Adaptive neuro-fuzzy inference system (ANFIS) and simultaneous perturbation stochastic approximation (SPSA) were applied to reduce the computational cost of the optimization model. An improved version of particle swarm optimization (PSO) was utilized to solve this problem. Al-Suhaili and Karim (2014) implemented an indirect S-O model based on the ANN model to find the optimum solution of hydraulic structure at minimum cost. In their study, the safety factors of HWRS were only considered for exit gradient and uplift pressure, disregarding sliding, overturning and eccentric load effects. The utilized method to generate training data and description of the data were undecided. Also, the ranges of the implemented cases were only applied for small HWRS (total head less than 10 m).

Hence, studies that have utilized the S-O model for optimum design of HWRS incorporating numerical seepage responses are scarce. Furthermore, incorporating the effect of the complex flow domain of seepage characteristics on optimum design has not been considered previously. Additionally, new formulations of the linked S-O model based on relatively new surrogate models (SVM, GPR) to find the optimum design HWRS have not been utilized. Also, integrating the effect of hydraulic conductivity or uncertainty of hydraulic conductivity has not been implemented within the context of S-O models.

2.7   Motivation and Scope

With the developments in numerical seepage simulation and its efficiency in providing an accurate solution for different problems integrating a complex seepage flow domain and non-homogenous and anisotropic soil parameters, there is motivation to advance a methodology based on linking the numerical simulation to the optimization model. The benefit of this methodology is to integrate accurate seepage simulation models with optimization models, and simultaneously to provide the safest and most economic design of HWRS. This methodology could not be implemented based on approximation and analytical seepage analysis methods. Also, by this methodology, many design safety factors related to HWRS may be incorporated to corroborate the safety of the HWRS.

Furthermore, the soil parameter uncertainty related to seepage characteristics, such as hydraulic conductivity which has a wide variation and uncertainty range (COV 200%-300%), may

affect HWRS safety. Quantifying the uncertainty in seepage characteristics due to uncertainty in estimating hydraulic conductivity was considered and applied based on a reliability based optimum design (RBOD) framework using the S-O model to determine the effect of the uncertainty in design parameters to the safety and minimum cost design of HWRS. Moreover, improving search efficiency of the S-O model related to the RBOD model in obtaining a global optimum solution with a certain reliability level was implemented based on multi-objective multi-realization optimization (MOMRO) technique. Using such a technique can improve the search process based on direct search technique and provide diverse alternatives of optimum solutions, which may approach the global optimum solution. Also, some optimum solutions based on the MOMRO technique are more applicable in some aspects of HWRS design requirements and field conditions. Furthermore, additional motivation is to provide an efficient and applicable combination of accurate numerical seepage simulation with an optimization based decision model to identify a feasible optimum solution (design). This was achieved by replacing the computationally expensive numerical simulation model with the expeditious surrogate model based on machine learning techniques.

From review of existing literature, it can be concluded that the previously developed approximate and analytical seepage analysis methods do not provide a precise solution, as their solutions have noticeable errors. In real fields, hydraulic conductivity is rarely seen in uniform, homogenous or isotropy conditions. Therefore, considering the variation of hydraulic parameters and flow conditions and effects on seepage characteristics is only possible by utilizing numerical methods. However, utilizing the numerical model solely provides accurate seepage characteristics for a predefined problem, and does not provide an explicit expression describing the relationship between the design variables related to seepage under HWRS.

Accordingly, there is a need to use an efficient methodology to find optimum design of HWRS and best combination of seepage control design variables for different conditions incorporating accurate seepage analysis and HWRS design requirements. Integrating important factors, such as safety and cost, could significantly improve design of HWRS and simultaneously provide an efficient cost design. Hence, the linked S-O technique is implemented in this study to achieve this goal. Optimum design of HWRS includes providing the best seepage control design variables with different upstream water levels and different scenarios of hydraulic conductivity. Seepage control design variables encompass optimum depths and orientation of many cut-offs and distances (aprons) between cut-offs.

As there are many (design) decision variables, and the relationship between these is nonlinear, and these variables influence the seepage characteristics of the candidate optimum

solution, the optimization problem is considered a complex task. Consequently, only the evolutionary optimization algorithm could solve such problems with some degree of confidence regarding global optimality. Hence, GA is utilized in this study to provide the global optimum solution for this problem.

To successfully and efficiently apply linked S-O techniques in this study, surrogate models are developed to imitate the numerical responses of seepage quantities. Identifying optimum design of HWRS based on direct linking of numerical model with the optimization model is an inefficient and time consuming process because the optimization algorithm (GA) based on direct search technique requires a large number of repeated solutions of nonlinear and complex numerical operations to seepage characteristics for each iteration. This process may lead to an infeasible solution and take a long time. Hence, developing an approximation seepage simulator (surrogate model) based on the machine learning technique can provide precise and expeditious responses for the S-O model to find the optimum solution. The surrogate model can be trained based on numerically simulated data sets encompassing the most effective design variables and seepage characteristics.

The linked S-O model was implemented in different scenarios with different machine learning techniques based on the purposes and the complexity of the seepage model related to the HWRS. S-O techniques include the developed surrogate models, and the formulation of the optimization task are presented in the following chapters. Specifically, in chapter three the S-O model based on ANN machine learning technique is implemented for a simple seepage conceptual model including two end cut-offs with apron (floor) between them. The chapter includes evaluations of the developed methodology and evaluations for developed surrogate models

3   Performance Evaluation of Genetic Algorithm and Artificial Neural Network Based Linked Simulation-Optimization Model for Optimal Design of Hydraulic Water Retaining Structures

A shorter version of this chapter has been published in the *Journal of Applied Water Engineering and Research.*

Al-Juboori, M & Datta, B. 2018 .*Performance evaluation of a Genetic Algorithm based linked simulation-optimization model for optimal hydraulic seepage related design of concrete gravity dams.* Journal of Applied Water Engineering and Research

The general concepts, theoretical background and literature review related to this chapter are covered in chapter two. This chapter highlights the procedure to apply the linked S-O methodology to find the optimum design of HWRS. Also, this chapter demonstrates to what extent the predictions of the developed surrogate models are trustworthy and applicable to be used instead of the numerical model. The findings and conclusion of this chapter are a foundation for the following chapters, which include more complex simulation and optimization models. The S-O methodology was applied on a simple conceptual model of HWRS including simple seepage scenarios of two cut-offs and one apron between them. Hydraulic conductivity is considered as homogenous isotropic. The ANN surrogate models are trained based on numerically simulated data sets, and then linked to the optimization solver (GA) to find the best seepage control variables and the best dimension of HWRS. The options and parameters of ANN and GA were carefully selected to attain ideal performance of these models.

3.1   Introduction

In addition to external hydrostatic and dynamic loads, seepage characteristics, such as uplift pressure and exit gradient values, resulting from seeping water are also critical design variables significantly affecting hydraulic stability of HWRS. Achieving accurate seepage analysis under hydraulic structures is a challenging task, especially for complex problems classified as nonlinear discontinuous problems (Chapuis et al., 2001; Harr, 1962). The complexity arises from several factors, such as the geometry of the flow domain under a hydraulic structure, soil properties, boundary conditions and the governing seepage equation, etc. The process of finding optimum economic design of HWRS, while incorporating accurate seepage analysis methods is a difficult task. Any feasible optimum solution must be based on reasonably accurate prediction of seepage characteristics. Only numerical seepage analysis methods, such as FEM, provide precise solutions.

Therefore, an alternative approach is utilized to achieve the optimum design based on linking the numerical seepage simulation model to the optimization model. Direct linking of the optimization model with the computationally demanding numerical simulation model is a computationally inefficient and time consuming procedure. The optimization solver (GA) based on direct search technique calls the simulation model a huge number of times to evaluate the objective function and constraints. For example, SEEP/W code may require one to two minutes to accomplish a run for one candidate solution, depending on the mesh size and complexity of the model. If GA starts with a limited population size for the first generation, e.g. 200, and the SEEP/W code is used for solving each candidate solution to evaluate the objective function, approximately six hours may be required to finish the evaluation of the first generation. To achieve the global optimum solution, the population size and number of generations need to be much larger. Further, the properties (genetic information) of each individual are modified and recombined many times to produce a new offspring by applying the crossover and mutation processes. These processes may be repeated several times and the fitness of each new candidate solution is evaluated by GA based on the SEEP/W solution to find the global optimum point. Hence, the directly linked S-O model needs an extensive computational process. Therefore, obtaining a global optimal solution for a particular seepage problem, using high performance processer unit, based on the directly linked S-O model may consume many days or even weeks. For instance, Dhar & Datta (2009) conducted a directly linked S-O model with a small aquifer system. The run time was 30 days utilizing relatively high qualification processors to find the optimum solution.

In addition to a computationally expensive process, the complexity of the problem decreases the adoptability of a robust direct linking of a rigorous numerical solution code within the S-O model. Design geometry and boundary conditions of the numerical model are different from case to case. Through the optimization process, seepage characteristic values and their locations are continuously changed from one numerical seepage simulation to another based on the candidate solution presented by GA. Alternatively, for computational efficiency through acceptable approximation of physical processes, the numerical model can be replaced with a surrogate model to provide accurate and fast approximation responses for different seepage scenarios. Hence, linking the surrogate model to the optimization model is computationally efficient compared to direct linking based on the numerical model.

One of the most conspicuous machine learning techniques to develop an efficient surrogate model is the ANN model. The ANN surrogate models were trained using many numerically simulated data utilizing GEO-STUDIO/ SEEP/W codes (Krahn, 2012). Additionally, the ANN models were rigorously tested using out of training data sets to measure the efficiency and predictive ability of the models. Within the linked S-O model, the GA calls the surrogate model numerous times iteratively to compare the fitness value of the objective function and evaluate the constraints. Furthermore, well

trained surrogate models can be used as an approximate seepage simulator and predictive model to precisely determine a particular seepage characteristic within the indicated ranges and conditions.

This chapter concentrates on developing surrogate models based linked S-O techniques to achieve optimal hydraulic design of HWRS. The optimization model is formulated to provide optimum hydraulic design, considering the safety and cost of HWRS, and integrate precise seepage simulation responses. The methodology is evaluated by various scenarios to demonstrate the efficiency and potential applicability of the methodology.

3.2   Numerical Seepage Simulation Model Based on Finite Element Method (FEM)

The numerical seepage simulation model utilized in this study is a finite element based model, SEEP/W, within Geo-studio modeling software (Krahn, 2012). The FEM code is used to solve the Laplace equation, as the seepage governing equation. FEM encompasses discretization of seepage flow continuum to small elements, defining material properties and physical boundary conditions. All equations of FEM are formulated at element nodes. The specified equation parameters are changed at each node based on location, properties and boundary condition for each node, which in turn represent surrounding elements. The general finite element form of the transient seepage equation is given by Eq. (3.1):

$$[K]\{H\} + [M]\{H\}, t = \{Q\} \tag{3.1}$$

Where: [K] = the element characteristic matrix;

[M] = element mass matrix;

{Q} = element applied flux vector;

{H} = vector of nodal heads;

t = time.

For steady state seepage, the terms {H}, t vanish, then the finite element equation can be expressed by Eq. (3.2):

$$[K]\{H\} = \{Q\} \tag{3.2}$$

The Gaussian numerical integration is used in SEEP/W to evaluate an element characteristic matrix [K]. For example, the integral form of [K] matrix is given by Eq. (3.3):

$$[K] = \tau \int_A ([B]^T [C] [B]) \, dA \tag{3.3}$$

Where: [B] = gradient matrix;

[C] = element hydraulic conductivity matrix;

τ = thickness of an element;

A= area of the element.

3.3   Conceptual Seepage Model

The conceptual seepage model was proposed for the illustrative HWRS design problem as shown in Figure 3.1. The variables and design parameters of this model are assumed based on many theoretical and practical considerations. Input variables (d_1, d_2, b and H) are assumed, as shown in Table 3.1, to cover wide ranges of expected problems in the real fields. Additionally, Tanchev (2014) recommended that the value of H must not be more than 40 m, because permeable soils have low bearing capacity values, and it is hard to bear the tremendous amount of hydrostatic pressure.

Table 3.1 Assumed range of input variables

	Description	Minimum value (m)	Maximum value (m)
d_1	Depth of cut-off in upstream side	1	40
d_2	Depth of cut-offs in downstream side	1	40
b	Half width of concrete HWRS (apron)	1	60
H	Upstream water head	1	40
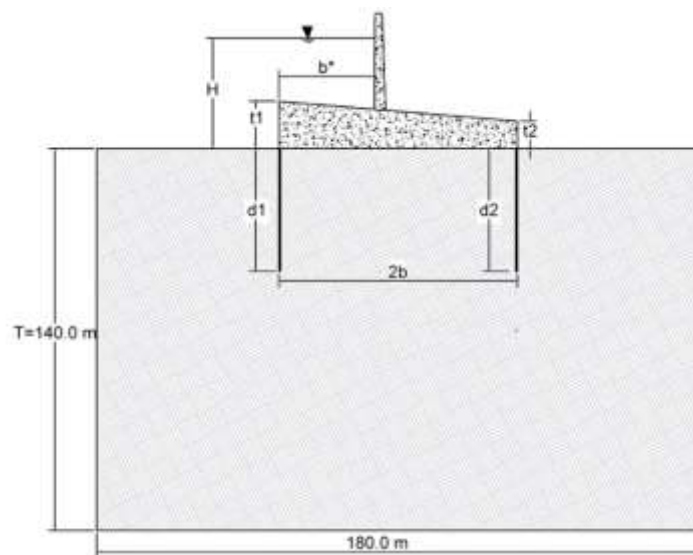
Figure 3.1 Conceptual seepage model

Furthermore, to satisfy the unconfined seepage flow condition, the ratio of the thickness of the permeable soil layer (T) to the half width of hydraulic structure (b) should be more than one, as shown in Figure 3.2 (Harr, 2012). Therefore, the soil layer thickness is assumed 140 m, which is more than double the maximum expected value of b (Table 3.2). This step guarantees that the unconfined flow

condition is achieved. Similarly, Figure.3.3 shows a strong effect of cut-off depth ratios (s/T) variation on the normalized discharge ratios (q/kh) for the (b/T) values less than 0.5 (unconfined flow condition). This means the influence of the embedded cut-off length has a significant effect on the unconfined flow condition.
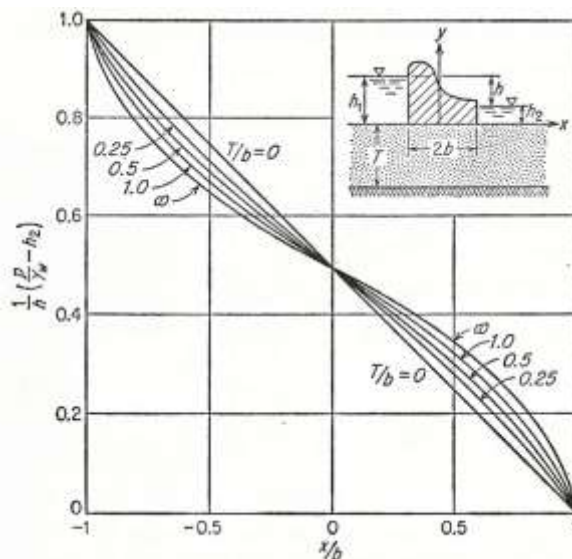
Figure 3.2 Comparing effect of soil layer depth to HWRS width on total head ratio (Harr, 1962)
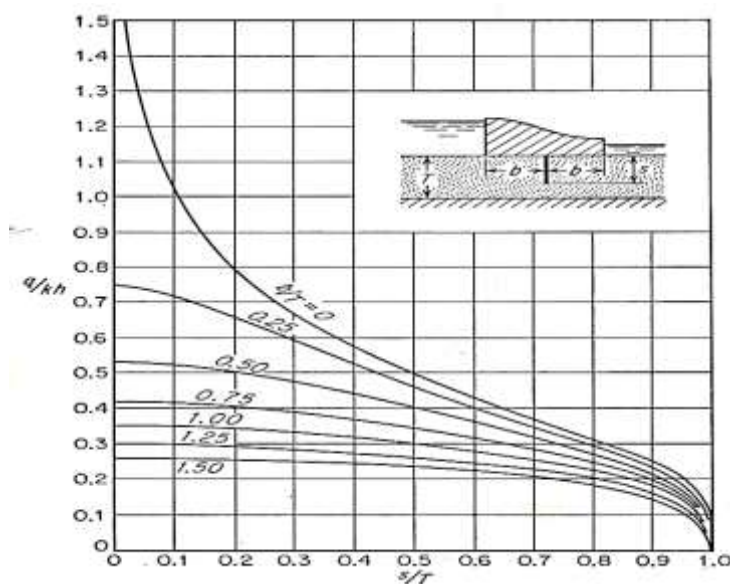
Figure 3.3 Effect of the cut-off embedment length on normalized discharge (q/kh) (Harr, 1962)

Moreover, Novak, Moffat, Natully and Narayanan(2007) suggested that major portion of the width of a HWRS floor (b*) should be within the upstream side. This length corroborates the stability of the HWRS, where upstream hydrostatic downward pressure and weight of floor counterbalance the substantial amount of the uplift pressure on the HWRS floor. On the other hand, the homogenous and

isotropic flow domain is assumed with the constant hydraulic conductivity value k= 5E-5 m/s, representing grained sand soils (Terzaghi et al., 1996).

3.4   Data Generation

Training of surrogate models is based on data sets simulated by numerical seepage modeling code (SEEP/W). Input data are the independent variables (d_1, d_2, 2b, H) randomly generated using the Latin hypercube sampling (LHS) method (Lin & Tang, 2015). The LHS method is a design of experiment (DOE) technique used to generate samples for experiments. This method provides local periodic information with equal probability that facilitates the training process to build an efficient surrogate model based on the input data and their numerical responses, i.e., the output data. The output data is obtained as a solution resulting from numerical seepage modeling for each input set. The most important output data are uplift pressure on the floor at the Us cut-off (θC) in kPa, uplift pressure on the floor at the downstream (Ds) cut-off (θE) in kPa and the exit gradient value (**ie**) at the toe of HWRS.

3.5   ANN Description

The ANN technique can explore complex, discontinuous and nonlinear relationships between data sets. The ANN captures the relationship between training input and output data sets to build an efficient surrogate model. Based on the generated data set related to the seepage system under HWRS, the ANN was used to build three surrogate models. These models provide accurate predictions of seepage characteristics without further utilizing numerical seepage simulation (SEEP/W code). A typical and simple ANN consists of input layer, hidden layer(s) and output layer. As shown in Figure 3.4, circles represent neurons, lines between layers represent weights, squares represent scalar biases, and X and Y vectors represent input and output data, respectively (Jain & Kumar, 2006).
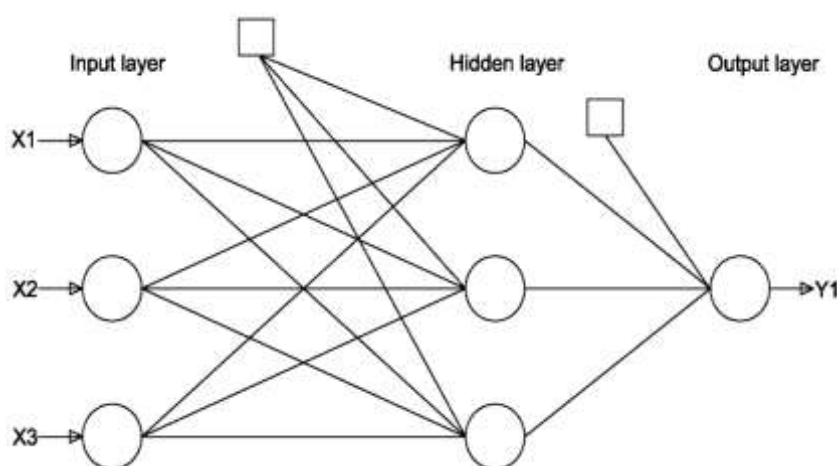
Figure3.4 Typical ANN architecture

The ANN tests all input and output data sets and learns, using ANN training rules, how changes in input data sets impact output data sets. The objective function of the ANN training algorithm is to

minimize the error between predicted and observed data. The ANN algorithm modifies the weights and biases several times until the best model is attained based on minimum mean square error (MSE) value, shown in Eq. (3.4) (Sivanandam et al., 2006).

$$MES \ = \frac{\sum_{I=1}^{N}(Y_g - Y_o)^2}{N}$$

(3.4)

Where: Y_g = target data;

Y_o = output of the ANN;

N = number of scenarios.

There are three kinds of training processes, supervised, unsupervised (self-learning) and reinforcement training (Sivanandam et al., 2006). In this study, feed-forward supervised training based on the Lievenberg-Marquardt algorithm was applied with a back propagation error. Matlab programing language was utilized to develop ANN models because Matlab is a versatile tool providing many options that can be modified to build perfect ANN models. Three ANN models were developed individually to approximately simulate each hydraulic seepage characteristic (θC, θE, **ie**). Generated input data sets of the four input variables (d_1, d_2, 2b and H(and their seepage simulation responses (θC, θE, **ie**) were utilized to build the ANN models. Input data passes through the input layer and training operations are performed in the forward direction. Outcomes of the output layer are compared with target values. Errors between ANN prediction and target values are distributed back on the weights and biases to modify their value. The forward training and back propagation error processes are repeated numerous times until the convergence is achieved between output data and target data (Jain & Kumar, 2006).

An example of mathematical expression of an ANN which has one hidden layer, **s** hidden neurons, **i** input variables and **m** output variables is given by Eq. (3.5):

$$Y_m = f_1 \left[\sum_{j=1}^{m} W_{ms}^o \ f_2 \left\{ \sum_{i=1}^{s} W_{si}^h \ x_i + b_s \right\} + b_m \right]$$

(3.5)

Where Y_m = output of the ANN;

x_i = input variables;

W_{ms}^o = connection weight between (s)th node of hidden layer and (m)th node of output layer;

W_{si}^h = connection weight for (i)th input variable and (s) th node of hidden layer;

f_1, f_2 = transformation functions;

b = bias factors.

3.5.1   Size of Training Data

Quantifying the required size for training data to develop an efficient surrogate model is one of the most difficult challenges of machine learning techniques. The difficulty arises from complexity of the relationship between input and output data, which is different from case to case. Often researchers use the trial and error procedure and check MSE or coefficient of determination (RSQ) until the developed model presents accurate results. However, Pruett and Hester (2016) increased training data sets many times and each time measured standard deviation error of predicted data based on the trained surrogate model. They considered that the data set adequate and the training surrogate model became efficient when standard deviation of the error is approximately constant. A similar concept was applied in this study to find the required data size to train ANN models. Therefore, the initial source data was generated and divided into two subsets: 70% for training and 30% for testing. The training/testing data sets were randomly selected without replacement from the source data. This process was repeated five times to generate five (5-fold) different training/testing data sets. Consequently, five ANN models were trained and tested using the 5-fold data. Average standard deviation and standardized error (standard deviation divided by the square root of data size) for the five developed models were computed for training and testing data. Then, source data was increased gradually and the same procedure was repeated for five new ANN models until standard deviation and standardized error did not substantially change. Results of the developed ANN models for different data size are presented in Figures 3.5, 3.6 and 3.7. Obtained results indicate that the data size of 500 sets (350/150) provides adequate ANN models.

	70/ 30	140 / 60	210/ 90	280 / 120	350 / 150
Training standarized error	0.2	0.1	0.7	0.5	0.6
Testing standarized error	0.4	0.1	1.2	1.1	1.0
Taining standar divietion	1.3	0.5	7.7	7.1	8.1
Testing standard devieation	2.3	0.6	11.4	12.0	11.9

Size of the data (training/testing)
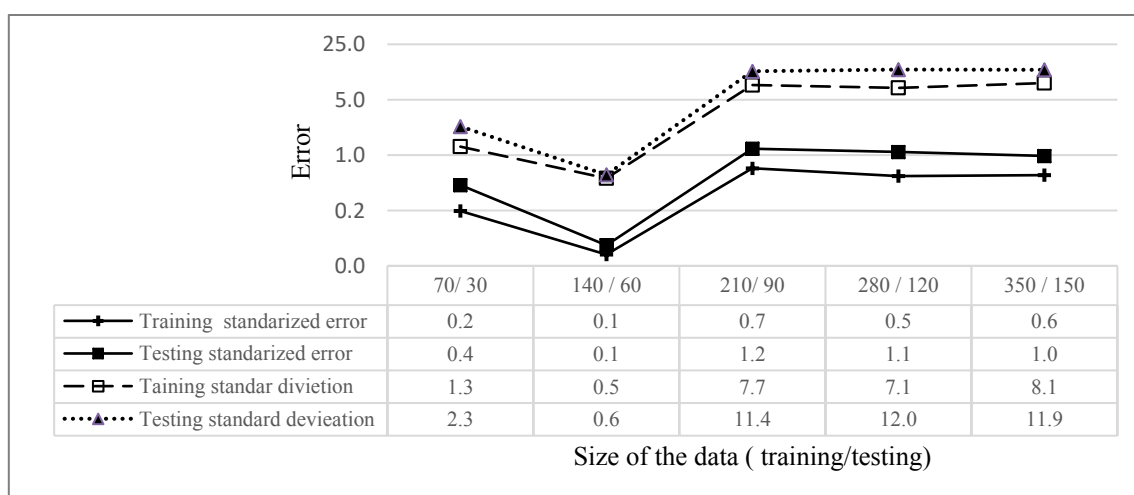
Figure 3.5 Standardized and standard deviation error for θC ANN model with different training/testing data size
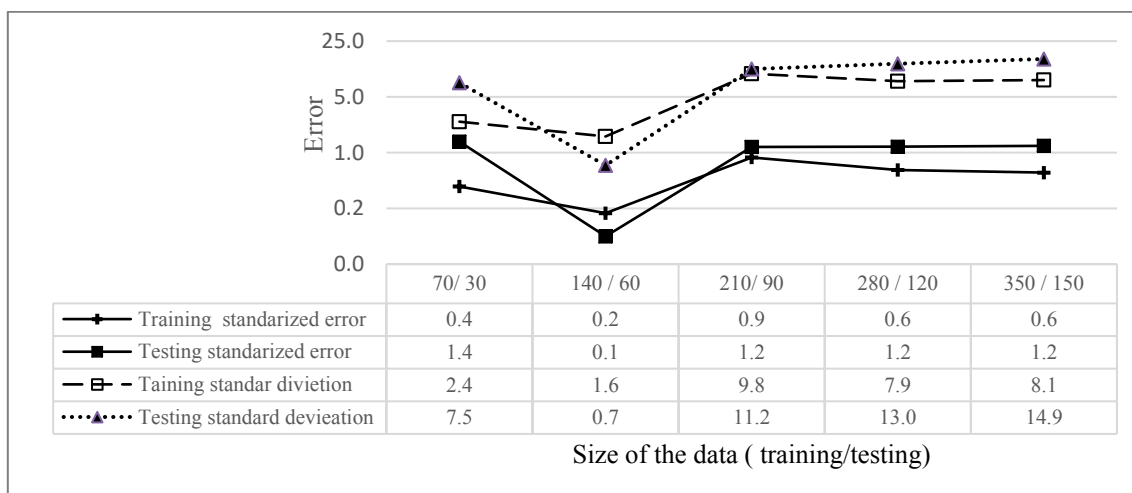
Figure 3.6 Standardized and standard deviation error for θE ANN models with different training/testing data size
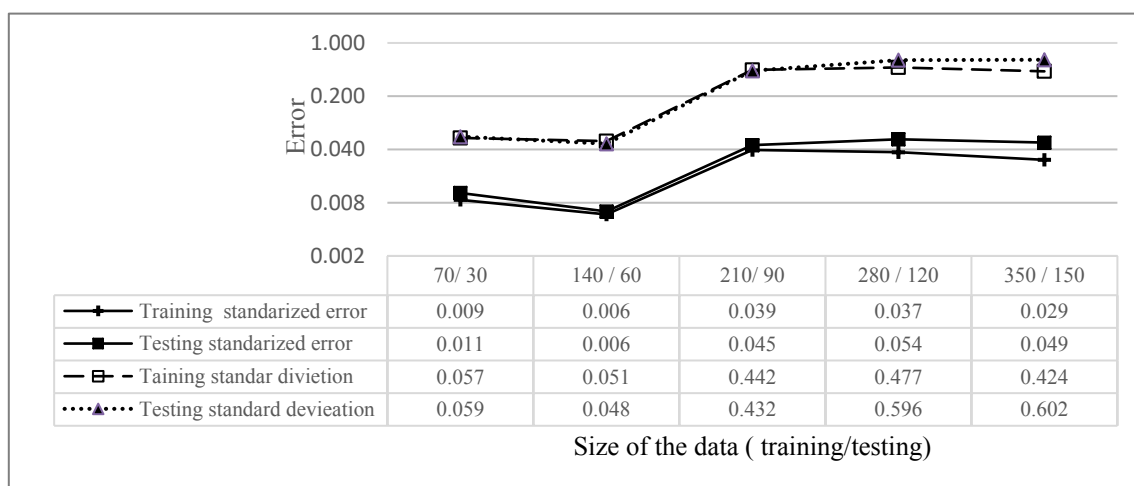
Figure 3.7 Standardized and standard deviation error for exit gradient ANN model with different training/testing data size

3.5.2 *Optimizing ANN performance*

ANN performance is based on several options and parameters, where these parameters can be modified to provide accurate and generalized surrogate models. Furthermore, performance of ANN is different from task to another task depending on relationship complexity between training data and data properties. Key parameters affecting ANN performance are: number of neurons, percentage of training to validation data, transfer function of hidden layer(s) and transfer function of the output layer. The most commonly utilized transfer functions are logsig, tansig, purelin and radbas (MathWorks, 2018).

In some previous studies, effective ANN parameters were selected based on the trial and error technique or user experience (Hamzaçebi, 2008; Jaddi, Abdullah, & Hamdan, 2013; Khaw, Lim, & Lim, 1995). The best model that can provide better data fit is chosen. However, more systematic and effective procedures, such as analysis of variance (ANOVA), Taguchi DOE method and other methods, have been used to maximize performance of ANN models.

The Taguchi DOE method (Cavazzuti, 2012) is one of the best tools utilized to attain optimum performance of a certain system (model, experiments, etc.) based on a small number of experiments. Based on data analysis, orthogonal array and signal noise ratio (S/N), Taguchi developed an efficient DOE method. Briefly, this method quantifies the impacts of effective variables (*control variables*) and *noise variables*, which have a trivial effect on experiment results. Depending on different performance measures, Taguchi successfully developed what he called *signal to noise ratio* (S/N) measures. These measures optimize variable performance and find the effective factors' combination, by which performance of the experiment (model) maximize or minimize the results (Cavazzuti 2012). The most prominent measures are *larger the better (LTB) and smaller the better (STB)*, which are used in this study and given by Eqs. (3.6) and (3.7).

Smaller the better equation *(STB):*

$$S/N = -10 \log\frac{1}{n}\left(\sum y^2\right) \tag{3.6}$$

Larger the better equation *(LTB)*:

$$S/N = -10 \log\frac{1}{n}\left(\sum \frac{1}{y^2}\right) \tag{3.7}$$

Where: y = responses of a certain factor combination in Taguchi DOE;

n = number of responses in the factor level combination.

To find the best parameters' combination of ANN models, the four factors with four levels of 16 runs Taguchi DOE (L4^4) were conducted, as shown in Table 3.2. The levels of each factor in Taguchi DOE represent the ANN parameters that can be modified in ANN training (Matlab) code for each experiment based on the same training/testing data set. Taguchi DOE was individually applied to the three seepage characteristics (θC, θE, ie). Taguchi analysis was accomplished using Minitab software and the SN ratio for each model was determined based on the RSQ for each experiment, as shown in Table 3.2.

Table 3.2 Taguchi Orthogonal Array Design L16 (4^4) with S/N ratio

Run	No of neuron (A)	Training/ validation ratio (B)	Transfer function of hidden layer (C)	Transfer function of output layer (D)	θC		θE		ie	
					Training RSQ	SNR	Training RSQ	SNR	Training RSQ	SNR
1	3	50/50	logsig	logsig	55	34.80	32	30.10	5	13.97
2	3	60/40	purelin	purelin	95	39.55	81	38.17	39	31.82
3	3	75/25	tansig	tansig	97	39.73	98	39.82	87	38.79
4	3	90/10	radbas	radbas	1	0.00	1	0.00	1	0.00
5	6	50/50	purelin	tansig	94	39.46	94	39.46	72	37.14
6	6	60/40	logsig	radbas	21	26.44	1	0.00	1	0.000
7	6	75/25	radbas	logsig	2	6.02	1	0.00	1	0.00
8	6	90/10	tansig	purelin	99	39.91	99	39.91	94	39.46
9	9	50/50	tansig	radbas	1	0.00	1	0.00	1	0.00
10	9	60/40	radbas	tansig	98	39.82	93	39.37	53	34.48
11	9	75/25	logsig	purelin	99	39.91	99	39.91	96	39.64
12	9	90/10	purelin	logsig	49	33.80	14	22.92	1	0.00
13	12	50/50	radbas	purelin	96	39.64	94	39.46	92	39.27
14	12	60/40	tansig	logsig	40	32.04	1	0.00	1	0.00
15	12	75/25	purelin	radbas	40	32.04	3	9.54	1	0.00
16	12	90/10	logsig	tansig	98	39.82	99	39.91	98	39.82

The Taguchi DOE analysis results for θC model shown in Figure 3.8 demonstrate that factors C1, C2 and D2, D3 have a parallel positive effect on S/N ratios of the θC ANN model. As Taguchi DOE is an approximation method, additional possible scenarios listed in Table 3.3 were implemented to find the best combination. Further experiments were implemented to find the best number of neurons between 12 and 9, i.e., level 3 and 4. The results of conformation experiments demonstrate that the model with 11 neurons provides the best fit. The final θC ANN model has 11 neurons, 60/40 training to validation ratio, *logsig* transformation function for the hidden layer and *purelin* transformation function for the output layer.

Table 3.3 Conformation experiments for different levels of C1, C2, D2 and D3 for θC ANN model

A	B	C	D	SN	Training	Testing	
					RSQ	RSQ	MSE
4	2	1	2	54.78	99.6	99.4	102.3
4	2	1	3	54.74	99.7	99.2	140
4	2	2	2	55.75	95.2	95.5	641
4	2	2	3	55.71	94.8	94.0	1045
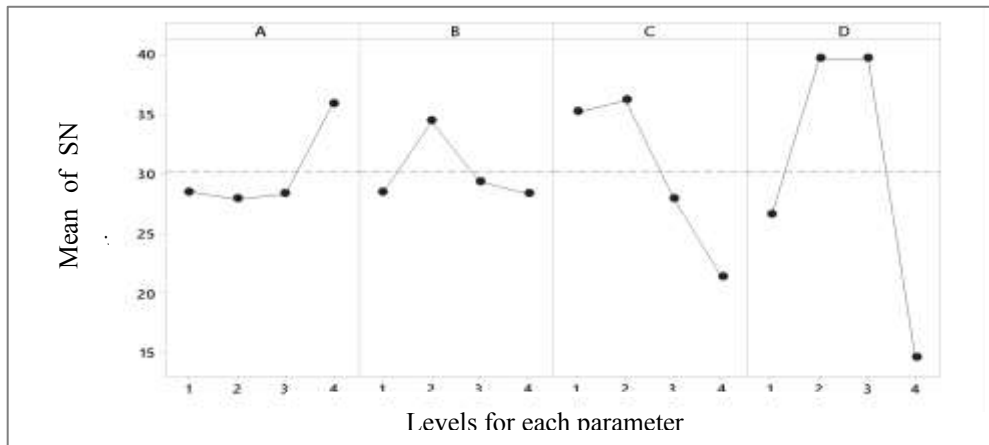
Figure 3.8 Main effects SN ratio (larger is better) of the θC ANN model

The same procedure was applied to the θE and **ie** ANN models and the result of Taguchi analysis is shown in Figures 3.9 and 3.10. The θE model has (A1B1C1D2) initial factors' combination, and the final combination is 4 neurons, 50/50 training to validation ratio, *logsig* transformation function for the hidden layer and *purelin* transformation function for the output layer. Similarly, the best factor combination for the **ie** model is (A1B1C1D3) and the final model has 5 neurons, 50/50 training to validation ratio, *logsig* transformation function for the hidden layer and *tansig* transformation function for the output layer.
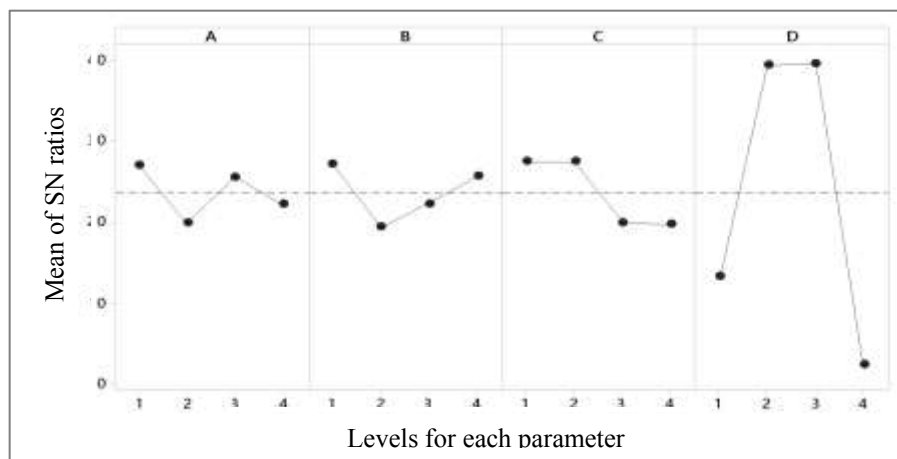
Figure 3.9 Main effects SN ratio (larger is better) of the θE ANN model
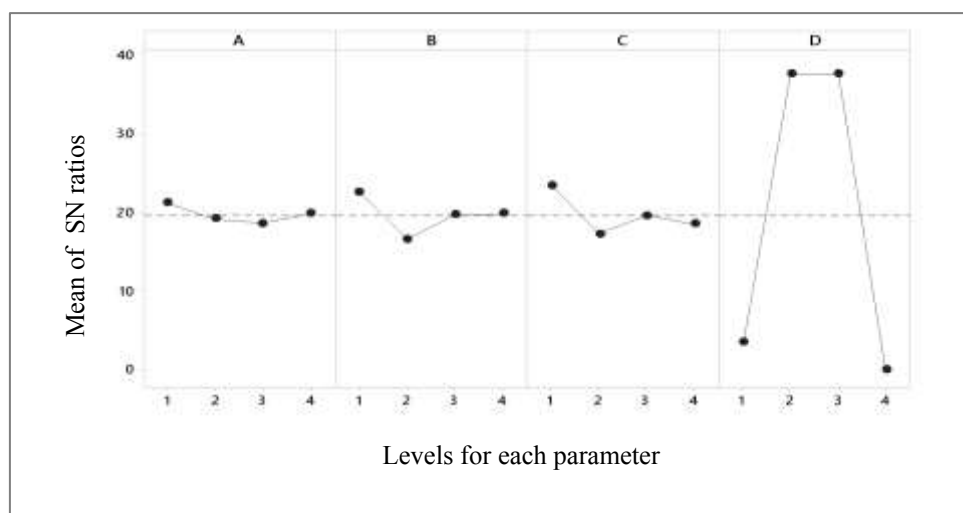
Figure 3.10 Main effects SN ratio (larger is better) of the exit gradient ANN model

3.5.3 Cross validation

Measuring the accuracy of the developed surrogate models related to seepage characteristics (θC, θE, ie) based on a single scenario of the training/testing data is a fragile technique. Alternatively, the multiple training/testing sets (cross validation (CV)) technique provides more understanding and precise estimation about prediction accuracy of the developed models for out of training data (Alpaydin, 2014). The CV process involves randomly dividing source data into **K** (5 to 10) folds without replacement. Each fold encompasses a unique data indexing for training and testing parts and is different to other folds. The CV technique ensures that every single point in data is used in the training and testing process. The training process was implemented **K** times. Error measures, such as MSE and RSQ, were recorded each run for training and testing sets. The average of measurements provides an accurate understanding of the model performance and a reliable prediction for detached data.

Based on ANN optimum parameters obtained by the Taguchi method, CV was conducted for each model. the source data was divided into five folds and new training processes were implemented five times with different (training/testing) sets. Results in Table 3.4 show robust predictions of the trained models with varied training and testing data sets. Although CV provides perfect understanding of model performance, it is a relatively expensive process and results of CV are used only to measure efficiency of the developed models. Therefore, after achieving a satisfactory CV results, the final models are different to CV models. The final model is trained on high percentage source data to provide an accurate prediction.

Table 3.4 Cross valuation results for different training / testing sets

CV-Set	ΘC				ΘE				Exit gradient			
	Training		Testing		Training		Testing		Training		Testing	
	RSQ	MSE	RSQ	MSE	RSQ	MSE	RSQ	MSE	RSQ	MSE	RSQ	MSE
set 1	99.8	27.57	99.4	113.5	99.1	68.16	98.8	148.2	95.1	0.017	93.8	0.006
set 2	99.7	41.5	99.7	30.17	98.4	142.5	98.3	132.6	97.6	0.008	91.4	0.02
set 3	99.8	31.8	99.1	94.1	98.5	143.7	98.16	103.4	97.4	0.007	98.1	0.007
set 4	99.6	51.8	99.7	59.6	99.4	47.77	98.5	145.1	97.8	0.005	91	0.056
set 5	99.6	53.98	99.6	43.07	99.1	82.25	99.33	45.63	95.9	0.013	96.8	0.006
average	**99.7**	**41.33**	**99.5**	**68.09**	**98.9**	**96.87**	**98.62**	**115**	**96.76**	**0.01**	**94.22**	**0.019**

3.6 Optimization Model

The optimization model was formulated to find safe and minimum cost design of HWRS that impounds a significant amount of water, considering the effects of seepage characteristics. Additionally, the hydraulic design requirements of HWRS were considered in the optimization model, such as flotation, sliding and overturning safety factors. The optimization model components are summarized as follows:

3.6.1 Decision vector X

The decision vector $X = [x_1, x_2, x_3... x_n]$ is a set of variables embedded in the objective function and/or constraints of the optimization model. Values of X are modified many times by GA until the minimum or maximum value of the objective function is achieved and simultaneously all constraints are satisfied. In this study, the decision vector ($X=[x_1, x_2, x_3, x_4, x_5, x_6]$) represents seepage design variables of the candidate design. Some of these variables describe the geometry of seepage control components and geometry of the HWRS. These variables are incorporated in the objective function and constraints, as shown in Eq. (3.8) to Eq. (3.32). The decision variables are defined as shown below:

$x_1 = (d_1)$ = Us cut-off length (m);

$x_2 = (d_2)$ = Ds cut-off length (m);

$x_3 = (2b)$ = width of hydraulic structure (m);

$x_4 = (b^*)$ = portion of the floor at the Us side (m);

$x_5 = (t_1)$ = thickness of the HWRS floor at Us (m);

$x_6 = (t_2)$ = the thickness of the HWRS floor at Ds (m).

3.6.2   Objective function f (x)

The objective function (f (x)) refers to the mathematical description of a certain value in a system or design to be minimized or maximized. Mostly, this function includes the decision variables. The optimization solver (GA) iterates and modifies the decision variables many times until the optimum value of the objective function is achieved. In this study, the objective function minimizes cost of the HWRS considering the cost of seepage prevention components. The objective function is shown in Eq. (3.8).

$$Minimize, \quad f(x) = C_1 V_1 + C_2 V_2 + C_3 V_3 \qquad (3.8)$$

Where C_1 and C_2 are costs coefficients related to construction Us and Ds cut-offs per unit volume (m^3), respectively. C_1 and C_2 can be expressed by Eqs. (3.9) and (3.10) as a function of the cut-off depth because construction cost of the cut-off is a critical stage and needs more time and effort with augmentation of cut-off depths. Further, theses functions were formulated based on the assumption that the cost could not represent a linear relationship with cut off depths, as the requirements, tools and field conditions to construct cut-offs less than 10 m (for example) in depth are generally different than when the depth of cut off is greater than 30, etc. Furthermore, these functions return high construction cost of deep cut-offs, which is undesirable in a minimum cost design optimization. However, it may be a feasible and good alternative for some HWRS which retain a high upstream water head value (H). However, the cost coefficient functions given by Eqs. 3.9 and 3.10 are only illustrative, and need to be carefully defined for each site condition. A typical plot of the costs per unit volume (C_1, or C_2) are shown in the Appendix B, as Figure B3.1. C_3 is construction cost of the floor per unit volume and equals $400/m^3$.

$$C_1 = x_1^3 + 20x_1^2 + 200\ x_1 + 400 \qquad (3.9)$$
$$C_2 = x_2^3 + 20x_2^2 + 200\ x_2 + 400 \qquad (3.10)$$

V_1 and V_2 are volume of Us and Ds cut-offs (m^3), respectively, which are given by Eqs. (3.11) and (3.12), where t_{s1}, t_{s2} are thicknesses of the Us and Ds cut-offs (assumed 0.5m), respectively; V_3 is volume of the floor (m^3) given by Eq. (3.13).

$$V_1 = x_1\ t_{s1} \qquad (3.11)$$
$$V_2 = x_2\ t_{s2} \qquad (3.12)$$
$$V_3 = \frac{(x_5 + x_6)\ x_3}{2} \qquad (3.13)$$

Where x_5, x_6 are computed utilizing Eqs. (3.14), and (3.15):

$$x_5 = \frac{1.3\ \theta C}{G_S - 1} \qquad (3.14)$$
$$x_6 = \frac{1.3\ \theta E}{G_S - 1} \qquad (3.15)$$

The values θC and θE are computed using the trained ANN models, which are linked with the optimization model. Hence, ANN models work as a function of (x_1, x_2 and x_3) or (d_1, d_2, 2b). Therefore, the X value is modified for each optimization iteration as a new candidate solution, until the optimum solution is achieved. As expression of Eqs. (3.8) to (3.15) are nonlinear and some decision variables (x_5, x_6) are based on complex nonlinear (ANN) surrogate model responses, the objective function and some constraints are considered nonlinear. Therefore, using evolutionary optimization algorithms, such as GA, is extremely effective to solve such nonlinear optimization tasks.

3.6.3 *Constraints defining simulated impact on the optimum design*

In order to define feasibility of any candidate optimal solution, the impact of decision variable values (i.e., depth of cut-offs, distance between cut-offs, floor thickness, etc.) on the candidate optimal solution needs to be predicted. Without accurate prediction of these impacts for each candidate design solution an optimum solution cannot be obtained. This aspect can be addressed by directly linking a numerical simulation model to compute the seepage characteristics, uplift pressure, exit gradient, etc. In the proposed methodology, because the optimization algorithm requires numerous runs of the numerical simulation model in order to identify an optimum solution, a trained and tested ANN based surrogate model was utilized as an approximate simulator and was introduced as a binding set of constraints (Eq. (3.16)) of the optimization model. The seepage characteristics are used to evaluate the objective function and constraints. Therefore, incorporating surrogate models in the optimization model represents an implicit equality constraint.

$$(\theta C, \theta E, ie) = f(x_1, x_2, x_3, H, k) \tag{3.16}$$

Additionally, ANN surrogate models are linked with other constraints because some design requirements and safety factors are based on the value of seepage characteristics. The general procedure of linking surrogate models with the optimization model is shown in Figure 3.11.
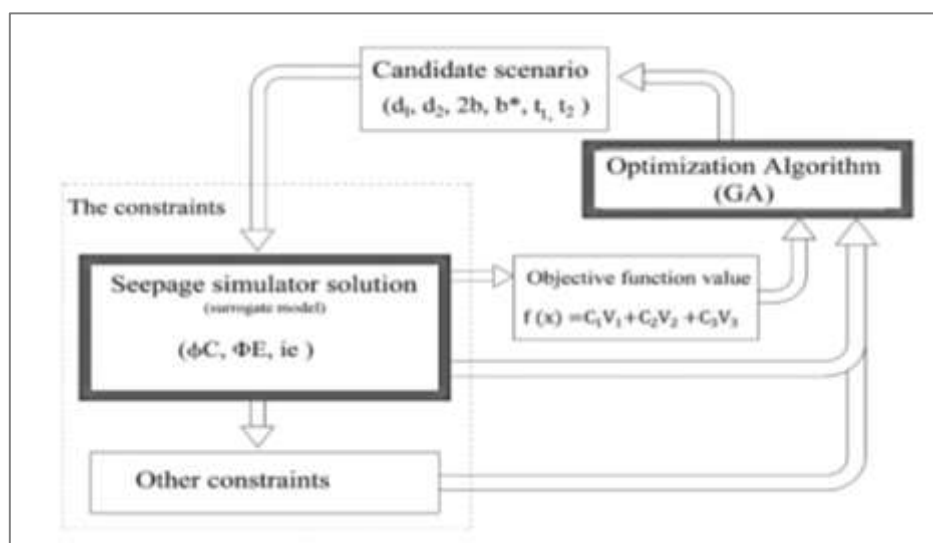
Figure 3.11 General schematic of the linked simulation-optimization model

3.6.4 Constraints defining design safety factors related to overturning, sliding, floatation, exit gradient and load eccentricity requirements

Design constraints represent particular conditions or design requirements and the optimal design must satisfy all these requirements in terms of permissible safety factors. In addition to simulation constraints discussed earlier, two types of constraints were incorporated: i) the design requirements to be complied with in terms of safety factors, and ii) the logical constraints, e.g., minimum permissible distance between cut-offs. Most of these constraints include the decision vector and are classified as nonlinear constraints as discussed below.

3.6.4.1 Flotation constraints

The standard stabilization criterion against uplift pressure provided by U.S. Army Corps of Engineers (1987) recommends that the uplift pressure safety factor for hydraulic structures with normal operation conditions is 1.5, whereas for construction and maintenance conditions with zero water level of upstream head (H) is 1.3. These factors were formulated as constraints, where Us uplift pressure (θC) must be less than the unit weight of concrete floor plus hydrostatic pressure near the first cut-off. Mostly, HWRS are constructed from concrete to efficiently resist external hydrostatic and dynamic pressures, and to provide the required weight to counterbalance external loads. The mathematical expressions for the two constraints are presented in Eq. (3.17) and (3.18):

$$g_1(x) = - \gamma_C\, x_5 - \gamma_w\, (H - x_5) + 1.5\, \theta_c\, \gamma_w \leq 0 \tag{3.17}$$

$$g_2(x) = - \gamma_c\, x_5 + 1.3\, \theta_c\, \gamma_w \leq 0 \tag{3.18}$$

Where:

γ_C = concrete weight density (25 kN/m^3);

γ_w = water weight density (9.81 kN/m^3);

H = total water head (m);

θ_c = uplift pressure at Us cut-off (kPa).

Also, Ds uplift pressure (θE) must be less than the unit weight of concrete floor near the second cut-off for normal conditions as shown in Eq. (3.19).

$$g_3(x) = - \gamma_c\, x_6 + 1.3\, \theta_E\, \gamma_w \leq 0 \tag{3.19}$$

3.6.4.2 Exit gradient constraint

The exit gradient (**ie**) is one of the most crucial design characteristics related to safety of HWRS. Physically, **ie** can be represented by the amount of hydraulic gradient dissipated at the last square of the stream-equipotential flow-net divided by length of the square (**ie** = Δh/L). In this study, actual **ie** value

is determined based on SEEP/W solution for each case. The exit gradient safety factor is computed by Eq. (3.20):

$$F.S = \frac{i_c}{ie}$$

(3.20)

Where i_c is the critical exit gradient and given by Eq. (3.21)

$$i_c = \frac{\gamma_{sub}}{\gamma_w} \quad or \quad i_c = \frac{(G_S - 1)}{(1 + e_s)}$$

(3.21)

Where γ_{sub} is submerged soil density; Gs is specific gravity of the soil; e_s is void ratio of the soil.

Soil properties are assumed mixed grained sand (γ_{sat} =21.2 kN/m^3), and that results in ic=1.15 (Terzaghi et al., 1996). Consequently, the minimum allowable safety factor for the exit gradient must be between three and five (Harr, 2012; Khosla et al., 1936). Therefore, the constraint is expressed by Eq. (3.22), considering the **ie** safety factor equals five:

$$g_4(x) = 5\, i_e\text{-}\, i_c \leq 0$$

(3.22)

3.6.4.3 *Sliding constraint*

HWRS resistance must be sufficient against sliding and shear forces along the contact surface between the HWRS foundation and soil surface or any horizontal joint within the body of HWRS. To examine HWRS safety against sliding, two soil parameters must be estimated: cohesion factor (C) and internal friction resistance factor (f= tan$\emptyset$), where $\emptyset$ is an internal soil friction angle. Tanchev (2014) recommended, for normal load conditions, a sliding safety factor (Ks) of 1.5, which can be determined by Eq. (3.23).

$$Ks = \frac{\sum V tan\emptyset + C\, B}{\sum W}$$

(3.23)

Where:

Ks = sliding safety factor;

$\sum W$ = resultant of horizontal forces acting on the HWRS;

$\sum V$ = resultant of all vertical forces;

C = cohesion resistance factor;

B = 2b = width of structures;

$\emptyset$ = internal friction angle.

The values of f and C are assumed as f= $tan\emptyset$=0.7 and C=20 kPa (Tanchev, 2014), and the constraint is expressed as shown in Eq. (3.24).

$$g_5(x) = 1.5 - K_s \leq 0 \qquad (3.24)$$

3.6.4.4 *The eccentric load condition and overturning constraint*

Overturning stability is another important concept in HWRS design. According to the U.S. Army Corps of Engineers (1987) recommendation, the resultant (R) of all acting forces on the HWRS force must be located at a distance (**e**) from the toe of the hydraulic structure for normal conditions. This means that R must be located within the middle third of the foundation width (2b). This condition corroborates the full compression zone under the hydraulic structure's foundation and prevents the probability of a tension zone, as shown in Figure (3.12). The resultant location (e) is determined by Eq. (3.25).

$$e = \frac{\Sigma M}{\Sigma V} \qquad (3.25)$$

Where:

ΣM = summation of applied moments (of forces) around the toe;

ΣV = summation of vertical forces acting on the HWRS.

The constraints are given by following equations.

$$g_6(x) = x_3 / 3 - e \leq 0 \qquad (3.26)$$

$$g_7(x) = e - 2/3 \times x_3 \leq 0 \qquad (3.27)$$

Also, Tanchev (2014) recommended that the design safety factor against overturning (F_{ovt}) must be more than 1.5 and can be expressed by Eq. (3.28)

$$F_{ovt} = \frac{M_{pas}}{M_{act}} \qquad (3.28)$$

Where

M_{pas} =passive moments about the toe, which stabilize the HWRS;

M_{act}=active moments about the toe, which weaken HWRS overturning stability. The constraint is given by Eq. (3.29).

$$g_8(x) = 1.5 - F_{ovt} \leq 0 \qquad (3.29)$$
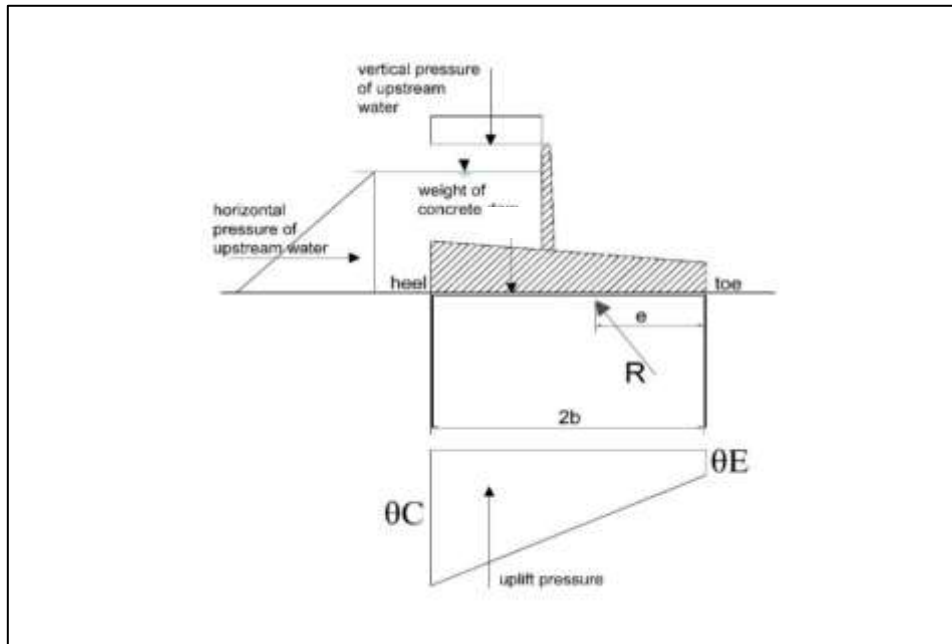
Figure 3.12 Free body diagram of the HWRS

3.6.4.5   *Other hydraulic logical constraints*

Most other constraints are logical and geometrical constraints; for instance, all the design variables must be in the positive range. Additionally, Tanchev (2014) mentioned that the minimum distance between two cut-offs is not less than the summation of cut-offs lengths. Moreover, the cut-off length must be less than 1.5 times of the total head. The formulation of these constraints is given by Eq. (3.30) to (3.32).

$$g_9(x) = x_1 - 1.5 \times h \leq 0 \tag{3.30}$$

$$g_{10}(x) = x_2 - 1.5 \times h \leq 0 \tag{3.31}$$

$$g_{11}(x) = x_4 - x_3 \leq 0 \tag{3.32}$$

3.6.5   *Genetic Algorithm (GA)*

GA is a non-traditional optimization algorithm widely utilized due to its efficiency in attaining global optimal solutions. Complex engineering optimization problems can be solved using GA. GA is an effective global optimization algorithm because GA: [1] has a parallel processing capability, [2] utilizes multiple offspring, [3] explores solutions in multi directions, [4] can easily eliminate dead directions and continue with more effective directions, [5] changes many parameters instantaneously, [6] randomly changes selected solutions and checks whether or not this provides improvements in solutions (Bajpai & Kumar, 2010).

GA randomly generates the initial population (individuals) covering the search design space. The fitness value of each individual is evaluated, then the high rank individual has a significant contribution to breed new individuals. The new generation is a combination of high rank parents and

new offspring (children). Children are generated by making crossover, or mutates for the genes' properties of selected parents. Hence, the new population inherits a large portion of parental characteristics. This process continues many times to find the optimum solution and stops when fitness value does not improve for new generations (Gen & Cheng, 2000; Haupt & Haupt, 2004; Rao, 2009).

Furthermore, GA can be used when the objective function or constraints are nonlinear, stochastic and have undefined derivatives. Because the objective function and constraints are based on ANN models, which is a non-differential function, it is extremely difficult to solve the optimization model using traditional optimization methods, which are based on the gradient search technique. Therefore, GA is a suitable choice to solve such optimization tasks. In the proposed linked S-O model, GA randomly generates many solutions and invokes ANN models many times to compute and evaluate the fitness value and constraints for each solution. These processes continue for many generations until the optimum solution is achieved.

3.6.6 *Maximizing GA performance*

There are many parameters and functions affecting GA performance. The impacts of these parameters must be explored before running GA. Population size, fitness scaling, selection, reproduction, migration crossover, mutation, stopping criterion and constraint parameters are the main parameters and functions that influence GA performance.

Many previous researchers used a non-systematic procedure to select GA parameters, such as the trial and error method, selecting default options and using their experience. Other researchers did not explain why they selected GA parameters in a particular combination (Al-Suhaili & Karim, 2014; Bornschlegell et al., 2012; Cojocaru et al., 2013; Datta et al., 2011; Dhar & Datta, 2008; Housh et al., 2012; Innal et al., 2015; Islam et al., 2015; Rajper & Amin, 2012; Singh, 2010, 2011). However, using such scenarios may not lead to ideal GA performance. Furthermore, varying a particular parameter individually, without considering other parameters, does not provide an insight into interactions between different GA parameters in different levels.

On the other hand, others systematically analysed and studied the influences of GA parameters on GA performance (Haines, Mills, & Filliben, 2012; Kolahan & Doughabadi, 2012; Koljonen & Alander, 2006; Pereira et al., 2005; Rand, Riolo, & Holland, 2006). From the review of previous research, it can be concluded that the most active parameters are population size, fitness scaling function, selection function, cross over fraction, cross over function and mutation function.

Studying comprehensive interactions between all GA parameters in different levels is a complex process and beyond of the scope of this research because extensive effort and time are required. Hence, the Taguchi DOE method was applied to provide an efficient parameter combination to

maximise GA performance with minimum experiment number (Dao, Abhary, & Marian, 2016; Majumdar & Ghosh, 2015).

The six factors (parameters) mentioned above with five experimental levels were considered in Taguchi DOE method L25 (5^6) using Minitab software, as shown in Table 3.5. The Taguchi DOE analyses were processed for different head value (10, 20, 30 and 40 m) to determine the GA fitness value for each run. To ensure the initial starting point of the GA is same for all DOE runs, Matlab optimization toolbox option "*Use random states from previous run*" was activated, which ensures an objective comparison for DOE results.

Table 3.5 Taguchi DOE for GA parameters with normalized fitness value for different head values

RUN	Population size	Fitness scaling function	Selection function	Cross over fraction	Cross over function	Mutation function	Normalized fitness value			
	A	B	C	D	E	F	10(m)	20(m)	30(m)	40(m)
1	50	Rank	Stochastic uniform	0.3	constraint dependent	Constraint dependent	0.911	0.782	1.000	0.723
2	50	Top Qty 0.2	Reminder	0.45	Scattered	Uniform Rate 0.01	0.221	0.545	0.839	0.201
3	50	Top Qty 0.30	Uniform	0.6	Single point	Uniform Rate 0.1	0.070	0.378	0.807	0.004
4	50	Top Qty 0.40	Roulette	0.75	two point	Uniform Rate 0.5	0.075	0.384	0.905	0.036
5	50	Top Qty 0.5	Tournament	0.9	Heuristic (1.2)	Adaptive Feasible	0.903	0.026	0.212	0.011
6	100	Rank	Reminder	0.6	two point	Adaptive Feasible	0.927	0.043	0.655	0.739
7	100	Top Qty 0.2	Uniform	0.75	Heuristic (1.2)	Constraint dependent	0.135	0.862	0.166	0.001
8	100	Top Qty 0.30	Roulette	0.9	constraint dependent	Uniform Rate 0.01	0.130	0.442	0.868	0.116
9	100	Top Qty 0.40	Tournament	0.3	Scattered	Uniform Rate 0.1	0.114	0.308	0.803	0.020
10	100	Top Qty 0.5	Stochastic uniform	0.45	Single point	Uniform Rate 0.5	0.041	0.263	0.842	0.010
11	200	Rank	Uniform	0.9	Scattered	Uniform Rate 0.5	0.023	0.013	0.909	0.003
12	200	Top Qty 0.2	Roulette	0.3	Single point	Adaptive Feasible	0.092	0.032	0.010	0.725
13	200	Top Qty 0.30	Tournament	0.45	two point	Constraint dependent	0.000	0.276	0.663	0.998
14	200	Top Qty 0.40	Stochastic uniform	0.6	Heuristic (1.2)	Uniform Rate 0.01	0.111	0.243	0.633	0.100
15	200	Top Qty 0.5	Reminder	0.75	constraint dependent	Uniform Rate 0.1	0.075	0.102	0.564	0.125
16	300	Rank	Roulette	0.45	Heuristic (1.2)	Uniform Rate 0.1	0.924	0.861	0.000	0.697
17	300	Top Qty 0.2	Tournament	0.6	constraint dependent	Uniform Rate 0.5	0.011	0.002	0.910	0.003
18	300	Top Qty 0.30	Stochastic uniform	0.75	Scattered	Adaptive Feasible	1.000	0.978	0.242	0.584
19	300	Top Qty 0.40	Reminder	0.9	Single point	Constraint dependent	0.957	1.000	0.884	0.062
20	300	Top Qty 0.5	Uniform	0.3	two point	Uniform Rate 0.01	0.072	0.236	0.815	0.041
21	400	Rank	Tournament	0.75	Single point	Uniform Rate 0.01	0.085	0.689	0.908	0.131
22	400	Top Qty 0.2	Stochastic uniform	0.9	two point	Uniform Rate 0.1	0.142	0.421	0.880	0.007
23	400	Top Qty 0.30	Reminder	0.3	Heuristic (1.2)	Uniform Rate 0.5	0.906	0.000	0.391	0.000
24	400	Top Qty 0.40	Uniform	0.45	constraint dependent	Adaptive Feasible	0.898	0.862	0.311	0.161
25	400	Top Qty 0.5	Roulette	0.6	Scattered	Constraint dependent	0.935	0.934	0.915	1.000

The resulting objective function for all experiments are normalized between 0 and 1 before starting Taguchi analysis, because there is a major variation in the fitness values for different head values, as shown in Table 3.5. A multiple response analysis was conducted for different head values to explore general performance of GA for different scenarios. The results showed that the best combination of the five factors is A3B2C3D4E5F3, as shown in Figure 3.13. This combination means that the population size is 300, the fitness scaling function is Top Qty 0.2, selection function is Uniform, the crossover fraction is 0.75, the crossover function is Heuristic (1.2), and the mutation function is Uniform Rate 0.1. Other GA parameters were the same as default Matlab options. One interesting inference seen from Taguchi results (Figure 3.12) is that increasing the population size does not guarantee improving GA performance. In this example problem, performance of GA deteriorated by increasing population size to 400 or 500 individuals.
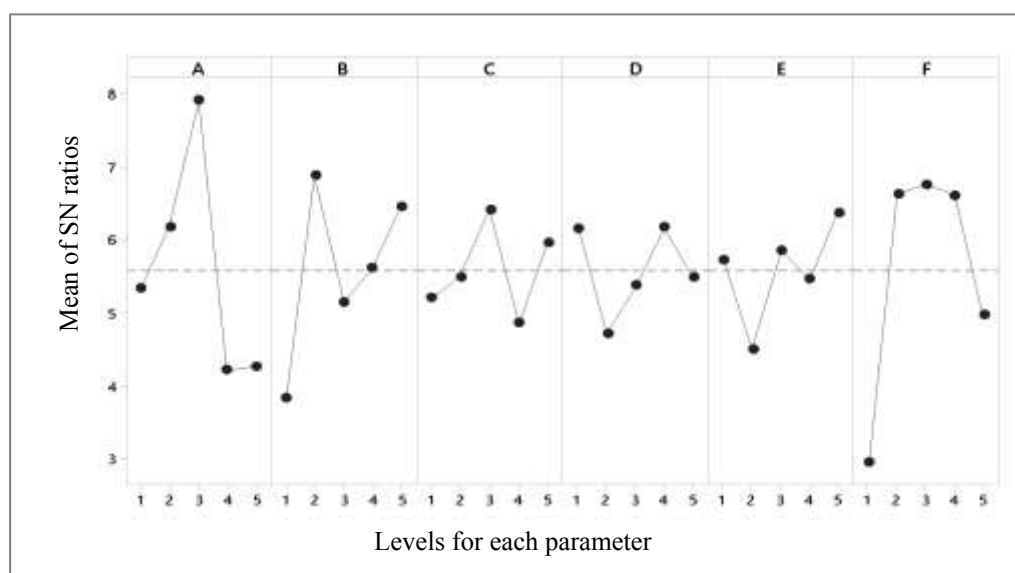
Figure 3.13 Main effects SN ratio (small is better) for GA parameters

Evaluation experiments based on Taguchi analysis results were conducted with three runs starting at different random initial generations. These experiments can help in measuring GA performance improvements with the best parameter combinations for different head values. The results are compared with the default Matlab options, as shown in Table 3.6. The comparison demonstrates that the best parameter combination significantly improves GA performance to find the optimum solution. The average of the minimum cost objective function obtained by the improved version of GA satisfy (on average) 17% cost reduction compared to the cost obtained by default GA options for the implemented cases.

Table 3.6 Comparison of the objective function values obtained by improved GA model and the MATLAB default parameter model.

	Exp. Run	H=10m	H=20m	H=30m	H=40m
Improved GA	1	52182.5	492412.8	2816276.3	10491423.7
	2	51947.4	492672.6	2816192.4	10480348.0
	3	51637.9	492315.5	2817477.8	10497979.9
Default GA	1	61442.42	693504.06	3099718.80	13740084.84
	2	52607.54	636480.18	3908556.00	10826865.39
	3	52451.07	640121.32	3943266.37	12124962.18
Percentage of Improvement	1	15.07	29.00	9.14	23.64
	2	1.25	22.59	27.95	3.20
	3	1.55	23.09	28.55	13.42

3.7   Results and discussion

3.7.1   ANN models

Three ANN models were successfully trained and tested to develop the surrogate models for (θC, θE, ie) individually, because each seepage characteristic has different attributes and ranges. Based on Taguchi DOE results and CV outcomes, robust ANN models were obtained. Many indicators and error coefficients were utilized to evaluate the accuracy of the developed models. In addition to MSE and RSQ, scatter index (SI) and bias parameter (Mentaschi, Besio, Cassola, & Mazzino, 2013; Moeini & Etemad-Shahidi, 2007) were implemented to measure the error between observed (simulated) data and predicted data. All these error indicators provide reliable evaluations of training and testing process accuracy for the developed models. The results were reasonable, as shown in Table 3.7.

Table 3.7 Description of the developed ANN models

ANN model	Number of neurons	Training/ validation ratio	Transfer function of hidden layer	Transfer function of output layer	Training				Testing			
					RSQ	MSE	SI	BIAS	RSQ	MSE	SI	BIAS
θC	11	60/40	Logsig	purlin	99.7	36.9	0.05	0.54	99.3	89.1	0.06	0.95
θE	4	50/50	Logsig	purlin	98.9	96.8	0.11	-0.53	99.1	67.16	0.09	0.29
Exit gradient	5	50/50	Logsig	tansig	97.5	0.009	0.28	-0.007	97.3	0.004	0.15	-0.004

The trained ANN surrogate models were used as generalized predictive models to determine the seepage characteristics of problems having similar ranges of training variables. Groups of ANN responses for each characteristic were used to develop the charts shown in Figures 3.14, 3.15 and 3.16

to easily determine the seepage characteristic for different scenarios as a percentage of H. These Figures reveal a noticeable effect of upstream cut-off depth (d_1) on **ie** values. This effect has been neglected by previous theories, such as Khosla's theory.
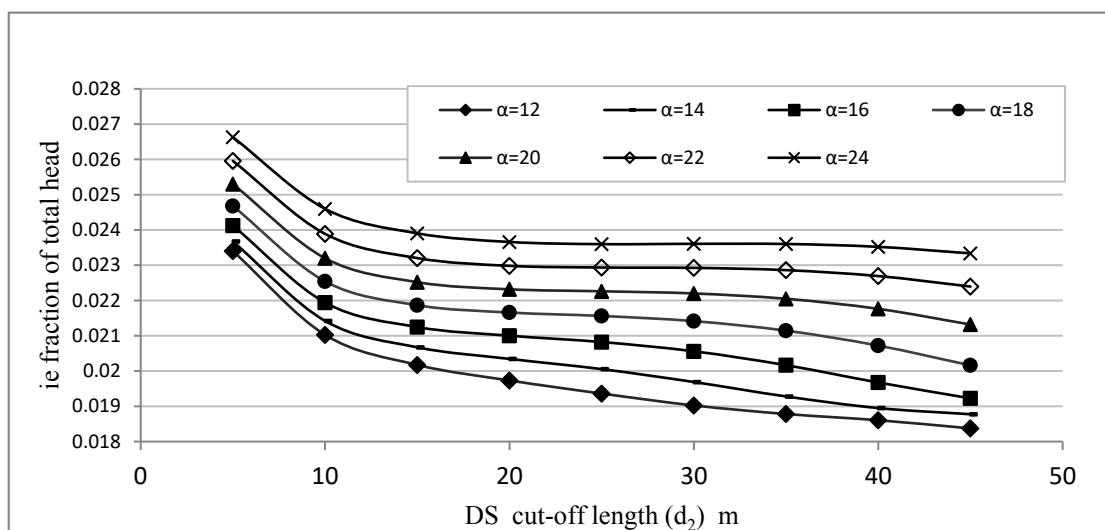
Figure 3.14 Chart for estimating the exit gradient based on the developed ANN model as a fraction of total head, α=2b/d₁
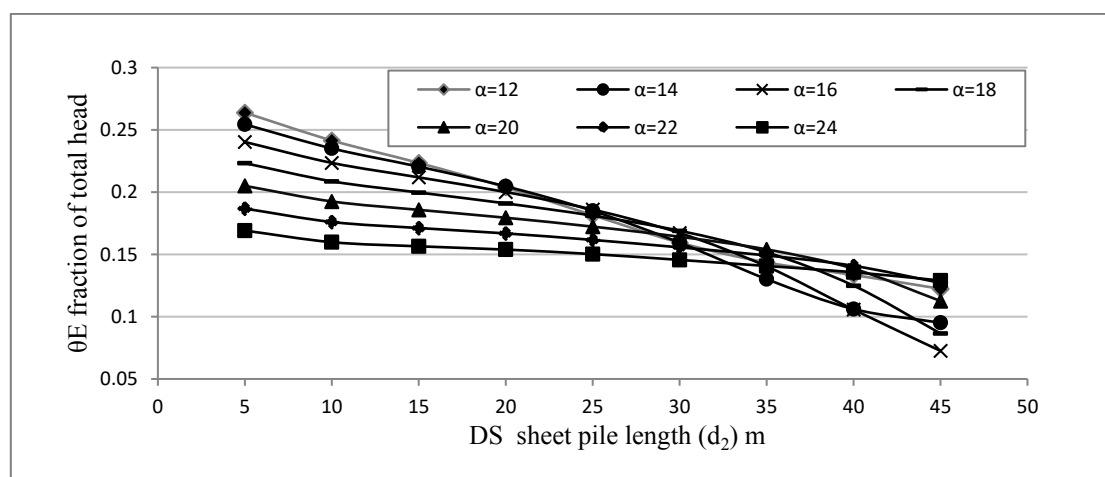
Figure 3.15 Chart for estimating the uplift pressure (θE) based on the developed ANN model as a fraction of total head, α=2b/d₁
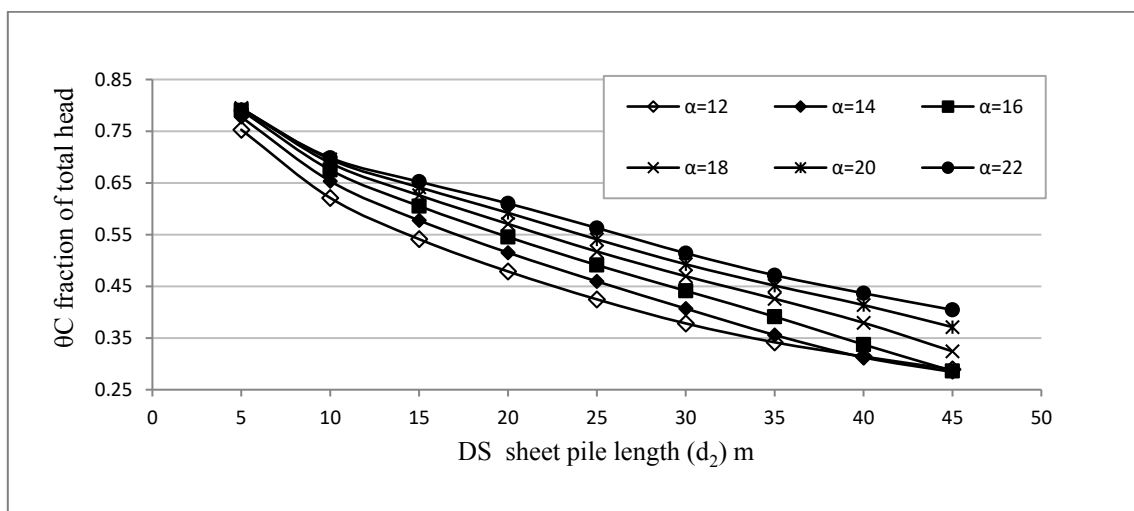
Figure 3.16 Chart for estimating the uplift pressure (θC) based on the developed ANN model as a fraction of total head, α=2b/d₁

Also, seepage characteristics could be determined using the scalar weights, scalar biases and transfer functions for each model, which are presented in Tables A 3.1, A 3.2, A 3.3, A 3.4, A 3.5 and A 3.6 in Appendix A. A mathematical example for the θE model was implemented and is described in the appendix. This example mathematically explains how ANN works based on the obtained weights, biases and transformation functions to determine seepage characteristics, and could be applied for any programming language.

Moreover, ANN models were successfully linked to the optimization model to provide an accurate seepage simulator. The developed ANN models worked smoothly and efficiently with GA. Each S-O run took approximately three minutes, which is an expeditious process to attain an optimum solution based on the approximate seepage simulator (ANN) and the GA direct search technique. Therefore, the ANN technique is a powerful method and provides accurate responses even with extreme points randomly presented by GA.

3.7.2 Simulation–Optimization model

The S-O technique was implemented for different H values ranging from 2 m to 40 m. The initial chromosomes of GA were randomly generated for each iteration. This ensures inclusion of a large portion of the search domain in the optimization process. Consequently, the possibility to attain the global optimum solution is increased. Results of the S-O model, including the design variables, design parameters, safety factors and optimum construction cost, are presented in Table 3.8. The design requirement of the HWRS and all the constraints were satisfied for each optimum solution.

Referring to Figure 3.17, optimum solutions for different H values show that d_1, d_2 make a considerable contribution in the hydraulic safety of HWRS. Nonetheless, the length of d_2 is relatively more important than d_1, because d_2 has a substantial impact on the **ie** value, which is the critical factor

in hydraulic design of HWRS. Approximately, the optimum ratio of (d_1/d_2) is 0.65 and it increases to 0.75 with head growth.
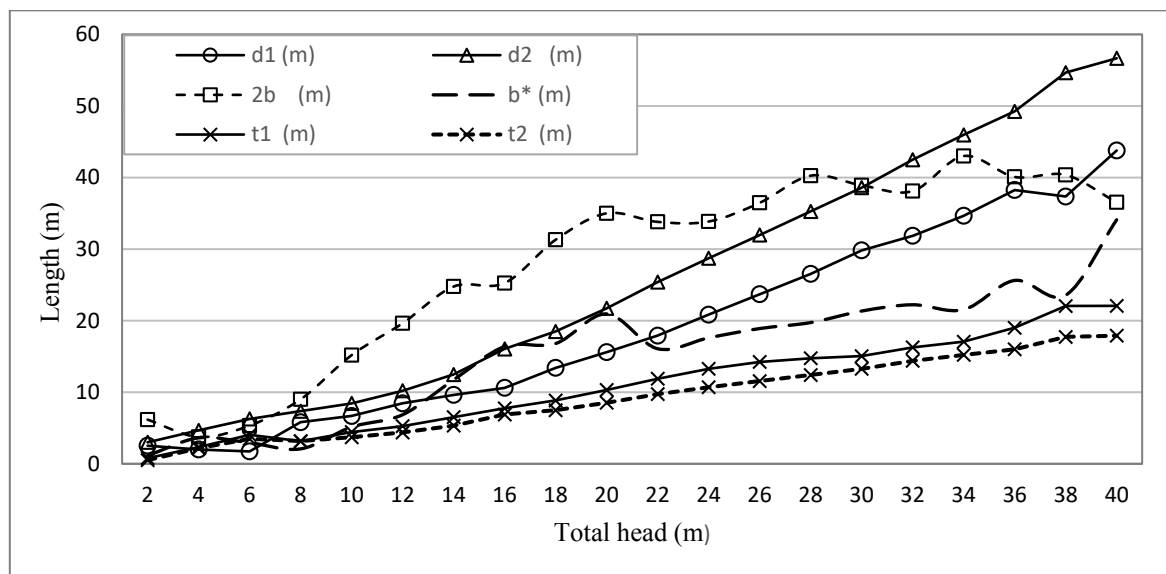
Figure 3.17 Optimum solution (d_1, d_2, 2b, b*, t_1, t_2) for different head values

On the other hand, the optimum width (2b) of HWRS effectively influences optimum hydraulic design of HWRS, because the total width is directly integrated in many safety factors, such as overturning, sliding and ie. The optimum ratio of 2b/(d_1+d_2) changed with head value. This ratio is 0.8 for H (0-10 m), 1 for H (10-20 m), 0.7 for H (20-30 m) and 0.4 for H (30-40 m). Reduction of the optimum HWRS width (2b) could be attributed to increasing floor thicknesses on the Us and Ds sides (t_1, t_2) with head increase, which results in an expensive design. Therefore, the S-O model reduced the total width and simultaneously augmented the depth of d_1 and d_2, which was an efficient and cost effective solution to reduce tremendous uplift pressure and exit gradient effects for large H values.

Moreover, b* considerably contributed to achieving optimum hydraulic design of HWRS. The weight of water head above b* (Figure 3.15) counterbalances uplift pressure and enhances the stability of HWRS. Hence, the optimum ratio of (b*/2b) ranges from (0.45-0.65) as seen in Figure 3.17. This means that the value of b* substantially contributed to the safety of HWRS and provides cheaper solutions. Usually, HWRS shape is without b* value. Therefore, replacing the volume of concrete (in case of b* = 0) by a sufficient volume of water is extremely cheaper solution when b* is a considerable value (0.45-0.65 of 2b).

Additionally, the values of t_1 and t_2 also affect optimum design of HWRS, which is logical as HWRS are partially based on its weight to resist hydrostatic and uplift pressure. The optimum ratio of t_1/H is approximately (0.5) and around (0.43) for t_2/H. All these design parameters and safety factors are integrated within the constraints, objective function and surrogate models.

Additionally, referring to Table 3.8, optimum cost can be approximately expressed as an exponential function with respect the water head (H), as shown in Eq. (3.33). This implies that construction cost for cases with a small H (less than 20 m) is significantly lower than cases with large H. For example, optimum cost is around ($490,000) for 20 m head, but when H attains 30 m the cost is almost six times that of the first case ($2,815,000). Therefore, the construction cost for HWRS exponentially increased with the head augmentation, especially for head values more than 20 m. That can be explained by two reasons: first, the construction cost of cut-offs dramatically increased with cut-off depth of, as the cost of cut-off is a function of its depth, see Eqs. (3.9) and (3.10). Second, when the head reached 20m or more, floor thickness values (t_1, t_2) became higher, which resulted in high construction cost. Roughly, the optimum hydraulic design of HWRS must include sufficient floor width (2b) ranging from H to 2H, upstream cut-off (d_1) ranging from 0.8H to1.25H, downstream cut-off (d_2) ranging from H to1.5H, upstream portion of the floor (b*) around 0.5(2b), upstream thickness (t_1) around 0.5H and downstream thickness (t_2) around 0.45H.

$$\text{HWRS}_{cost} = 6407 \text{ EXP } 0.1992 \text{ H}, \qquad \text{RSQ}= 0.98 \qquad\qquad (3.33)$$

Table 3.8   Optimization – simulation model results with SEEW and Khosla evaluations

head (m)	Optimum design vector						Optimization-simulation results							SEEPW result (evaluation)			Khosla result (evaluation)		
							The safety factors			Other results			cost $						
	d1 (m)	d2 (m)	2b (m)	b* (m)	t1 (m)	t2 (m)	K_s	F_over	e	θC S-O (m)	θE S-O (m)	Exit gradient S-O		θC SEEPW (m)	θE SEEPW (m)	Exit gradient SEEPW	θC Khosla (m)	θE Khosla (m)	Exit gradient -Khosla
2	2.54	3.00	6.17	1.15	0.79	0.52	8.75	2.50	3.57	0.9	0.6	0.23	4,758.28	1.2	0.9	0.16	1.2	0.9	0.17
4	2.00	4.67	3.76	3.62	2.32	2.17	2.52	1.81	1.32	2.7	2.5	0.23	8,639.49	2.8	2.6	0.24	3.1	2.1	0.26
6	1.73	6.27	5.33	2.94	4.05	3.49	1.92	1.63	1.86	4.7	4.0	0.23	17,151.23	4.5	4.2	0.27	5.0	3.6	0.28
8	5.81	7.35	9.01	2.09	3.15	3.18	1.67	1.75	3.49	3.6	3.7	0.23	30,778.05	4.5	4.2	0.26	4.9	3.7	0.31
10	6.68	8.44	15.18	5.14	4.43	3.71	2.23	2.20	7.56	5.1	4.3	0.23	51,835.99	5.8	4.9	0.27	5.9	4.7	0.31
12	8.46	10.21	19.64	6.86	5.26	4.38	2.29	2.29	10.08	6.1	5.0	0.23	83,799.48	7.0	5.8	0.26	7.0	5.6	0.30
14	9.62	12.48	24.76	11.73	6.51	5.33	2.60	2.46	13.06	7.5	6.2	0.23	132,730.48	8.4	6.8	0.25	8.4	6.6	0.28
16	10.61	16.05	25.25	16.38	7.76	6.89	2.55	2.44	12.58	8.9	7.9	0.23	209,207.30	9.8	8.5	0.24	10.0	8.0	0.27
18	13.41	18.50	31.30	16.80	8.85	7.49	2.60	2.45	16.23	10.2	8.6	0.23	323,012.77	10.8	9.2	0.23	10.9	8.8	0.25
20	15.59	21.73	35.00	20.95	10.32	8.53	2.68	2.46	18.02	11.9	9.8	0.23	492,431.87	12.0	10.4	0.23	12.2	9.8	0.24
22	17.91	25.39	33.80	16.08	11.89	9.74	2.05	2.10	16.42	13.7	11.5	0.23	731,887.59	13.1	12.2	0.22	13.7	10.8	0.24
24	20.84	28.72	33.85	17.60	13.28	10.70	2.07	2.17	16.36	15.3	12.3	0.23	1,060,131.96	14.1	13.1	0.22	15.2	11.4	0.24
26	23.69	31.97	36.46	18.90	14.23	11.56	2.04	2.17	17.59	16.4	13.3	0.23	1,497,531.19	15.1	14.2	0.22	16.6	12.1	0.23
28	26.54	35.27	40.26	19.73	14.75	12.41	2.04	2.20	19.61	17.0	14.3	0.23	2,072,930.37	16.2	15.2	0.22	17.8	13.0	0.23
30	29.82	38.59	38.91	21.34	15.04	13.27	1.59	1.91	17.17	17.0	15.1	0.23	2,815,829.91	17.0	16.2	0.22	19.8	13.0	0.23
32	31.86	42.49	38.11	22.22	16.27	14.39	1.74	2.07	17.02	18.8	16.6	0.23	3,766,369.50	18.5	18.0	0.22	22.4	13.1	0.22
34	34.65	45.96	43.01	21.54	17.06	15.21	1.77	2.10	19.82	19.7	17.5	0.23	4,963,850.86	19.6	19.0	0.21	23.3	14.3	0.22
36	38.25	49.24	40.09	25.62	19.01	16.00	1.65	1.99	17.17	21.9	18.5	0.23	6,451,119.34	20.6	20.2	0.21	26.7	13.1	0.22
38	37.35	54.66	40.36	23.56	22.05	17.73	1.56	1.88	16.73	25.4	20.4	0.23	8,369,651.45	22.9	22.6	0.21	30.1	14.0	0.21
40	43.78	56.66	36.54	34.10	22.07	17.90	1.52	1.77	12.58	25.5	20.6	0.23	10,472,071.86	23.1	22.9	0.22	35.4	9.5	0.21

3.7.3 Evaluation

An objective evaluation of the methodology was conducted to assess the performance of developed ANN models and the linked S-O model. Basically, the evaluation processes included comparing the predicted seepage characteristics value based on ANN / S-O models to solutions of numerical simulation and other methods for the resulting optimum solutions.

3.7.4 The ANN model evaluation

Forty different scenarios of d_1, d_2, 2b and H were randomly generated using LHS. The seepage models based on these values are solved/simulated by the developed ANN models, numerical seepage code and Khosla's theory. The evaluations showed a superior match between ANN and SEEP/W results for uplift pressure and **ie** values, as shown in Figures 3.18, 3.19, 3.20 and Table 3.9. The ANN predictions did not precisely match Khosla's solutions as much as the numerical solution. This can be assigned to two factors: first, the ANN model was not trained based on Khosla's solutions. Second, the approximation and empirical assumptions utilized in Khosla's equations affect the accuracy of Khosla's solutions. Furthermore, irregular results were presented by Khosla's theory for uplift pressure values. This could be attributed to Khosla's empirical correction formula for mutual interference between cut-offs, which is the last term in Eqs. (3.35) and (3.36). This term provides illogical values and affects the uplift pressure value strongly when the ratio of $(d_1/2b)$ or $(d_2/2b)$ is more than 1. The calculation of **ie** value and uplift pressure (percentages from a total head (H)) by Khosla's theory are given by Eqs. (3.34) to (3.37):

$$IE_{Khosla} = \frac{h}{\pi * \Lambda * d_2} \tag{3.34}$$

$$\%\emptyset_{C\,Khosla} = 100 - \frac{1}{\pi}COS^{-1}\left(\frac{\Lambda - 2}{\Lambda}\right) + 19\sqrt{\frac{D}{b'}}\ \left(\frac{d + D}{2b}\right) \tag{3.35}$$

$$\%\emptyset_{E\,Khosla} = \frac{1}{\pi}COS^{-1}\left(\frac{\Lambda - 2}{\Lambda}\right) - 19\sqrt{\frac{D}{b'}}\ \left(\frac{d + D}{2b}\right) \tag{3.36}$$

$$\Lambda = \frac{\sqrt{1+\alpha^2}+1}{2}, \quad \alpha = \frac{2b}{d}, \tag{3.37}$$

Where

b' = distance between two cut-offs (m);

2b = total width of the floor (m);

d = depth of the cut-off at which uplift pressure is determined (m);

D = depth of the cut-off which affects neighbouring pile (m).
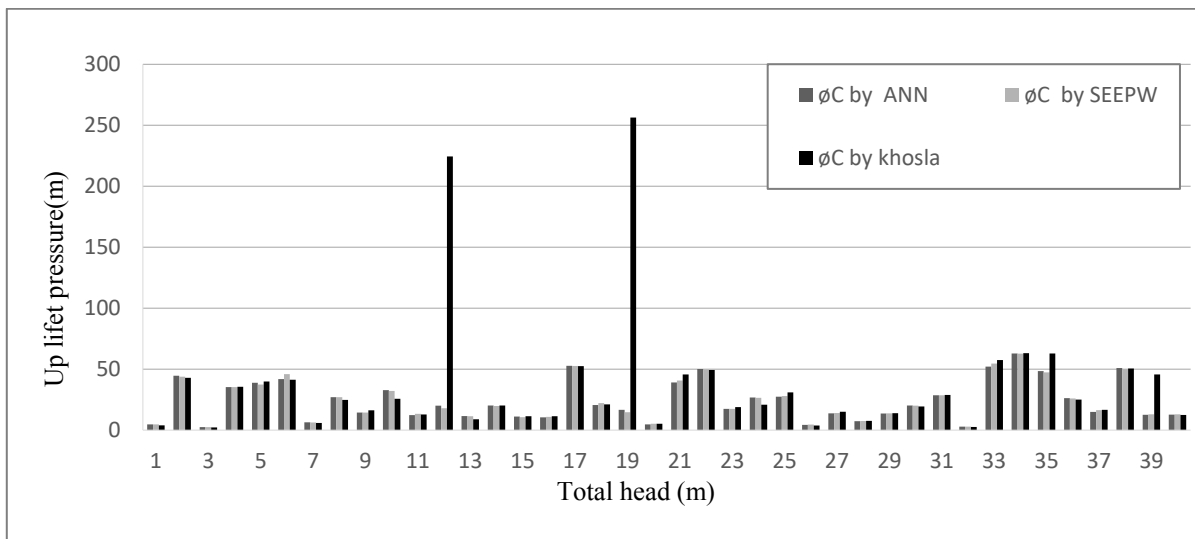
Figure 3.18 Comparison of ANN solution with SEEP/W and Khosla's solutions (Exit gradient)
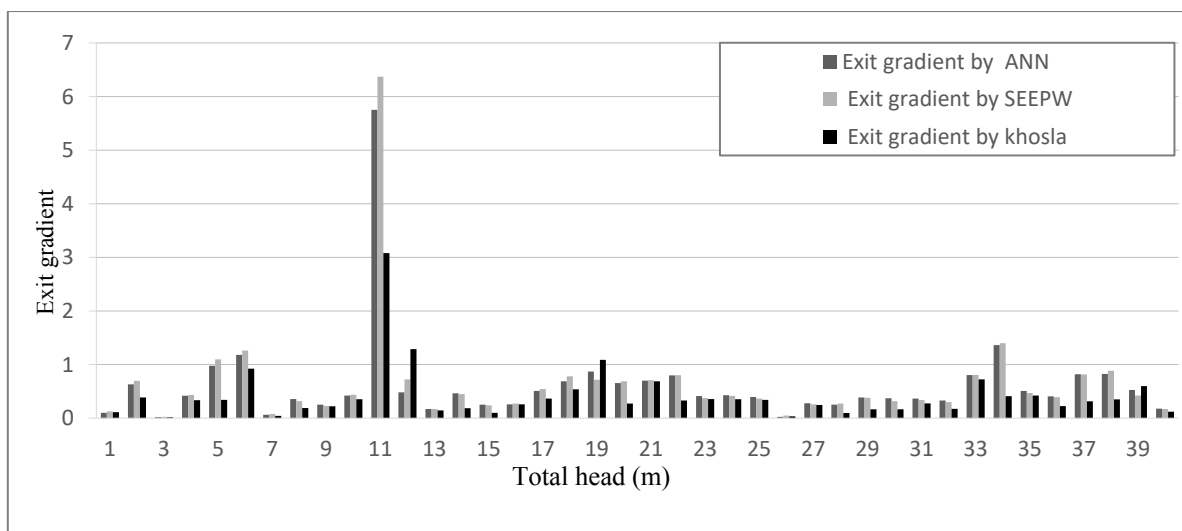
Figure 3.19 Comparison of ANN solution with SEEP/W and Khosla's solutions (θC)
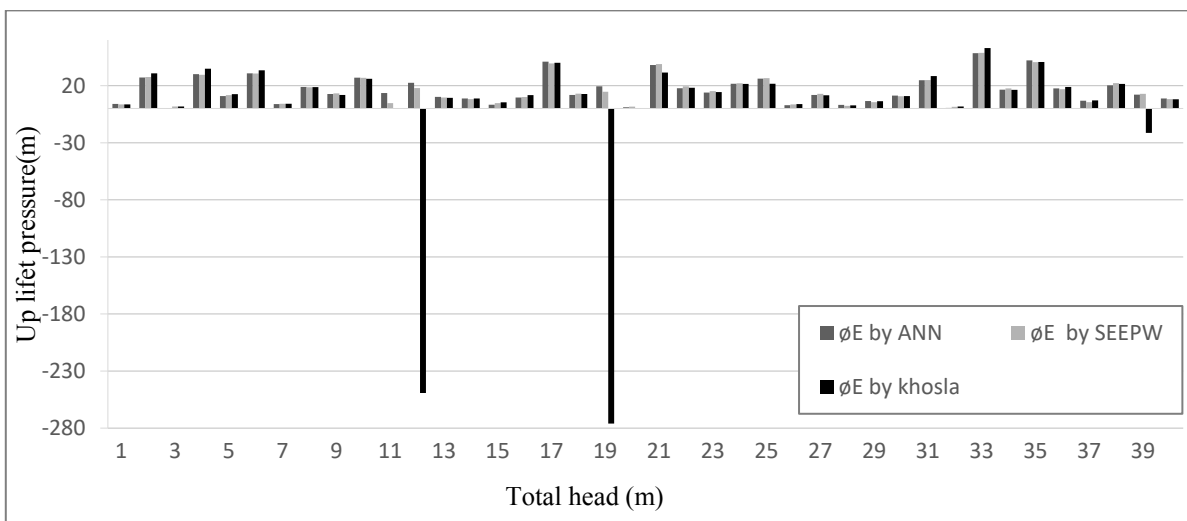
Figure 3.20 Comparison of ANN solution with SEEP/W and Khosla's solutions (θE)

3.7.5 S-O model evaluation

Seepage characteristic values related to optimum solutions obtained by the S-O model were evaluated to verify that the surrogate model responses within S-O model are accurate. The optimum solutions were solved by the numerical seepage modeling and Khosla's method. The resulting seepage characteristic values obtained by these methods and seepage characteristic of the optimum solution given by S-O technique are shown in Figures. 3.20, 3.21, 3.22 and Table 3.9.

Broadly, S-O solutions totally agreed with SEEP/W solutions for uplift pressure and **ie** values. However, there are minimal deviations for **ie** and uplift pressure values for a few points. This is expected performance for any approximation and surrogate model, and may be attributed to imperfect training of the developed ANN models for data located beyond or near the training ranges. For example, for cases having H value between 32 and 40 m, the optimum d_2 value was more than 40m (Table 3.8), whereas the maximum training range for d_2 is 40 m.

Moreover, all **ie** values attained ultimate allowable value (0.23) to achieve the safety factor value (5), which can be clearly observed in Figure 3.22. This means **ie** values substantially and critically impact S-O the optimal solutions and safety of HWRS design. Therefore, the S-O model modifies the decision vector to provide ultimate allowable safe **ie** value. Hence, that might influence efficiency of S-O solutions for some cases compared to the numerical solution.

Comparing with Khosla's solutions, a good match is obtained for most results. Nevertheless, there were considerable deviations, as clearly seen in Figures 3.20, 3.21 and 3.22, which could be attributed to the same reasons discussed earlier in the context of ANN evaluation. There is a noticeable deviation of Khosla's solution for the large HWRS scenarios (large H value) for uplift pressure value. Also, for exit gradient values, Khosla's solutions present a noticeable error for small HWRS instances (low H value). Hence, there are some imprecise solutions and limitations in applying Khosla's theory.

Generally, the linked S-O model provided precise and computationally efficient results. Therefore, this methodology is potentially applicable for a real life minimum cost optimal design. However, it is recommended to adequately expand training data range to obtain accurate solutions using trained ANN models for different cases of HWRS design.
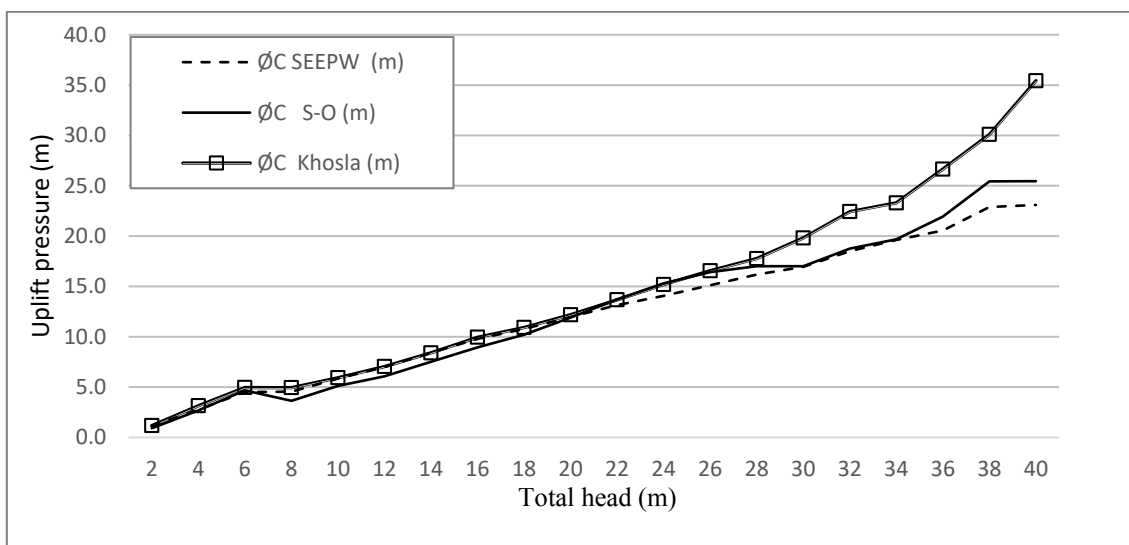
Figure 3.21 Comparison of seepage characteristics (θC) of the optimum obtained by S-O model, Numerical model (SEEP/W) and Khosla's theory
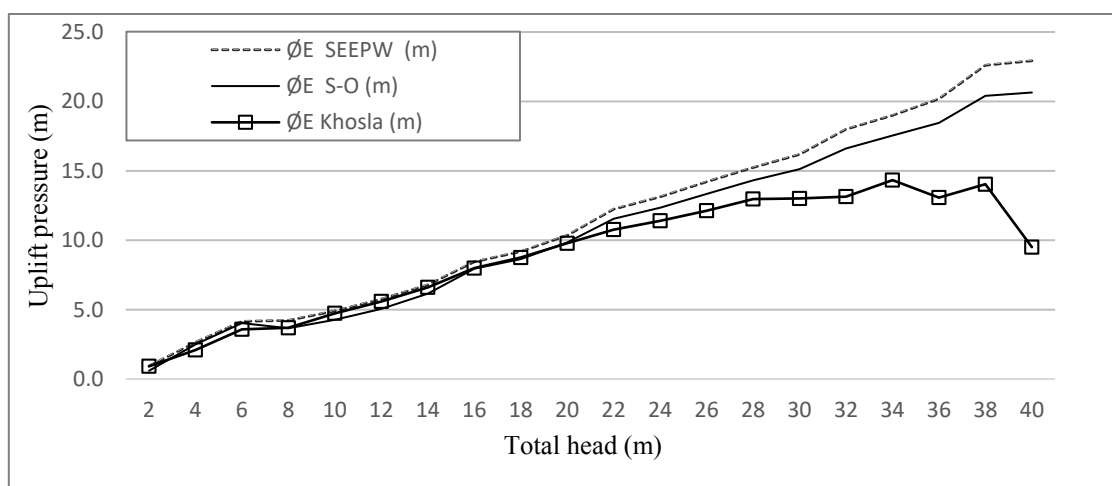
Figure 3.22 Comparison of seepage characteristics (θE) of the optimum obtained by S-O model, Numerical model (SEEP/W) and Khosla's theory
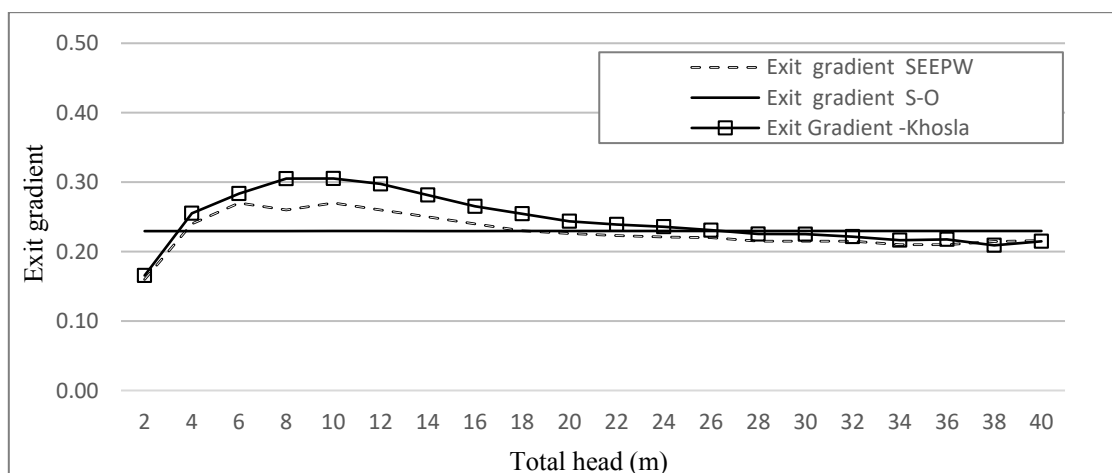
Figure 3.23 Comparison of seepage characteristics (Exit gradient) of the optimum obtained by S-O model, Numerical model (SEEP/W) and Khosla's theory

Table 3.9 Evaluation of S-O optimum solutions with SEEP/W and Khosla's solutions

No	Assumed data				S-O Result			SEEP/W result			Khosla result		
	d1	d2	2b	H	θC ANN	ΘE ANN	Exit gradient ANN	θC SEEPW	ΘE SEEPW	Exit gradient SEEPW	θC Khosla	ΘE Khosla	Exit gradient Khosla
1	28.5	14.5	44.78	10.78	5.42	4.01	0.10	4.76	3.65	0.13	3.98	3.62	0.11
2	30.5	21.5	106.73	79.03	43.71	27.19	0.63	43.82	27.51	0.70	42.96	30.78	0.39
3	5.5	38.5	77.23	2.98	2.78	0.38	0.02	2.47	1.76	0.02	2.27	1.71	0.02
4	27.5	35.5	68.38	59.53	35.54	30.07	0.42	35.28	29.54	0.43	35.59	34.79	0.34
5	20.5	5.5	112.63	63.43	39.22	10.88	0.98	37.33	11.69	1.10	39.83	12.52	0.34
6	6.5	11.5	32.98	67.33	46.59	30.72	1.18	45.88	30.67	1.26	41.34	33.47	0.92
7	13.5	28.5	94.93	8.83	5.71	3.90	0.06	6.32	4.12	0.08	5.90	4.11	0.04
8	14.5	31.5	91.98	38.08	26.39	18.84	0.36	27.08	18.62	0.32	24.83	18.79	0.19
9	37.5	30.5	47.73	30.28	14.11	12.77	0.25	14.42	13.22	0.23	16.32	11.84	0.22
10	36.5	32.5	71.33	61.48	30.77	26.94	0.42	32.13	26.79	0.44	25.73	26.05	0.35
11	9.5	0.5	9.38	47.83	18.20	13.47	5.75	13.38	4.72	6.37	12.85	0.10	3.08
12	**38.5**	**18.5**	**6.43**	**77.08**	18.08	22.47	0.48	17.91	17.91	0.72	**224.42**	**-249.16**	1.29
13	35.5	29.5	62.48	22.48	11.06	10.18	0.17	11.35	9.61	0.17	8.88	9.31	0.15
14	18.5	9.5	100.83	32.23	20.19	8.79	0.46	19.79	8.18	0.45	20.19	8.76	0.19
15	31.5	10.5	118.53	20.53	11.33	3.24	0.25	10.55	4.73	0.24	11.45	5.42	0.10
16	8.5	16.5	18.23	16.63	9.89	9.58	0.26	10.85	9.97	0.27	11.42	11.76	0.26
17	10.5	37.5	74.28	69.28	54.50	41.07	0.51	52.57	39.53	0.54	52.43	40.05	0.37
18	34.5	8.5	56.58	55.63	21.84	11.91	0.69	22.22	12.97	0.78	21.09	12.63	0.54
19	**25.5**	**15.5**	**3.48**	**53.68**	16.81	19.41	0.87	14.73	14.73	0.72	**256.34**	**-275.95**	1.09
20	39.5	1.5	41.83	18.58	2.95	1.01	0.65	5.19	1.66	0.69	5.26	-0.21	0.27
21	15.5	25.5	24.13	65.38	40.40	38.12	0.70	40.72	38.87	0.71	45.71	31.43	0.69
22	2.5	12.5	97.88	57.58	50.43	17.75	0.80	49.73	19.42	0.80	49.31	18.11	0.33
23	26.5	20.5	38.88	36.13	19.14	13.94	0.41	17.40	15.20	0.38	18.82	14.39	0.36
24	32.5	27.5	59.53	51.73	26.77	21.74	0.43	26.48	22.16	0.42	20.90	21.56	0.35
25	16.5	33.5	30.03	41.98	28.48	26.16	0.39	27.90	26.53	0.37	30.92	21.65	0.34
26	22.5	39.5	83.13	6.88	3.85	2.91	0.03	4.51	3.58	0.05	3.81	3.88	0.03
27	23.5	24.5	35.93	26.38	15.63	11.86	0.28	14.03	12.77	0.26	15.11	11.62	0.25
28	17.5	4.5	80.18	12.73	7.40	3.12	0.25	7.44	2.38	0.27	7.58	2.69	0.10
29	21.5	7.5	86.08	24.43	13.77	6.58	0.39	13.73	5.60	0.38	13.93	6.39	0.17
30	11.5	17.5	89.03	28.33	19.73	11.28	0.37	20.03	10.78	0.32	19.36	10.91	0.17
31	19.5	36.5	53.63	43.93	29.21	24.71	0.37	28.61	24.88	0.34	28.87	28.34	0.28
32	4.5	2.5	15.28	4.93	2.20	0.53	0.33	2.82	1.44	0.30	2.65	1.74	0.17
33	7.5	26.5	27.08	73.18	55.64	48.45	0.81	54.53	48.75	0.81	57.50	52.97	0.72
34	3.5	6.5	109.68	75.13	64.24	16.43	1.36	62.75	17.56	1.40	63.08	16.30	0.41
35	0.5	34.5	21.18	49.78	48.32	42.20	0.51	47.35	40.65	0.47	62.85	40.71	0.42
36	29.5	23.5	103.78	45.88	25.88	17.62	0.41	26.02	16.92	0.39	24.99	18.85	0.22
37	24.5	3.5	65.43	34.18	16.57	6.82	0.82	16.38	5.53	0.82	16.65	7.05	0.32
38	12.5	13.5	115.58	71.23	51.85	20.22	0.82	50.03	22.29	0.88	50.51	21.47	0.35
39	33.5	19.5	12.33	40.03	13.81	12.13	0.53	12.91	12.89	0.42	45.66	-21.35	0.60
40	1.5	22.5	50.68	14.68	13.58	8.71	0.18	13.01	8.16	0.17	12.41	8.06	0.12

3.8   Conclusion

This chapter presents a methodology to develop and validate the linked S-O technique in the hydraulic design of HWRS integrating the numerical responses of nonlinear seepage characteristic values. The biggest challenges in directly linking the complex optimization model to the numerical simulation model is that the method is computationally expensive and time consuming. Therefore, efficient ANN surrogate models were built to imitate numerical seepage responses. The developed models were successfully and efficiently linked to the optimization model to find the optimum hydraulic design of HWRS based on expeditious surrogate model responses. Systematic method is used to find the optimum training data size for ANN models. The ANN and GA parameters were carefully selected based on Taguchi DOE analysis to improve their performance. This procedure improved GA

performance by 17 % and significantly increased prediction preciseness of ANN models. The cross validation technique was implemented to evaluate ANN performance with different training/testing data combinations. The cross validation results demonstrated that the developed ANN surrogate models provide sufficient accuracy.

The S-O model was implemented for different H values ranging from 2 m to 40 m to find the optimum hydraulic design of a HWRS. In general, the optimum hydraulic design variable values of the HWRS can be summarized as: d_1/d_2 ratio ranges from (0.7-0.8), $2b/(d_1+d_2)$ ratio increases with H value growth from 0.8 to 1 then drops to 0.7 and 0.4, (b*/2b) ranges from (0.45-0.65), t_1/H is approximately 0.5, t_2/H is 0.43 and the optimum construction cost could be estimated based on H value using the equation ($HWRS_{cost}$ = 6407 e 0.1992 H). One of the most important inference of the results is that the inclusion of b* value in the optimization model significantly reduces construction cost of HWRS.

The optimum solutions obtained by the S-O model demonstrate that the most important design variable is **ie** (exit gradient). As **ie** value drastically influences the HWRS design and construction cost, it is recommended that future studies quantify uncertainty of the exit gradient safety factor and related parameters and variables, and how it affects minimum cost design.

The optimum solutions presented in this study could be used to select the optimum combination of (d_1, d_2, 2b, b*, t_1, t_2) for specific (H) value in design HWRS. Additionally, seepage characteristics could be directly obtained using the provided charts or by substituting input variables in ANN equations (in appendix A). However, application of these techniques is limited by the assumed ranges of the design variables.

Extensive evaluations to the optimum solutions based on ANN predictions were performed by comparing the seepage characteristic of the optimum solution obtained by the S-O model to the seepage characteristic resulting from numerical simulation of optimum solutions. The S-O and ANN predictions demonstrated good agreement with the numerical solutions. Therefore, the proposed methodology is potentially applicable to minimum cost and safe optimal hydraulic design of HWRS integrating accurate seepage modeling.

In Chapter Four, the S-O methodology is applied to the comprehensive conceptual seepage model. This model included ten cut-offs and varied inclination for each cut-off. The locations of cut-offs varied also. The SVM surrogate model is utilized in this problem to provide a robust prediction for seepage characteristics. Also, the effects of hydraulic conductivity and anisotropic hydraulic conductivity are studied in the next chapter.

4 Coupled Simulation-Optimization Technique for Optimum Hydraulic Design of Hydraulic Water Retaining Structures Constructed on Anisotropic and Non-homogenous Permeable Soil

Parts of this chapter were published, as per following details:

Al-Juboori, Muqdad, and Datta, Bithin (2018) *Linked simulation-optimization model for optimum hydraulic design of water retaining structures constructed on permeable soils.* International Journal of GEOMATE, 14 (44). pp. 39-46.

Al-Juboori, Muqdad, and Datta, Bithin (2018) *Minimum Cost Design of Hydraulic Water Retaining Structure by Using Coupled Simulation Optimization Approach.* KSCE Journal of Civil Engineering, in press.

In this chapter the S-O based methodology is implemented for a comprehensive scenario, incorporating different features of hydraulic conductivity and many seepage prevention components (cut-offs). The aim of this chapter is to find optimum design of HWRS, the most effective variable/parameters in the optimum design of HWRS, and how the variation of hydraulic conductivity affects optimum design of HWRS.

4.1 Introduction

An obvious concern in designing HWRS is the limitation of seepage prevention components, especially for high water head, to provide a safe design. Often seepage prevention components of most constructed projects are end cut-offs (upstream and downstream) with an apron between them. Also, with limited orientation, lengths and number of cut-offs, and width of the apron, the opportunity to find a feasible optimum solution using a linked S-O technique is reduced. On the other hand, including the effects of different scenarios of hydraulic conductivity and its anisotropic ratio on the optimum HWRS is an important concept that must be considered in optimum design of HWRS. Moreover, studying soil stratification based on different values of hydraulic conductivity and its effects on optimum design of HWRS is another concept that needs to be considered in optimum HWRS design.

Hence, a comprehensive conceptual model is proposed. This model includes ten cut-offs distributed along the apron of the HWRS. The lengths, orientation of cut-offs and distance between them (apron) are considered variables. These variables are used to build surrogate models and within the S-O model the optimum value of these variables can be achieved. Based on optimum solutions, which provide a safe and minimum cost design of HWRS considering seepage impacts, the most important and active sets with their optimum value could be identified.

On the other hand, seepage characteristics are affected by soil properties. Soil properties in real fields vary with different locations and directions and rarely exhibit homogenous isotropic hydraulic

conductivity (Lambe & Whitman, 1969). Hence, hydraulic conductivity of the flow domain is proposed as a variable value, and is included in three different layers, and anisotropic ratio for each layer is varied as well. The depth of each layer is another variable incorporated in the conceptual model. The precise values for uplift pressure and exit gradient in non-homogenous anisotropic soils with different boundary conditions could only be determined using numerical simulation, specifically the finite element method (FEM).

This chapter concentrates on studying the effect of soil properties on optimum solution, and finding the most important and effective seepage control components for optimum design of HWRS. The S-O methodology involved formulating the optimization model to minimize construction cost. Also, many constraints were proposed to represent the safety factors and design requirements of HWRS. The hybrid genetic algorithm (HGA) was based on the support vector machine (SVM) surrogate model responses (seepage characteristics) to evaluate the objective function and constraints to select the optimum decision variable. The SVM surrogate models were trained and tested by a large amount of numerically simulated data sets. The input variables were randomly generated, then numerically simulated to determine seepage characteristics (output variables). Additionally, optimum solutions obtained using the S-O model were evaluated by numerically simulating the optimal solutions and comparing seepage characteristics resulting from the S-O to the numerical solution results. More details about the developed S-O approach and related models are covered in the following sections.

4.2 Seepage conceptual model and data generation

The first step in developing a surrogate model is to propose a comprehensive conceptual model. This model includes all expected parameters and variables affecting design of HWRS. Based on the conceptual model, many scenarios of input data could be generated and simulated to find the corresponding seepage characteristic (output data) for each scenario. Each scenario represents a specific numerical simulation seepage model and includes different features and soil properties.

The comprehensive numerical model is shown in Figure 4.1. The variables of the comprehensive conceptual model are processed through the optimization model to find the most important design variables that provide a safe, economic and optimum solution. The geometry of the assumed numerical model comprised ten cut-offs (sheet piles) with varied positions, length and orientation. Additionally, three subsoil layers were assumed and the principle (horizontal) hydraulic conductivity (k_x) and anisotropic ratio (k_y/k_x) varied for each layer and for each case. As a result, the contribution of each variable involved in the comprehensive model to the optimal design could be explored for different boundary conditions.

The prescribed range of each design variable and parameter, shown in Table 4.1, was selected carefully to satisfy the flow condition and other design requirements, as discussed in Section 3.3. Also,

the ranges of hydraulic conductivity and anisotropic ratio were proposed to cover a wide range of expected real life hydraulic conductive and anisotropic ratios and were based on many studies and experimental data (Beckwith, Baird, & Heathwaite, 2003; Burger & Belitz, 1997; Greenkorn, Johnson, & Shallenberger, 1964; Terzaghi et al., 1996).
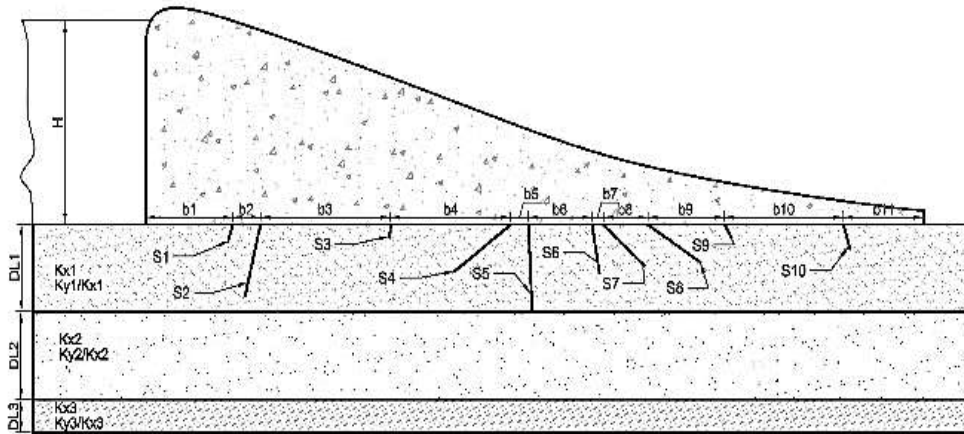
Figure 4.1 Seepage conceptual model scheme

The second step is to randomly generate numerous and different seepage scenarios, then simulate them by the numerical model. In each scenario, the design variables of the numerical model were completely different to other scenarios. The input and output variables for each scenario represented one data set. The 41 input variables included in the conceptual model were: total upstream water head (H), ten cut-off depths (d_1, d_2 ,... d_{10}), their angles (β_1, β_2,... β_{10}), distance (width) between cut-offs (b_1, b_2,.... b_{10}), three subsoil layers depths (LD_1, LD_2, LD_3), their hydraulic conductivity in a horizontal direction (k_{x1}, k_{x2}, k_{x3}) and their anisotropic ratio ($k_y/k_x)_1$, ($k_y/k_x)_2$, ($k_y/k_x)_3$, respectively.

Latin hypercube sampling method (LHS) (Cox & Reid, 2000) was used to randomly generate data sets within the specified range. Statistical description of the input data is listed in Table 4.1. The input data and their corresponding simulated responses (output data) was utilized to train and build SVM surrogate models. The output data for each case was obtained by simulating the input data for the same case using the numerical simulation model. The most important seepage design characteristics for each numerical seepage model were uplift pressure in front (PEi) and behind (PCi) each single cut-off (S_1, S_2, ... S_{10}) in addition to the exit gradient (**ie**) at the toe of the hydraulic structure. Hence, it was required to develop 21 surrgate models, one surrgate model for each seepage characteristic.

Table 4.1 Statistical description of the generated data

Input variable	Unite	Min	Max	Average	Std.
H	m	2	100	50.61	28.11
$b_1, b_2, ... b_{11}$	m	1	120	60.37	34.26
$d_1, d_2, ... d_{10}$	m	0	60	29.98	17.37
$\beta_1, \beta_2, ... \beta_{10}$	dgree	30	150	90.4	34.11
LD_1, LD_2, LD_3	m	5	100	53.67	27.01
k_{x1}, k_{x2}, k_{x3}	m^3/day	0.01	20	10.04	5.78
$(k_y/k_x)_1, (k_y/k_x)_2, (k_y/k_x)_3$	-	0.1	1.5	0.80	0.40

Seepage characteristics varied for each scenario and were affected by different parameters (input parameters), such as upstream water head, soil properties, flow geometry, cut-off depths, etc. Achiveing adequately trained surrogate models to predict seepage characteristics for complex problems provides good understanding of the effects and contribution of each parameter and variable on seepage characteristics. As a result, based on surrogate model responses the optimizaiton model could select the most important variable which provides safety and most efficient construction cost of HWRS.

4.3   Variable importance analysis

Variable importance or feature selection analysis is an important step which must be implemented before training surrogate models to select and incorporate active input design variables in building required surrogate models to predict a certain seepage characteristic. There are 41 input variables (Table 4.1) and 21 output seepage characteristics, and it is unexpected that all input variables play a significant role in training the surrogate model of a particular seepage characteristic. Therefore, a feature selection technique was utilized to find the most important variables contributing to prediction of a particular output variable.

Using this technique provides two advantages. First, accuracy of the surrogate model increases because the training process including many input variables deteriorates training quality of the surrogate model. Each input variable produces a specified amount of error. Consequently, with a huge amount of predictors (input variables/parameters) accumulate error becomes larger and this may lead to an inadequate surrogate model. Additionally, mixing uncontrollable predictors with controllable variables substantially affects the training process (Cavazzuti, 2012). Consequently, ill-trained surrogate models are produced and prediction accuracy is unsatisfied. Second, surrogate model speed responses, trained on large number of input variables, is less compared to the surrogate model trained on a small number of input variables. The expeditious responses of surrogate models are considered an important factor to successfully develop S-O approaches. The surrogate models would be invoked by the optimization solver numerous times to evaluate the related objective function and constraints.

Variable importance analysis comprises of passing generated data sets used for training surrogate models to the feature selection model. Analysis results demonstrate the importance level of

each input variable and its contribution in calculation of the output variable. Based on feature selection results, surrogate models can be trained using the active and important sets of input variables. The variable importance process was conducted for each output seepage characteristic variable to find the most relevant input variable. Two techniques were utilized for variable importance analysis: the first is based on beta standardized coefficient and the second is based on the random forest (RF) regression, as discussed below.

4.3.1 Variable importance analysis using Beta weight (standardized coefficient)

The standardised regression coefficient, or beta weight coefficient, was used to find the contribution of each predictor (input variable) for the specified dependent variable (output variable). Calculation of the standardized coefficient involves converting variables to z-score (matric-free or standardized score). This means that all dependent and independent variables have zero mean and one variance. Hence, variable importance is measured based on the variation of standard deviation values of dependent and independent variables. Consequently, a reliable and objective comparison could be achieved to determine actual variable contribution. The greatest absolute value of standardized coefficient for a specific input variable means that the variable considerably correlated to the output variable (Gail, Krickeberg, Samet, Tsiatis, & Wong, 2007; Pallant, 2007; Schumacker & Lomax, 2004). The beta coefficient (β_c) for multi-predictors regression model was determined using Eq. (4.1):

$$\beta_c = b \frac{\sigma_x}{\sigma_y} = \frac{\sum(z_x\ z_y)}{\sum(z_x^2)} \tag{4.1}$$

Where:

σ_{x_j}, σ_y = standard deviation of X and Y, respectively;

b = unstandardized coefficient from the normal regression model;

z_x, z_y = z-score for X and Y variables, respectively, and is determined by the Eq. (4.2).

$$Z = \frac{x - \bar{x}}{\sigma_x} \tag{4.2}$$

Also, β_c could be determined by Pearson product–moment correlation coefficient (r_{xy}) as shown in Eq. (4.3).

$$\beta_c = r_{xy} = \frac{Cov\ (x,y)}{\sigma_x\ \sigma_y} \tag{4.3}$$

Where: Cove (x,y) is the covariance of x and y,

For two variables, the standardized beta coefficients β_{c1}, β_{c2} are given as shown in Eqs. (4.4 and 4.5).

$$\beta_1 \quad = \frac{r_{x_1} - r_{x_2} r_{12}}{1 - r_{12}^2} \tag{4.4}$$

$$\beta_2 \quad = \frac{r_{x_2} - r_{x_1} r_{12}}{1 - r_{12}^2} \tag{4.5}$$

4.3.2 *Variable importance analysis using Random Forest (RF)*

By developing machine learning techniques and its applications, the random forest (RF) technique has played a significant role in solving many complex problems related to machine learning techniques and data analysis, such as prediction tasks and variable importance analysis. Basically, variable importance analysis via the RF technique is based on the random permutation of a certain predictor, then measuring the influences on the target variable. The difference between the permuted and non-permuted model responses reflects the importance of that variable (Strobl, Boulesteix, Zeileis, & Hothorn, 2007).

Generally, the RF technique combines many individuals of a classification tree and it is important to note that 36.8% of training datasets are not incorporated for any individual tree. This percentage is called 'out of the bag' (OOB) of the tree. Prediction accuracy of the random forest model can be determined based on mean square error (MSE) of OOB datasets, as shown in Eq. (4.6):

$$OOB\_MSE \quad = \frac{1}{n} \sum_{i=1}^{n} (y_i - \widehat{\overline{y}}_{i,OOB})^2 \tag{4.6}$$

Where: $\widehat{\overline{y}}_{i,OOB}$ refers to the average prediction value from all trees for i datasets, which have been OOB. Accordingly, Breiman (2001) developed a measure (criterion) based on permuting a particular variable, called 'MSE reduction' to estimate variable importance, which can be determined as shown in Eq. (4.7).

$$OOBMSE_t = \frac{1}{n_{OOB,t}} \sum_{\substack{i=1 \\ i \in OOB_t}}^{n} (y_i - \widehat{y}_{i,t})^2 \tag{4.7}$$

Where $\widehat{}$ refers to predicted values;

OOB_t = {i: observation i is OOB for tree t};

$n_{OOB,t}$ = number OOB datasets in tree t.

This means that variable X_j would not have a significant impact on model prediction if randomly permuting X_j in OOB data and would not influence on the value of $OOBMSE_t$ determined by Eq. (4.8).

$$OOBMSE_t(X_{j\,permuted}) = \frac{1}{n_{OOB,t}} \sum_{\substack{i=1 \\ i \in OOB_t}}^{n} (y_i - \widehat{y}_{i,t}(X_{j\,permuted}))^2 \qquad (4.8)$$

Therefore, measuring permutation for Xj variable in tree **t** using the difference $[OOBMSE_t(X_{j\,permuted}) - OOBMSE_t]$ provides a significant understanding of Xj variable importance. When the difference approaches zero, this reflects that the variable is not integrated in any tree split, which means the contribution of this variable is negligible (Genuer, Poggi, & Tuleau-Malot, 2010; Grömping, 2009).

After accomplishing the feature selection analysis, results were listed from the first and second method in Tables B4.1 to B4.21 (Appendix B). Approximately, the two methods provide the same sets of controllable variables for each seepage characteristic. The highest rank input variables were chosen as active variables to be incorporated in training data. Variables with an importance index between (100 to ≈ 0.01) were considered effective variables. Even though there were few variables with a low variable importance index, they were incorporated in training surrogate model. Incorporating such variables, from physical meaning, may have some effect and can provide an efficient surrogate model. Also, the feature selection methods may have some uncertainty or approximation in the obtained results.

4.3.3 *Variable importance results and discussion*

As seen from variable importance results (Tables B4.1 to B4.21) the controllable variable, its sequences and ranks are different for each dependent variable. For example, the controllable variable related to PE2 is different to PE3. This variation may be attributed to noise in provided data and close resulting ranks for the most controllable variables. Hence, it is more systematic and efficient to provide the same sequential input variables for training the surrogate model to predict the values of PCi or PEi. This particularly helps provide more uniform formulation and programing code of the linked S-O approach for such a complex model. Therefore, in addition to the rank of each independent variable, the number of appearance of each independent variable is also considered for different locations of PCi or PEi values. This also provides a good indicator of variable importance to select a variable to be in the most controllable factors, as shown in Tables 4.2 and 4.3.

Table 4.2 Appearance of the important variables in the PEi model

PE_1	PE_2	PE_3	PE_4	PE_5	PE_6	PE_7	PE_8	PE_9	PE_{10}
H	PC_1	PC_2	PC_3	PC_4	PC_5	PC_6	PC_7	PC_8	PC_9
b_1	b_2	b_3	b_4	b_5	b_6	b_7	b_8	b_9	b_{10}
β_1	β_2	β_3	β_4	β_5	β_6	β_7	β_8	β_9	β_{10}
d_1	d_2	d_3	d_4	d_5	d_6	d_7	d_8	d_9	d_{10}
-	d_1	d_2	d_3	d_4	d_5	d_6	d_7	d_8	d_9
-	β_1	β_2	β_3	β_4	β_5	β_6	β_7	β_8	β_9
-	$(k_y/k_x)_1$	$(k_y/k_x)_1$	$(k_y/k_x)_1$	$(k_y/k_x)_1$	$(k_y/k_x)_1$	$(k_y/k_x)_1$	$(k_y/k_x)_1$	-	$(k_y/k_x)_1$
k_{x1}	k_{x1}	-	-	-	-	-	-	-	-
k_{x2}	-	-	k_{x2}	-	-	k_{x2}	-	-	-
layer depth1	-	-	-	-	-	-	-	-	layer depth$_1$
layer depth2	-	layer depth$_2$	-	-	-	-	-	-	layer depth$_2$
-	-	-	-	-	$(k_y/k_x)_2$	-	-	$(k_y/k_x)_2$	-

Table 4.3 Appearance of the important variables in the PCi model

PC_1	PC_2	PC_3	PC_4	PC_5	PC_6	PC_7	PC_8	PC_9	PC_{10}
PE_1	PE_2	PE_3	PE_4	PE_5	PE_6	PE_7	PE_8	PE_9	PE_{10}
d_1	d_2	d_3	d_4	d_5	d_6	d_7	d_8	d_9	d_{10}
-	d_1	d_2	d_3	d_4	d_5	d_6	d_7	-	-
d_2	d_3	d_4	d_5	d_6	d_7	d_8	d_9	d_{10}	-
b_1	b_2	b_3	b_4	b_5	b_6	b_7	b_8	b_9	-
b_2	b_3	b_4	b_5	b_6	-	-	-	-	-
β_1	β_2	-	β_4	-	β_6	-	-	-	β_{10}
$(k_y/k_x)_1$	$(k_y/k_x)_1$	$(k_y/k_x)_1$	-	-	-	-	$(k_y/k_x)_1$	-	$(k_y/k_x)_1$
k_{x1}	-	-	k_{x1}	-	k_{x1}	-	k_{x1}	k_{x1}	k_{x1}
-	-	-	-	-	-	-	-	$(k_y/k_x)_2$	$(k_y/k_x)_2$
-	-	-	-	-	-	-	-	layer depth$_2$	layer depth$_2$
-	layer depth1	-	-	layer depth$_1$	-	-	-	-	-

Consequently, the widespread controllable variables of PEi and PCi related to cut-off (Si) are shown in Table 4.4. These results were selected based on quantifying importance rankings and the most repetitive variables related to the dependent variable (PCi or PEi) for the ten cut-offs. Therefore, a comprehensive combination of independent variables was utilized to be the predictors of PEi or PCi variables. Predictors of the exit gradient variable, mentioned in Table B4.21, were selected based on results of variable importance analysis. The dependent variables PE10, PC10, PE1 and PC1 have a special location; therefore, the variable combination is slightly different to other dependent variables of the same class.

Table 4.4 Final combination of predictors for each seepage characteristic

	PE_1	PE_2 to E_9	PE_{10}	PC_1	PC_2 to PC_9	PC_{10}
1	b_1	bi	b_{10}	b_1	bi	b_{10}
2	d_1	$di\text{-}1$	b_{11}	b_2	$bi+1$	b_{11}
3	β_1	di	d_9	d_1	$di\text{-}1$	d_9
4	DL_1	$\beta\, i\text{-}1$	d_{10}	d_2	di	d_{10}
5	DL_2	$\beta\, i$	β_9	β_1	$di+1$	β_{10}
6	k_{x1}	DL_1	β_{10}	DL_1	βi	DL_1
7	$(k_y/k_x)_1$	DL_2	DL_1	DL_2	DL_1	DL_2
8	k_{x2}	k_{x1}	DL_2	k_{x1}	DL_2	k_{x1}
9	$(k_y/k_x)_2$	$(k_y/k_x)_1$	k_{x1}	$(k_y/k_x)_1$	k_{x1}	$(k_y/k_x)_1$
10	H	k_{x2}	$(k_y/k_x)_1$	k_{x2}	$(k_y/k_x)_1$	k_{x2}
11	-	$(k_y/k_x)_2$	k_{x2}	$(k_y/k_x)_2$	k_{x2}	$(k_y/k_x)_2$
12	-	$Pci\text{-}1$	$(k_y/k_x)_2$	pe_1	$(k_y/k_x)_2$	Pe_{10}
13	-	-	Pc_9	-	pei	-

Variable importance analysis significantly decreases the number of input variables for each model. For example, input variables for the PEi surrogate model is 12 and for PCi is 13, which are less than the total number (41) of independent variables for each dependent variable. After feature selection is conducted and the most important variables in each model are identified, the surrogate model could be trained based on these results.

4.4 Support Vector Machine surrogate model

The support vector machine (SVM) is one of the most popular machine learning techniques and has recently been implemented for different nonlinear and complex engineering problems. The SVM is a regression and classification technique that provides generalized responses and is less affected by the overfitting phenomena (Alpaydin, 2014).

The SVM algorithm selects from training data sets an efficient hyperplane, by which a good separation can be achieved. As long as the boundary (margin) of the hyperplane is far from the center of the hyperplane, good prediction ability of the SVM model can be attained (Figure 4.2). The multi-objective optimization task of the SVM algorithm concentrates on defining the best data sets that provide an efficient classification and maximize margin widths of the hyperplane. Therefore, SVM is less constrained by training data and prediction ability for unseen data sets is robust (Alpaydin, 2014; Kramer, 2016).
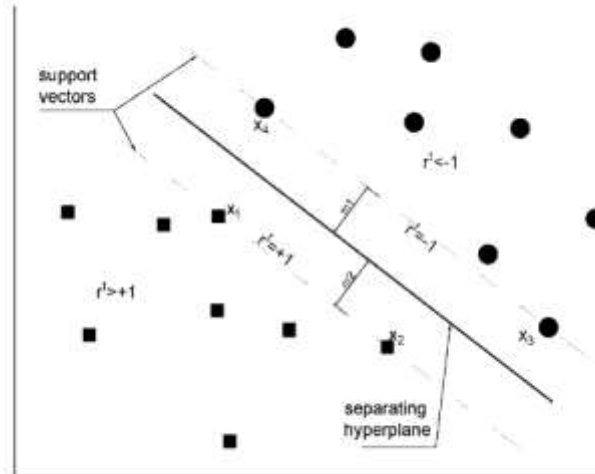
Figure 4.2 Linear separation support vector (two classes)

A normal vector $W = (w, .., w_d)^T \in R^d$ and a point $\mathbf{x_0}$ on the hyperplane could be used to describe the hyperplane $\mathbf{A}$ as: $\mathbf{A} = \{ x \in R^d : w^T x + w_0 = 0 \}$. Then, assuming there are two classes +1 /-1 and sample $X = \{x^t, r^t\}$, where $r^t = +1$ if $x^t \in C_1$ and $r^t = -1$ if $x^t \in C_2$, as shown in Eq. (4.9a) and (4.9b):

$$(W^T x^t + w_0) \geq +1 \quad for \quad r^t = +1 \tag{4.9a}$$

$$(W^T x^t + w_0) \leq -1 \quad for \quad r^t = -1 \tag{4.9b}$$

Eq. (4.8) and Eq. (4.9) can be written as Eq. (4.10):

$$r^t (W^T x^t + w_0) \geq +1 \tag{4.10}$$

So, according to Eq. (4.10), the instances must not be located on the hyperplane ($\geq +0$) only, but also must be at a distance ($\geq +1$) away to provide better separation. Then, the best separating hyperplane is the one which has maximum margin $\boldsymbol{m} = \frac{1}{||w||} + \frac{1}{||w||} = \frac{2}{||w||}$ or the minimum norm $\frac{1}{2} ||w||^2$; therefore, the optimization task can be formulated as shown below:

$$\text{Minimize: } \frac{1}{2} ||w||^2$$

$$\text{Subject to: } r^t (W^T x^t + w_0) \geq +1, \quad \forall t$$

This optimization problem can be solved by finding $\mathbf{W}$ and w_0 to define the optimal hyperplane having an efficient margin $\mathbf{m}$ and the decision boundary, which is called support vectors (Alpaydin, 2014; Kramer, 2016). This optimization task can be solved by using Lagrange multipliers, as shown in Eqs. (4.11 to 4.14).

$$L_p = \frac{1}{2} \, ||w||^2 - \sum_{t=1}^{N} \alpha^t \, [\, r^t (W^T x^t + w_0) - 1] \tag{4.11}$$

$$L_p = \frac{1}{2} \, ||w||^2 - \sum_{t=1}^{N} \alpha^t r^t \, (W^T x^t + w_0) - 1] \quad + \sum_{i=1}^{N} \alpha^t \tag{4.12}$$

$$\frac{\partial L_p}{\partial W} = 0 \; \rightarrow \quad W = \sum_{t=1}^{N} \alpha^t r^t x^t \tag{4.13}$$

$$\frac{\partial L_p}{\partial w_0} = 0 \; \rightarrow \quad \sum_{t=1}^{N} \alpha^t r^t = 0 \tag{4.14}$$

Substitute Eq. (4.13 and 4.14) in Eq. (4.11) then:

$$L_d = -\frac{1}{2}(\boldsymbol{w^T w}) - \boldsymbol{w^T}\frac{1}{2}\sum_{t=1}^{N} \alpha^t r^t x^t - w_0 \sum_{t=1}^{N} \alpha^t r^t \; + \sum_{t=1}^{N} \alpha^t \tag{4.15}$$

$$= -\frac{1}{2}(\boldsymbol{w^T w}) + \sum_{t=1}^{N} \alpha^t \tag{4.16}$$

$$L_d = -\frac{1}{2}\sum_{t=1}\sum_{s=1} \alpha^t \alpha^s r^t r^s \, x^{t\,T} x^s + \sum_{t=1}^{N} \alpha^t \tag{4.17}$$

So, L_d is maximized with respect to α^t only and subjected to the constraints $\sum_{t=1} \alpha^t r^t = 0$, and $\alpha^t \geq 0$, $\forall t$. By solving the Eq. (4.17) using the quadratic programing method, the value α^t is equal to zero for most cases and sets of x^t that have $\alpha^t > 0$ are support vectors. Additionally, **W** is the weighted sum of instances selected as support vectors. Therefore, sets of vectors located on the margin satisfy $r^t(W^T x^t + w_0) = 1$. Then, w_0 can be easily determined from any support vector using $w_0 = r^t - W^T x^t$. The majority of training instances have $\alpha^t = 0$ at which $r^t(W^T x^t + w_0) \geq 1$. These sets are located away from the decision boundary and rarely affect hyperplane parameters. Therefore, SVM algorithm is influenced by the training vector located close to boundaries (Alpaydin, 2014; Kramer, 2016).

The SVM technique was utilized to build surrogate models to imitate the numerical responses of seepage within the S-O model. Matlab programing language was utilized to develop surrogate models because Matlab is a versatile tool including many options that can be modified to build efficient SVM surrogate models. Twenty one models were built to determine the uplift pressure in front and behind each cut-off and exit gradient near the toe of the HWRS. These models were trained based on 1,500 scenarios of numerically simulated data.

For each uplift pressure dependent variable, two different SVM models were built and trained on different training/testing data sets randomly selected from source data, as shown in Table B4.22. A

basic version of the ensemble surrogate model based on an average of the two models was developed. This procedure provides a more robust and accurate prediction. Also, any uncertainty arising from source data or surrogate model prediction could be reduced by using the ensemble surrogate model. For exit gradient three different models were developed.

Seventy five percent of the simulated data was utilized for training and 25% was used for testing. Predictors for each model were selected based on variable importance results. The coefficient of determination for RSQ and MSE for the training and testing phases are listed in Table B4.22. Parameters for each SVR model were carefully selected after several iterations of trial and errors until best RSQ and less MSE value were achieved. The most influencing parameters on SVM performance were type of kernel function, box constraint and epsilon. The kernel function used in this study was second order polynomial, which provided precise predictions compared to other kernels.

4.5   Optimization model

A constrained optimization model was formulated as an S-O model to determine optimum design of HWRS. The optimization model includes a large number of decision variables (32) and several constraints. Also, the optimization solver evaluates the objective function and constraint values based on 21 ensemble surrogate model responses. This makes the optimization problem a complex task. Safety factors and other hydraulic design requirements represent imposed constraints of the optimization model within the S-O model. The best value of each design/decision variable was selected by the optimization algorithm to provide a safe and economic design. Therefore, for such optimization tasks, the hybrid genetic algorithm (HGA) was used. The HGA is a combination of two optimization algorithms: GA and interior point algorithm (IPA), as discussed in the next chapter. The HGA provided a global optimum solution and has the ability to deal with a complex problem.

Matlab programing language was used to implement the optimization model. The parameters of GA were: population size 2,000, elite count 10 and crossover fraction 0.8, function tolerance1e-6, constraint tolerance1e-3 and the remaining GA options were left to default Matlab options. The parameters of the IPA were: max function evaluations 10,000, max iterations 1,000, optimality tolerance 1.00E-04, function tolerance 1.00E-04, step tolerance 1.00E-04 and constraint tolerance 1.00E-04.

4.5.1   *Formulation of the optimization model*

The goal of the optimization model is to find the optimum decision vector X, providing the minimum construction cost objective function $(f(X))$ and safe HWRS design, which satisfies all design requirements, i.e., the optimization constraints. The decision vector represents the most important design variables of the HWRS model. Design variables from x_1 to x_{11} represent width between cut-offs $(b_1, b_2...b_{11})$, the variables from x_{12} to x_{22} represent depth of cut-offs $(d_1, d_1,...d_{10})$ and variables from x_{23} to x_{32} represent inclination angles for cut-offs (β_1, β_2,... β_{10}) (Figure 4.1). The objective function

represents construction cost of HWRS considering the substructure components related to seepage design. The objective function includes the decision vector and some design parameters. Formulation of the optimization model includes the following steps:

$$\text{Find the decision vector } X = \begin{Bmatrix} x_1 \\ x_2 \\ . \\ . \\ . \\ . \\ . \\ . \\ x_{32} \end{Bmatrix} = \begin{Bmatrix} b_1 \\ b_2 \\ . \\ . \\ . \\ b_{11} \\ d_1 \\ d_2 \\ . \\ . \\ . \\ d_{10} \\ \beta_1 \\ \beta_2 \\ . \\ . \\ . \\ \beta_{10} \end{Bmatrix}$$

Which minimizes the cost objective function shown in Eq. (4.18)

$$f(X) = c_f \sum_{x=1}^{11} T_i\, x_i + c_c\, t_c \sum_{x=12}^{21} x_i \quad \forall\, T, x \tag{4.18}$$

Where: c_f = cost of constructing the body of the HWRS (\$500); t_c = thickness of the cut-off, which is constant (1 m); Ti= thickness of each width between cut-offs (b_1, b_2 … b_{11}), for example T_2= (t_2+t_3)/2 ,etc. Thickness value (ti) is determined based on uplift pressure values PCi or PEi as shown in Eq. (4.19).

$$t_i = \frac{1.3\,(\text{PCi or PEi})}{G_S - 1} \quad \forall\, i, \text{PCi}, \text{PEi} \tag{4.19}$$

c_c = construction cost of cut-offs, which is a function of depth(d) and inclination angle (β), as shown in Eq. (4.20). It may be difficult to drive an inclined cut-off; therefore, the cost function incrported angle values to reflect increase in associated cost. Practically, there is no specific techniques to implement deep inclined cut-offs. However, a complementary version of Trench Cutter Machine (TCM) may be able to construct a deep inclined cut-offs in future. Such machines include ultrasonic measuring devices and computerized technology used for constructing complex trench systems (BAUER Group, 2016; O'Brien, Dann, Hunter, & Schwermer, 2005)

$$c_c^i = 0.05di^2 + 200\ di + 0.0698\ \beta i^2 - 12.558\ \beta i + 565.93 \ \forall\, i, \beta, d \tag{4.20}$$

72

The PCi and PEi values are based on candidate decision variables, which are randomly presented by the HGA solver. The decision variable values are modified in each optimization iteration as a candidate solution until the optimum solution is achieved. As a consequence, the objective function of this problem is classified as nonlinear because the expressions in Eqs. (18) to (20) are nonlinear, and some of the constraint values are based on nonlinear numerical surrogate model responses based on SVM model.

The decision vector is subject to the constraints similar to the sets of constraints presented in chapter two. These constraints were applied in the comprehensive design model in this chapter. The difference in this model is that there are many values of uplift pressure to be considered for the flotation safety factor and other specified safety factors. Because of the complexity of the problem, the portion (b*) of the floor on upstream side has not been considered in this chapter. Involving this variable in the optimization model makes the formulation of the optimization task more complex. The other logical and boundary constraints are also applied for each variable as discussed in chapter two.

4.6   Results and discussion

Many synthetic instances were proposed and implemented using the linked S-O model to find the influences of different hydraulic parameters and variables on the optimum solution. The important variables, such as upstream water head, hydraulic conductivity for the first layer and anisotropic for the first layer, were selected to find their effects on the optimum solution. Also, an evaluation phase was applied to measure efficiency and accuracy of the developed methodology to attain the optimum solution. Hence, the following results and discussion is categorized based on the effects of the variables or parameters through the S-O model.

4.6.1   Head variation effects

The linked S-O was implemented for different head values ranging from 20 m to 100 m. Other parameters were kept constant, such as hydraulic conductivity for all layers ($k_x = 5$ m/day), anisotropic ratio (($k_y/k_x)_1 = 1$) and depth of soil layers (50 m). The obtained optimum solutions can figure out the vital variables of all the provided design (decision) variables. This means that the optimization solver selects the design variables that provide safe and cost efficient design of HWRS for the optimum solution.

In general, the resulting optimum solutions demonstrated that contribution of variables b_1 to b_8 and d_2 to d_8 in the safety of HWRS was insignificant, as shown in Figures 4.3, 4.4 and Table B4.23. The optimum value for these variables approached to zero. In contrast, values b_9, b_{10}, b_{11}, d_9 and d_{10} had a vital role in the optimum design of HWRS. These variables, for most implemented cases, presented considerable values and were relatively varying with the variation of head values. The function of d_9 is to reduce PC9 and PE10 uplift pressure and exit gradient value. More importantly, the function of d_{10} is to directly reduce exit gradient value, which is the most critical seepage characteristic. The function

of b_9 and b_{10} is to provide a sufficient weight for stability of the HWRS, reduce the uplift pressure and provide sufficient width to counterbalance overturning and sliding forces.

Other important variables were β_9 and β_{10}, which are related to d_9 and d_{10}, respectively. The values of other inclination angles (β_1 to β_8) had a trivial value because the value of d_1 to d_8 approached zero. The optimum value of β_{10} is150 degrees. This is logical, as making the inclination angle of the last cut-off toward downstream (>90 degrees) substantially decreased exit gradient value. This can be attributed to the augmentation of the streamline length of seeping water, particularly when β_{10} reached 150 degrees. Thus, time and travel distance of seeping water would increase, which can reduce exit gradient value. The optimum value of β_9 was 30 degrees in all implemented cases. Such inclination angle can reduce uplift pressure under b_{10}. This aids to decrease the construction cost of HWRS. Furthermore, since predicting exit gradient value (using surrogate model) is based on PC_{10} value (Table B4.21), decreasing PE_{10} value by reducing β_9 value aids to reduce the exit gradient value also. Additionally, β_9 with a value less than 90 degrees contributes to reducing the exit gradient value, because small β_9 value (<90 degrees) increases seeping water stream length.

Approximately, it seems that effective and general optimum design of HWRS must include two upstream and downstream cut-offs and the width (b_{10}) between them, plus the width (b_9) on the upstream side. These widths are necessary to provide sufficient weight for the HWRS to resist the external hydrostatic loads and uplift pressure, and the width plays a vital role in the optimum design to satisfy HWRS design requirements (constraints), such as the sliding, overturning and eccentric load conditions. The downstream cut-off must have an inclination angle up to 150 degrees toward downstream. The upstream cut-off must have an inclination angle 30 degrees toward upstream.
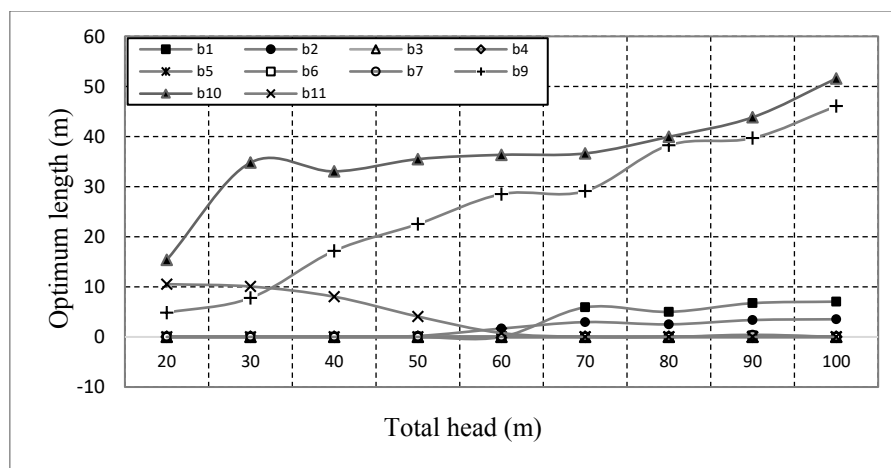
Figure 4.3 Optimum width between cut-offs of the implemented cases for different head values
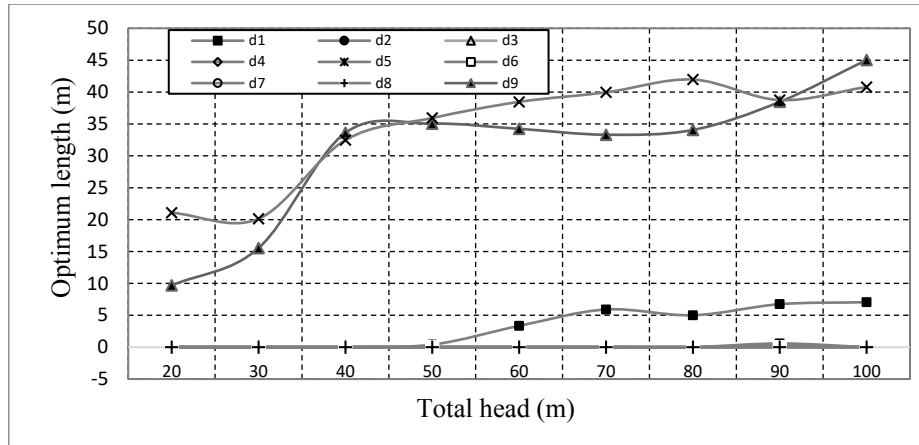
Figure 4.4 Optimum cut-off depths for the implemented cases for different head values

For the implemented cases, with high head value (> 60 m), the depth of first cut-off (d_1) makes a contribution to the optimum design of these cases (Figure 4.4). The optimization solver increased d_1 to minimize construction cost, because d_1 is effective in reducing uplift pressure at the downstream side of the HWRS and this aids to reduce the cross section of HWRS and cost of the HWRS. Also, construction cost of deep cut-offs (> 40 m) is less cost efficient (Eq. (4.20)). Therefore, the optimization solver increased the depth of the first cut-off, which is a cheaper option for optimum design of HWRS. Hence, the function of d_1 is to reduce high uplift pressure, which could not be solely faced by d_9, d_{10}, b_9 and b_{10}.

On the other hand, all the optimum solutions satisfied the safety factors and requirements of HWRS design. For all implemented cases, the optimum solution attained the minimum allowable value of the exit gradient safety factor (5), as shown in Table 4.5. This reflects the significance of the exit gradient safety factor in HWRS design and how the exit gradient safety factor affects the construction cost of HWRS because exit gradient value is mainly controlled by the depth and inclination angle of the last cut-off (d_{10}, β_{10}), which are indispensable and expensive components to reduce the exit gradient value.

Table 4.5 Safety factors for different values of H

H	Exit gradient safety factor	e value	Overturning safety factor	Sliding safety factor
100	5	36.11	1.60	1.50
90	5	31.52	1.59	1.50
80	5	28.60	1.59	1.50
70	5	24.90	1.59	1.50
60	5	22.46	1.64	1.74
50	5	20.79	1.69	1.96
40	5	19.44	1.77	2.30
30	5	19.61	1.86	3.09
20	5	10.28	1.81	2.76

The minimum allowable **e** distance was achieved for all obtained optimum solutions, as can be seen in Figure 4.5 and Table 4.5. This reflects the important contribution of this safety factor in HWRS stability and the crucial effect of this factor in attaining the optimum solution. Achieving the minimum allowable **e** value reveals that the optimization model provides a safe and cost efficient solution. The **e** value is the location of the resultant force R (Chapter Three).
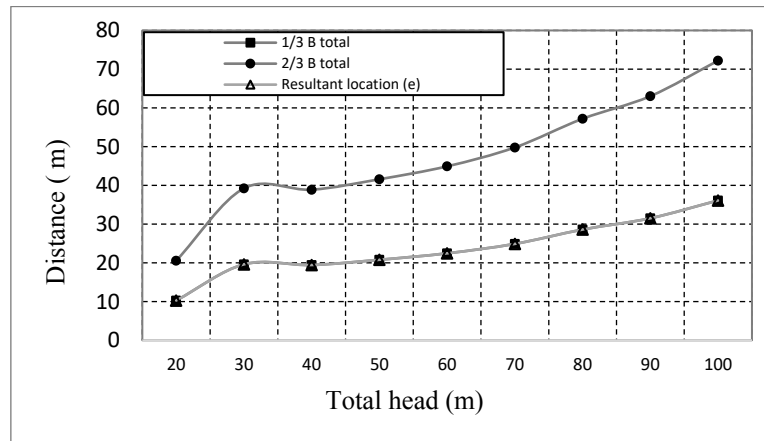
Figure 4.5 Optimum location of load resultant (R) for different values of head

Moreover, in some implemented instances (H > 60) the sliding and overturning safety factors approached the minimum allowable safety factors (Table 4.5). This refers to the extensive hydrostatic horizontal and uplift pressure created due to high upstream water head. The sliding and overturning safety factors ensure that the optimum solution satisfies, at least, the minimum allowable value of these safety factors. This could be attained by increasing the weight of the HWRS, which could be achieved by increasing the thickness and width of the HWRS floor. Hence, the HGA optimization solver based on the direct search process was efficient to satisfy safe design at minimum cost.

As clearly seen, all constraints have significant interactions and restrictions for decision variables. This means the search process for optimum solution of such a problem is complex and computationally expensive. Therefore, each run of the S-O model took approximately three hours, including the parallel computing technique based on Matlab programing language. Hence, the direct link of numerical simulation to the optimization model (if that was a case) is an inefficient method with a huge number of evaluations for the objective function and prescribed constraints.

The total construction cost curve, shown in Figure 4.6, demonstrates that construction cost increased dramatically with head augmentation. Approximately, the average construction cost per meter of upstream water head per meter width is: $24,000 for H between 10 m to 40 m, $40,000 for H between 50 m to 70 m, and $50,000 for H between 80m to 100m. This implies that construction cost of a single HWRS impounding water head (H) equal to 100 m is more expensive than constructing three HWRS

impounding H equal to 40 m. This may be attributed to the high construction cost value for deep cut-offs with large inclination angle (Eq. (4.20)) to provide a safe exit gradient for the high value of H.
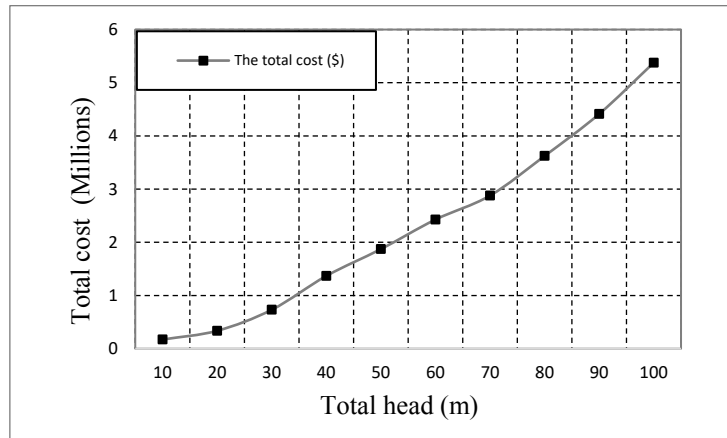
Figure 4.6 Minimum cost optimum design of HWRS for different values of head

Figure 4.6 shows optimum thickness values for different locations along the width of HWRS versus different H values. The t_{19} and $t_{20,}$ for example, represent floor thicknesses before and after cut-off S_{10}. The values of t_1 to t_{15} are not presented in the figure, because these values are approximately constant and similar to t_{16}. This is logical, considering widths (b_1 to b_8) and cut-offs depths (d_1 to d_8) between these thicknesses are almost zero (Table B4.23). Mainly, significant variation could be seen at t_{17}, t_{18}, t_{19} and t_{20}. This reflects the effects of seepage control components (cut-offs and width of the floor) at these locations in reducing uplift pressure, and the required thickness. To prevent the optimization solver from presenting inapplicable thicknesses, the minimum allowable thickness is restricted to 1 m. Therefore, for all the implemented cases, the value of t_{20} was 1 at which uplift pressure approached zero.
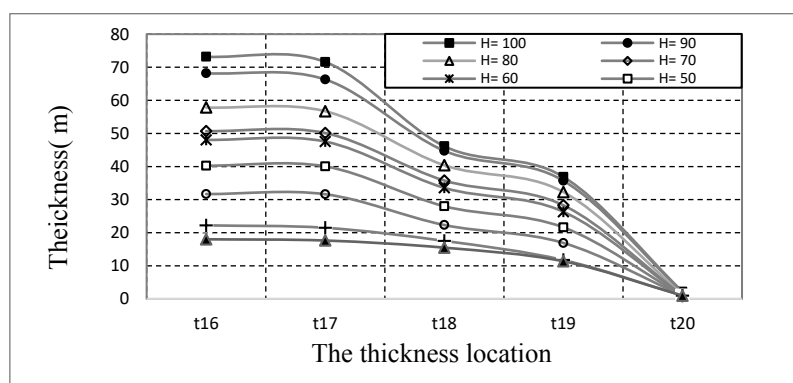
Figure 4.7 Optimum floor thickness of HWRS for different values of head

4.6.1.1 *Evaluate optimum solutions for different H*

To evaluate the accuracy of the S-O technique, the seepage characteristics of optimum solutions obtained based on the S-O model were compared to the seepage characteristics resulting from numerical

simulation of optimum solutions, which were processed as input variables for the simulation model. The results of evaluation revealed high agreement of S-O solutions with numerical solutions, as shown in Figures 4.7 to 4.12 and Table B4.24. However, there was a slight deviation for predicted uplift pressure and exit gradient values in some cases. This deviation can be attributed to weak learning of SVM for unseen or extreme data. The majority of optimum solutions included extreme values. For example, b_2 to b_8 and d_1 to d_8 values approached zero (minimum value). Also, inclination angles for S_9 and S_{10} reached 30 degrees (the minimum value) and 150 degrees (the maximum value), respectively. Although the optimum solution included extreme values, SVM models based the S-O approach precisely predicted uplift pressure and exit gradient values.

In general, for all implemented cases, average of mean absolute error (MAE) of the predicted uplift pressure was 1.01, which is acceptable for such complex problems. The MAE for predicted exit gradient values was 1.1e-3. However, few predicted exit gradient values had noticeable error. Additionally, the bar charts below demonstrate accuracy of predicted uplift pressure and exit gradient. These bar charts include 5% (+/- 2.5%) error indications. Hence, the evaluation results demonstrate the efficiency of the developed methodology in achieving optimum design of HWRS considering minimum cost and safety requirements in the design.
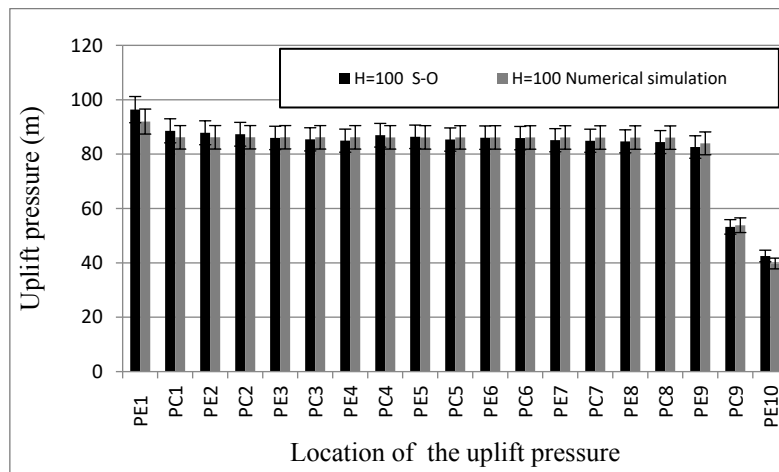
Figure 4.8 Evaluation results for different locations of uplift pressure (H=100 m)
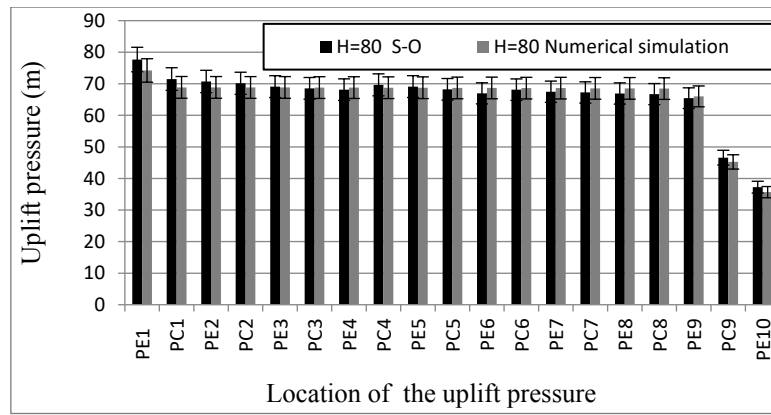
Figure 4.9 Evaluation results for different locations of uplift pressure (H=80 m)
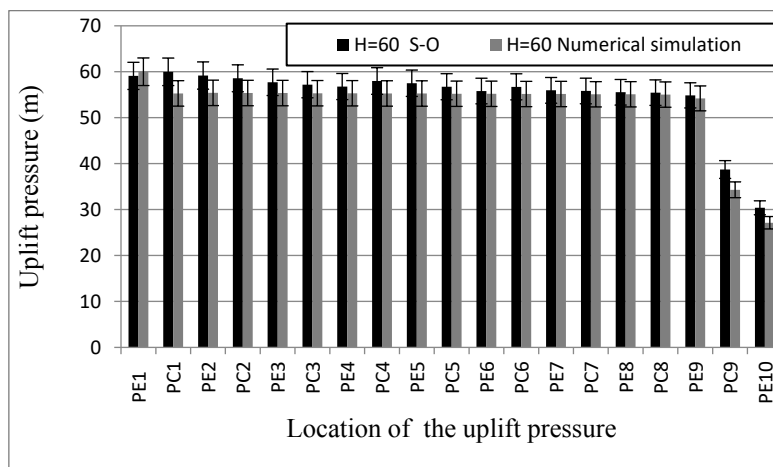
Figure 4.10 Evaluation results for different locations of uplift pressure (H=60 m)
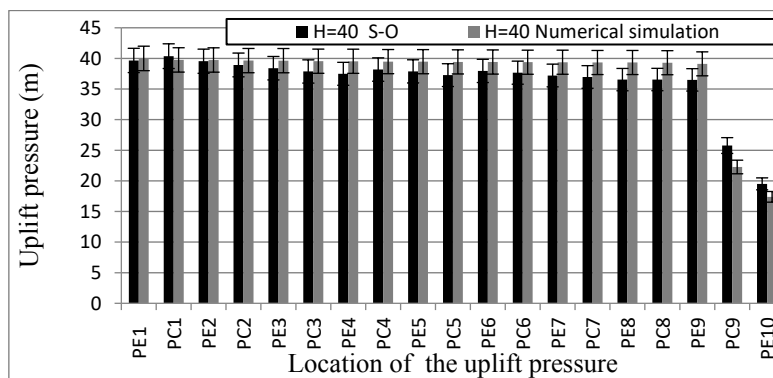
Figure 4.11 Evaluation results for different locations of uplift pressure (H=40 m)
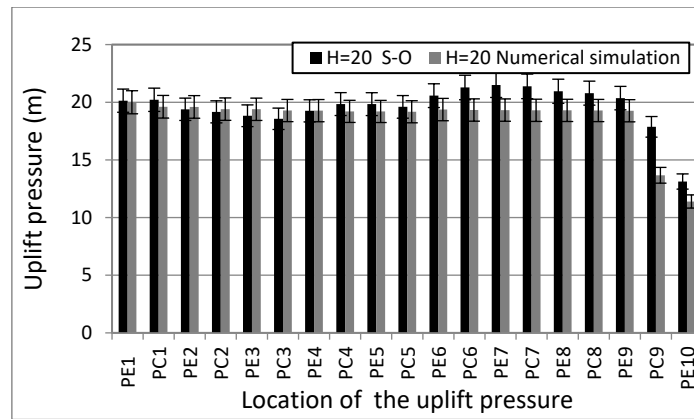
Figure 4.12 Evaluation results for different locations of uplift pressure (H=20 m)
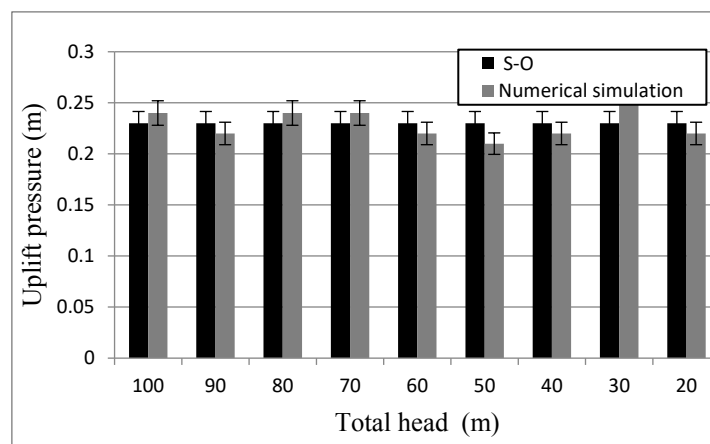
Figure 4.13 Comparison of exit gradient of the optimum design to the numerical solution

4.6.2 *Hydraulic conductivity (k_{x1}) and anisotropic ratio ($k_y/k_x)_1$ effects*

The same procedure applied to study the effects of upstream water head was implemented to quantify effects of hydraulic conductivity (k_{x1}) and anisotropic ratio ($k_y/k_x)_1$ of the first layer. The first layer is the nearest layer to the foundation of HWRS (Figure 4.1), and soil parameters of this layer are expected to significantly influence seepage characteristics. The effect of ($k_y/k_x)_1$ was studied by assuming eight different values ranging from 0.1 to 1.5. Ten different values of k_{x1} ranging from 0.01 m/day to 20 m/day were specified and processed using the S-O technique. The value of other design variables and parameters were left constant. For example, k_x and (k_y/k_x) of the second and third layers were 5 m/day and 1, respectively. The upstream head, i.e. H, value was 50 m and depth of the three layers equaled 50 m. Other variables were considered the decision variables to be obtained by the optimization solver as an optimum solution for each implemented case.

Generally, obtained optimum solutions revealed that increase of ($k_y)_1$ and ($k_y/k_y)_1$ ratio significantly decreased total cost of HWRS, as shown in Figures 4.13 and 4.14. The reason for this is when k_{x1} increases with the constant anisotropic ratio (($k_y/k_x)_1 = 1$), seeping water can move easily from

the high pressure zone (upstream) to the low pressure zone (downstream). Consequently, pore-water pressure underneath HWRS and exit gradient values decrease. Thus, deep cut-offs and significant width between cut-offs are not needed.

Similarly, when the anisotropic ratio $(k_y/k_x)_1$ is large with specified hydraulic conductivity (k_{x1} = 5), the seeping water motion in the vertical direction becomes faster and the exit gradient value becomes smaller compared to the exit gradient value obtained for small values of $(k_y/k_x)_1$ ratio. Hence, for high values of $(kx)_1$ and $(k_y/k_x)_1$, the optimum value of d_9, d_{10}, b_9 and b_{10}, which are the most effective variables, decreased and consequently the optimal cost declined.
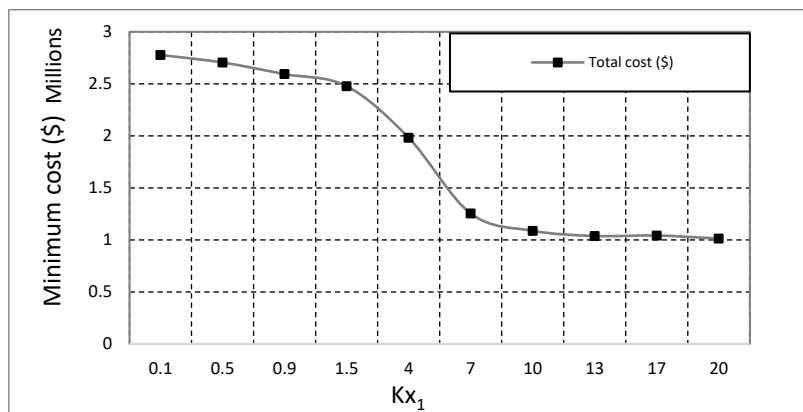
Figure 4.14 Minimum cost for optimum design of HWRS for different values of k_{x1}
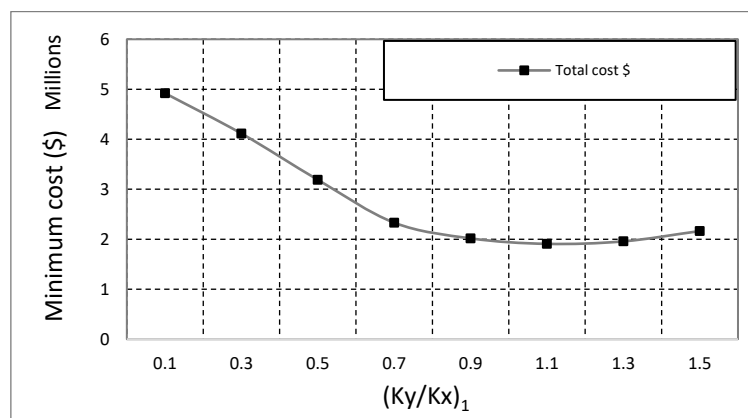
Figure 4.15 Minimum cost for optimum design of HWRS for different values of $(k_y/k_x)_1$

Low anisotropic ratios (0.1 to 0.6) drastically increased the construction cost, as shown in Figure 4.14. The reason is that optimum values of d_9, d_{10}, b_9 and b_{10}, β_9, β_{10} were relatively large to counterbalance the effect of high uplift pressure, satisfy design safety factors and yield a safe exit gradient value (< 0.23). Also, for the same reasons, there was a large optimum construction cost for low k_{x1} values ranging between 0.01 m/day and 4 m/day.

For the $(k_y/k_x)_1 > 1$ and $k_{x1} > 5$ m/day, the optimum solutions and design variables were approximately the same and construction cost was almost at the same level. One possible reason for

this outcome with the example problems presented here, is that soil properties of the second and third layers have more influence on seepage characteristics than the first layer, as they have smaller $(k_y/k_x)_1$ and k_{x1} values than values of $(k_y/k_x)_1$ and k_{x1} for the first layer. Hence, the seepage characteristics did not change with variation in hydraulic conductivity; therefore, the optimum solution was almost same. This results in a more or less constant construction cost with varied soil properties of the first layer and constant soil properties of the second and third layers.

The resulting optimum design of HWRS for the implemented cases satisfied all safety factors and design requirements. For small values of $(k_y/k_x)_1$ and k_{x1}, the exit gradient safety factor and safe eccentric distance played a crucial role in the optimum solution, compared to other safety factors. This is evident as these safety factors reached the maximum or minimum allowable limit to satisfy design requirements, while the optimum design attained minimum construction cost. Tables 4.6, 4.7 and Figures 4.15, 4.16 demonstrate the safety factor variations for different values of $(k_y/k_x)_1$ and k_{x1}, respectively. However, with augmentation of k_{x1} and $(k_y/k_x)_1$, exit gradient and eccentric distance had less impact on safety factors in the optimum solutions. Consequently, the sliding and overturning safety factor approached the minimum allowable limits and had more influence with increasing $(k_y/k_x)_1$ and k_{x1} values. The reason is that the seepage characteristic decreases with an increase in $(k_y/k_x)_1$ and k_{x1} values, and that aids to satisfy the minimum allowable limits of all safety factors.

Table 4.6 Safety factors for the implemented cases for different k_{x1}

k_{x1}	Exit gradient safety factor	e value	Overturning safety factor	Sliding safety factor
0.10	5.00	28.75	1.83	2.38
0.50	5.00	27.95	1.82	2.33
0.90	5.00	27.17	1.81	2.30
1.50	5.00	25.94	1.79	2.25
4.00	5.00	21.84	1.72	2.04
7.00	5.00	19.39	1.61	1.50
10.00	5.00	19.11	1.59	1.50
13.00	5.00	19.37	1.59	1.50
17.00	5.00	20.02	1.60	1.50
20.00	5.00	21.01	1.61	1.50
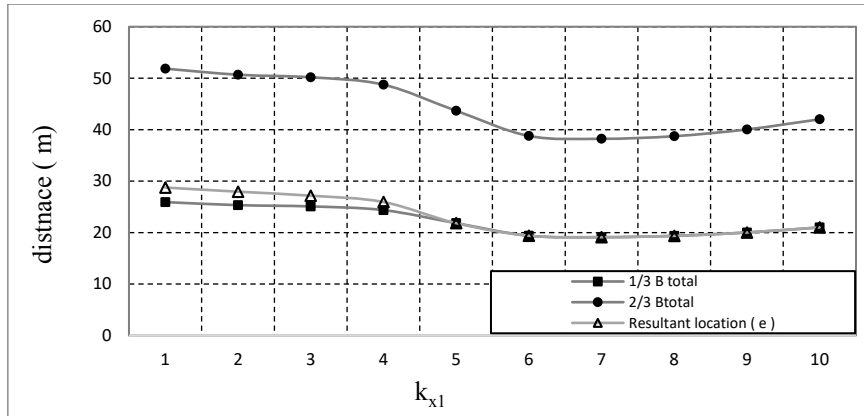
Figure 4.16 Resultant(R) location for different values k_{x1}

Table 4.7 Safety factors for the implemented cases for different $(k_y/k_x)_1$

$(k_y/k_x)_1$	Exit gradient safety factor	e value	Overturning safety factor	Sliding safety factor
0.1	5.0	91.4	2.0	6.5
0.3	5.0	64.1	1.9	5.7
0.5	5.0	41.7	1.9	3.8
0.7	5.0	23.9	1.8	2.2
0.9	5.0	22.7	1.7	2.1
1.1	5.0	22.3	1.7	2.0
1.3	5.0	22.1	1.7	2.1
1.5	5.0	23.7	1.8	2.2
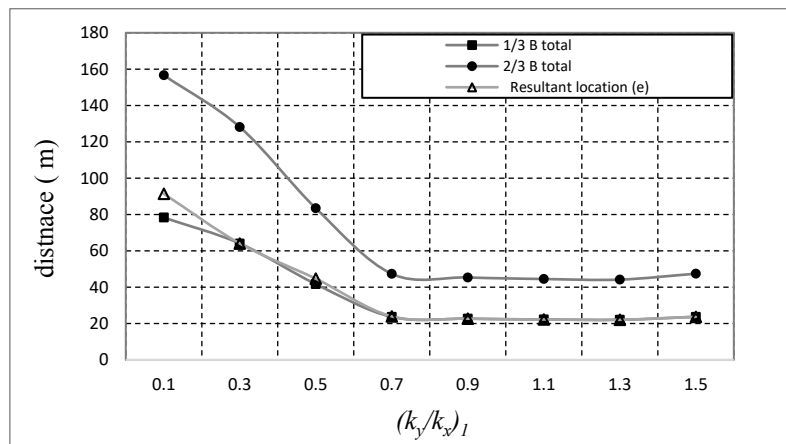
Figure 4.17 Resultant (R) location for different $(k_y/k_x)_1$ values

The S-O results demonstrated that the contribution of b_1 to b_8 and d_1 to d_8 to the safety of HWRS was insignificant, because the optimum value of those variables approached zero, as shown in Figures 4.17 and 4.18. Therefore, inclination angles (β_1, β_2, … β_8) were negligible because they are related d_1 to d_8. Optimum solutions for HWRS were based on increasing the value of b_9 and b_{10} to counterbalance the uplift pressure values, and based on augmenting d_9, d_{10} and β_{10} to decrease the exit gradient value.

Also, there is a significant contribution for d_9 associated with the minimum value of β_9 to decrease uplift pressure beneath b_{10}, which represents a large portion of the HWRS floor.

Additionally, the optimization solver particularly increased d_{10} and β_{10} values to satisfy the safe exit gradient value, even it is a more expensive option (Eq. 4.20). These variables were more effective at reducing exit gradient value, which is the most critical safety factor. Also, increasing these values, particularly provides an effective and minimum cost alternative. Augmentations of these values lengthened the seeping water stream line; consequently, the exit gradient value particularly, and other seepage characteristics were decreased. Hence, the optimum value of β_{10} equalled 150 degrees, which is the maximum specified limit for this variable. For the same reason, the inclination angle of cut-offs at upstream (β_9) approached the minimum allowable limit (30 degrees) for all implemented cases, as shown in Tables B4.25 and B4.27.

Simultaneously, to corroborate stability of HWRS and satisfy related safety factors, the required optimum width of HWRS was provided by b_9 and b_{10}. Furthermore, the uplift pressure on the downstream side decreased with total width augmentation, contributing to reducing the exit gradient value. Therefore, the values of b_9 and b_{10} mainly provide an efficient cross section and weight to resist external loads and uplift pressure, and partially reduce the uplift pressure and exit gradient value.
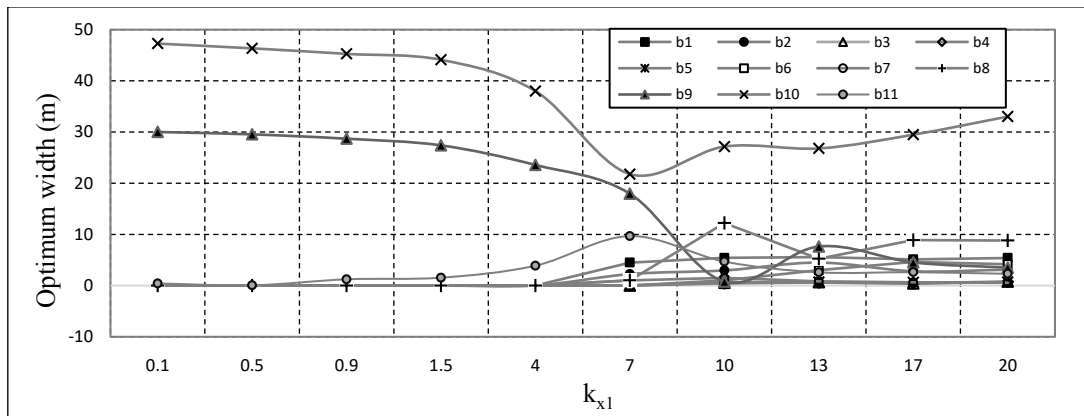
Figure 4.18 Optimum width between cut-offs of HWRS for different values k_{x1}
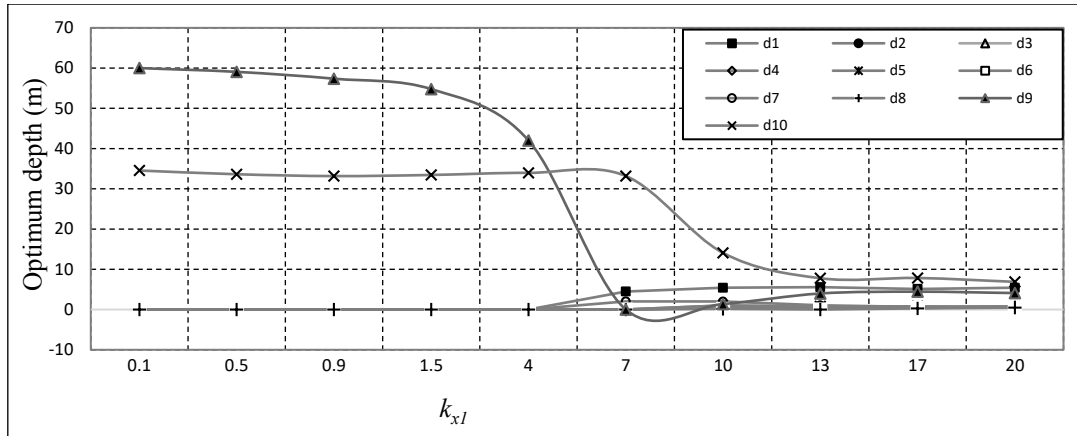
Figure 4.19 Optimum cut-off depths of HWRS for different values k_{x1}
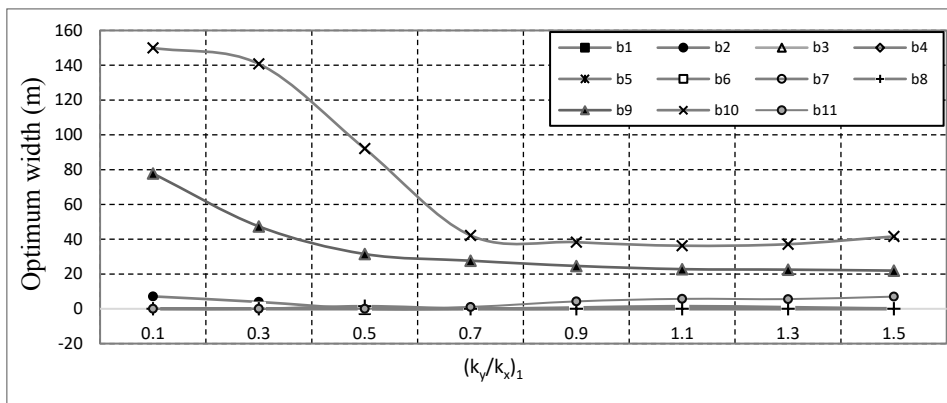
Figure 4.20 Optimum width between cut-offs of HWRS for different values $(k_y/k_x)_1$
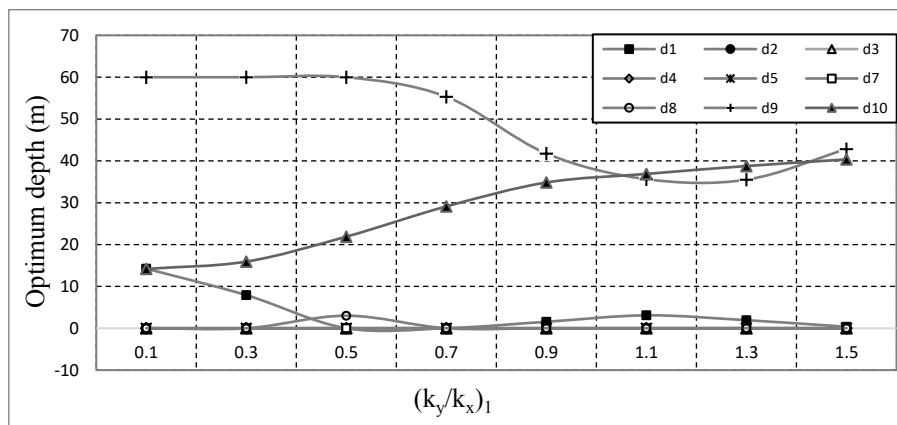
Figure 4.21 Optimum cut-off depths for different values $(k_y/k_x)_1$

For small value of ky/ky, which results in high uplift pressure and high exit gradient value, the optimization solver provided a depth for the upstream cut-off (S1) (Figure 4.20) to reduce the effect of uplift pressure. This value with the provided d_9, d_{10}, b_9 and b_{10} can provide a safe and minimum cost design.

In a few cases, including high value k_{x1}, the value of d_9, d_{10} declined and the value of d_1 increased, as shown in Figure 4.18. For these cases, the exit gradient safety factor became less controllable and the optimization solver searched for a cheaper alternative. Therefore, the optimization solver decreased the more costly and significant depth of d_9, d_{10} and slightly increased the depth of d_1. This solution provides the most cost efficient and safe HWRS design.

4.6.2.1 *Evaluate optimum solutions for different values of $(k_y/k_x)_1$ and k_{x1}*

The same procedure utilized to evaluate optimum solutions of the implemented cases with different head values was used to evaluate optimum solutions resulting due to the variation of k_{x1} and $(k_y/k_x)_1$ values. The evaluations demonstrated that the developed surrogate models based on the SVM technique within the S-O model provided accurate predictions of seepage characteristics for the optimum solutions located within the training range. However, prediction accuracy of surrogate models was slightly less for a few extreme optimum solutions (out of training ranges). In general, maximum error percentages of predicted seepage characteristics compared to numerical seepage simulation solutions were less than ±10 %. The MAE of predicted uplift pressure at specified locations compared to numerical solutions for different values of $(k_y/k_x)_1$ and k_{x1} is presented in Tables 4.7 and 4.8. Also, the MEA for exit gradient value of implemented cases with different values of k_{x1} was (0.0272) and was (0.0386) for the implemented cases with different values of $(k_y/k_x)_1$. However, there were slight deviations for a few cases in predicted exit gradient values compared to the numerical solutions (Figures 4.39 and 4.40), which may be attributed to imprecise learning of the exit gradient surrogate model for out of training data sets.

In general, performance of the utilized surrogate models within the S-O model was within acceptable ranges. The predicted uplift pressure and exit gradient values for these cases were precise and within safe limits. Also, the evaluation process demonstrates that the SVM technique can be used to develop accurate and efficient surrogate models for complex problems, including many design variables. Some evaluation results are represented in Figures 4.22 to 4.41, including five (±2.5%) percentage error.

Table 4.8 Mean absolute error for predicted uplift pressure at specified locations of HWRS for different $(k_x)_1$

k_{x1}	0.01	0.05	0.1	0.2	0.3	0.4	0.5	0.6	0.7	0.8	0.9	1	2	4	6	8	10
MAE (m)	5.39	5.18	5.39	5.22	5.33	4.44	4.89	3.07	4.66	4.47	3.86	3.70	2.43	2.18	1.14	3.38	2.61

Table 4.9 Mean absolute error for predicted uplift pressure at specified locations of HWRS for different $(k_y/k_x)_1$

$(k_y/k_x)_1$	0.1	0.2	0.3	0.4	0.6	0.8	1	1.2	1.4	1.5
MAE(m)	0.74	5.85	5.37	2.03	2.28	2.25	1.71	0.62	0.80	2.27
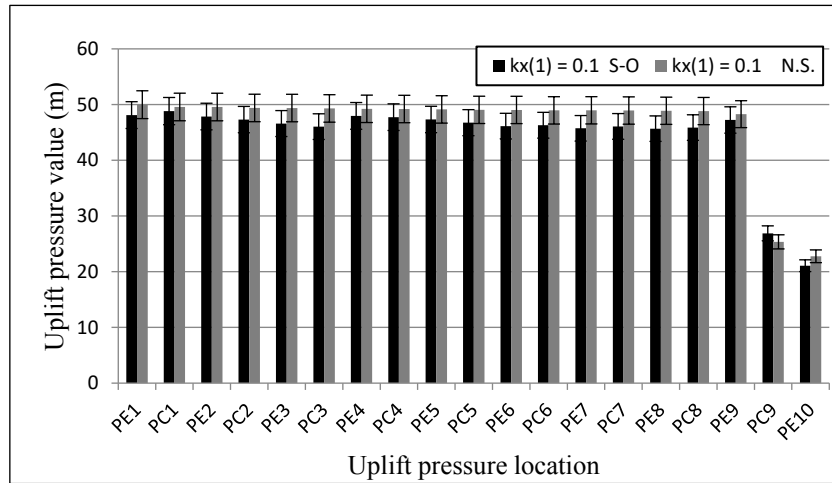
Figure 4.22 Evaluation results for different locations of uplift pressure (k_{x1}=0.1 m/day)

* N.S. =Numerical solutions (SEEPW)
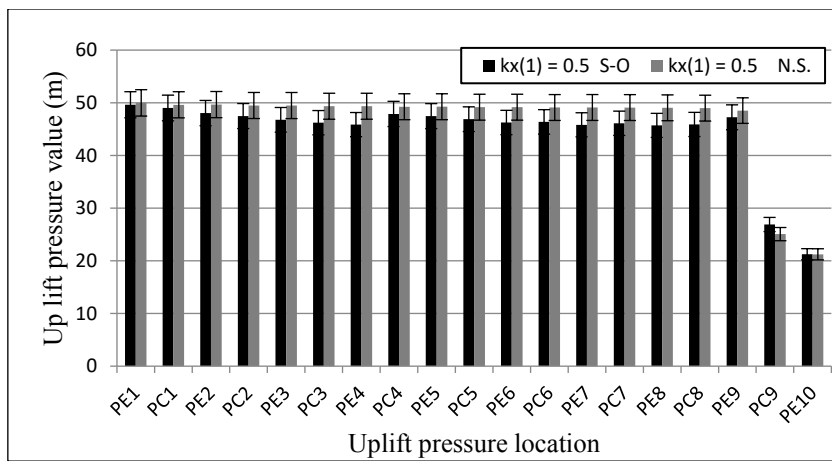
Figure 4.23 Evaluation results for different locations of uplift pressure (k_{x1}=0.1 m/day)
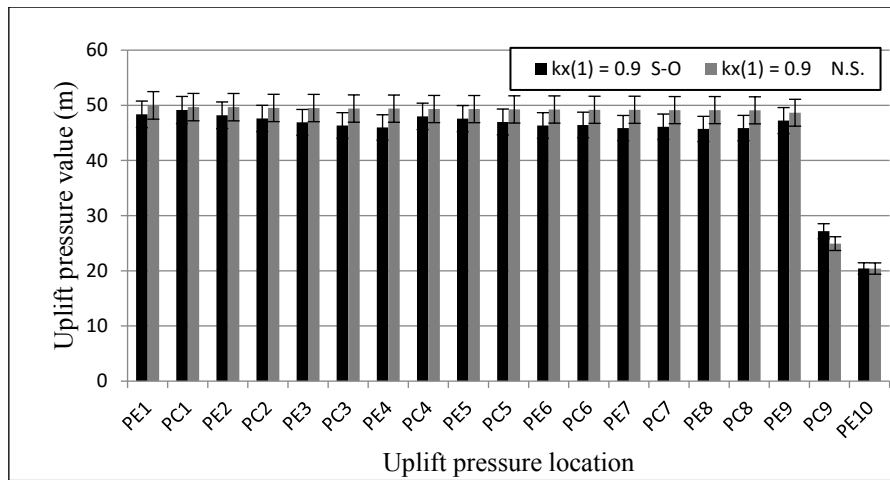
Figure 4.24 Evaluation results for different locations of uplift pressure (k_{x1}=0.1 m/day)
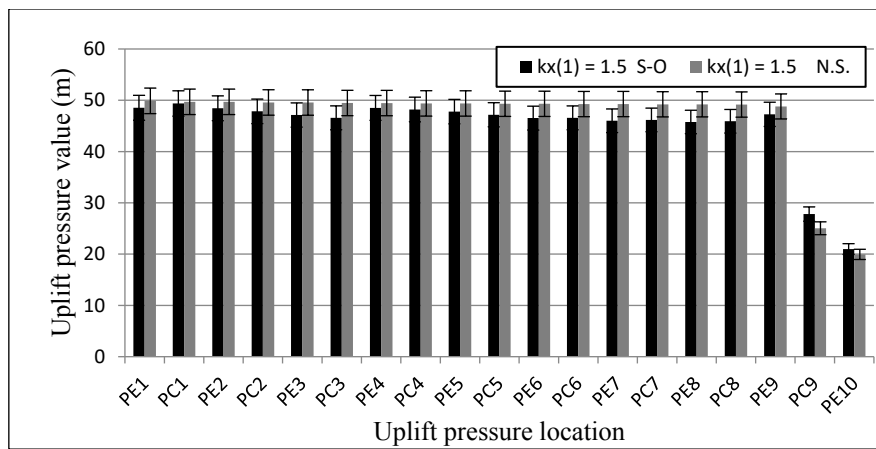
Figure 4.25 Evaluation results for different locations of uplift pressure (k_{x1}=0.1 m/day)
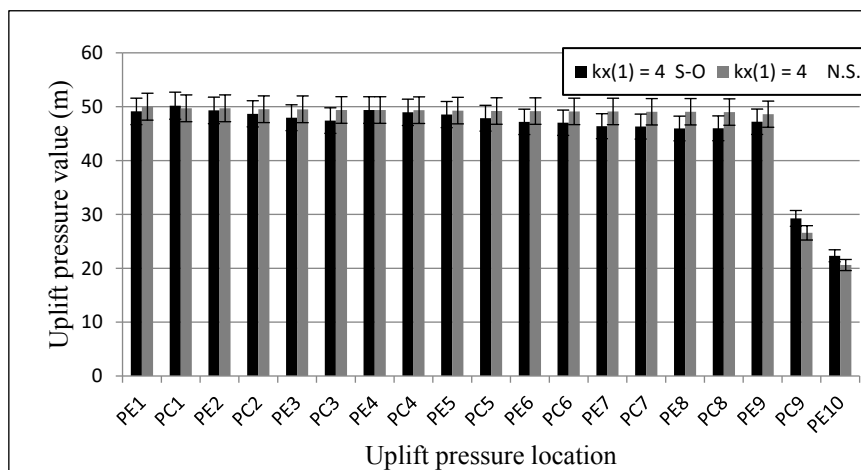
Figure 4.26 Evaluation results for different locations of uplift pressure (k_{x1}=0.1 m/day)
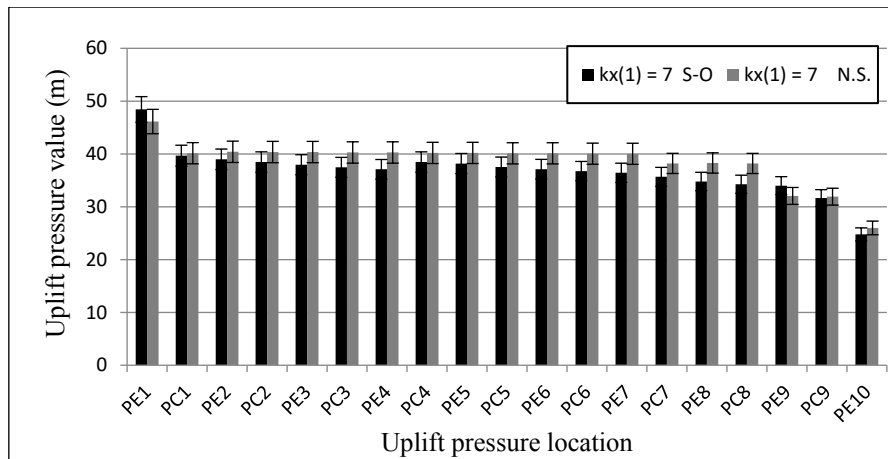
Figure 4.27 Evaluation results for different locations of uplift pressure (k_{x1}=0.1 m/day)
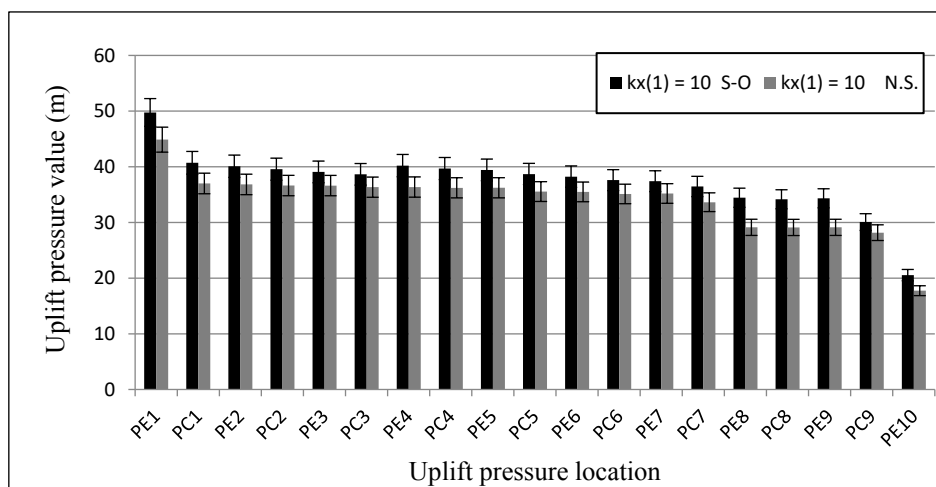
Figure 4.28 Evaluation results for different locations of uplift pressure (k_{x1}=0.1 m/day)
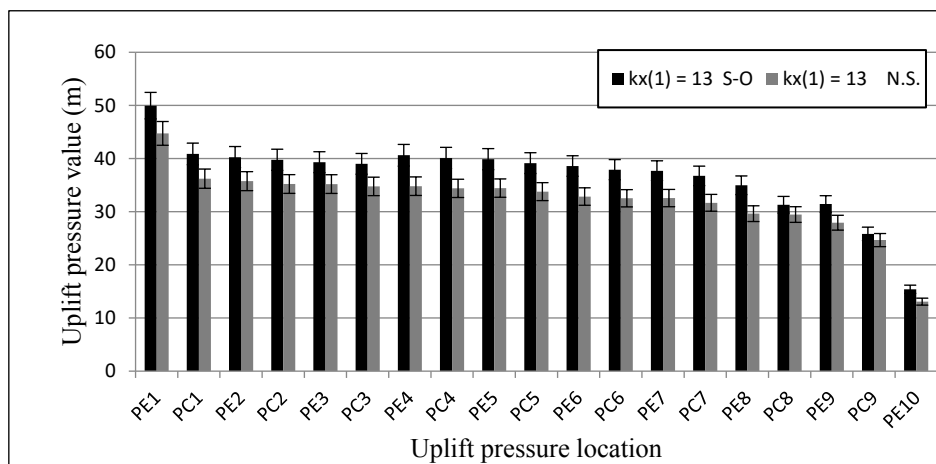
Figure 4.29 Evaluation results for different locations of uplift pressure (k_{x1}=0.1 m/day)
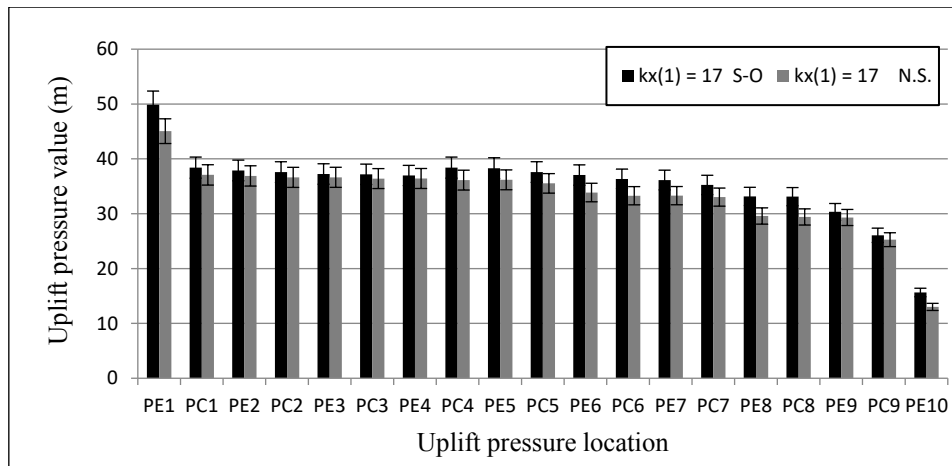
Figure 4.30 Evaluation results for different locations of uplift pressure (k_{x1}=0.1 m/day)
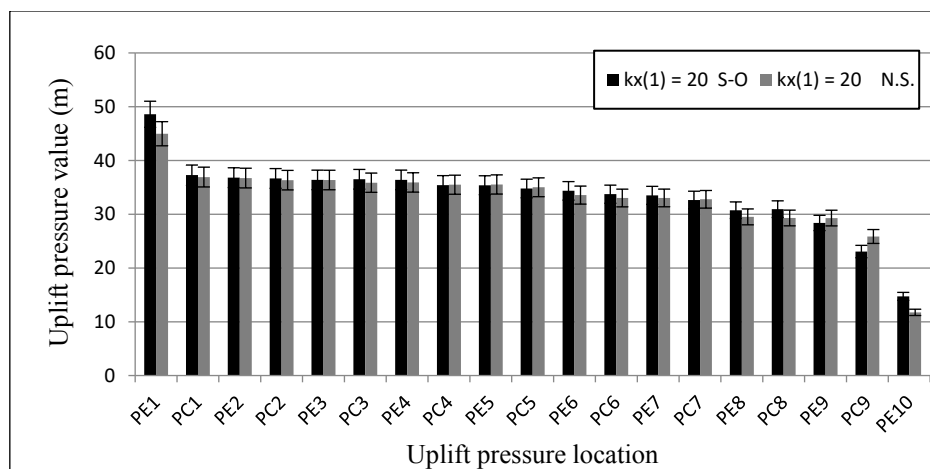
Figure 4.31 Evaluation results for different locations of uplift pressure (k_{x1}=0.1 m/day)
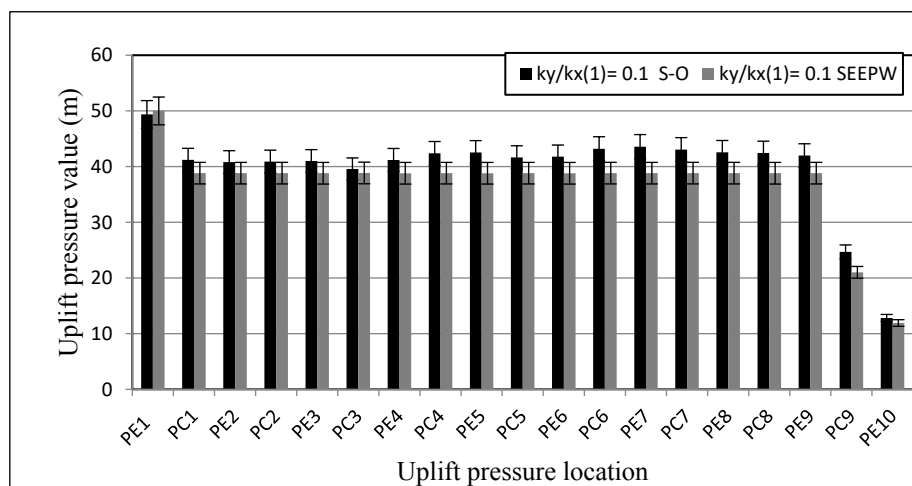
Figure 4.32 Evaluation results for different locations of uplift pressure (($k_y/k_x)_1$=0.1)

90
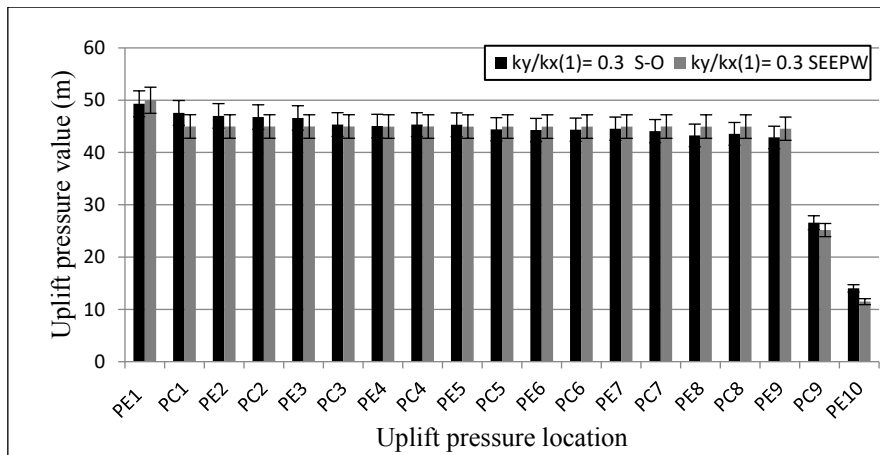
Figure 4.33 Evaluation results for different locations of uplift pressure ($(k_y/k_x)_1=0.3$)
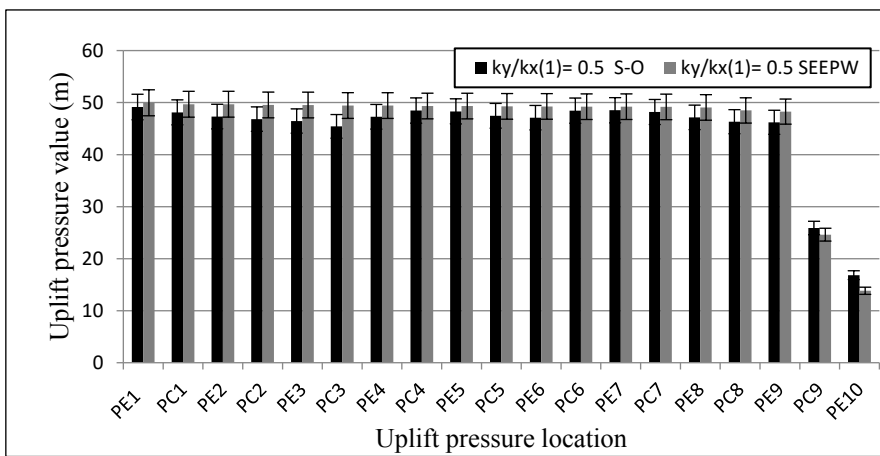
Figure 4.34 Evaluation results for different locations of uplift pressure ($(k_y/k_x)_1=0.5$)
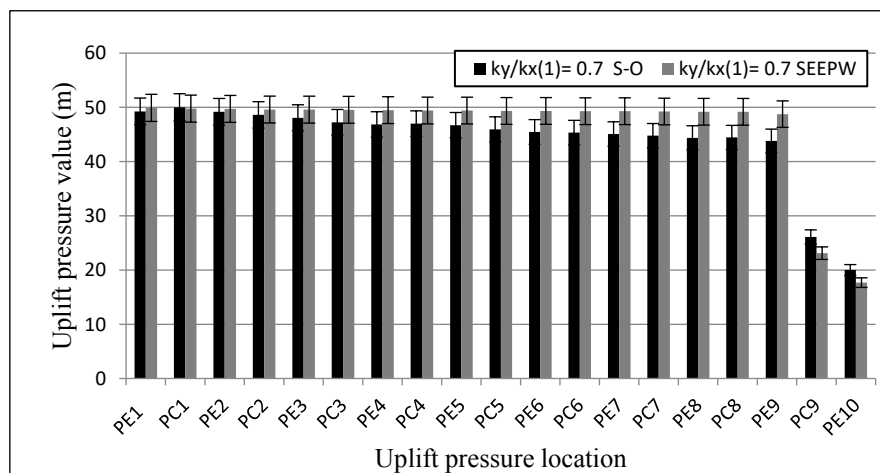
Figure 4.35 Evaluation results for different locations of uplift pressure ($(k_y/k_x)_1=0.7$)
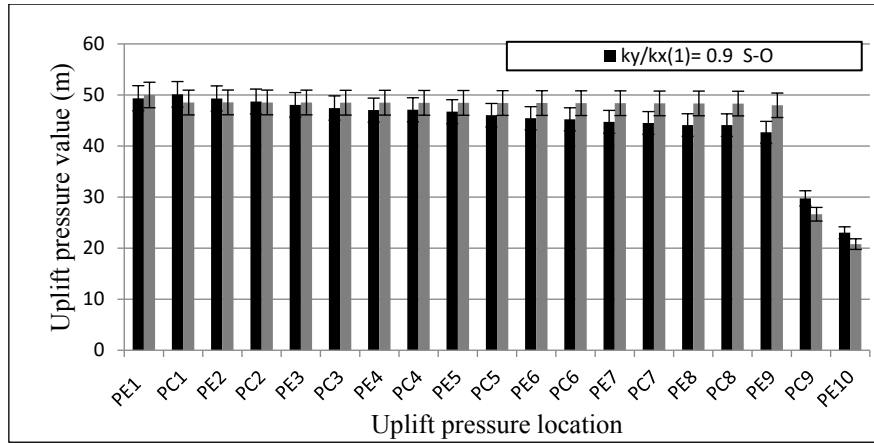
Figure 4.36 Evaluation results for different locations of uplift pressure ((k_y/k_x)$_1$=0.9)
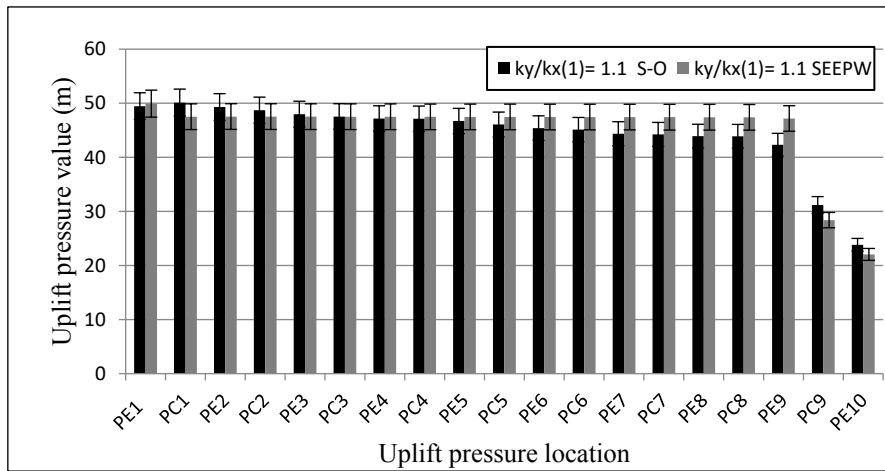
Figure 4.37 Evaluation results for different locations of the uplift pressure ((k_y/k_x)$_1$=1.1)
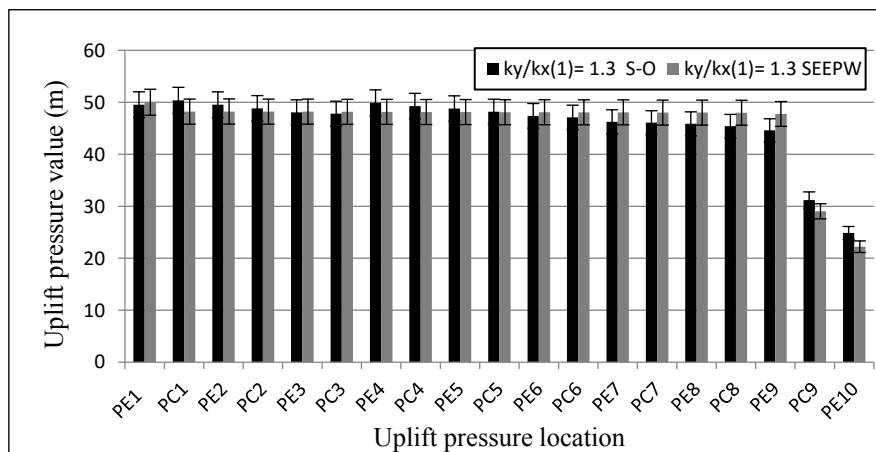
Figure 4.38 Evaluation results for different locations of uplift pressure ((k_y/k_x)$_1$=1.3)
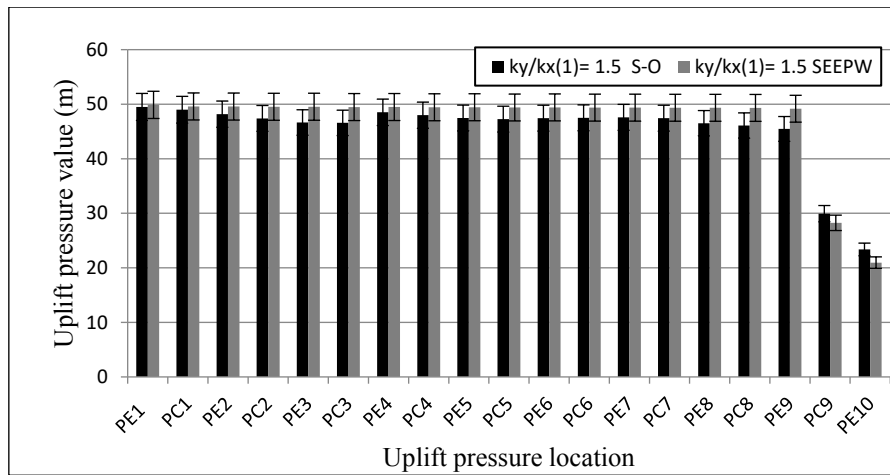
Figure 4.39 Evaluation results for different locations of uplift pressure ((k$_y$/k$_x$)$_1$=1.5)
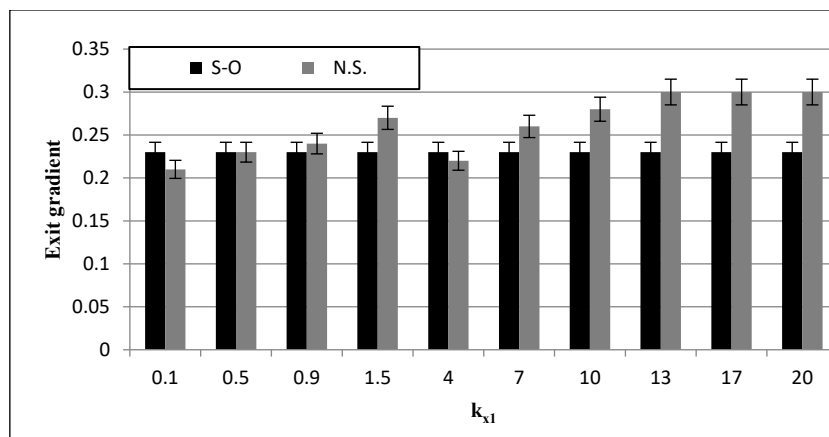
Figure 4.40 Exit gradient evaluation results for different values of (k_{x1})
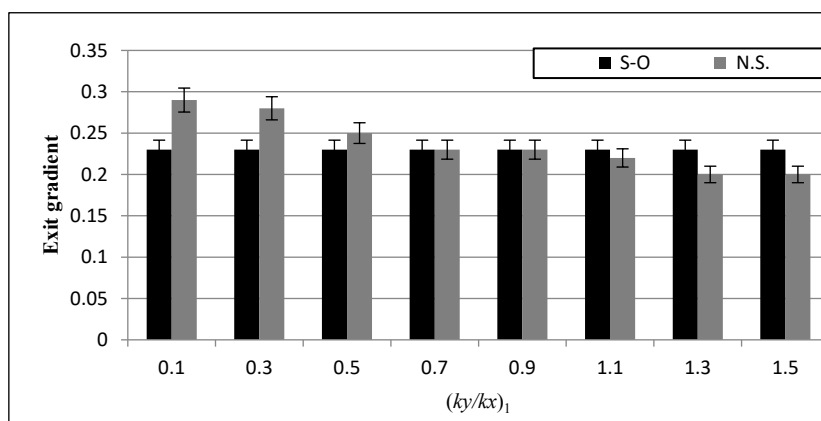
Figure 4.41 Exit gradient evaluation results for different values of (k$_y$/k$_x$)$_1$

4.7   Conclusion

In this chapter, the S-O methodology was successfully applied to study the effects of design parameters and variables, such as hydraulic conductivity and upstream head, on the optimum design of

HWRS. Also, this chapter focuses on identifying the most effective and optimum design variable combination to produce an efficient optimum design of HWRS.

Twenty one ensemble surrogate models were developed based on the SVM technique utilizing 1,500 numerically simulated data sets. The simulated data was generated based on a comprehensive conceptual model including many cut-offs, many widths between cut-offs and varied inclination angle for each cut-off. Before training the surrogate models, variable importance analysis was implemented using beta standardized coefficient and random forest techniques. This significantly decreased the number of the incorporated input variables related to each seepage characteristic. Hence, expeditious and accurate surrogate models were developed. These surrogate models were successfully linked to the HGA. Based on the surrogate model responses, HGA evaluated the objective function and constraints, which represent the design requirements and safety factors related to HWRS.

In general, the obtained optimum solution of the implemented cases demonstrated that there were many unnecessary design variables, such as b_1 to b_8, d_1 to d_8 and related inclination angles. This means that the optimum solution for most implemented cases must include upstream and downstream cut-offs, upstream apron (width) b_9 and an apron (b_{10}) between cut-offs. The optimum inclination angle for the upstream cut-offs was 30 degrees and for downstream cut-offs was 150 degrees. For some cases classified as a critical cases, such as when upstream water head reaches 60m or more, or when $(k_y/k_x)_1$ ratio approaches 0.5 or less, the optimum solution must include a depth (d_1) for the first cut-offs.

Deep cut-offs downstream significantly reduced exit gradient value, especially when the inclination angle was more than 90 degrees. In contrast, the upstream cut-offs were adequate in decreasing uplift pressure, especially when the inclination angle was less than 90 degrees. The widths (b_9 +b_{10}) were necessary to provide a sufficient weight for the HWRS to resist external hydrostatic loads and uplift pressure. Also, these widths played a vital role in optimum design to satisfy HWRS design requirements (constraints), such as sliding, floatation, overturning and eccentric load conditions.

All design requirements and safety factors were satisfied for all implemented cases. Exit gradient value was the most critical seepage design variable significantly affecting the obtained optimum solution. The minimum allowable value of the exit gradient safety factor was achieved for all implemented cases. This reflects the significance of the exit gradient value. For the same reason, the eccentric load condition had a crucial role in the obtained optimum solutions.

High upstream water head significantly increased construction cost. Construction cost (per meter of water head) for small HWRS is cheaper than construction cost of HWRS with a high water head. On the other hand, the effect of hydraulic conductivity on optimum design of HWRS was significant. Low hydraulic conductivity and anisotropic ratio substantially augmented minimum construction cost.

The evaluation process for S-O methodology demonstrated that the obtained optimum solutions (designs) of HWRS were the most efficient solutions because all design safety factors and conditions were satisfied. Furthermore, optimum cost (objective function) was rationally varied with variation of upstream water head, k_{x1}, $(k_y/k_x)_1$ values. Additionally, the evaluation results demonstrated that the SVM technique can be used to develop accurate and efficient surrogate models for complex problems. The HGA optimization solver based on the direct search process was efficient to satisfy safe design at minimum cost. Finally, the linked S-O approach is considered an adequate technique to attain the optimum solution for complex problems related to design of HWRS incorporating the seepage characteristic effects in the obtained optimum design.

The next chapter focuses on hybridizing the genetic algorithm (GA) to the interior point algorithm (IPA) to improve performance of the optimization solver based the coupled S-O model. The advantages of using HGA are discussed and applied to a few illustrative problems presented in Chapter Five.

5 Global Optimum Hydraulic Design of Hydraulic Water Retaining Structures Constructed On Anisotropic Permeable Soil Utilizing Interior Point Algorithm Based Hybrid Genetic Algorithm

A similar version of this chapter is under review for publication in the ISH Journal of Hydraulic Engineering as shown below:

Al-Juboori, Muqdad, and Datta, Bithin (2018) *Optimum hydraulic design of concrete gravity dams founded on anisotropic soils: utilizing interior point algorithm based hybrid genetic algorithm*. ISH Journal of Hydraulic Engineering, <u>Under Review.</u>

5.1 Introduction

This chapter is a continuation of Chapter Four. Similar surrogate models, methods and the same formulation of the optimization model mentioned in Chapter Four were utilized in this chapter. However, this chapter focuses on improving performance of the genetic algorithm (GA) optimization solver based on the linked simulation-optimization (S-O) approach to improve the possibility of obtaining a global optimum solution.

Due to complexity of the optimization model, including many surrogate models and constraints incorporated in linked S-O models, attaining the global optimum solution for such problems based on the GA is difficult. Hence, GA based on the direct search technique is hybridized with the interior point algorithm (IPA) based on the gradient search technique to find the global optimum solution. The hybrid genetic algorithm (HGA) optimization solver based the linked S-O technique was utilized to find the optimum design of the comprehensive model of HWRS constructed on anisotropic soils. The optimization model minimizes construction cost and provides safe HWRS design.

The optimization task, which involves a large number of decision variables and constraints, is based on SVM-surrogate model responses and is considered a complex task. Therefore, a powerful optimization solver must be used to find the global optimum solution. One of the most prominent direct search optimization solvers is GA, which is an evolutionary solver and effective for complex optimum decision problems. However, for such complex problems, GA performance may deteriorate, decreasing the possibility of identifying a global optimal solution (Kolda, Lewis, & Torczon, 2003). Hence, this study focuses on improving GA performance to attain the global optimum design for HWRS constructed on permeable anisotropic soils. The proposed procedure involves hybridizing the GA based direct search technique with a gradient search algorithm, such as the IPA. Efficiency of HGA is tested by incorporating HGA in the linked S-O approach to find the optimum design of HWRS involving the

effect of anisotropic hydraulic conductivity and related seepage characteristics. Furthermore, this study compares performance of HGA with performance of standard GA and standard IPA when they are applied separately. In the following section, the developed methodology is described and obtained results based on different algorithms are discussed.

5.2 Seepage conceptual model and data generation

The conceptual model includes all relevant parameters and design variables which may affect HWRS design. As a result, hydraulic effects of each parameter on seepage characteristics could be determined. Generated data, the conceptual model and the design variables are the same as those utilized in Chapter Four. However, the properties of the flow domain are different. Hydraulic conductivity is considered the same for the entire flow domain, as shown in Figure 5.1. This means that there is no stratification in the flow domain and there is a single value of hydraulic conductivity (k_x) and anisotropic ratio (k_y/k_x) for the entire flow domain. Utilized surrogate models in Chapter Four could be used in this study with minimal modification, considering the new adjustment of hydraulic conductivity. Based on the surrogate model responses, the optimization model within the S-O approach could select the most important variables, which provide a safe and the most cost-efficient construction design.
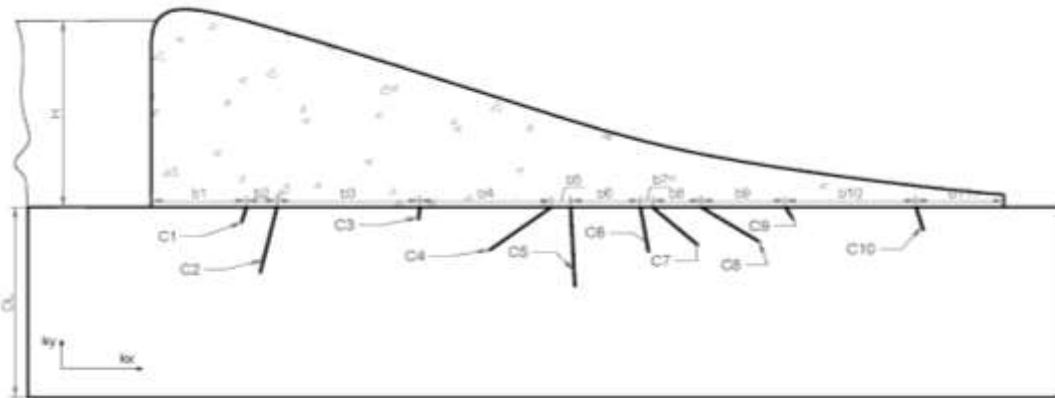
Figure 5.1 Conceptual seepage model

5.3 Support vector machine surrogate model

The support vector machine (SVM) surrogate models developed in Chapter Four were utilized to predict the seepage responses within the optimization model (see section 4.4). Matlab programing language was utilized to develop SVM models. Fifteen hundred scenarios of numerically simulated data were used to train SVM models. Twenty one ensemble surrogate models were built to determine uplift pressure (PEi, PCi) in front and behind each cut-off, and the exit gradient near the toe of the HWRS.

5.4 Optimization model

5.4.1 Interior point algorithm (primal-dual):

The interior point algorithm (IPA) can be used to solve constrained linear and nonlinear optimization problems involving inequality constraints. The IPA is profoundly and quickly able to find an optimum solution, even for large scale problems (Lesaja, 2009; Liu, Tso, & Cheng, 2002; Mulligan & Ahlfeld, 2002). IPA processes many iterations to find the optimal solution from the (pre-defined) interior point located in the feasible region of the search space.

Concisely, to understand the process of IPA, formulation of the optimization problem must be transferred from the general (primal) form to the standard form (dual), as shown in Table 5.3. Each inequality constraint, i.e., g (x), is converted to an equality constraint by adding a slake variable (s_i). Also, a new inequality constraint ($s_i \geq 0$) is assumed to ensure the slack variable is not less than zero to satisfy the original inequality constraints (Parkinson, Balling, & Hedengren, 2013). The new and original equality constraints are converted to standard form sets of equality constraints (c (x) = 0).

Table 5.1 Formulation for the interior point algorithm

General form	Standard form	Barrier function form
Objective function $$min_{x \in R^n} \quad f(x)$$ Inequality constraint $$g_i(\text{x}) \geq b \quad i = 1, 2, \dots, \text{m}$$ or $$g_i(\text{x}) - \text{b} - s_i = 0 \quad i = 1, 2, \dots, \text{m}$$ $s_i \geq 0$ (support inequality constraint) Equality constraint $$h_j(\text{x}) = 0 \quad j = \text{m} + 1, \dots, \text{k}$$	$$min_{x \in R^n} \quad f(x)$$ *s.t.* $$c(\text{x}) = 0$$ $$x_i \geq 0$$	$$min_{x \in R^n} \quad f = f(x) - \mu \sum_{i=1}^{m} \ln(x_i)$$ *s.t.* $$c(\text{x}) = 0$$

In the second step, the original and slack variables inequality constraints ($x_i \geq 0$) are involved in a barrier function and embedded as a part of the objective function. The barrier function must be defined in the second derivative. The logarithmic function, shown in Table 5.3, ensures attaining a positive value of x_i, which has the same action as the inequality constraint. The term of the barrier function goes to (+) infinity when x_i approaches zero from the positive side, i.e., from the feasible region. Additionally, as the objective function minimizes the μ value, the barrier term becomes steeper and sharper (Parkinson et al., 2013). This could guarantee that the x_i value becomes a positive value and the IPA searches in the feasible space. Also, for a small μ value there is a critical barrier at zero. Hence, the IPA avoids breaching this barrier because the potential optimal (or sub-optimal) solution for IPA is inside the locale search space and it is demanding for IPA to move to the next search space.

The next step is to integrate equality constraints ($c(\mathrm{x}) = 0$) into the objective function using Lagrangian multipliers (Eq. (5.1)), and differentiate the resulting equation with respect to x, λ, then make them equal to zero (Eq. (5.2)). Then, the Karsh-Kuhn-Tucker (KKT) conditions for the barrier problem can be derived.

$$L(X,\lambda) = f(x) - \mu \sum_{i=1}^{m} \ln(x_i) + c(\mathrm{x})\,\lambda \tag{5.1}$$

$$\nabla L(X,\lambda) = \nabla f(X) - \mu \sum_{i=1}^{m} \frac{1}{x_i} + \nabla c(\mathrm{x})\,\lambda = 0 \tag{5.2}$$

Where λ instances is the Lagrangian multiplier vector and its size equals the number of equality constraints.

let $z = \frac{\mu}{x}$, then $Z\,X\,e - \mu e = 0$, where **e** is the unite vector and Z, X, as shown below.

$$Z_k = \begin{bmatrix} z_1 & 0 & 0 \\ 0 & z_2 & 0 \\ 0 & 0 & z_n \end{bmatrix} \qquad X_k = \begin{bmatrix} x_1 & 0 & 0 \\ 0 & x_2 & 0 \\ 0 & 0 & x_n \end{bmatrix} \qquad e_{m\times 1} = \begin{bmatrix} 1 \\ : \\ : \\ 1 \end{bmatrix}$$

Then, the modified version of KKT equations are given in Eqs. (5.3) to (5.5):

$$\nabla L(X,Z,\lambda) = \nabla f(x) - Z + \nabla c(\mathrm{x})\lambda = 0 \tag{5.3}$$

$$c(x) = 0 \tag{5.4}$$

$$XZ\,e - \mu\,e = 0 \tag{5.5}$$

By applying the Newton Raphson method, we can solve these equations to find the search direction d_k^X, d_k^λ, d_k^Z for the iteration k, then update x_k, λ_k, Z_k values for the next new iterations, as shown in Eq. (5.6):

$$\begin{bmatrix} W_k & \nabla c(x_k) & -I \\ \nabla c(x_k)^T & 0 & 0 \\ Z_k & 0 & X_k \end{bmatrix} \begin{pmatrix} d_k^x \\ d_k^\lambda \\ d_k^z \end{pmatrix} = - \begin{pmatrix} \nabla f(x_k) - Z_k + \nabla \lambda_k\, c(x_k) \\ c(x_k) \\ X_k Z_k e - \mu_j\, e \end{pmatrix} \tag{5.6}$$

Where W_k is given in Eq. (5.7)

$$w_k = \nabla_{xx}^2\, L(x_k,\lambda_k,z_k) = \nabla_{xx}^2\, (f(x_k) - z_k + c(x_k)^T \lambda_k)) \tag{5.7}$$

A new symmetric equation resulting from the rearrangement of Eq. (5.7) could be easily solved, as shown in Eq. (5.8) (Lesaja, 2009)

$$\begin{bmatrix} W_k + \Sigma_k & \nabla c(x_k) \\ \nabla c(x_k)^T & 0 \end{bmatrix} \begin{pmatrix} d_k^x \\ d_k^\lambda \end{pmatrix} = - \begin{pmatrix} \nabla f(x_k) + \nabla\, c(x_k)\, \lambda_k \\ c(x_k) \end{pmatrix} \tag{5.8}$$

Where $\Sigma_k = X_k^{-1} Z_k$

It is then easy to find d_k^X, d_k^λ and d_k^Z, and by providing an appropriate step size (α) it is easy to move to the next point and explore the search direction using the merit function. Merit function measures the objective function plus the absolute value of the constraint. The α is accepted if it reduces the merit function, as shown in Eq. (5.9).

$$merit = f(x) + v \sum |c(x)| \tag{5.9}$$

Convergence criteria for the interior point algorithm are satisfied when KKT conditions are satisfied with a specified tolerance, as shown in Eqs. (5.10), (5.11) and (5.12).

$$\max |\nabla f(X) - z + \nabla c(x)| \leq \epsilon_{tol} \tag{5.10}$$

$$\max |c(x)| \leq \epsilon_{tol} \tag{5.11}$$

$$\max |XZe - \mu e| \leq \epsilon_{tol} \tag{5.12}$$

By providing a starting point, the algorithm rechecks the constraints and objective function violation until an optimum solution is satisfied. In conclusion, the obtained optimum solution by IPA is based on the start point located in the feasible space and gradient of the objective function. However, if the optimization problem is a complex problem including many constraints and decision variables, many feasible search regions, which satisfy the constraints, could be identified, but only one includes the global optimal solution. For such problems, the optimum solution by IPA probably converges in local minima. Therefore, the IPA provides a local optimal solution and rarely the global solution can be attained based on IPA.

5.4.2 Genetic algorithm

This section briefly discusses the reasons behind GA deficiency in finding the global optimum solution for complex problems. Because the optimization theory for GA has been extensively studied, this chapter disregards the formal description of GA, which can be found in Chapter Four and (Gen & Cheng, 2000; Haupt & Haupt, 2004; Rao, 2009). The GA has a high possibility to find a global optimum solution, because the GA examines search domains using a large number of individuals and simultaneously checks improvement direction of the objective function and constraints. However, for large scale problems encompassing many decision variables and constraints, convergence of the GA to the global optimum solution is difficult (Kolda et al., 2003).

The GA solution is based on many iterations of the natural selection process, from the initial population to last generation. The weakness of the GA is highlighted by understanding that the selection process of individuals from one generation to next generation is continuously implemented to the genes with preferable properties. Individuals with a low-grade (score) die out (Dorsey & Mayer, 1995). This

means that the contribution of all parents to generate the next offspring is not equal. It may be possible to find a better solution next to low-grade individuals, if they were still surviving. However, convergence of the GA does not occur with equal possibility of parents to produce the next generation.

Additionally, crossover and mutation ratios are other factors affecting GA performance. When a high crossover ratio is used, i.e., 0.5 or more, the GA pulls out the majority of individuals to a particular point. In contrast, the mutation process creates new and different individuals, which may explore the entire search space and lead the GA to the global optimum solution. However, convergence of the GA with a high mutation ratio is difficult (MathWorks, 2015). Hence, for the prominent ratio of cross over (0.6-0.8), the mutation effect to explore the entire space is limited because the number of newly created individuals is smaller than high-grade individuals. Then, the number of high-grade individuals significantly grows for the next generations and the majority of populations have the same properties. Subsequently, tolerance of the objective function and constraint for all individuals are satisfied and convergence criteria are achieved. Therefore, the objective function at the optimum point founded by GA may not have a zero gradient, but it satisfies the stopping criteria. As a result, the crossover and mutation ratio, which are the most important parameters for GA, must be accurately identified for each problem to attain the global optimum solution.

Other important parameters of the GA, such as population size, fitness scaling function, selection function, cross over function and mutation function, also affect GA performance. These parameters depend on optimization task nature and complexity. Therefore, for each problem, GA parameter combinations must be prudently selected using particular search and feature section methods to improve GA performance (Haines et al., 2012; Kolahan & Doughabadi, 2012; Koljonen & Alander, 2006; Pereira et al., 2005; Rand et al., 2006). This process is a demanding and time consuming task, especially for a large population size. From this point, it can be concluded that GA efficiently explores the most search space, even for complex problems, because it is based on a random and direct search technique (Dorsey & Mayer, 1995). However, to approach the global optimum solution for a complex problem using GA there is a requirement to set up several options and parameters of the GA accurately and efficiently. Hence, for complex problems it is difficult to converge to the global optimum solution (zero grade point) based on standard GA. In this study, therefore, GA is hybridized with the IPA based gradient search technique.

5.4.3 *Hybrid genetic algorithm (HGA)*

The weakness of GA to find the global optimum solution for a complex problem may be addressed by hybridizing the GA with a gradient search algorithm, such as IPA. Improvement of the hybrid genetic algorithm (HGA) can be attributed to high efficiency of GA to explore the entire search space. Also, GA quantifies the best optimum search region from many regions, because GA, in contrast IPA, has the ability to expeditiously change the properties of the population and explore the entire space,

especially for the first few generations. Additionally, IPA can efficiently and quickly approach to the zero gradient local minima of the objective function. Furthermore, the ability of IPA to move from a search space to another is limited, because the objective function would approach to infinity when IPA reaches the boundary (constraints) of a specific search space.

In this study, the complexity of the problem arises from many factors. For example, the number of decision variables is 32, the number of constraints is 70 and the objective function and constraints are nonlinear. Also, 21 ensemble SVM surrogate models are involved in the objective function and constraints. The optimization solver evaluates the fitness value and constraint violations based on the surrogate model responses. Additionally, even though SVM provides high prediction accuracy in the training and testing phase, the relationship between seepage design variables and design parameters is complex. As a result, performance of SVM surrogate models is expected to decline with the extreme data presented by the optimization solvers, which significantly affects convergence of the optimization solver.

Basically, the HGA process involves normal start of the GA with a random population. After many generations, the GA converges to the best optimum point in the search space. This point is the starting point of the local-based gradient search algorithm (IPA). The IPA algorithm searches from a point to the next point for the best direction that leads to the zero gradient point. Therefore, IPA efficiently attains the optimum solution for the local search space with a predefined point. Hence, a combination of random direct search technique based GA with the gradient search technique based IPA may lead to the global optimum solution.

5.4.4   *Formulation of the optimization model*

The optimization model is formulated to determine optimum design of HWRS. The best value of each design/decision variable is selected by the optimization solver to provide safe and economic design. Safety factors and other hydraulic design requirements represent the constraints of the optimization model within the S-O model.

Formulation of the optimization model is similar to optimization formulation in Chapter Four. Constraints and minimum cost objective function are also the same. The optimization model within the S-O technique explores the effects of the anisotropic ratios. Also, the effect of utilizing HGA is studied by comparing the obtained optimum solutions of the optimization models based on different optimization algorithms, such as HGA, GA and IPA.

5.5   **Results and discussion**

The linked S-O model was implemented to find the optimum solution of HWRS with different anisotropic ratios ranging from 0.1 to 1.5, as shown in Table 5.3. The value of other variables was left constant; for example, hydraulic conductivity was 5 m^3/day, upstream head, i.e., H, value was 100 m

and depth of subsoil was constant at 150 m. The remaining variables were considered as decision variables to be obtained by the optimization solver as an optimum solution.

5.5.1 *Optimization solvers efficiency*

To determine how HGA enhances and improves optimization results, the S-O technique was implemented with the specified optimization solvers (GA, HGA and IPA) for different values of anisotropic ratio. For each optimization solver within the S-O model, and for each single anisotropic value, the S-O model was implemented twice, utilizing different and random start points. This arrangement was undertaken to achieve an accurate and objective examination of algorithm performance for different scenarios. Parameters of GA and IPA are listed in Table 5.2, and the remaining parameters were left the same as default Matlab settings. Parameters of HGA are the same for the combination of the two algorithm's parameters, and are exactly as the same as those shown in Table 5.2.

Table 5.2 Options and parameter values for GA and IPA

GA parameters		IPA parameters	
Population Size	500	Max Function Evaluations	10000
Elite Count	3	Max Iterations	1000
Crossover Fraction	0.65	Optimality Tolerance	1.00E-04
Migration Direction	'both'	Function Tolerance	1.00E-04
Function Tolerance	1.00E-04	Step Tolerance	1.00E-04
Constraint Tolerance	1.00E-04	Constraint Tolerance	1.00E-04
Use Parallel	true	Use Parallel	true

The most important result of this study was the objective function values obtained by HGA, which were significantly less than the objective function value obtained by standard GA. As shown in Figure.5.2, the two different GA implementations provided less economic design compared with HGA solutions. The two iterations of HGA provided exactly the same objective function value and optimum solutions, even when HGA started from a different random starting point. In contrast, the GA optimum solution for the first time was different to the second time. Performance of GA proved that solutions resulting from GA were not the global optimum solution. As seen in Table 5.3, the percentage of improvement of optimum construction cost was a considerable value, which sometimes reached more than 50 %.
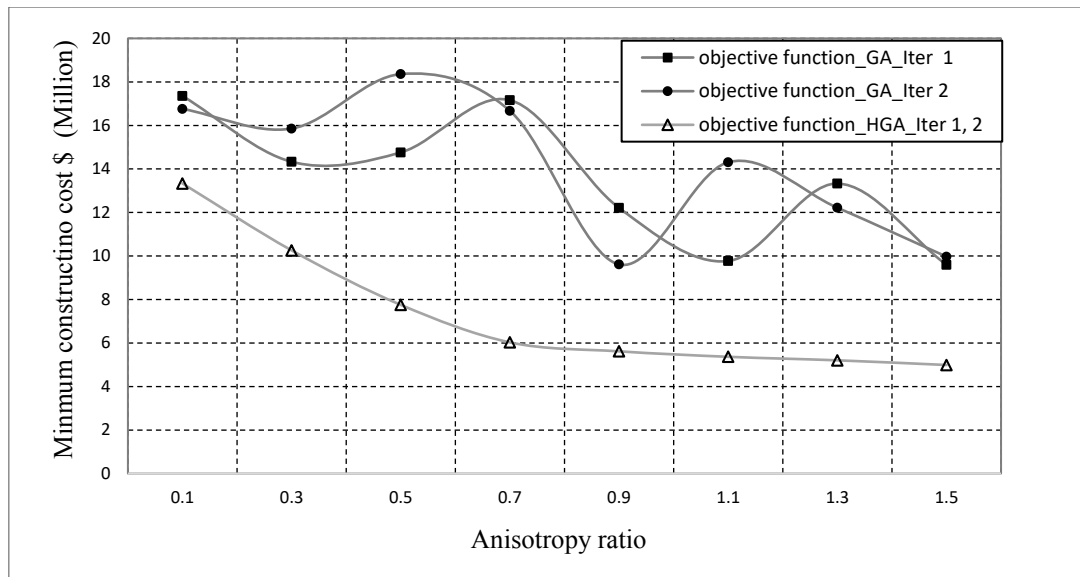
Figure 5.2 Objective function by HGA and GA

Table 5.3 Objective function values obtained by HGA and GA for different k_y/k_x ratio

k_y/k_x	Objective function _HGA_Iter 1, 2	Objective function _GA_Iter 1	Improvement percentage for the first iteration	Objective function _GA_Iter 2	Improvement percentage for the second iteration
0.1	13,333,370.86	17,354,151.09	23.17	16,760,144.36	20.45
0.3	10,258,627.47	14,330,295.53	28.41	15,855,989.49	35.30
0.5	7,753,981.80	14,759,779.64	47.47	18,360,589.05	57.77
0.7	6,030,451.81	17,163,655.36	64.86	16,671,226.89	63.83
0.9	5,618,499.23	12,211,401.29	53.99	9,611,843.27	41.55
1.1	5,367,411.11	9,766,642.65	45.04	14,310,283.98	62.49
1.3	5,205,080.84	13,329,024.09	60.95	12,219,413.38	57.40
1.5	4,991,124.45	9,592,305.68	47.97	9,971,288.64	49.95

However, GA performance could be improved if the the population size is significantly increased. This test was conducted for the case that includes a 1.5 anisotropic ratio. The standard GA code based linked S-O technique was applied with two random start points and 5,000 population size using a relatively high quality process unit (Intel(R) Core™ i7-2600 CPU@ 3.4GHz_3.4GHz, RAM 8.00 GB, 64x-based processor). The results, shown in Table 5.4, demonstrated that new objective function values obtained by GA were better than when the population size was 500 (Table 5.3). However, HGA results were still the best. That means, even with large population size, attaining the global optimum using GA is difficult. Moreover, the time consumed by HGA was considerably less than time consumed by the standard GA. Therefore, time efficiency is another advantage of using HGA. The computational time consumed by HGA was approximately 13 times less compared with the time consumed by the standard GA with high population size. Also, the global optimum solution was not guaranteed by the GA.

Table 5.4 Performance efficiency of HGA and GA ($k_y/k_x=1.5$)

	Run	Population size (GA)	Objective function ($)	Time (Sec.)
Standard GA	First	5000	8.247e 6	8543.44
	Second	5000	7.8603e 6.	8413.26
HGA	First & second	500	4.9911e 6.	652.41

The S-O model with the IPA solver was also implemented twice for each case. The IPA did not present any feasible solution even with different random starting points. However, for the first run of the case including anisotropic ratio equal to 1.1, the optimum solution by IPA was a feasible solution and the same as the HGA solution, as shown in Table 5.5. This means there is an opportunity to approach global optimum solutions by IPA, if IPA starts (initial point) in the same search space of the global optimum solution. The exit flag (-2) in Table 5.5 means that the relative maximum constraint violation exceeded the allowable tolerance, whereas the exit flag (+1) means the relative objective function tolerance, the constraints tolerance and optimality tolerance (less than 1e -4) were satisfied (MathWorks, 2015).

Table 5.5 Stopping condition and objective function values of IPA

ky/kx	objective function – Iter 1	exit Flag	objective function – Iter 2	exit Flag
0.1	13066713	-2	16092694	-2
0.3	7847945	-2	5681176	-2
0.5	5988833	-2	7711078	-2
0.7	6050421	-2	6106638	-2
0.9	5930869	-2	6633099	-2
1.1	**5367411**	**1**	5451110	-2
1.3	4887445	-2	5188936	-2
1.5	4948707	-2	5066211	-2

5.5.2   *S-O solutions result*

As the best optimum solutions are attained by HGA, only these results are considered in the discussion to find the effect of anisotropic ratio on the optimum solution. Eight different anisotropic ratios varying from 0.1 to 1.5 were implemented in the linked S-O model.

The majority of optimum solutions were based on input design variables b_9, b_{10}, d_9 and d_{10} to provide a safe and cost effective solution, as shown in Table 5.6. In general, with a low anisotropic ratio (k_y/k_x) the values of b_9, b_{10}, d_9 and d_{10} were large and gradually decreased with increase of (k_y/k_x) value. This is logical and can be attributed to the exit gradient safety factor consequences. The exit gradient values increase with decrease of anisotropic ratio. Therefore, the optimization solver provided an efficient depth (d_{10}), which is the most controllable variable in reducing exit gradient value. Also, inclination angle β_{10} reached the maximum limit of 150 degrees. Although, it is an expensive alternative to provide deep cut-offs with maximum inclination angle (see Eq. (4.20)), it was the optimum option to

attain a safe exit gradient value. A deep downstream cut-off (d_{10}) encompassing inclination angle toward downstream considerably decreases the exit gradient value. Constructing inclined cut-offs either at the upstream location with an angle less than 90 degrees or, at the downstream location with an angle more than 90 degrees, increases the stream path for seeping water. This would reduce seepage characteristics impacts, particularly exit gradient, for HWRS design.

Table 5.6 Optimum solutions based on HGA

Design variables	ky/kx							
	0.1	0.3	0.5	0.7	0.9	1.1	1.3	1.5
b1	0.01	0.01	0.01	0.01	5.48	8.70	9.78	11.35
b2	30.01	30.00	0.01	4.56	3.84	4.45	5.79	6.37
b3	0.01	0.01	0.01	0.01	0.01	0.10	0.91	0.70
b4	0.01	0.01	0.01	0.01	0.01	0.01	0.01	0.01
b5	0.01	0.01	0.01	0.01	0.01	0.01	0.01	0.01
b6	21.05	0.01	0.01	0.01	0.01	0.01	0.01	0.01
b7	51.04	22.84	0.01	0.01	0.01	0.01	0.01	0.01
b8	30.01	134.12	0.01	0.01	0.01	0.01	0.01	0.01
b9	**150.00**	**30.01**	**72.23**	**50.17**	**47.67**	**43.02**	**38.96**	**35.77**
b10	**41.64**	**41.71**	**60.00**	**53.20**	**46.88**	**48.38**	**48.57**	**55.14**
b11	0.01	0.01	4.75	0.01	0.01	0.01	1.24	1.26
d1	**60.00**	**60.00**	0.01	**9.11**	**7.67**	**8.70**	**9.78**	**11.35**
d2	0.01	0.01	0.01	0.01	0.01	0.19	1.81	1.39
d3	0.01	0.01	0.01	0.01	0.01	0.01	0.01	0.01
d4	0.01	0.01	0.01	0.01	0.01	0.01	0.01	0.01
d5	0.01	0.01	0.01	0.01	0.01	0.01	0.01	0.01
d6	42.09	0.01	0.01	0.01	0.01	0.01	0.01	0.01
d7	60.00	45.66	0.01	0.01	0.01	0.01	0.01	0.01
d8	0.01	0.01	0.01	0.01	0.01	0.01	0.01	0.01
d9	**60.00**	**60.00**	**60.00**	**55.15**	**47.14**	**41.77**	**37.50**	**35.59**
d10	**23.28**	**23.42**	**60.00**	**51.25**	**46.61**	**41.88**	**40.00**	**35.88**
dd	0.01	0.01	0.01	0.01	0.01	0.01	0.01	0.01
β1	140.71	135.11	150.00	148.96	141.41	135.71	131.26	126.85
β2	106.89	106.71	76.15	83.81	83.87	85.29	85.70	86.58
β3	92.34	94.70	113.14	119.49	123.15	127.22	132.67	135.12
β4	86.53	88.34	100.78	106.38	108.32	110.80	113.72	113.77
β5	62.37	54.52	46.31	55.23	57.06	60.11	63.68	68.27
β6	150.00	150.00	150.00	150.00	150.00	150.00	150.00	142.88
β7	147.33	150.00	107.21	142.94	133.49	134.77	140.83	143.44
β8	104.05	150.00	30.00	30.00	30.00	30.00	30.00	30.00
β9	**30.00**	**30.00**	**30.00**	**30.00**	**30.00**	**30.00**	**30.00**	**30.00**
β10	**150.00**	**150.00**	**150.00**	**150.00**	**150.00**	**150.00**	**150.00**	**150.00**

On the other hand, augmentation of b_9, b_{10} and d_9 partially contributed to reducing the exit gradient value, because uplift pressure of a specific point was used with other design variables (b_i, d_i, β_i, k_x, (k_y/k_x)) to predict the next point uplift pressure. This means that exit gradient value is influenced also by values of b_9, b_{10}, and d_9 due to their effects on the uplift pressure behind the last cut-off, which influences exit gradient value. The values of b_9, b_{10} and their thicknesses enhanced stability for HWRS to satisfy the sliding, overturning and eccentric load requirements. These variables provide sufficient weight to counterbalance external hydrostatic loads and uplift pressure. Moreover, d_9 decreases uplift pressure value under b_{10} to decrease the floor thickness and construction cost. The inclination angle β_9 reached the minimum boundary 30 degrees, which is the most effective inclination angle to reduce uplift pressure underneath the HWRS.

In some optimum solutions, as shown in Table 5.6, there are noticeable contributions related to d_1 and b_2 values, especially for small anisotropic ratios, which are the most critical scenarios. For the cases (k_y/k_x = 0.1 to 0.3), the length of d_9 and d_{10} within the specified range are not solely adequate to provide a safe HWRS design. Hence, the d_1 value significantly reduces the uplift pressure for the rest of the structure (Figures 5.4 and 5.5) and consequently decreases construction cost. Additionally, an increase in d_1 value partially contributed to a decrease in exit gradient value due to d_1 effects in reducing uplift pressure under the HWRS.

When the anisotropic ratio increased (>0.5), the load resultant distance **e** became more controllable in the optimization process. The **e** value of the optimum solutions reached the minimum allowable limit (B/3) to provide safer and cheaper solutions, as shown in Figure 5.3. Therefore, **e** value also plays a significant role in safety of HWRS. The sliding constraint has significant effects on optimal design of HWRS. The minimum allowable value of the sliding safety factor is 1.5, as shown in Table 5.7. For small anisotropic ratio, the seepage characteristics are more critical and exit gradient value is high. Consequently, for these cases the exit gradient value is more controllable in optimum design of HWRS. However, when anisotropic ratio decreases, exit gradient value also decreases. This allows other safety factors, such as the sliding and overturning safety factor, to approach to the minimum allowable limit. Hence, an economical design could be achieved (Table 5.7, Figure. 5.3).
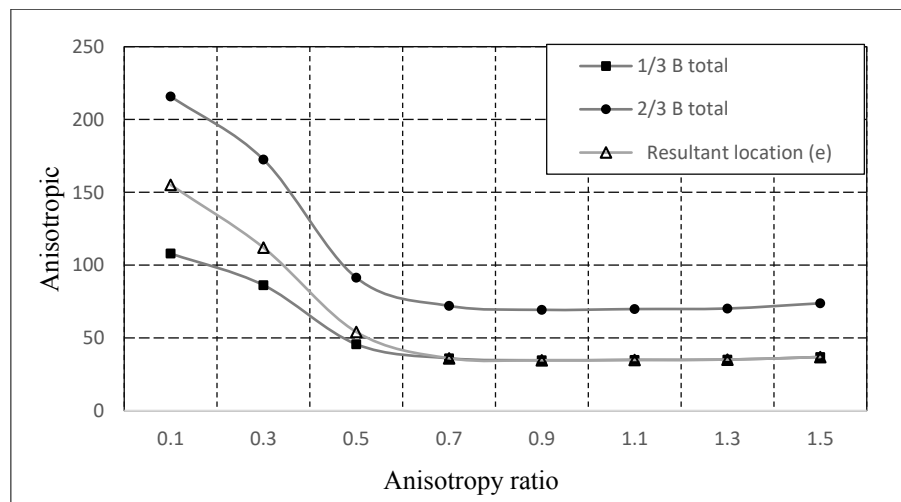
Figure 5.3 Load resultant location (e)

Table 5.7 Safety factors for the optimum solution for different ky/kx ratios

ky/kx	Exit gradient	Resultant location	Over turning	Sliding
0.1	5	155.09	2.09	3.45
0.3	5	112.02	1.99	2.68
0.5	5	54.10	1.81	2.03
0.7	5	36.00	1.62	1.57
0.9	5	34.64	1.59	1.50
1.1	5	34.90	1.59	1.50
1.3	5	35.10	1.59	1.50
1.5	5	36.88	1.60	1.50

Total construction cost of HWRS decreases with an increase in anisotropic ratio. This may be attributed to the high construction cost for deep cut-offs due to significant inclined angles. Also, the huge thickness and length of b_9 and b_{10} considerably increase the construction cost. With high anisotropic ratio, exit gradient values have less impact on the safety of HWRS design, as the seeping water movement through soil becomes easier, especially in the vertical direction. Consequently, large depths of d_{10} and d_9 are not necessary, instead the optimization solver provides sufficient thickness, which is a cheaper solution, to counterbalance uplift pressure.

5.5.3 *Optimum solution evaluations*

To evaluate the accuracy of the S-O technique, the obtained optimum solutions were solved using the seepage numerical modeling code. Agreement of seepage characteristics obtained by the S-O model with those obtained by the numerical solution reflects the accuracy of the S-O technique. Evaluation results demonstrated good agreement between the seepage characteristics of the optimum solutions and the numerical solutions, as shown in Figure 5.4 to Figure 5.12 (5% error bar charts).

However, in some cases there were slight deviations for the uplift pressure and exit gradient values. These deviations may be attributed to weak learning of SVM surrogate models for unseen or extreme data. The most optimum solutions presented by HGA were extreme scenarios. For example, values of b_2 to b_8 and d_2 to d_8 approached zero. Also, values of d_9 and d_{10} reached the upper limit (60 m) and inclination angles β_9 and β_{10} reached the boundary limits (30 and 150 degrees), as shown in Table 5.6. In general, although optimum solutions included an extreme value, SVM surrogate models base S-O models presented an accurate prediction related to seepage characteristics. Maximum percentages of error of the predicted uplift pressure were less than (+/- 10%), which are accepted for such complex problems. On the other hand, the predicted exit gradient values, shown in Figure 5.12, were in total agreement with the numerical solution results. However, a few cases have noticeable deviation, as in the first scenarios (anisotropic ratio = 0.1), which might be attributed to weak learning of the SVM model for the range of values lying on the periphery of training data sets.
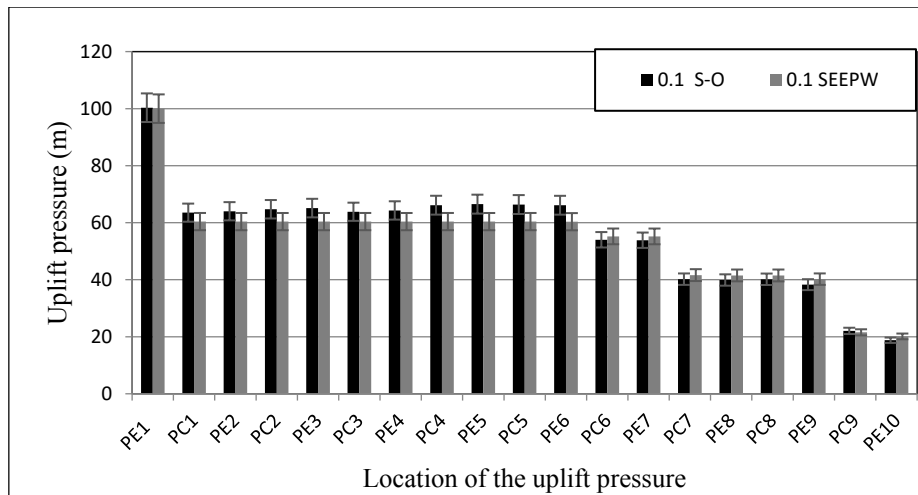
Figure 5.4 Evaluation results for different locations of the uplift pressure (ky/kx =0.1)
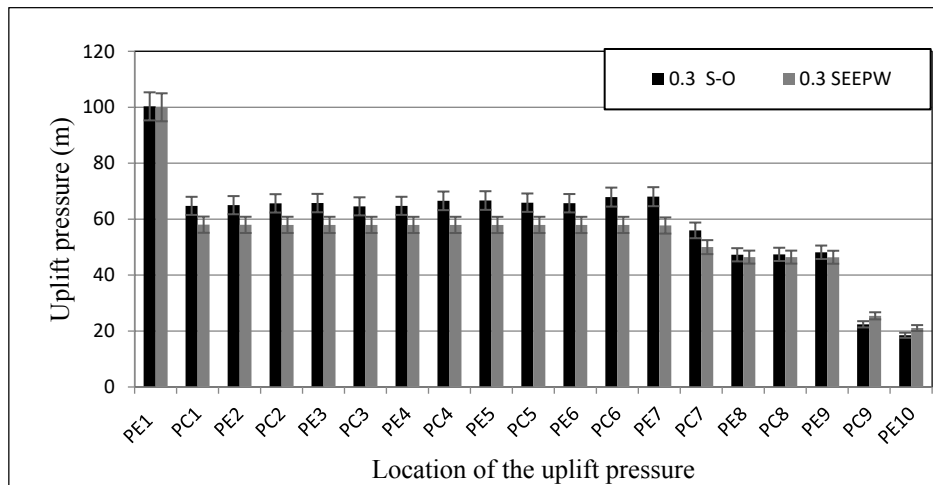
Figure 5.5 Evaluation results for different locations of the uplift pressure (ky/kx =0.3)
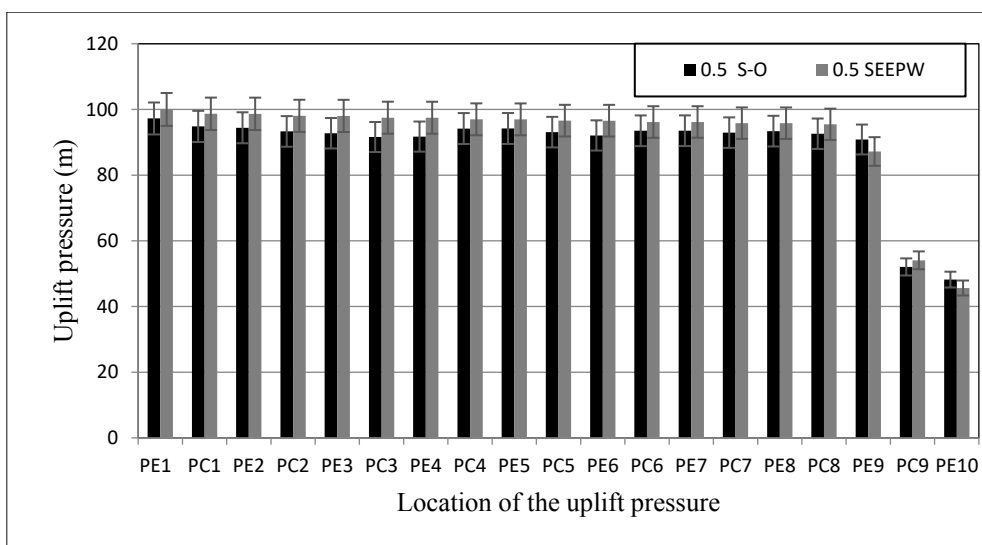
Figure 5.6 Evaluation results for different locations of uplift pressure (ky/kx =0.5)
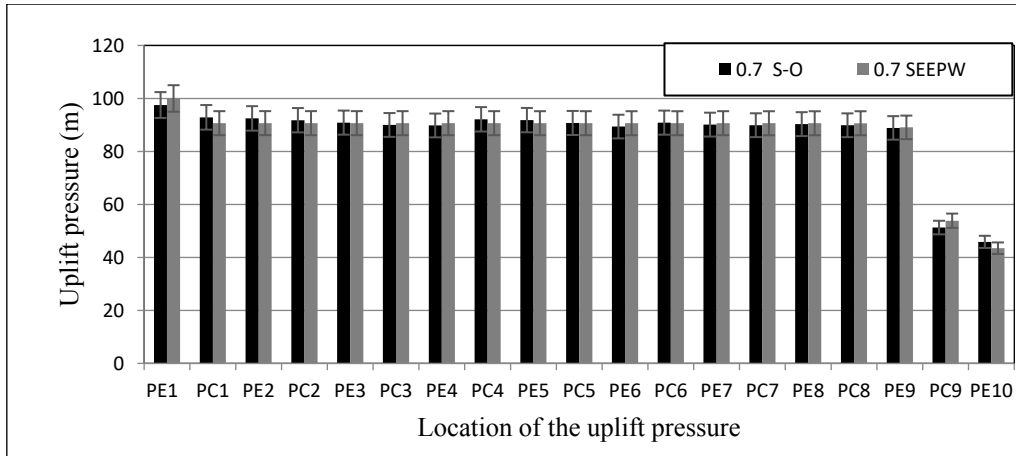
Figure 5.6 Evaluation results for different locations of the uplift pressure (ky/kx =0.7)
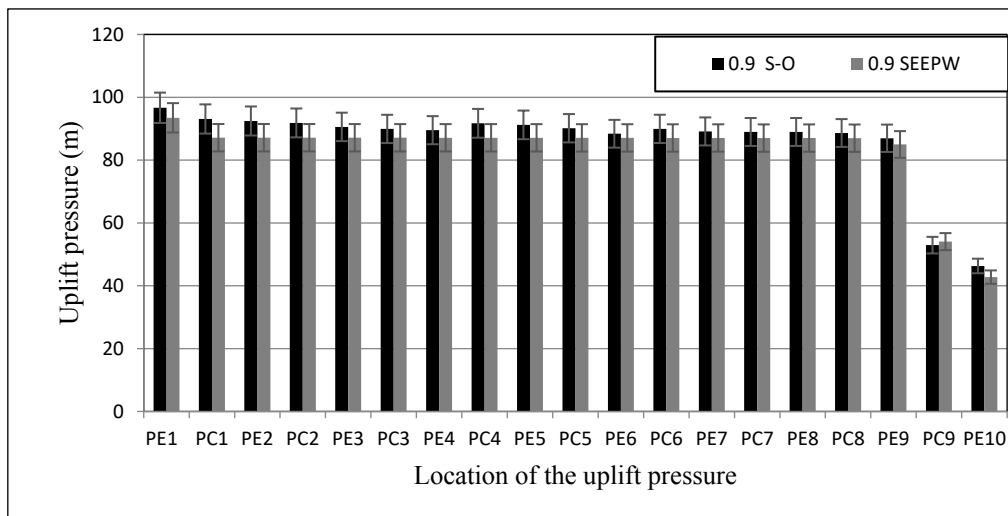
Figure 5.7 Evaluation results for different locations of uplift pressure (ky/kx =0.9)
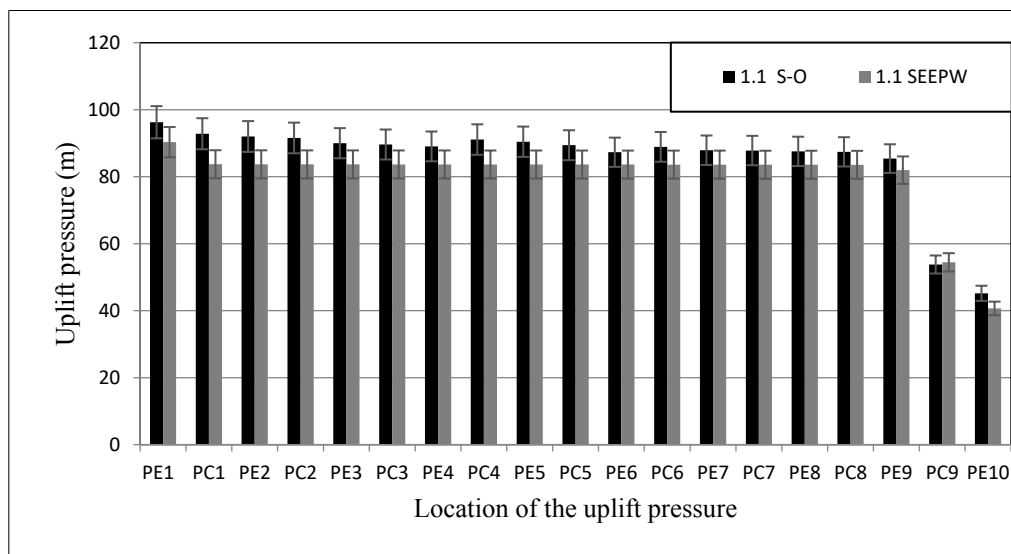
Figure 5.8 Evaluation results for different locations of uplift pressure (ky/kx =1.1)
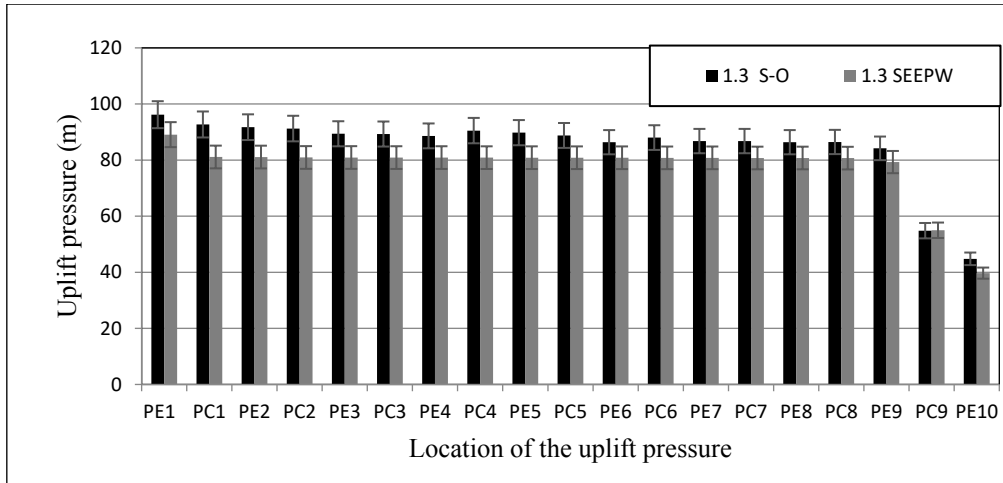
Figure 5.9 Evaluation results for different locations of uplift pressure (ky/kx =1.3)
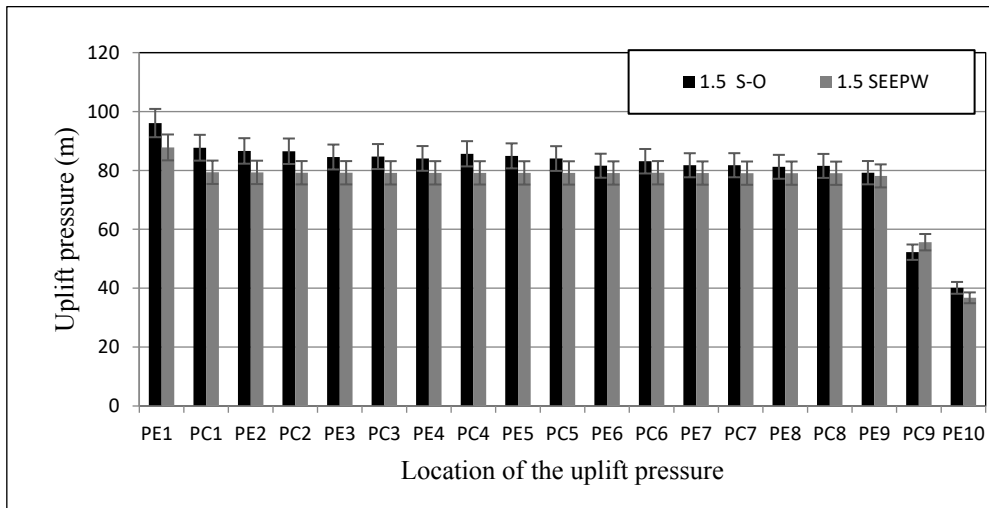
Figure 5.10 Evaluation results for different locations of uplift pressure (ky/kx =1.5)
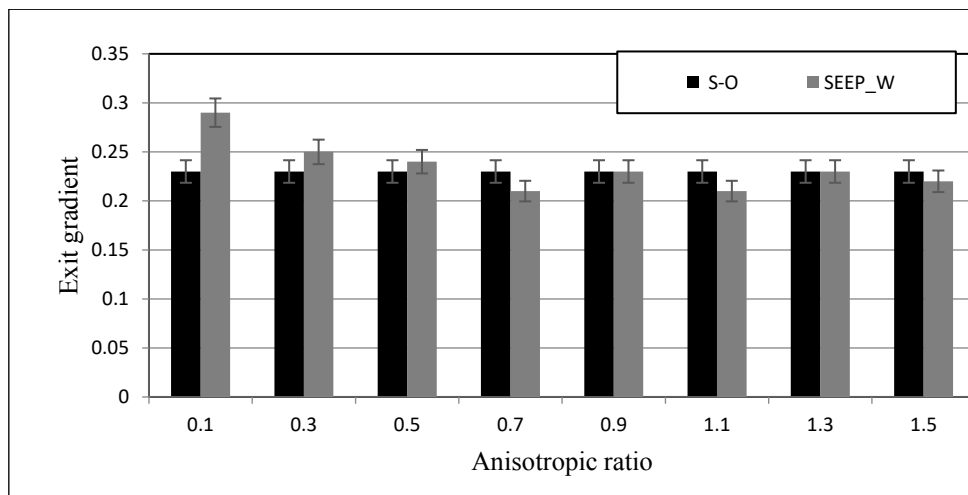
Figure 5.11 Exit gradient evaluation for different anisotropic ratios

5.6   Conclusion

Attaining global optimum design of HWRS incorporating several constraints, and based on several seepage characteristic responses of many surrogate models, is an almost unachievable task without improvement in efficiency of the utilized optimization solvers. This study presented a new methodology to expeditiously find the global optimum solutions by hybridizing the GA based direct search method with the IPA based gradient search method. The HGA was applied to find optimum design of HWRS incorporating the seepage characteristics based on an anisotropic hydraulic conductivity flow domain. The linked S-O model utilized well trained and tested SVM surrogate model responses to evaluate the objective function and constraints. Optimization results demonstrated that efficiency of the HGA was enough to find the global optimum solution compared with standard GA and IPA. The HGA efficiently provides a more economic and safer HWRS design. The percentage of improvement in the objective function value (construction cost) was between 20% and 50 %, which is of substantial value for large scale construction projects. Even though population size of the GA was increased to 5,000 individuals, optimum solutions from HGA based on 500 individuals was the best. Also, the computing time efficiency of HGA to find the optimum solution was about 13 times faster compared to standard GA based on 5,000 populations.

Physically, reducing anisotropic ratio (k_y/k_x) significantly increases construction cost due to augmentation of the seepage characteristics, especially exit gradient value. The optimum solutions for many cases were based on the six effective variables d_9, d_{10}, b_9, b_{10}, $\beta9$ and β_{10}. The main role of the widths b_{10} and b_9 with sufficient thickness was to provide an efficient cross section counterbalancing the significant uplift pressure and hydrostatic forces. The role of d_9 was to reduce uplift pressure under the HWRS, especially when β_9 reached the minimum value (30 degrees). Additionally, reduction of uplift pressure due to increasing d_9 significantly reduced the uplift pressure at the end of HWRS; then the exit gradient value declined. The value of d_{10} had a direct effect in reducing the exit gradient value, especially when β_{10} reached 150 degrees. In general, all HWRS hydraulic design requirements and safety factors were satisfied. The exit gradient safety factor was the most controllable factor for the optimum solutions; however, when anisotropic ratio increased the allowable resultant distance (e) and sliding safety factor were also acting as controllable factors and affecting optimum solutions.

The accuracy of solutions obtained in the evaluation processes demonstrated that the S-O methodology is applicable for finding the optimum solution of HWRS. Even though most optimum solutions were extreme scenarios, i.e., lying on the periphery of the training data set, maximum SVM prediction errors were less than 10%. Accordingly, the linked S-O technique incorporating HGA is a powerful methodology and can be applied to find global optimum solutions for complex problems.

Future recommendations to address the limitations of this study are: [1] extensively study the effect of GA and IPA parameters and find the optimum combination of these parameters to improve

their performance; [2] the training range of training data could be expanded to provide more accurate responses for extreme data; [3] different machine learning techniques, such as genetic programing (GP) or fuzzy neural network (FNN), which are expected to provide precise predictions (surrogate model) for design variable of complex problems should be explored.

The reliability based optimum design is implemented in Chapter Six. The uncertainty in seepage quantities due to the uncertainty in estimating the hydraulic conductive is incorporated in the S-O model to quantify the reliability of HWRS design based on the multi-realization optimization technique.

6 Reliability Based Optimum Design of Hydraulic Water Retaining Structure Constructed on Heterogeneous Porous Media: Utilizing Stochastic Ensemble Surrogate Model Based Coupled Simulation Optimization Model

A similar version of this chapter is under review for publication in the Journal of Life Cycle Reliability and Safety Engineering as shown below:

Al-Juboori, Muqdad, and Datta, Bithin (2018) *Reliability based optimum design of hydraulic water retaining structure constructed on heterogeneous porous media: utilizing stochastic ensemble surrogate model based coupled simulation optimization model.* Journal of Life Cycle Reliability and Safety Engineering, <u>Under Review.</u>

This chapter studies the effects of uncertainty and variation in hydraulic conductivity on the optimum design of HWRS. Different realizations (random field) of heterogeneous hydraulic conductivity were sampled from a constant mean and varied standard deviation log-normal distribution. The objective of this study was to integrate the reliability concept in the linked simulation optimization (S-O) technique to address uncertainty of the seepage characteristics due to uncertainty of hydraulic conductivity. The reliability based optimum design (RBOD) framework was implemented utilizing multiple realization optimization techniques based on GPR stochastic ensemble surrogate models. The S-O model based RBOD was formulated to find the most cost-effective HWRS design that satisfies a specified degree of reliability.

6.1 Introduction

Seepage characteristics under hydraulic water retaining structures (HWRS) significantly impact the hydraulic serviceability and stability of such structures. Seepage quantities are influenced by the hydraulic conductivity value and its spatial and directional variations. Homogenous isotropic hydraulic conductivity soils are rarely seen in the field. As Lambe & Whitman (1969, p. 275) reported, "unfortunately, the soils are generally nonhomogeneous and anisotropic", even in one single layer there is no uniform homogenous soil properties (Freeze, 1975). Therefore, in the geotechnical and structural design codes, uncertainty due to analysis methods, loads and parameter variations have been strongly considered (ACI Committee American Concrete Institute& International Organization for Standardization, 2011; European Committee For Standardization, 2004). Uncertainty in soil parameters arises from different sources, as follows: [1] spatial and direction variations of inherited soil properties

as a result of the environmental effect on sediment conditions, [2] shortage in the number of required samples, [3] error in measurement of soil properties and statistical analysis error. Soil properties and hydraulic conductivity especially have a large covariance 200-300% value, which means uncertainty level of hydraulic conductivity is high (Baecher & Christian, 2005).

As uncertainty level increases, the expected risk increases, especially for huge projects such as nuclear power plants and large water retaining structures. Hence, design and safety factors must be conservative. Therefore, many studies have been conducted to study the effect of uncertainty and soil properties variations on the reliability of designs (Baroni, Zink, Kumar, Samaniego, & Attinger, 2017; Christian, Ladd, & Baecher, 1994; Deng, Li, Qi, Cao, & Phoon, 2017; Duncan, 2000; Hicks, Nuttall, & Chen, 2014; Hicks & Spencer, 2010; Popescu, Deodatis, & Nobahar, 2005). Specifically, for groundwater and seepage for hydraulic structures most studies have concentrated on stochastic analysis of seepage characteristics based on different realizations of hydraulic conductivity generated from different probability distribution functions (PDF) or different sets of mean and standard deviation (Ahmed, 2012; Griffiths & Fenton, 1993, 1997; Le, Gallipoli, Sanchez, & Wheeler, 2012). The important conclusion of such studies was that the degree of uncertainty drastically influenced seepage characteristics, which may negatively affect the design performance and safety.

All traditional techniques used to quantify uncertainty and measure the reliability of design are based on statistical parameters of involved variables. Reliability in this context refers to actual performance of the design compared to expected performance. A majority of conducted studies are based on conventional reliability methods, such as first order reliability method (FORM), first order second moment (FOSM) method, reliability index method, point estimation methods and the Hasofer-Lin approach or geometrical reliability method. These methods are based on mean (μ), variance (σ^2), covariance (cov) and probability density function (PDF) of involved parameters or variables and a particular performance criteria integrated in reliability analysis. Generally, the reliability index or probability of failure (P_f) for a design can be computed based on a certain safety factor criteria and a particular value of μ, σ. On the other hand, Monte Carlo simulation (MCS) method, which is based on randomly generated data from specific PDF, μ and σ, can be used to determine P_f. The MCS method is based on involving a large number of random data in calculation of a certain safety factor criteria, then the probability of failure is determined based on the number of unsuccessful samples to the total number of samples (Baecher & Christian, 2005).

Recently, new techniques have been developed based on numerical simulation to evaluate reliability. For example: Griffiths and Fenton (2004) used the random finite element method; Zhu, Wang, Li, Liu, and Cheng (2017) utilized the weighted dynamic response surface method; a non-intrusive stochastic finite element method was implemented by Jiang, Li, Zhang, and Zhou (2014), and the multi response surface method was used by Deng et al. (2017). These methods were based on

stochastic simulation of the design based on the random field concept integrated with the finite element method considering spatial variability of soil parameters. In other studies, the computationally expensive numerical models were replaced with stochastic response surface models to explore the reliability of the design (Mollon, Dias, & Soubra, 2009, 2010).

Although satisfying high reliability level of a certain design provides a more reliable design, this may negatively impact on the efficiency of other aspects, such as the construction cost, etc. Hence, a number of studies incorporated reliability in the optimization model to improve design and acquire more information about the impact of reliability on optimum design, considering the uncertainty in design parameters (Bayer, de Paly, & Bürger, 2010; Singh & Minsker, 2008; Sreekanth & Datta, 2011; Tee, Khan, Chen, & Alani, 2014; Zhang, Zhang, & Tang, 2011). The majority of these studies demonstrated that the RBOD approach was a computationally expensive and difficult task, especially with stochastic noisy constraints and objective functions. Also, only evolutionary optimization solvers based on the direct search technique, such as the anti-colony optimization (ACO) and genetic algorithm (GA), could be utilized in similar optimization problems.

In the present study, the reliability based optimum design (RBOD) framework was implemented using a multiple realization optimization technique. As directly linking the numerical simulation code to the RBOD model is a demanding task, sets of precisely trained ensemble stochastic surrogate models were imbedded in the linked S-O technique based RBOD framework. Each surrogate model imitated the numerical seepage modeling responses based on a particular field of heterogeneous hydraulic conductivity. Characteristics of each random field were based on certain values of μ and σ of log-normal PDF. Hence, each surrogate model represented a certain degree of uncertainty of a specific seepage quantity. The process to quantify the reliability of design within the RBOD framework was based on determining the number of stochastic responses, satisfying a particular constraint of the total number of surrogate models (stochastic responses) in the ensemble. For example, for each safety factor, candidate design with 60 % reliability must satisfy at least 60 % of stochastic safety factors computed based on stochastic seepage values using many surrogate models. These surrogate models were trained and tested based on different seepage data sets resulting from the numerical simulation of different seepage modelling and different scenarios of heterogeneous hydraulic conductivity.

The objective function of the optimization model is the minimum construction cost of HWRS. Reliability level was formulated as an additional constraint, continually controlling all stochastic constraints until the desired reliability level is achieved for each single iteration of the optimization model. Reliability constraints, stochastic constraints and deterministic constraints were simultaneously evaluated with the objective function to attain the optimum solution. The majority of the constraints and objective function were based on the ensemble surrogate model responses within the S-O model.

The optimization task in the present study is considered complex. Hence, the optimization solver and machine learning technique had to be efficient and accurate enough to provide reliable and accurate solutions. Therefore, GA was utilized as an optimization solver for this task. The GA is widely used to solve complex optimization problems in different engineering applications. Additionally, the Gaussian process regression (GPR) machine learning technique was utilized in S-O models to precisely imitate numerical model responses under different conditions. Many researchers dealing with geotechnical and civil engineering problems have demonstrated that GPR precisely predicted certain responses compared to other machine learning techniques, such as support vector machine and back propagation neural network (He et al., 2017; Kang et al., 2015; Kang et al., 2017; Li et al., 2017; Pal & Deswal, 2010; Samui & Jagan, 2013).

This study concentrated on developing the RBOD framework to find optimum HWRS design at minimum cost, considering a particular level of reliability to address uncertainty in hydraulic conductivity and seepage quantities. This objective could be established by formulating a constrained multi-realization optimization model based linked S-O technique utilizing GA optimization solver and incorporating many stochastic ensemble GPR surrogate models. The minimum cost objective function and stochastic constraints within the S-O model were based on the responses of ensemble surrogate models. Reliability constraints were simultaneously integrated into the S-O model and were based on the ensemble surrogate responses to quantify the reliability of the design. Each surrogate model in the ensemble model was trained and tested based on large data sets simulated by a numerical seepage modeling code (SEEP/W) (Krahn, 2012). Predictions of each surrogate model represented one of the seepage characteristics based on a particular random field involving different realizations of heterogeneous hydraulic conductivity.

The following sections present and discuss the seepage model and data generation, theory of GPR, measuring the performance of the developed surrogate models, formulation of the RBOD model, results and discussion, evaluation of the developed methodology and conclusion.

6.2 Conceptual seepage model and design of experiments

Generally, seepage analysis for heterogeneous hydraulic conductivity of the flow domain based on the closed form solution is impractical. Furthermore, mathematical seepage analysis for homogenous isotropic hydraulic conductivity with complex geometry is a convoluted process. However, the numerical solutions based on the finite element method (FEM) provide precise solutions for complex problems compared to experimental observations and other numerical method solutions (Shahrbanozadeh et al., 2015).

Therefore, in the current study, FEM code based-Geo-Studio/SEEP/W software (Krahn, 2012) was utilized to simulate seepage problems. However, each iteration (run) of the numerical simulation of seepage modeling with heterogeneous hydraulic conductivity takes a long time. For example,

simulation time for two randomly selected cases drawn from the hydraulic conductivity field with standard deviation 2.95, 3.65 m/day was 1:27.34 and 3:25.14 minutes, respectively. These simulations were conducted utilizing a high speed processor unit (Core™ i5-4570 CPU@ 3.20 GHz, RAM 8.00 GB, 64x-based processor). Consequently, it is time consuming and inefficient to directly link the numerical model to the optimization model. The justification being that the optimization solver is based on a direct search evolutionary algorithm, which invokes numerical responses numerous times to evaluate the constraints and objective function for each individual in each generation of the search process. This might take many weeks to find the optimum solution for one S-O run (Dhar & Datta, 2009; Mollon et al., 2009, 2010). Additionally, reliability constraints increase complexity of the problem and the required time for each run of the S-O model because additional iterations are required to evaluate reliability of the design. Moreover, quantifying the reliability requires responses of many numerical stochastic simulations encompassing different realizations of the hydraulic conductivity field. Attaining and incorporating such responses requires a large number of iterations and longer time.

Alternatively, the numerical seepage model can be replaced by expeditious surrogate models. The surrogate model can be trained and tested based on numerous data sets simulated using the numerical seepage modeling code. Then the trained surrogate model could efficiently and accurately predict seepage characteristics even for out of training data sets without a need to use the numerical simulation model.

The first step to building a surrogate model is to propose a conceptual seepage model for HWRS integrating the design variables and parameters. Based on the conceptual model shown in Figure 6.1, input data could be generated. Important design variables influencing seepage quantities were upstream cut-off (d_1), downstream cut-off (d_2), total width of HWRS (b), upstream water head (H), and hydraulic conductivity characteristics.
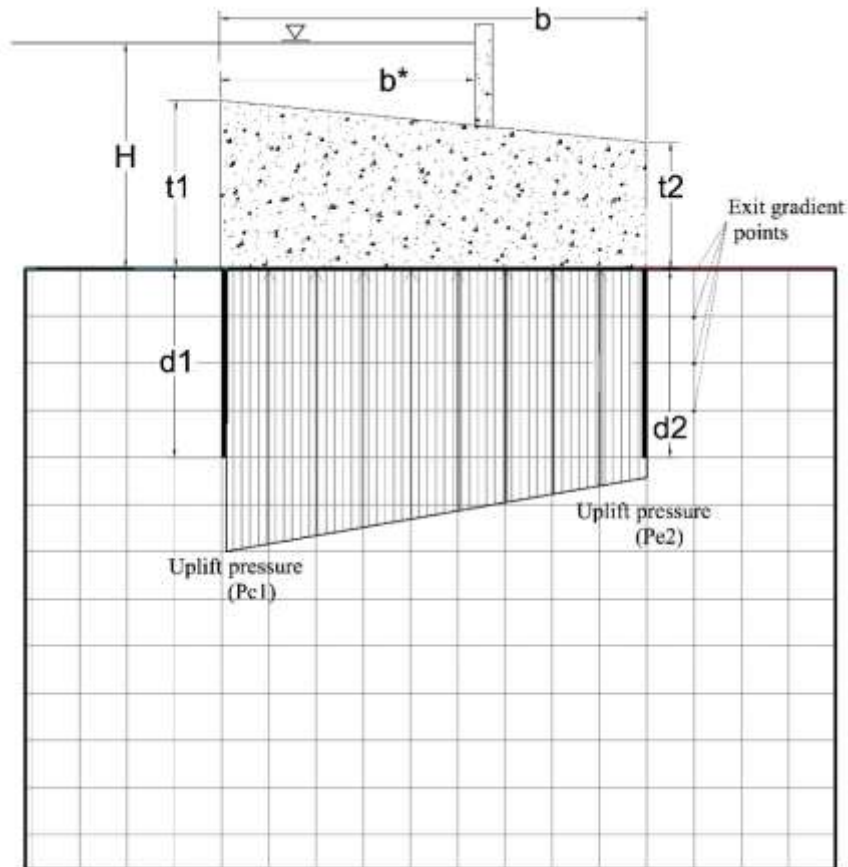
Figure 6.1 Conceptual model of HWRS

Input data comprised 150 sets of seepage design variables (d_1, d_2, b, H), randomly generated utilizing the Halton sequences (HS) method (Loyola, Pedergnana, & García, 2016). The HS provides more uniform distribution for generated data compared with other methods, such as the Latin hypercube sampling method (LHS). A sample of random data generated for HWRS width (b), shown in Figure 6.2, demonstrates how the HS method uniformly covers all variable ranges. In contrast, the LHS leaves some spots without any point and provides many adjacent points in the same place. Therefore, data sets generated by the HS method are the best distributed data for the machine learning process (experiments). The proposed ranges of design variables were 0-80 m for d_1 and d_2 and 0-150 m for b and H. These ranges were supposed to cover all expected optimum solutions obtained for different upstream head value. Furthermore, in the real field, the most constructed HWRS could be seen within these limits.
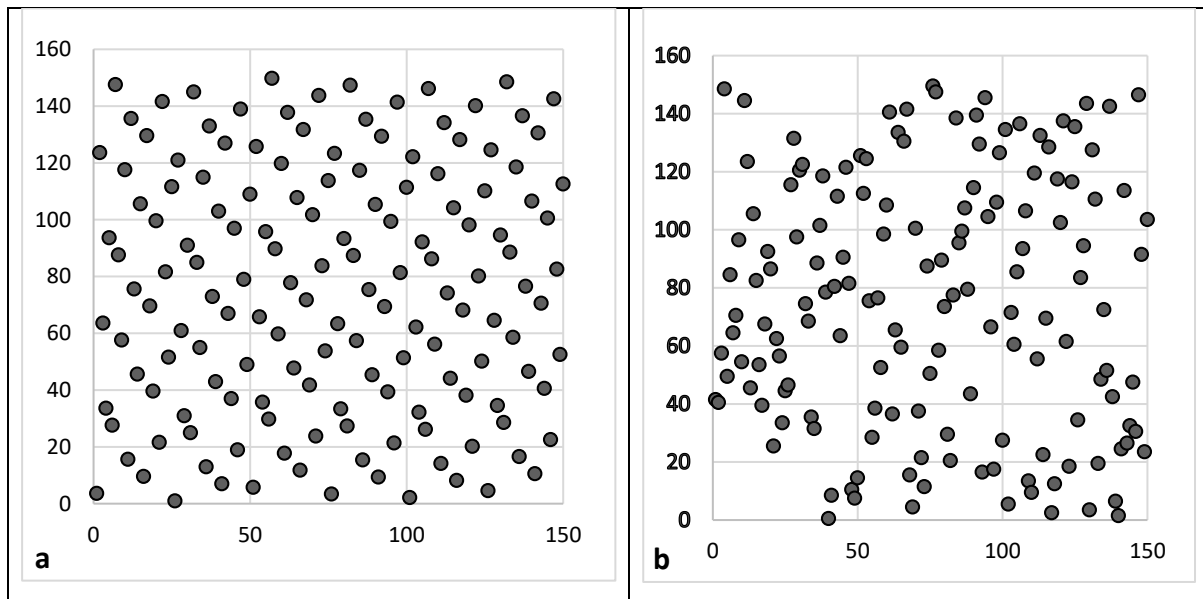
Figure 6.2 Random data sampling using a) HS method b) LHS method for width of HWRS [b (0-150) m]

Heterogeneous hydraulic conductivity was assumed to be a random field sampled from log-normal distribution. Random field properties were based on a defined mean and standard deviation. Five standard deviations (0.85, 1.55, 2.25, 2.95 and 3.65) were assumed based on constant mean (2 m/day). Although, there is no explicit relationship between the standard deviation and mean, the expected values of standard deviation range between (0.5 to 2 μ). Hence, using Eq. (6.1), the prescribed five values of standard deviation can be generated.

$$\sigma_i = \sigma_{min+} \, i \left(\frac{\sigma_{max} - \sigma_{min}}{5 \times \mu} \right), \qquad i = 1, 3, \ldots 9 \tag{6.1}$$

Where σ_{min} is the minimum value of standard deviation (0.5 m/day), σ_{max} is the maximum value of standard deviation (4 m/day).

A Box-Muller approach (Ross, 2014) was used to generate a log-normal distribution with a particular value of μ and σ random field. A subroutine code to generate the distribution was written in C#, then linked to the seepage modeling code to define hydraulic conductivity value to each element in the FEM numerical model. A randomly selected sample of actual hydraulic conductive random field defined in the FEM models is shown in Figure 6.3, which decidedly matches log-normal distribution.
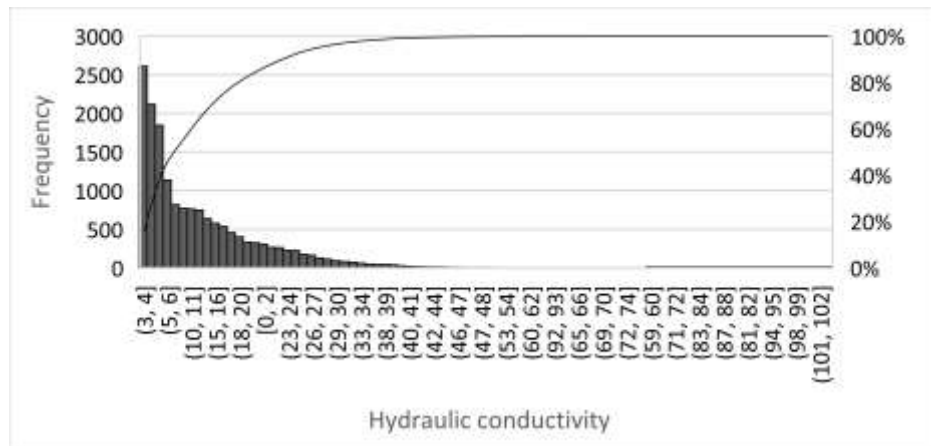
Figure 6.3 Log-normal histogram for a sample of (μ = 2, σ = 0.85)

Based on each standard deviation value, a random field of hydraulic conductivity was generated and incorporated in the numerical seepage model. As unlimited realizations could be generated from a log-normal distribution with a certain value of standard deviation, each input data set (d_1, d_2, b, H) was simulated with four different random realizations (random field) of the same standard deviation value. Then, the simulated data sets used for training a surrogate model for a particular seepage characteristic was 600 sets. This procedure ensures that the different numerical responses with different hydraulic conductivity realizations are recorded and incorporated in surrogate model training data. Figure 6.4 represents different realizations of hydraulic conductivity for the same case and how it affects the exit gradient value (contour) shown in Figure 6.5.
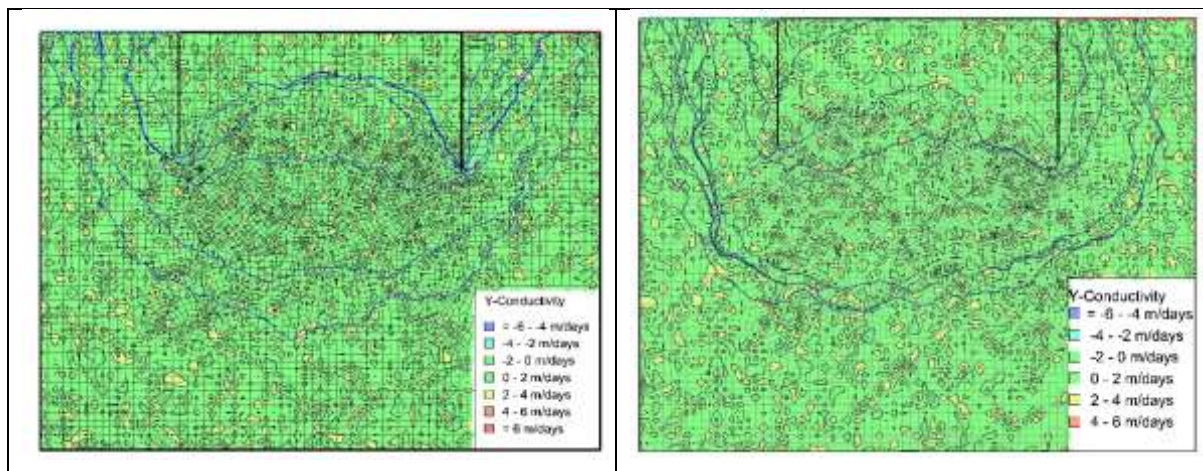
Figure 6.4 Different realizations of hydraulic conductivity for same standard deviation value
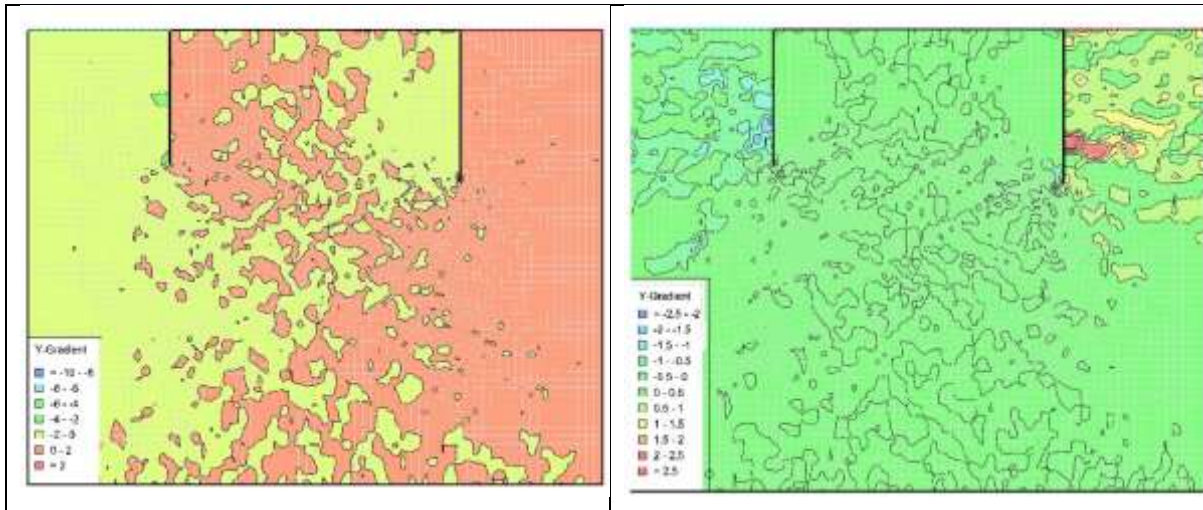
Figure 6.5 Effect of different realizations (for same σ value) of hydraulic conductivity variation on exit gradient contour

Accordingly, the varied seepage quantities, such as uplift pressure on the upstream side (Pc_1), downstream uplift pressure (Pe_2) and exit gradient (ie) value, were determined by the numerical seepage modeling code four times for each input data set (case). Furthermore, because exit gradient value is more critical than other quantities and hydraulic conductivity varies randomly, four points, shown in Figure 6.1, were selected at which exit gradient values were determined for each simulation. Determining four values of exit gradient and ensuring each value was within allowable limits ensured safety for HWRS constructed on a heterogeneous flow domain. Hence, each training data set for a single surrogate model included one set of input design variables (d_1, d_2, b, H) and four stochastically varied sets of output data (Pc_1, Pe_2, ie_1, ie_2, ie_3, ie_4). Therefore, the responses of surrogate models reflect variation of seepage characteristics obtained from the four scenarios of random hydraulic conductivity. For each seepage design variable, five surrogate models were trained to imitate different responses, reflecting the effect of five different hydraulic conductivity random fields drawn from the five log-normal distributions. As a result, 30 surrogate models were built in this study to develop six ensemble stochastic surrogate models linked to the optimization model within the RBOD framework. Each ensemble surrogate model involved five surrogate models, and each represented numerical simulation responses for different hydraulic conductivity random fields for a particular standard deviation value. Based on these stochastic responses, reliability of the design could be quantified.

Deterministic surrogate models were developed separately to compare stochastic optimum solutions with deterministic solutions. Deterministic responses were used to train three surrogate models (Pc_1, Pe_2, ie) based on expected hydraulic conductivity ($\sigma = 0$, $\mu = 2$). Deterministic surrogate models were incorporated in the deterministic S-O model to find the optimum solution of HWRS for different head values.

6.3   Gaussian process regression (GPR) model

Gaussian process regression (GPR) is a stochastic machine learning technique. The Gaussian process involves generalization of the (joint) multivariate Gaussian, which may include a finite collection of random variables following Gaussian distribution. GPR uses probabilistic methods to measure uncertainty of the regression model by defining the distribution of the solution, which likely follows Gaussian distribution. The GPR technique can explore several relationships between training data sets using a finite number of parameters. The best relationship is the one which perfectly matches training data (Rasmussen, 2004). The GPR machine learning technique is selected for current S-O model because many researchers observed that the performance of GPR is even better than SVM and ANN models, as discussed in section 2.5.3.

Primarily, the GPR technique is based on the assumption that there is high probability that $f(x)$ matches $f(x')$ when vector x is adjacent to x'. This relationship (function) can be identified by finding distribution of data utilizing mean function $(m(x))$ and covariance function $k(x, x')$. The covariance function provides good indication of similarity between x and x', and measures corresponding functions' similarity. By incorporating the Bayesian inference statistical concept, the known (observed) data set becomes a conditional distribution (posterior probability) based on an unknown distribution function. The unknown function is based on many random vectors following Gaussian distribution (Rasmussen, 2004; Shi & Choi, 2011).

6.3.1   Gaussian process for regression

Let us assume the function between input (x) and output (y) can be expressed by two terms: f(x) the signal term and ϵ noise term, as shown in Eq. (6.2).

$$y = f(x) + \epsilon \tag{6.2}$$

Where, the noise term follows normal distribution $(\epsilon \sim \mathcal{N}\ (0, \sigma_\epsilon^2))$, the noise term refers to randomness of observations. The signal $f(x)$ term is considered a random variable and follows Gaussian distribution using the Gaussian process, as shown in Eq. (6.3).

$$f(x) \sim \mathcal{GP}\big(m(x), k(x, x')\big)\ ,\quad \text{x} \ni \mathbb{R} \tag{6.3}$$

Where, m(x) is the mean function, which refers to the average of all functions evaluated at point (x), $m(x) = \mathbb{E}[\ f(x)]$. Usually, the prior mean function is taken (0) to make the posterior computations cheaper and because the information of the prior distribution of the unknown function is insufficient. $k(x, x')$ refers to the covariance function measuring dependence of function values for different input points (x and x'), as shown in Eq. (6.4).

$$k(x, x') = \mathbb{E}[\ \big(f(x) - m(x)\big)\big(f(x') - m(x')\big)] \tag{6.4}$$

The covariance function represents the kernel of the Gaussian by which the correlation between two points can be obtained. The kernel function may be any function identifying correlation between two points and can be utilized for $\mathbb{D}$ dimension data. Often, the radial basis function (RBF) is used as a kernel function for GPR. RBF may be varied to increase or reduce correlation between points, providing desired smoothness. Over fitting and under fitting phenomena can be avoided by modifying the length scale (λ) and signal variance (σ_f^2) to provide better fit of the resulting function (Eq. (6.5)).

$$k(x, x') = \sigma_f^2 \exp\left(-\frac{\|x - x'\|}{2\,\lambda^2}\right) \tag{6.5}$$

Theoretically, the function can be represented by a vector of points. Therefore, to find the function vector, a sample of a large number of points is drawn from the multivariate Gaussian distribution (prior distribution) with $\mathbb{D}$ dimension data at an arbitrary point X_*. Then, the covariance matrix for all points is determined. This matrix represents correlation between all points, as shown below. Then, by using the prior mean function $m(X_*) = 0$ and the covariance (kernel) matrix, the values of $f(X_*) = [\,f(X_1^*), f(X_2^*), f(X_n^*)\,]^T$ can be sampled from multivariate distribution, as shown in Eq. (6.6).

$$f(X_*) \sim \mathcal{N}\left(0, k(X_*, X_*)\right) \tag{6.6}$$

$$k(X_*, X) = \begin{bmatrix} k(x_1^*, x_1) & k(x_1^*, x_2) & \dots & k(x_1^*, x_n) \\ k(x_2^*, x_1) & k(x_2^*, x_2) & \dots & k(x_2^*, x_n) \\ \vdots & \vdots & \ddots & \vdots \\ k(x_n^*, x_1) & k(x_n^*, x_2) & \cdots & k(x_n^*, x_n) \end{bmatrix}$$

If the training data is $\{X, f(X)\}$ and test (proposed) data set is $\{X_*, (X_*)\}$ drawn from multiverse normal distribution, then f_* is the unknown function to be found using the GPR technique. Using conditional probability, i.e., posterior distribution, the new data sets (function) drawn from multivariate normal distribution must comply with the observed data set, then condition probability distribution can be written as given in Eq. (6.7).

$$\begin{bmatrix} f_* \\ f \end{bmatrix} = \sim \mathcal{N}\left(0, \left(\begin{bmatrix} K(x\ x) & K(x\ x_*) \\ K(x_* x) & K(x_* x_*) \end{bmatrix}\right)\right) \tag{6.7}$$

The resulting function vector $f(X_*)$ is totally controlled by the observed data set, ignoring the uncertainty in this data and assuming the observed data is the actual function value. More practically, the noise term (ϵ) must be included to provide a more generalized function, as indicated earlier in Eq. (6.2). Therefore, the distribution can be written as:

$$\begin{bmatrix} y \\ f \end{bmatrix} = \sim \mathcal{N}\left(0, \left(\begin{bmatrix} K(x, x) + \sigma_f^2\,I & K(x, x_*) \\ K(x_*, x) & K(x_*, x_*) \end{bmatrix}\right)\right)$$

Where $\sigma_f^2 \, \boldsymbol{I}$ is scale identity matrix. After some manipulation, the posterior $p(\,f_*|y, X, X_*)$ is considered Gaussian distribution with mean $K(x_*, x)\,[K(x,x) + \sigma_f^2 \, \boldsymbol{I}]^{-1}\boldsymbol{y}$ and covariance matrix $[K(x_*x_*) - K(x_*, x\;)[K(x,x) + \sigma_f^2 \, \boldsymbol{I}]^{-1}K(x, x_*)$. Then f_* can be defined based on the mean function and kernel function, as shown in Eq. (6.7) (Rasmussen, 2004; Roberts et al., 2013).

The GPR surrogate models were implemented using Matlab. Parameters of the utilized GPR are shown in Table 6.1. After many iterations of trial and error, we found that the listed parameters provided a better prediction. The rest of the GPR options were similar to Matlab default options.

Table 6.1 Properties of the GPR technique

	Properties	Value
1	Prediction method	Exact
2	Kernel function	Squared exponential kernel with a separate length scale per predictor
3	Fit method	Exact
4	Basis function	Constant

6.3.2 Surrogate model performance

Building a surrogate model to use in the S-O approach is a delicate task. Although surrogate models provide an expeditious alternative to numerical models, the training and testing phases need to be established carefully and accurately. Performance of surrogate models must be precisely evaluated before being used in the S-O approach. Efficiency and accuracy of developed surrogate models increase robustness of the linked S-O based RBOD technique. The evaluation strategy is based on many statistical error measures (indices). Each measure is based on different criteria and involves different statistical variables. In addition to conventional error measures, such as mean square error (MES) (Eq. (6.12)), standard deviation of error (STD_ERROR) and mean error (M-Error), these measures are briefly described below, with more information found in (Gupta, Sorooshian, & Yapo, 1999; Moriasi et al., 2007).

Correlation coefficient (R): this measure provides an indicator to evaluate the linear relationship between observed and predicted data. The range of R is between -1 and +1. Criteria to determine R are shown in Eq. (6.8). Value of R greater than 0.5 is acceptable.

$$R = \frac{\sum_{i=1}^{n}(\hat{y}_i - \bar{\hat{y}})\;(y_i - \bar{y})}{\sqrt{\sum_{i=1}^{n}(\hat{y}_i - \bar{\hat{y}})^2(y_i - \bar{y})^2}} \tag{6.8}$$

Where $\hat{y}$ is predicted data; y is observed data; and $\bar{y}$, $\bar{\hat{y}}$ refers to mean of observed and predicted data, respectively.

Nash-Sutcliffe efficiency (NSE): this normalized coefficient measures residual variance to measured data variance. The range of NSE is between -∞ and +1. NSE values between 0 and 1 are considered accepted and perfect performance of the model is achieved when NSE value attains 1. The NSE index can be determined using Eq. (6.9).

$$NSE = 1 - \left[\frac{\sum_{i=1}^{n}(\hat{y}_i - y_i)^2}{\sum_{i=1}^{n}(y_i - \bar{y})^2} \right] \tag{6.9}$$

Percent bias (PBIAS): is used to provide a perspective of how much the average of predicted data is larger or smaller than counterpart observed data. Positive values indicate that the model is an overestimation and negative values indicate the model is an underestimation. The ideal value of PBIAS is 0. The PBIAS measure criteria is shown in Eq. (6.10).

$$PBIAS = \frac{\sum_{i=1}^{n}(y_i - \hat{y}_i) \times 100}{\sum_{i=1}^{n}(y_i)} \tag{6.10}$$

Root mean square error to standard deviation ratio (RSR): The RSR ratio is a standardized index error measure. It provides indication of the error ratio to the standard deviation of observed data, as shown in Eq. (6.11). The RSR value is equal to or greater than zero, and the prefect prediction is obtained when RSR approaches zero.

$$RSR = \frac{RMSE}{STD_{obs}} = \frac{\sqrt{\sum_{i=1}^{n}(y_i - \hat{y}_i)^2}}{\sqrt{\sum_{i=1}^{n}(y_i - \bar{y})^2}} \tag{6.11}$$

$$MSE = \frac{\sum_{i=1}^{n}(\hat{y}_i - y_i)^2}{n} \tag{6.12}$$

All statistical error measures and indices discussed above were used to evaluate developed surrogate models for training and testing data. All surrogate models satisfied error measure limits. The majority of surrogate models provided high accuracy predictions and most of index values reached optimum values. Some surrogate models, especially exit gradient models of high standard deviation (3.65) cases, provided slightly deviated predictions, but were within ideal ranges. Samples of testing and training error measures corresponding to each model are listed in Table 6.2. Also, some samples of graphic training and testing results for different models are shown in Figure 6.6 to Figure 6.11, giving good inference about performance of the GPR technique to imitate the complex relationship related to seepage characteristics incorporating uncertainty in some design parameters.

Table 6.2 Samples of surrogate model training testing error measures

	ie_1		ie_2		ie_2		ie_2		pc_1		pe_2	
	train	test	train	test	train	test	train	test	train	test	train	test
MSE	0.17	0.28	0.107	0.121	0.09	0.25	0.14	0.12	3.09	5.69	9.76	8.78
STD-ERROR	0.42	0.53	0.327	0.344	0.30	0.50	0.37	0.34	1.76	2.35	3.13	2.94
M-error	0.00	-0.05	0.000	-0.066	0.00	0.05	0.00	-0.04	0.00	0.52	0.00	0.51
NSE	0.54	0.37	0.696	0.428	0.74	0.73	0.64	0.54	1.00	0.99	0.99	0.98
RSR	0.68	0.80	0.551	0.757	0.51	0.52	0.60	0.68	0.06	0.07	0.12	0.13
PBIAS	0.00	-9.74	0.000	-12.08	0.00	6.83	0.00	-5.77	0.00	1.05	0.00	1.68
R	0.73	0.64	0.830	0.710	0.86	0.88	0.80	0.77	0.99	0.99	0.99	0.99
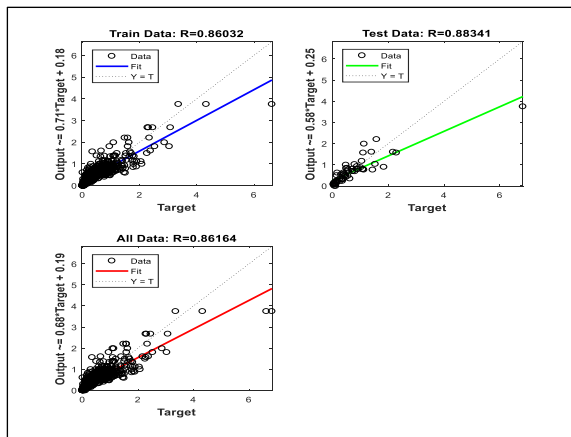
Figure 6.6 Training-testing R index for the surrogate model (ie_3) (STD=2.25 m/day)
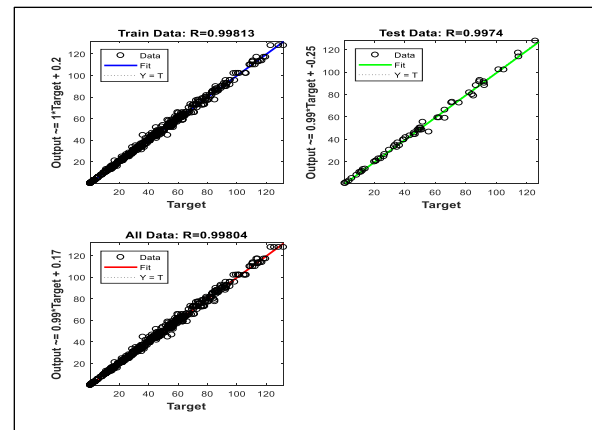
Figure 6.8 Training-testing R index for the surrogate model (PC_1) for (STD=2.25 m/day)
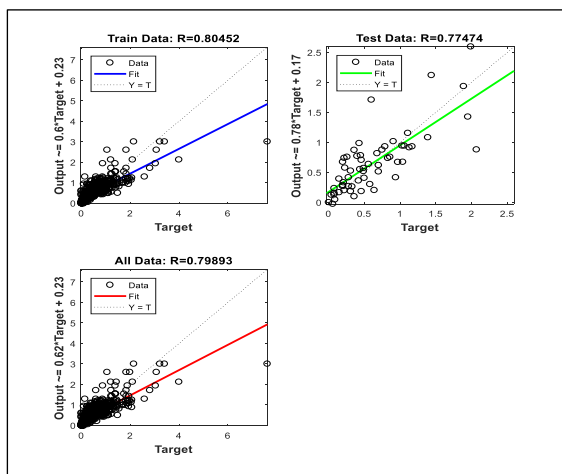
Figure 6.7 Training-testing R index for the surrogate model (ie_4) (STD = 2.25 m/day)
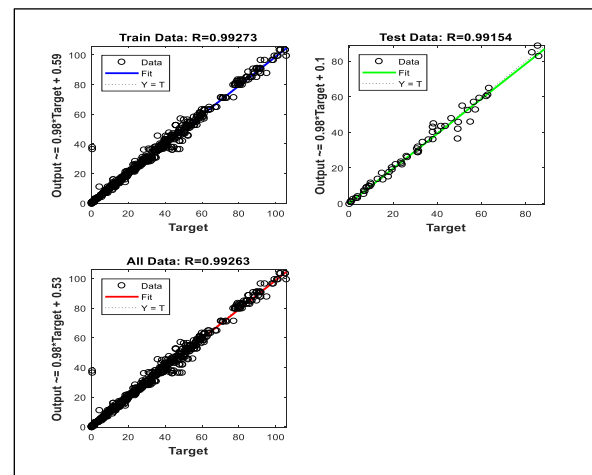
Figure 6.9 Training-testing R index the surrogate model (PE_2) (STD = 2.25 m/day)
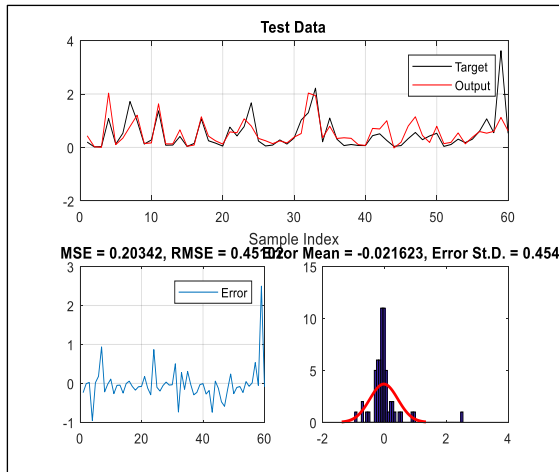
Figure 6.10 ie₂ surrogate model prediction for test data (STD = 2.95 m/day)
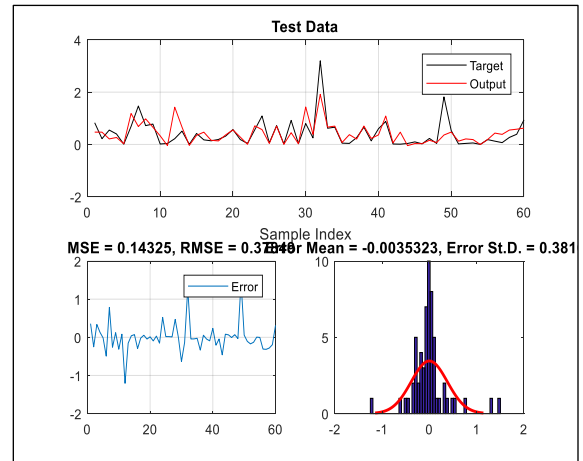
Figure 6.11 ie₁ surrogate model prediction for test data (STD = 2.95 m/day)

129

6.4 Formulating the reliability based optimization model

The aim of the optimization model is to find the optimum design of HWRS restricted by a particular level of reliability. As performance criteria of seepage are based on developed surrogate models, it is more applicable to use the multiple realization technique based on the stochastic S-O model to find the optimum solutions. The multiple realization 'stacking' optimization approach has been used by many researchers (Chan, 1993; Feyen & Gorelick, 2005; Sreekanth & Datta, 2011). In some previously conducted multiple realization optimization models, the reliability degree was specified in advance and the optimization process stopped when post optimality multi-realization criteria reached the desired level. Similarly, in this study reliability level was specified beforehand and the optimum design of HWRS satisfied that level of reliability at minimum cost, based on the multi-realization optimization technique. This can be achieved when the optimum solution satisfies a certain number of stochastic responses of all safety factors (constraints) of total incorporated responses. This means a particular reliability value (**n/m**) could be established within the S-O model by imposing candidate design to satisfy **n** stochastic constraints of the total number (**m**) of constraints based on safety factors of HWRS design. Each stochastic constraint is based on responses of **m** surrogate models within the stochastic ensemble surrogate model. For each safety factor, the reliability value **n/m** of the optimum design represents that at least (any) **n** stochastic constraints of all involved stochastic constraints (**m**) in the S-O model must be satisfied. Reliability is considered 100% when **m/m** of all constraints are satisfied and considered 50% when **0.5m/m** of stochastic constraints are satisfied, etc.

It is also important to note that some stochastic design variables, such as thickness of the floor upstream and downstream (t_1, t_2), involved in computation of the objective function are based on stochastic ensemble surrogate models. Therefore, to provide safe design the maximum values of each thickness were considered in determining the objective function.

The multiple realization optimization based RBOM using stochastic S-O model was formulated as:

Find $X = \{x_1, x_2, x_3, x_{4,}\} = \{d_1, d_2, b, b^*\}$

Minimize the construction cost of the HWRS:

$$f(X) = c_f \, x_3 \, \frac{\max \, (t_1^m) + \max(t_2^m)}{2} + t_c \sum_{s=1}^{2} c_s^c \, x_s \tag{6.13}$$

Subject to:

$$FS\_ie_i^m = \varepsilon_i^m \, (H, d_1, d_2, b, k_m, ie_{crt}) \qquad \forall \, i, m \tag{6.14}$$

$$FS\_ie_i^m \geq FS_{exit} \qquad \forall \, i, m \tag{6.15}$$

$$FS\_FL_{US}^m = \epsilon^m (H, d_1, d_2, b, k_m) \quad \forall \, m \tag{6.16}$$

$$FS\_FL_{US}^m \geq FS_{uplift} \quad \forall \, m \tag{6.17}$$

$$FS\_FL_{DS}^m = \gamma^m (H, d_1, d_2, b, k_m) \quad \forall \, m \tag{6.18}$$

$$FS\_FL_{DS}^m \geq FS_{uplift} \quad \forall \, m \tag{6.19}$$

$$k_m = Log \, normal \, (M, \delta) \quad \forall \, m \,, \quad k_m \in (0, \infty) \tag{6.20}$$

Where t_1^m, t_2^m represents stochastic thickness of the floor at the upstream and downstream sides (Figure (6.1)), respectively. These thicknesses were determined utilizing (**m**) stochastic surrogate models. c_f is the cost of constructing the floor per cubic meter ($400/m³); c_s^c is construction cost of the cut-off per cubic meter, which is a function of depth of the cut-off, as shown in Eq. (6.21)(similar to Eq. (3.9) and (3.10)), t_c is thickness of the cut-off and is equal to 1.0 m.

$$c_s^c = x_s^3 + 20 \, x_s^2 + 200 \, x_s + 400 \quad \forall \, s \tag{6.21}$$

$FS \, ie_i^m$ are **m** realizations of the exit gradient safety factor determined based on m surrogate models $\{\varepsilon_i^m( )\}$ and for each location (i) there are **m** realizations of the exit gradient safety factor. ie_{crt} is the critical exit gradient value (1.15). FS_{exit} is the minimum allowable exit gradient safety factor, which was considered 3 in current optimization model because achieving an optimum solution based on exit gradient safety factor value equal 5 was difficult (Harr, 2012; Khosla et al., 1936). $FS \, FL_{US}^m$, $FS \, FL_{DS}^m$ are the stochastic safety factors to impose the weight of upstream and downstream floor of HWRS to safely counterbalance uplift pressure ($Pc_1{}^m$, $Pe_2{}^m$) (Bligh, 1915; U.S. Army Corps of Engineers, 1987). The $FS\_FL_{US}^m$, $FS\_FL_{DS}^m$ were computed by **m** stochastic surrogate models $\{\epsilon^m( )\}$, $\{\gamma^m( )\}$, respectively.

Additionally, as explained in Chapter Three, there were many other stochastic safety factors based on the stochastic responses of uplift pressure ensemble surrogate models ($Pc_1{}^m$, $Pe_2{}^m$). These safety factors represent requirements of HWRS design, such as eccentric load condition limits, sliding and overturning safety factors (Garg, 1987) . Other logical and boundary constraints were utilized to prevent the optimization solver from presenting illogical and negative values. The total number of stochastic constraints was 10 and each had to satisfy different realization of seepage quantities. A flow chart of RBOD using the stochastic S-O model is shown in Figure 6.12.
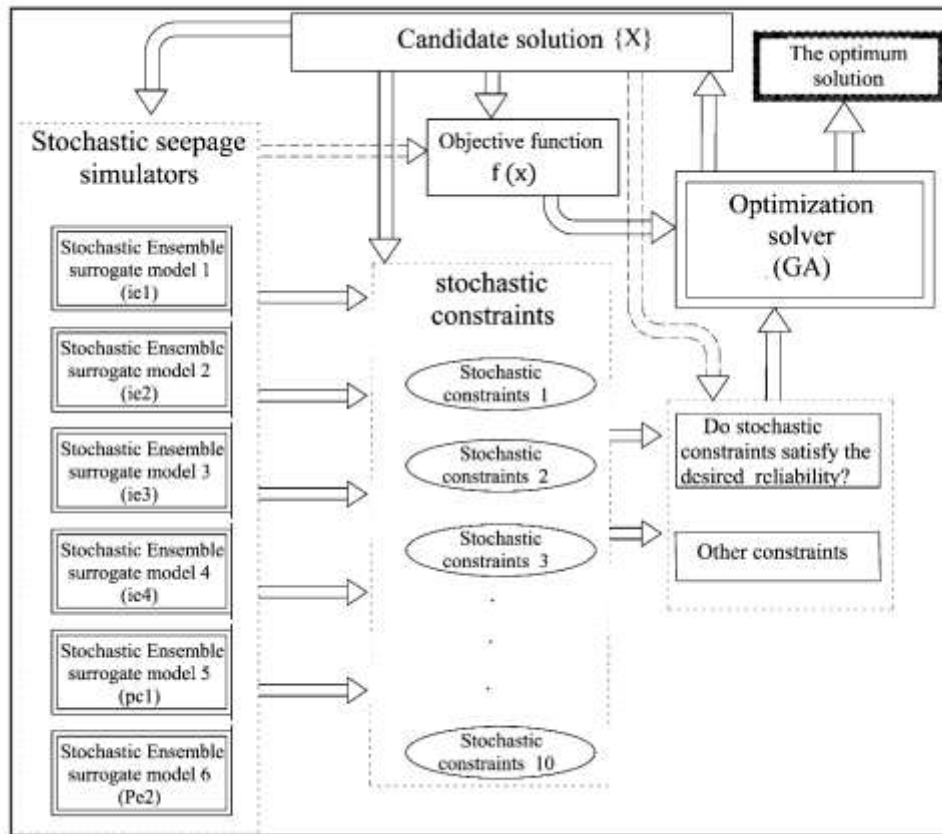
Figure 6.12 Illustrative formulation of reliability based stochastic S-O model

The genetic algorithm (GA) also was used for this optimization task because GA is a powerful optimization solver. The parameter combination of GA was selected by many processes of trial and error. GA parameters in this study were: population size 2,000; elite count 20; crossover fraction 0.6; objective function tolerance 1e-6; constraint tolerance1e-6; with the remaining GA parameters the same as default Matlab options.

6.5   Computational efficiency of the S-O model

The optimization task in such formulation is computationally expensive and time consuming, especially when the GA based direct search technique is utilized incorporating responses of many stochastic ensemble surrogate models. Furthermore, a large population is required to obtain an almost global optimum solution by GA. Consequently, optimization processes take longer.

Two strategies were employed to significantly increase linked S-O computational efficiency. The first was to use parallel processing based on a multicore computation processor. This option in Matlab distributes computing tasks to multi workers (cores), which doubles computing efficiency. The second strategy was nested function formulation. Usually, the objective function and constraint codes are written in two detached files, where the surrogate models are uploaded separately to each code and then the optimization algorithm continually invokes these codes to separately evaluate the constraints

and objective function. Such operations are implemented numerous times in the optimization model. Hence, the optimization model takes a long time to find the optimum solution. In contrast, by employing a nested function framework, both the constraints and objective function codes are written in the same file (nested function). Surrogate models are uploaded at one time to the nested function and the resulting objective function and constraint values are directly utilized by the optimization solver. This strategy accelerates computational speed by around 100% (MathWorks, 2015).

6.6   Results and discussion

The RBOD framework based on stochastic S-O methodology was applied to illustrative hypothetical cases to study the effect of reliability on optimum design of HWRS. In these cases, average hydraulic conductivity (2 m/day) and the five prescribed standard deviations were used to generate different scenarios of heterogeneous hydraulic conductivity. Upstream head values (H) were 10m, 20m, 40m, 60m, 80m and 100m. The S-O models were implemented with different reliability levels (20%, 40%, 60%, 80% and 100%). The percentage of reliability only reflects the uncertainty of seepage quantities under HWRS due to uncertainty of heterogeneous hydraulic conductivity. The objective function of the optimization model was minimum construction cost of HWRS. Constraints represent the hydraulic requirements and safety factors related to design of hydraulic structures, as discussed in Chapter Three.

The effect of the reliability on optimum design of HWRS could be clearly seen by comparing obtained minimum construction costs for different reliability levels, as shown in Figure 6.13. As logically expected, augmenting the reliability significantly increased construction cost. For instance, construction cost of HWRS impounded 100 m water head with 100% reliability was around $143 million/m, whereas the cost was $102 million/m with 60% reliability. This infers that considering reliability substantially affects design of HWRS. Furthermore, ignoring hydraulic conductivity uncertainty may result in unsafe design, although deterministic safety factors are used. The deterministic optimum design, based on constant hydraulic conductivity (2m/day), is also presented in Figure 6.13. In general, the minimum deterministic cost curve was below the 60% reliability curve. However, only when the head reached 80 m, the deterministic model move above the 60% reliability curve. This provides general understanding that equivalent reliability of the deterministic design can be considered as 50 % to 60 %, which is an unsatisfactory reliability level for such an important structure. Consequently, deterministic safety factors, especially exit gradient, should be at least twice the actual values actually achieved as per deterministic modeling.
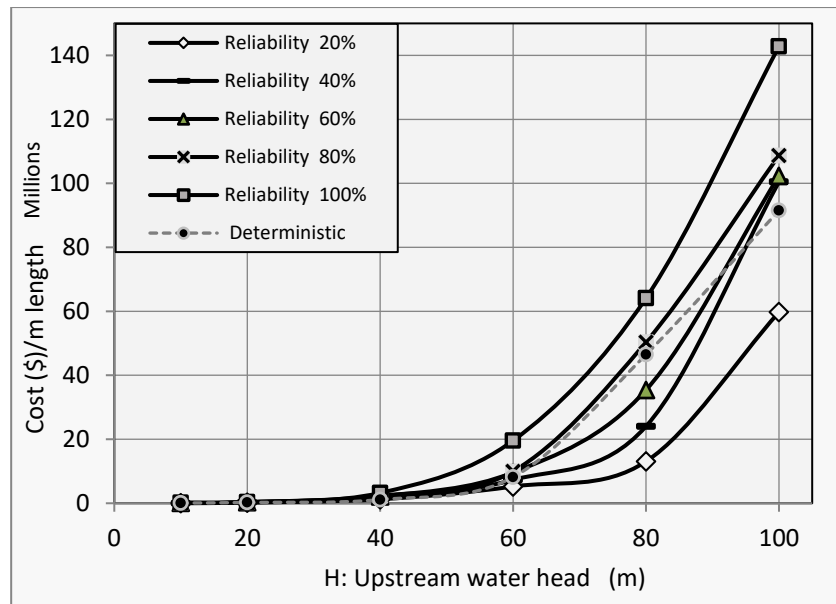
Figure 6.13 Optimum cost of HWRS for different reliability levels and different head values

The optimum lengths for upstream cut-off (d_1) versus different levels of reliability for different head values are shown in Figure 6.14. The main role of d_1 is to directly reduce the uplift pressure under the floor of HWRS and, indirectly, to reduce exit gradient value. This is because the exit gradient value proportions to uplift pressure value located before downstream cut-offs. In general, optimum length of d_1 decreased with reduced head value. In contrast, optimum length of d_1 was augmented by increasing degree of reliability. However, for some values, especially with 100% reliability at H (80, 40) m, optimum length was less than other reliability levels. This can be explained by considering that the objective function minimizes construction cost. Therefore, the optimization solver presents minimum construction cost for each case separately, as long as the decision vector satisfies constraints. On the other hand, because the surrogate model responses are stochastic responses, it is extremely difficult to expect the optimum value with different reliability levels. Furthermore, if the optimization solver could provide an optimum solution that satisfies, for example, three of five (60% reliability) stochastic constraints, that does not guarantee the optimum solution with 80% reliability is close to the 60% solution. The justification being that additional stochastic constraint may require a larger value of that variable, e.g. d_1, which significantly increases the objective function value. Consequently, the optimization solver (GA) changes the direction of search and continues with a more promising direction that provides lesser cost. Moreover, while the objective function is minimum construction cost, the optimum solution with a certain reliability level does not promise to follow the general trend of the other reliability levels. For instance, the optimum value for d_1 at H equal to 80m with reliability 100% was unexpectedly less than other values. That may be logical if the values of d_2, b and b* are considered simultaneously for this case. The value of d_2, shown in Figure 6.15, for the same case was extremely larger than other reliability levels because d_2 is more important to reduce the crucial exit gradient value to the safe limit.

134

On the other hand, optimum value of d_2, shown in Figure 6.15, proportionally increased with an increase in level of reliability. This design variable is the most important variable as it controls exit gradient value. In reliability results, the majority of violated constraint was due to the exit gradient safety factor. Therefore, the optimum solution for d_2 with 100% reliability presents the highest value for different H values to satisfy all stochastic responses due to uncertainty of heterogeneous hydraulic conductivity.

Therefore, the optimum solution for each component of the decision vector must be simultaneously considered with other components in the same case. Thus, the optimization task for such problems is complex. Obtaining the optimum solution based on different reliability levels, including stochastic constraints, needs continuous variation of search directions for the optimum solution. Consequently, with such complex formulation of the stochastic optimization model, the GA efficiently provided the optimum solutions based on the minimum cost objective function.

There are two aspects possibly affecting the performance of the optimization algorithm. First, the complexity of the optimization model prevents the GA from finding the global optimum solution (Dorsey & Mayer, 1995). Increasing the reliability level augments the number of stochastic constraints, which restricts the GA searching process and decreases the possibility to find a feasible solution. Second, although in general the training accuracy level of surrogate models was within standard error limits, such as NASH and R, etc., there was weak prediction in some extreme ranges. Such predictions may affect the optimization process. Also, this may be attributed to training data which was based on different realizations of hydraulic conductivity drawn from different values of standard deviation. This could decrease the efficiency of prediction for some surrogate models and may affect the optimum solution.
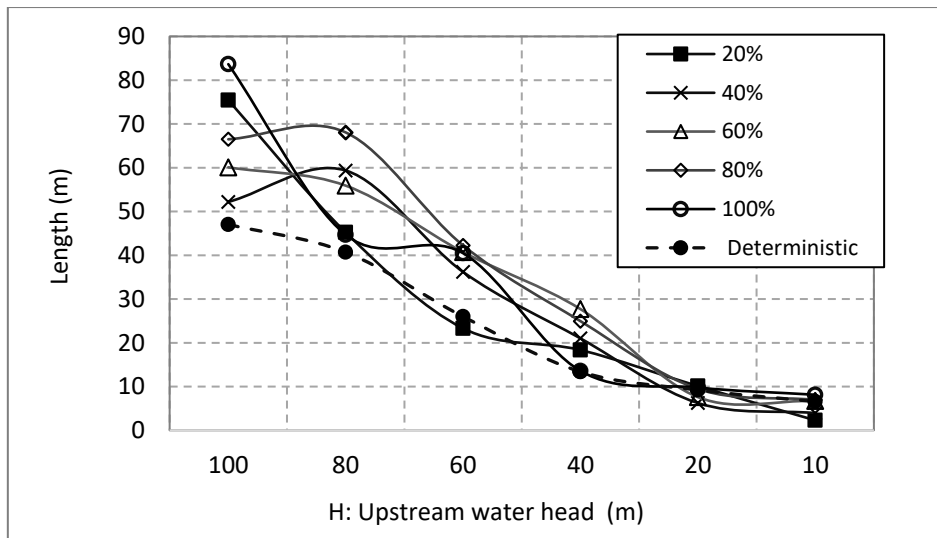
Figure 6.14 Optimum length of upstream cut-off (d_1) for different reliability levels and different head values
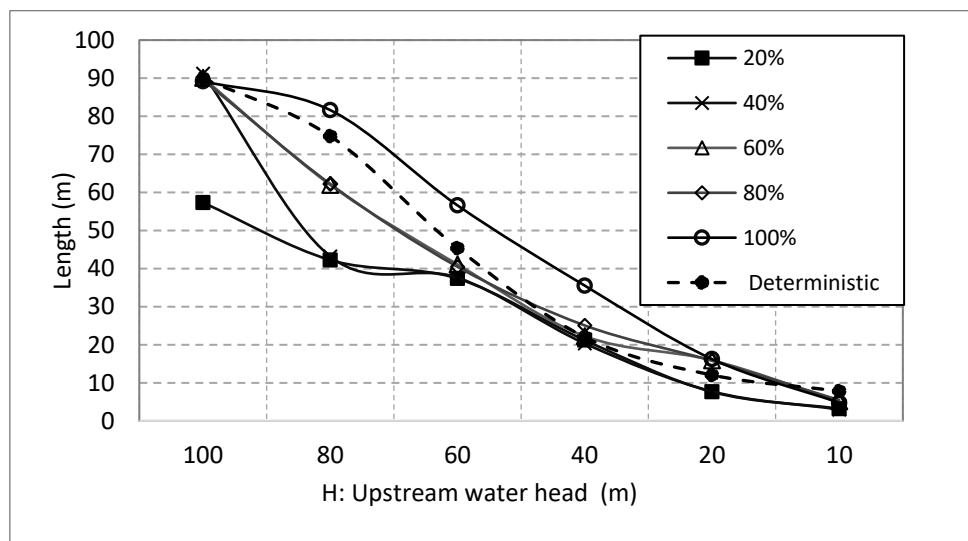
Figure 6.15 Optimum length of downstream cut-off (d_2) for different reliability levels and different head values

Figure 6.16 shows optimum values for the total width (b) of HWRS. Optimum length of b is the lowest value for high reliability for different head values. This can be explained by two reasons. First, the objective function is minimum cost. Accordingly, the minimum cost scenarios may be satisfied with any one of five stochastic constraints that provide minimum cost. For example, optimum width (b) with 20% reliability had more than 100% reliability at H = 80m. Simultaneously, the optimum depth of downstream cut-off for the same H value with reliability of 100% was much larger than when reliability was 20%. Therefore, as the objective function is minimum cost, there are many different scenarios that provide minimum cost regarding different reliability levels. Second, the role of b is to provide a sufficient weight to counterbalance the uplift pressure on the HWRS and to provide sufficient width satisfying the sliding, overturning constraints and preventing the eccentric load condition. As the most critical safety factor was the exit gradient, the b value did not play as much of a critical role in the optimization process as d_2. Hence, the optimization solver decreased the value of b and simultaneously

136

increased the value of b*, which provided additional weight coming from upstream water (Figures 6.17, 6.1). However, for high reliability levels (60 %, 80 %, 100 %), the optimum b value increased when H approached 10 m. This is due to additional weight resulting from upstream water, covering b*, was not enough to satisfy the uplift pressure and other safety factors. The additional water height was low because the floor thickness value on the upstream side approached 10 m. As a result, the GA increased b value to satisfy the required conditions and safety factors.
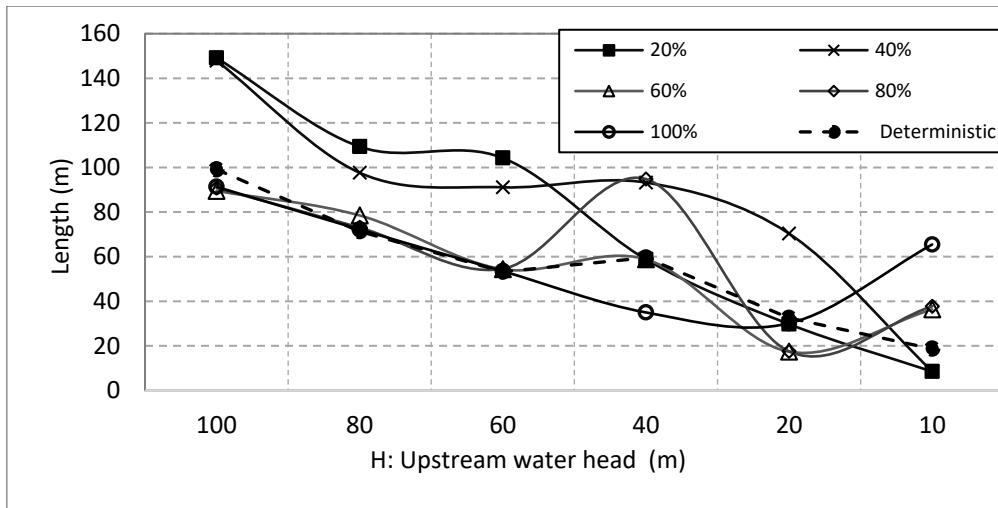
Figure 6.16 Optimum length of the total width (b) for different reliability degree and different head value
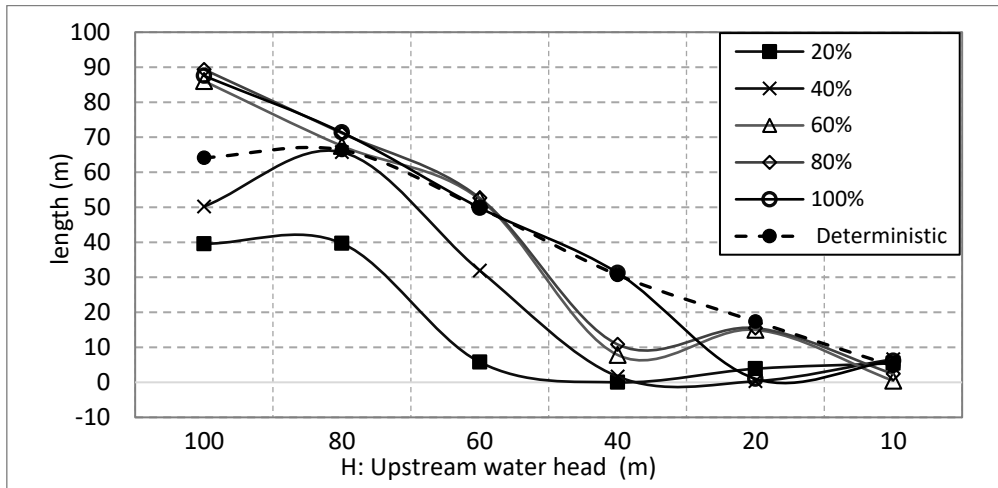
Figure 6.17 Optimum length of (b*) for different reliability degree and different head value

The surrogate models' responses in each ensemble are varied based on the training data set, which is based on different realizations of hydraulic conductivity. Figure 6.18 demonstrates the varied ie_1 responses of the five surrogate models for a hundred randomly selected cases of (d_1, d_2, b, b*, H). The perdition for each surrogate model was diverse from case to case. For example, in case 41, the predictions for ie_1 were (2.89, **3.14**, 1.91, 1.56, 1.63), for case 23 (**2.10**, 1.94, 1.73, 1.54, 1.42) and for case 80 (0.88, 0.86, 0.91, 0.79, **1.05**), which were predicted by (ie_1 (0.85), ie_1 (1.55), ie_1 (2.25), ie_1

(2.95), ie_1 (3.65)), respectively. The ie_1 (0.85), for example, refers to the exit gradient surrogate model (for the first point) trained using data set simulated based on numerical model including heterogeneous hydraulic conductivity drawn from Log-normal distribution ($\mu = 2$, $\sigma = 0.85$). This concludes that the performance of the surrogate models is unsystematically varied form cases to case; it might also explain to some extent the variation of the optimum solution behaviour.
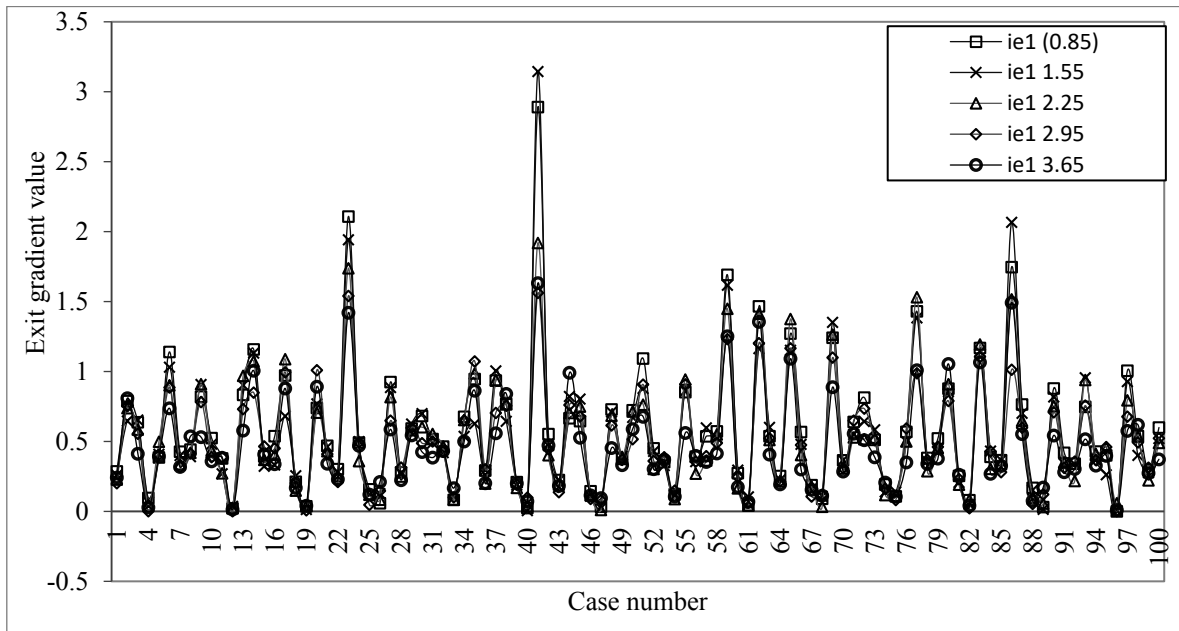
Figure 6.18 Sample of surrogate model (ie_1) prediction from different stochastic surrogate models

6.7 Evaluation of results

Usually, in the deterministic S-O techniques, efficiency of the developed methodology can be assessed by comparing seepage characteristics of the optimum design obtained by S-O methodology to seepage characteristics obtained by the numerical seepage modeling for the same optimum solution. However, in the RBOD optimum solution, each single optimum solution represents a particular level of reliability and different realizations of hydraulic conductivity. Consequently, the evaluation method must incorporate the reliability degree and hydraulic conductivity uncertainty for each optimum solution. As a result, each solution must be evaluated at least 50 times; five times for the five σ values and at least 10 times to integrate different realizations of hydraulic conductivity for each σ value to quantify reliability. Implementing and presenting such a procedure for all results is time consuming and does not suit time-limited research.

To evaluate the optimum solution, random samples of optimum solutions were selected. The evaluation process included comparing seepage characteristics of the selected optimum solution with numerical model seepage characteristics of the same case, incorporating 10 different realizations of hydraulic conductivity randomly generated based on a particular standard deviation value. Additionally,

the evaluation was implemented only for exit gradient value, because the exit gradient value is the most critical variable and is impacted by hydraulic conductivity uncertainty.

Conducted evaluations, shown in Table 6.2, include different samples of optimum solutions from different reliability levels. The exit gradient value for four locations (points) (ie_1, ie_2, ie_3, ie_4) were evaluated for each case. The exit gradient value for each case had to be equal or less than 0.383, satisfying an exit gradient safety factor of 3 or more. To validate reliability for each optimum solution, the seepage modeling code was run ten times with new random realizations of hydraulic conductivity for each new iteration. The number of exit gradient values satisfying the allowable limit for each location divided by the total number of iterations (10) provided the actual reliability level. Additionally, standard deviation values were randomly assigned to each case.

Table 6.3 displays evaluation results for four samples of optimum solutions, with violated exit gradient values highlighted in grey. It is clear that actual reliability level for each optimum design matched the proposed reliability for the optimum solution. Average actual reliability level of case B was more than desired reliability (60%). In contrast, average actual reliability of case C was slightly less than desired reliability (80%). This can be attributed to two reasons. First, hydraulic conductivity is a completely random field and each new realization of hydraulic conductivity is totally different to training realizations. Hence, when the number of iterations is increased to 100, for example, more understanding can be achieved for actual reliability. Second, the number of surrogate models grouped in the stochastic ensemble surrogate model was five, which may not be enough to efficiently and accurately quantify reliability level. Furthermore, the allowable error in surrogate model predictions slightly affected optimum solutions and actual reliability.

In general, the proposed technique to evaluate reliability of the optimum design was validated and provides good indication and understanding of design reliability. Consequently, the RBOD framework using stochastic S-O models based on multiple realization optimization technique provides a reliable and optimum solution, significantly matching the actual reliability of the design. Furthermore, stochastic S-O methodology based on many ensemble surrogate models trained using the GPR technique is computationally efficient and provides accurate results for reliability based optimum design of HWRS.

Table 6.3 Evaluation results for four randomly selected optimum solutions

Case A	σ = 2.95	Rel = 60%			Case B	σ = 2.25	Rel =60%		
optimum design	H	d1	d2	b	optimum design	H	d1	d2	b
	80	55.91	61.9	78.48		10	6.73	5.16	36.33
Iteration	ie1	ie2	ie3	ie4	Iteration	ie1	ie2	ie3	ie4
1	0.25	0.15	0.27	0.39	1	0.53	0.27	0.15	0.18
2	0.3	0.386	0.32	0.22	2	0.24	0.22	0.25	0.15
3	0.39	0.25	0.91	0.93	3	0.23	0.25	0.2	0.17
4	0.47	0.24	0.55	0.74	4	0.42	0.17	0.023	0.266
5	0.16	0.32	0.52	0.94	5	0.09	0.27	0.387	0.18
6	0.14	0.69	0.66	0.05	6	0.098	0.22	0.26	0.18
7	0.74	0.43	0.43	0.68	7	0.159	0.121	0.64	0.21
8	0.09	0.21	0.19	0.05	8	0.1	0.15	0.329	0.16
9	0.03	0.32	0.27	0.22	9	0.183	0.24	0.23	0.3
10	0.08	0.29	0.06	1.02	10	0.107	0.26	0.28	0.21
Actual reliability	70%	70%	70%	50%	Actual reliability	80%	100%	80%	100%
Case C	σ = 2.95	Rel =80%			Case D	σ = 3.65	Rel =80%		
optimum design	H	d1	d2	b	optimum design	H	d1	d2	b
	100	66.50	89.59	90.77		40	24.95	25.08	94.80
Iteration	ie1	ie2	ie3	ie4	Iteration	ie1	ie2	ie3	ie4
1	0.84	0.56	0.47	0.7	1	0.02	0.25	0.24	0.02
2	0.61	0.42	0.34	0.39	2	1.18	0.72	0.14	0.49
3	0.4	0.3	0.26	0.33	3	0.035	0.13	0.11	0.199
4	0.21	0.32	0.52	0.36	4	0	0.28	0.39	0.11
5	0.04	0.16	0.39	0.27	5	0.89	0.51	0.31	0.26
6	0.05	0.03	0.57	0.56	6	0.13	0.15	0.13	0.15
7	0.23	0.34	0.21	0.28	7	0.19	0.129	0.11	0.22
8	0.29	0.17	0.19	0.23	8	0.12	0.39	0.5	0.41
9	0.16	0.28	0.33	0.17	9	1.28	0.72	0.08	0.05
10	1.23	0.87	0.229	0.18	10	0.1	0.14	0.25	0.8
Actual reliability	70%	70%	60%	70%	Actual reliability	70%	60%	80%	70%

6.8   Conclusion

Incorporating reliability in optimization models is an advanced technique and there are limited studies dealing with such reliability testing. This may be attributed to complex formulation of the optimization model, in addition to associated computational burden, particularly when the optimization model is linked to direct numerical simulation modeling. The uniqueness of the current study was consideration of uncertainty of seepage characteristics resulting from random field hydraulic conductivity, representing a fully heterogeneous flow domain under HWRS. This study successfully and efficiently restricted optimum design of HWRS to a desired reliability level based on many expeditious stochastic ensemble surrogate models combined with a direct search optimization algorithm (GA).

The issue of time consuming and computationally expensive optimization problems were partially addressed utilizing nested function and parallel computing techniques. These preparations improved model efficiency (solution speed) about four times, compared to the normal model's computation speed. The GA solver based multiple realization optimization technique was used in this

study incorporating many stochastic safety factors (constraints) and minimizing construction cost of HWRS. Several sets of well-trained surrogate models utilizing the GPR machine learning technique were grouped in many ensemble stochastic surrogate models to be integrated in the linked stochastic S-O model. Reliability level was quantified by determining the percentage of successful or violated scenarios within the RBOD framework.

The developed methodology was implemented for many hypothetical cases impounding different upstream water head values to find the minimum construction cost of HWRS with varied reliability levels. Results demonstrated that high reliability value augments construction cost of HWRS. Furthermore, uncertainty of heterogeneous hydraulic conductivity and related seepage characteristics strongly affect HWRS design. As the objective function minimizes construction cost based on stochastic responses of the ensemble surrogate model, some optimum decision vectors (d_1, d_2, b, b*) were irregular, compared to the deterministic trend. Deterministic results based on a constant value (2 m/day) of hydraulic conductivity compared to stochastic results show that reliability of the deterministic is located between 50% and 60%. The 50% reliability of design means the opportunity for all stochastic constraints to violate the limits is high, which may lead to failure of HWRS. As a result, the deterministic safety factors must be greater than the utilized value to satisfy at least 80% reliability for all cases. This would be true if we considered that utilized deterministic safety factors addressing uncertainty in hydraulic conductivity only.

The most important design variable was downstream cut-off depth (d_2). This variable substantially controls exit gradient value, which is the most critical seepage characteristic. This was clear when a comparison was conducted for the number of violated exit gradient values with the desired reliability level (Table 6.2). Also, the 100% reliability curve for d_2 was the maximum value for all implemented cases.

The main role of upstream cut-off (d_1) was to reduce uplift pressure on the foundation of HWRS. The b and b* provide a sufficient weight to safely counterbalance uplift pressure values and to satisfy other design requirements, such as sliding, overturning and eccentric load conditions. Incorporating the b* value in the optimization model drastically decreases construction cost because the additional cheap weight resulting from water pressure covering the upstream side of HWRS decreases required thickness and width of HWRS (Figure.6.1).

The developed surrogate models based on the GPR machine learning technique were evaluated by many statistical error measures and all built surrogate models provided an accurate prediction corresponding to different error and performance indices for training and testing phases. This infers that GPR provides robust surrogate models, even when training data is based on random realizations of hydraulic conductivity based on different standard deviation values.

Results of RBOD were evaluated to find efficiency of multiple realization optimization techniques in quantifying reliability of the design. Results of the evaluation demonstrated that the proposed methodology can provide an optimum design with a predefined reliability agreeing with actual reliability level. However, there was a slight deviation of some evaluation results, which could be overcome by increasing the number of evaluation iterations and number of surrogate models in the stochastic ensemble surrogate models. Finally, the proposed methodology is applicable to find a reliability based optimum design of HWRS and it can be applied to find the optimum reliable solution for similar problems in different disciplines.

To improve the performance of the methodology and overcome some limitations of this study, it is recommended that future studies incorporate more random realizations of hydraulic conductivity for each case and separately train each surrogate model corresponding to each set of realizations. However, this procedure may need a super high speed processor unit as the number of surrogate models is huge. Also, the optimization solver (GA) performance could be improved by optimizing the GA parameter using Taguchi method, for example, and hybrid GA with gradient search optimization techniques. Also, it is recommended to consider uncertainty of some parameters in the design, such as soil cohesion factor (C), internal friction factor (f) and variables related to the critical exit gradient value.

Some limitations of this study reported in this chapter are addressed in Chapter Seven. A more realistic formulation is proposed based on multi-objective multi-realization technique, utilized to quantify uncertainty in seepage characteristics due to uncertainty in estimation of hydraulic conductivity. The number of surrogate models incorporated in each stochastic ensemble surrogate model is also increased. The 'vectorized' optimization technique is utilized to increase computational efficiency of the RBOD based on linked S-O models.

7 Optimum Design of Hydraulic Water Retaining Structures Incorporating Uncertainty in Estimating Heterogeneous Hydraulic Conductivity Utilizing Stochastic Ensemble Surrogate Models within Multi-Objective Multi-Realization Optimization Model

A similar version of this chapter is submitted and under review for publication in the Journal of Computational Design and Engineering, as shown below:

Al-Juboori, Muqdad, and Datta, Bithin (2018). *Optimum Design of Hydraulic Water Retaining Structure Incorporating Uncertainty in Estimating Heterogeneous Hydraulic Conductivity Utilizing Stochastic Ensemble Surrogate Models within Multi-Objective Multi-Realization Optimization Model.* Journal of Computational Design and Engineering, Under Review.

This chapter addresses some study limitations mentioned in Chapter Six. Data sets generated by the numerical model utilized in the Chapter Six are same for this chapter. However, the number of surrogate models within the ensemble stochastic surrogate model and the amount of training data for each surrogate model are different. Also, formulation of the optimization model and optimization solver are different.

The objective of this chapter is to improve the search technique based the optimization solver using the non-dominated sorting genetic algorithm (NSGA-II) to find the global optimum solution for reliability based optimum design (RBOD) by improving the efficiency and formulation of the linked S-O model. Also, this chapter adequately represents multi-realization of heterogeneous hydraulic conductivity by increasing the number of surrogate models incorporated in ensemble stochastic surrogate models. A limitation of this study reported in Chapter six was the difficulties in attaining a truly optimum solution, especially for high reliability levels (large number of constraints). This issue can be overcome by modifying formulation of the multi-realization optimization model, utilizing a multi-objective optimization solver, which helps decrease the number of stochastic constraints and provides less restrictive search process to find optimum solutions.

7.1 Introduction

The reliability based optimum design (RBOD) technique was utilized in this study to quantify the uncertainty in estimation of seepage characteristics due to uncertainty in estimation of heterogeneous hydraulic conductivity (HHC). This included incorporating reliability measures in minimum cost design of HWRS utilizing the multi-realization optimization technique based on many stochastic ensemble surrogate models. To improve efficiency and accuracy of the RBOD model and

direct search optimization solver, a new approach was utilized. This approach was based on the multi-objective multi-realization optimization (MOMRO) model. The advantage of this approach is that some stochastic optimization constraints based on many ensemble surrogate models were formulated as a second objective function to be minimized in the MOMRO model. Stochastic constraints used to impose the HWRS design to satisfy safe exit gradient values were formulated as a second stochastic objective function. The multi-objective optimization solver minimizes two stochastic objectives: the exit gradient and construction cost. Desired reliability levels are implicitly incorporated in objective functions and explicitly as constraints. This significantly improves search efficiency for the utilized solver, i.e., multi-objective non-dominated sorting genetic algorithm-II (NSGA-II) and aids in exploring more feasible candidate solutions in the search space.

A number of GPR surrogate models were trained using numerous data sets resulting from numerical seepage simulation integrating different random fields of HHC drawn from log-normal distribution with specified coefficient of variation values (COV) (42.5%, 77.5%, 112.5%, 147.5%, 182.5%). Desired reliability was assigned beforehand and achieved by allowing the optimum solution to satisfy a certain fraction (ratio) of stochastic constraints and objective functions based on responses of the developed surrogate models. In addition to impacts of uncertainty in estimating HHC on seepage quantities, the effect of uncertainty was also considered for other safety factors related to design of HWRS, such as flotation, overturning, sliding and eccentric loading safety factors.

Incorporation effects of soil parameter uncertainty in an optimization model for a particular design have rarely been considered in previous geotechnical research or in hydraulic structure studies as it is a demanding task. Incorporation of reliability in design of HWRS provides a safe design and more understanding of uncertainty consequences. However, more conservative design results in inefficient cost of the designed structure. Minimizing construction cost is an important goal in huge engineering constructions, such as HWRS. More importantly, efficient cost design of HWRS may significantly reduce total construction cost as a massive amount of construction material and engineering effort are required for such projects. Hence, in this study, to find a trade-off between these two opposing aims, i.e., safety and cost, the RBOD framework was utilized to find safe design with the desired reliability at minimum cost.

The objective of this study was to find a safe, reliable and minimum cost optimum design of HWRS incorporating uncertainties in estimation of HHC. The RBOD framework was implemented based on a more efficient and productive approach using the multi-objective multi-realization optimization (MOMRO) technique. The MOMRO integrated many stochastic responses from well-trained surrogate models based on GPR machine learning techniques. These stochastic responses represented the uncertainties in estimation of particular seepage design variables, which were embedded in stochastic constraints and objective functions of MOMRO. The reliability criterion is quantified by

imposing reliability constraints by which optimum design satisfies the condition that a specified fraction of surrogate model responses in the ensemble of surrogate models satisfies imposed design constraints. Estimated reliability of the design can be based on this ratio of the number of surrogate models satisfying design criteria to total number of models in the ensemble. Or, the number of predicted stochastic responses which are to be satisfied can be imposed as an equivalent probability constraints to reflect the specified reliability of design criteria. The simulation model and formulation of optimal design model are discussed in the following sections.

7.2   Linked simulation–optimization (S-O) model

The direct linking of numerical seepage modeling based on finite element method (FEM) code to the RBOD model is often very difficult or an impossible task for many reasons. Model geometry and boundary condition need to be varied for each new candidate decision vector presented by the optimization process. The FEM mesh number, properties and location also vary.

Furthermore, direct linking of the numerical model to the RBOD model is a time consuming task, as the NSGA-II invokes the numerical model numerous times to evaluate objective functions and constraints for all individual candidate solutions generated by the optimization solver. Numerical seepage simulation for scenarios/cases, including heterogeneous hydraulic conductivity (HHC), takes more time than simulation time of scenarios/cases which include only homogenous hydraulic conductivity. For example, simulation time of a case has a HHC drawn from log-normal distribution (μ = 2, COV = 182.5%) was 2.37 minutes. This simulation was implemented on a relatively high speed processor unit (Intel(R) Core™ i7-2600 CPU@ 3.4GHz_3.4GHz, RAM 8.00 GB, 64x-based processor). If direct linking of the simulation model to the optimization model is technically possible, and population size is 1,000 and generation number is 100, the optimization algorithm needs 100,000 iterations to evaluate constraints and objective functions to approach the optimum solution. Then, one optimization run requires 3,950 hours (based on 2.37 minutes for each iteration), which is an unproductive process. Direct linking of S-O models had been proposed earlier and a similar conclusion has been attained by other researchers (Dhar & Datta, 2009; Mollon et al., 2009, 2010). Hence, indirect linking of the S-O model was adopted in this study by training many efficient surrogate models to precisely imitate numerical seepage responses.

7.3   Conceptual seepage model and design of experiments

The steps used to generate data were same as those mentioned in Chapter Six. Input design variables and seepage characteristics were also the same. The number of generated data for input design variables was 150 random cases. However, as random field HHC was used, the number of simulations for each input design variable was 20, including 20 different realizations of HHC for each case to cover a wide range of uncertainty in HHC. Each single realization represented a unique and randomly varied distribution of hydraulic conductivity values of finite elements in the numerical model. Five log-normal

distributions with different standard deviations (σ) 0.85 m/day, 1.55 m/day, 2.25 m/day, 2.95 m/day, 3.65 m/day (COV 42.5%, 77.5%, 112.5%, 147.5%, 182.5%) and constant mean (μ = 2 m/day) were proposed to generate different HHC. Therefore, from a particular log-normal distribution, four realizations were randomly generated and used in numerical seepage simulation for each case of input variables (d_1, d_2, b, H). The Geo-Studio/SEEP/W numerical code (Krahn, 2012) was used to simulate each case separately. As a result, each input data set was simulated 20 times to generate different (stochastic) output data sets reflecting uncertainty of seepage characteristics due to random variation of HHC.

Output data sets encompassed uplift pressure on upstream and downstream sides (Pc_1, Pe_2) and exit gradient value of four locations (ie_1, ie_2, ie_3, ie_4), as shown in Figure 7.1. Exit gradient values were considered for four points to provide more safety to HWRS design for a heterogeneous flow domain. For each input data set (d_1, d_2, b, H), there were 20 different scenarios of seepage characteristic output sets (Pc_1, Pe_2, ie_1, ie_2, ie_3, ie_4) associated with 20 different HHC realizations. For each output design seepage variable, 20 surrogate models were trained and tested to imitate stochastic numerical responses. For each seepage quantity, the stochastic ensemble surrogate model was developed, containing 20 surrogate models. Therefore, for a single input data set 20 stochastic responses were obtained by the ensemble surrogate model to be processed in the MOMRO model based on the RBOD technique.
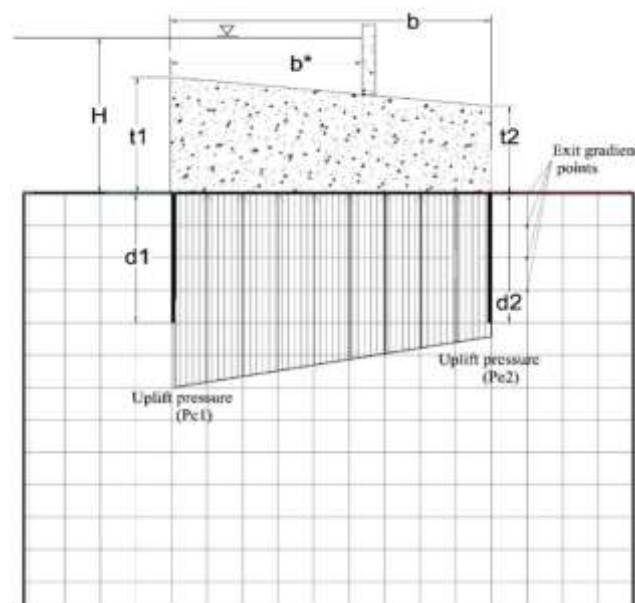
Figure 7.1 Conceptual model of the HWRS

Similar to Chapter Six, the Box-Muller (Ross, 2014) method was utilized to generate an uncorrelated random field drawn from log-normal distribution (μ, σ). Examples of different realizations of random fields for the same characteristic of log-normal distribution are presented in Figures 7.2-A1 and 7.2-A2. Furthermore, the effect of these realizations on exit gradient and uplift pressure

distributions are presented in Figures 7.2-B1, 7.2-B2 and 7.2-C1, 7.2-C2. These Figures demonstrate a significant variation of seepage quantities due to different realizations of HHC.
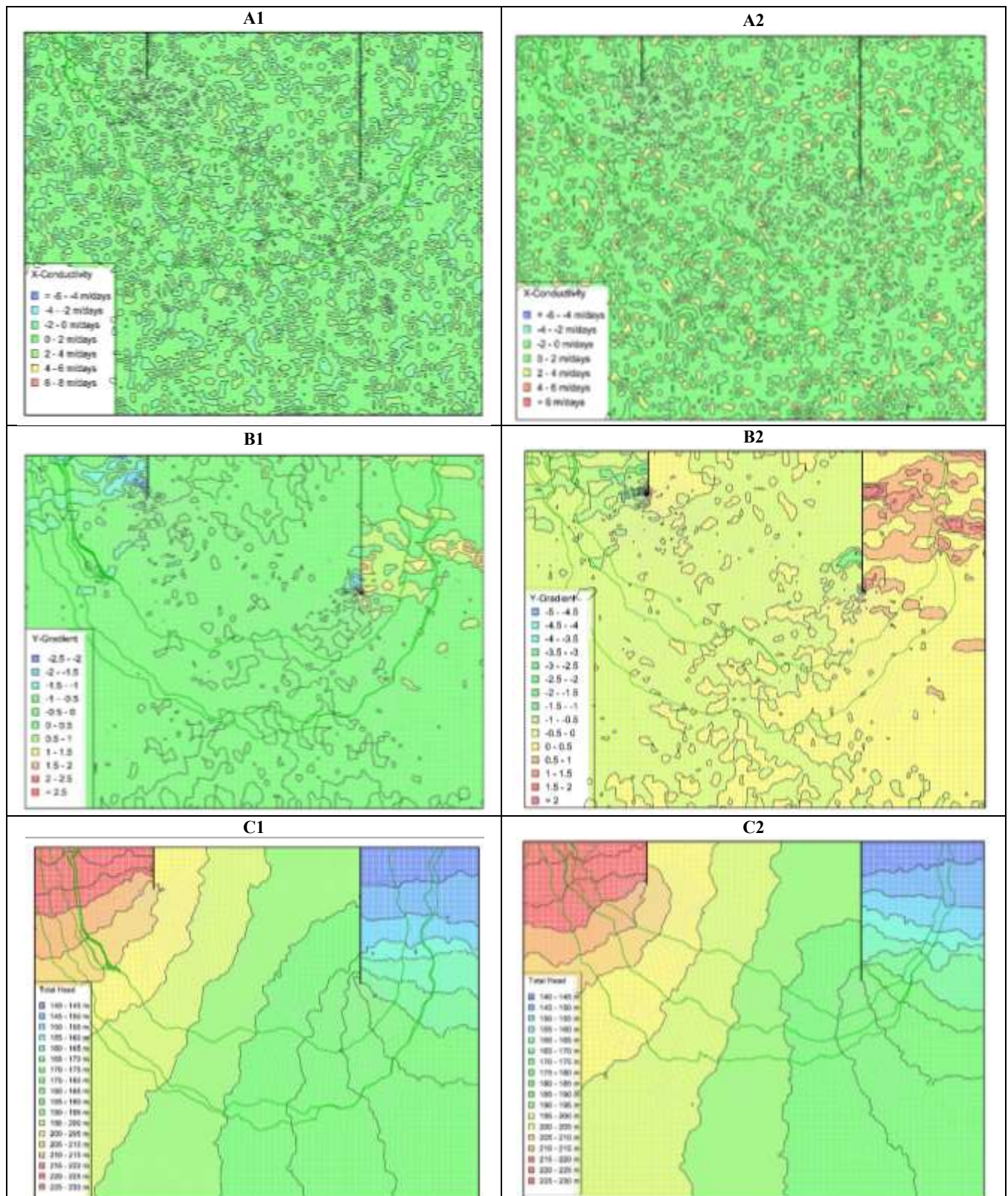
Figure 7.2 A randomly selected case, including different realizations of HHC (A_1, A_2) drawn from the same log-normal distribution ($\mu=2$, $\sigma=3.65$). B_1, B_2 represent effect of the different realization of HHC (A_1, A_2) on the exit gradient distribution. C_1, C_2 represent effect of the different realization of HHC (A_1, A_2) on total head distribution

7.4 Design and evaluation of surrogate models

Similar to Chapter Six, GPR machine learning was used to develop 120 surrogate models utilized to build six stochastic surrogate models. For each surrogate model, training and testing data included 150 sets (cases). Source data related to each design variable was divided into training and testing data sets. Since, it is recommended to put the majority of the data in training part (Alpaydin, 2014), and the testing part does not affect performance of the surrogate model, 90% of source data was used for training and 10% was used for testing. The generalization ability of GPR surrogate models was examined by evaluating prediction accuracy of surrogate models outside training data sets. Testing error should be close to training error and both must be within the prescribed range of error measures. However, because source data resulted from stochastic numerical simulations, training and testing results, especially for cases with a high COV random field, were slightly less robust.

Developed GPR surrogate models were trained using Matlab programing language. The parameters of GPR, listed in Table 7.1, were carefully selected after many trial and error iterations to satisfy best prediction and less error for training and testing phases. Furthermore, different scenarios of training/testing data were randomly selected and tested to find the best set of GPR parameters for each surrogate model. Other parameters were left the same as default Matlab values.

Table 7.1 Parameters of the GPR technique

Properties	Value
Prediction method	Exact
Kernel function	Squared exponential kernel with a separate length scale per predictor
Fit method	Exact
Basis function	Constant

The training/testing performance of surrogate models must be accurately evaluated before using them in the RBOD model. Developed GPR surrogate models were evaluated using many error measures (see Chapter Six) and statistical evaluation indices. These error measures were applied to all surrogate models. The majority of surrogate models presented perfect training and testing performance. Although, testing prediction efficiency of some models was less than the optimum range, predictions of these models were within acceptable ranges, particularly for exit gradient surrogate models for cases including high uncertainty (COV = 182.5%, COV = 147.5%). Samples of training and testing results of developed surrogate models are presented in Table 7.2 and Figures 7.3 to 7.8. These results reflect accurate training using GPR technique for noisy training data sets influenced by the uncertainty of HHC.

Table 7.2 Samples of surrogate model training testing error measure

	ie1 (2.95/B)		ie2(1.55/C)		ie3(1.55/D)		ie4 (2.95/A)		pc1(3.65/C)		pe2(3.65/B)	
	train	**test**	**train**	**test**	**train**	**test**	**train**	**test**	train	test	train	test
MSE	0.00	0.03	0.02	0.05	0.05	0.07	0.07	0.06	20.52	12.08	4.16	24.73
STD-ERROR	0.00	0.19	0.14	0.22	0.22	0.27	0.27	0.24	4.55	3.52	2.05	4.95
M-error	0.00	0.01	0.00	0.03	0.00	0.06	0.00	0.02	0.00	-0.73	0.00	-1.35
NSE	1.00	0.71	0.93	0.67	0.81	0.74	0.81	0.70	0.97	0.99	0.99	0.98
RSR	0.00	0.54	0.26	0.57	0.43	0.51	0.44	0.55	0.16	0.11	0.08	0.16
PBIAS	0.00	3.66	0.00	5.51	0.00	11.11	0.00	5.32	0.00	-1.64	0.00	-3.24
R	0.99	0.88	0.96	0.82	0.90	0.87	0.91	0.84	0.98	0.99	0.99	0.99
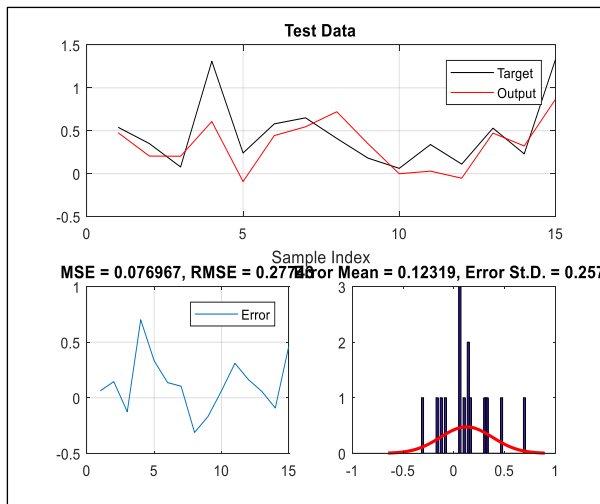
Figure 7.3 ie₄ surrogate model prediction for test data (σ=2.95-D*)
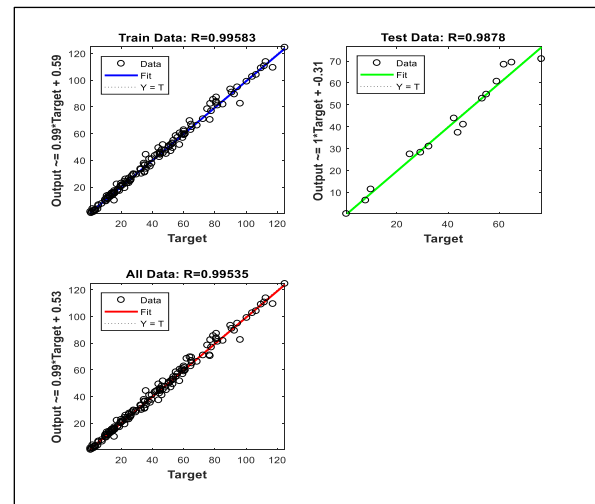
Figure 7.5 Training-testing R index for the surrogate model (ie₄) (σ=2.25-C)
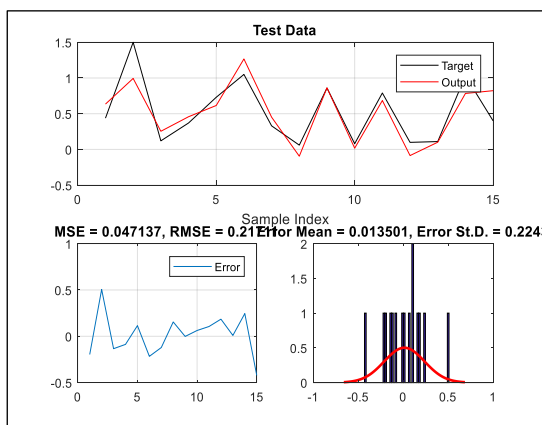
Figure 7.4 Pc1 surrogate model prediction for test data (σ=3.65-D)
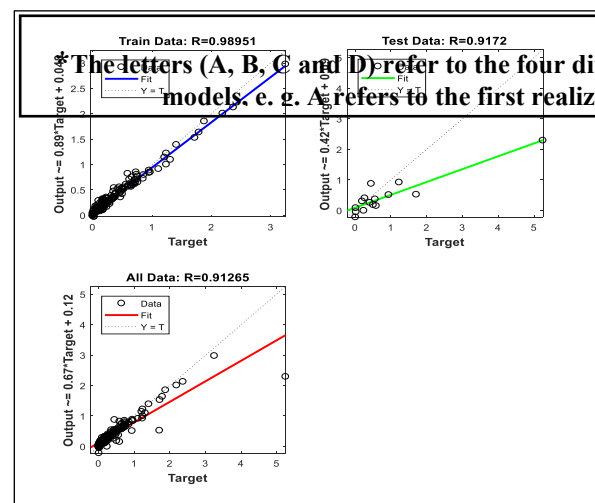
*The letters (A, B, C and D) refer to the four different realiza... models. e. g. A refers to the first realization and B re...

Figure 7.6 Training- testing R index for the surrogate model (ie$_2$) (σ=3.65-B)
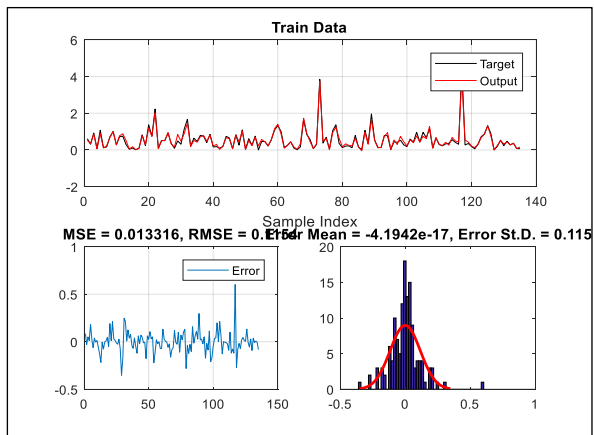
Figure 7.7 ie$_2$ surrogate model training performance (σ=2.95-A)
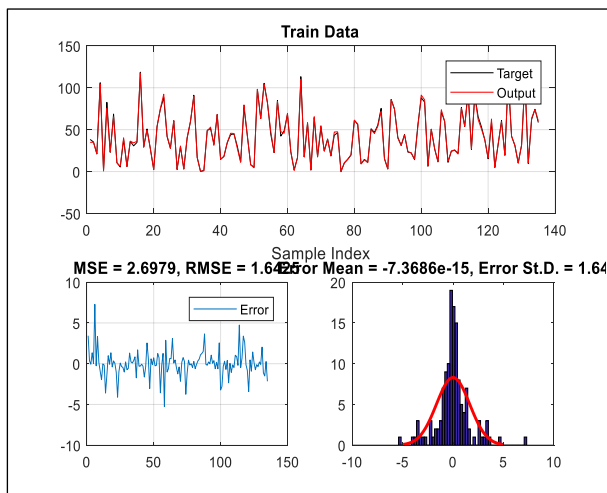
Figure 7.8 Pc1 surrogate model training performance (σ=2.95-D)

7.5 Multi-objective multi-realization optimization model

Formulation of a multi-realization optimization model based on a single objective function with numerous stochastic constraints may lead to a sub-optimum solution or infeasible solution. The RBOD approach required imposition of a large number of explicit constraints which needed to be satisfied as binding conditions for a feasible solution. Many attempts were made to formulate the RBOD model for this study with a large number of stochastic surrogate models (120 surrogate models) based stochastic constraints using a single objective function, but the majority of obtained solutions were infeasible. Some earlier studies compared performance of multi-objective and single objective optimization models (Yapo, Gupta, & Sorooshian, 1998; Zakaria, Jamaluddin, Ahmad, & Loghmanian, 2012). These studies concluded that a multi-objective formulation may provide more efficient solutions than those obtained by a single objective model. Such conclusions seem to have been based on the premise that if a large number of constraints are replaced by an objective function not ensuring a certain specified level at which these constraints need to be satisfied, the computation becomes more flexible and possibly more efficient. As multi-realization technique based reliability required a large number of stochastic constraints, the optimal solution search process based on evolutionary algorithms may produce an infeasible solution. Searching efficiency decreases with increasing number of constraints and complexity of the problem (Dorsey & Mayer, 1995; Kolda et al., 2003). Furthermore, incorporating a large number of stochastic constraints makes determining improvement of the searching process difficult because stochastic constraints for each iteration provide different responses reflecting uncertainties in design parameters and variables.

Therefore, a new formulation of the RBOD model was adopted in this study to improve the searching process for such complex optimization tasks. The most important stochastic constraints are exit gradient constraints as they are significantly influenced by HHC uncertainty and have critical impacts on HWRS design and safety. These constraints were transformed as a second objective function to be minimized in addition to the first objective function related to HWRS construction cost. Hence, the multi-objective optimization formulation was implemented to significantly decrease the number of constraints and improve searching efficiency. Reliability was included for exit gradient (objective function) and also implemented for stochastic constraints using a multi-realization technique.

The optimum solution of the multi-objective function is not a single solution. Instead, sets of the optimum solution are presented. Each coupled solution of consecutive solutions reflects improvement in the first objective and deterioration in the second. Hence, there is no solution explicitly better than other solutions and the HWRS designer has many alternatives from which to select the best optimum HWRS design.

7.6   Non-dominated sorting genetic algorithm-II (NSGA-II)

In many engineering applications two or more conflicting objectives are possible. Improving one objective requires sacrifice of other conflicting objectives and vice versa. Hence, it is difficult to present a single solution of a multi-objective optimization model and instead a set of non-dominated sorting optimum solutions (Pareto optimum solutions) are generated. The multi-objective formulation does not result in the optimum solution for each objective function separately as a single objective function. There are many in between solutions at which perfect performance of the design can be found (Burke & Kendall, 2005).

The procedure of NSGA-II to attain the Pareto optimal front, the process of obtaining non-dominated solutions, and selecting optimal sets, are briefly described here. The non-dominated optimum solution X dominates the solution Y, if X is not worse than Y in all objective functions values and X is better than Y in one objective. The NSGA-II is a population based search algorithm, similar to the genetic algorithm (GA) (Gen & Cheng, 2000).

NSGA-II starts with N number of random initial populations, P_0. Thereafter, ordinary GA operations, such as binary tournament selection, crossover and mutation operations, are performed to generate an offspring population (Q_t) of size N. The P_0 and Q_t are combined to generate 2N populations and the best non-dominated sorting individuals are used to fill different ranks of Pareto fronts (slots), one by one. The highest rank non-dominated front is selected first, then the second, etc. As there are 2N individuals and all non-dominated fronts cannot cover more than N individuals all exceeded individuals are rejected (Zakaria et al., 2012).

The selection process to fill the last slot is slightly different, because it probably has two parts and all the individuals in this slot have a same rank. Population of the first part is within N size, and the second part of the population is more than N, which must be deleted, as described in Figure 7.9. However, instead of an unsystematic process to fill the last slot, the crowding distance measure is used to select more diverse individuals.
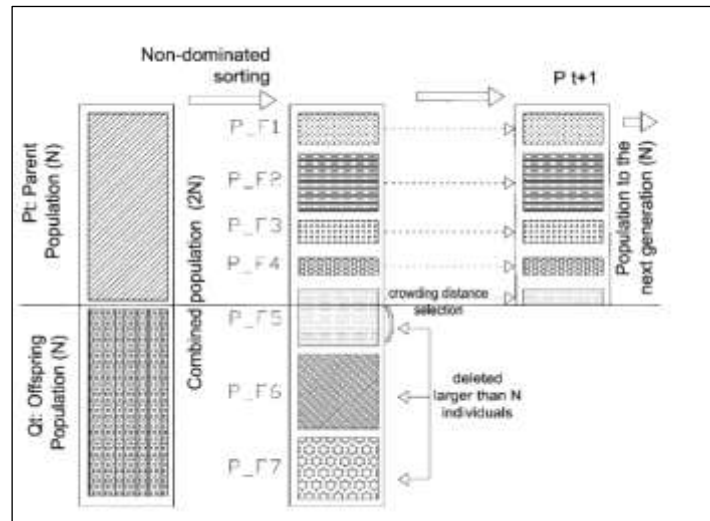
Figure 7.9 Non-dominated sorting and Pareto front selection process (NSGA-II)

Crowded distance is a second preference (measures) after non-dominated rank. If two solutions classified for the same Pareto front, then the solution resulting from less crowded area (larger crowding distance (d_i)) is the winner. Determining crowding distance for solution **i** is based on the two neighbouring solutions located either side of **i** in the Pareto front. Distance d_i represents average cuboid side lengths determined based on location of the nearest solutions (i+1, i-1), as shown in Figure 7.10 (Burke & Kendall, 2005). Crowding distance (d_i^m) for solution **i** for each objective function (f^m, m = 1, 2,…, M) is given by Eq. (7.1).

$$d_i^m = d_i^m + \frac{f_{i+1}^m - f_{i-1}^m}{f_{max}^m - f_{min}^m}$$

(7.1)

These processes continue until each front is filled and non-dominated sorting and crowding distance classification are implemented for the new generations until the stopping criteria is achieved (Burke & Kendall, 2005). Many researchers have utilized NSGA-II in finding optimum solution trade-off for competing objective functions, finding that performance of NSGA-II was efficient (Bekele & Nicklow, 2007; Deb, 2001; Dhar & Datta, 2009; Rajabi-Bahaabadi, Shariat-Mohaymany, Babaei, & Ahn, 2015; Sreekanth & Datta, 2010, 2014; Yandamuri, Srinivasan, & Murty Bhallamudi, 2006).
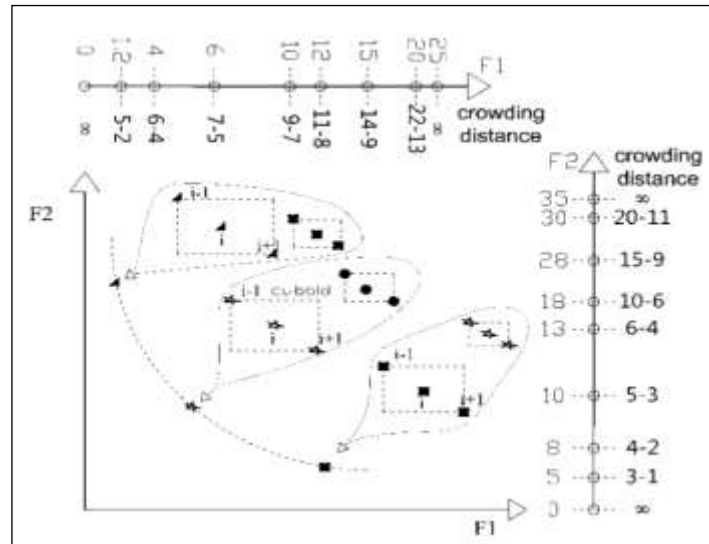
Figure 7.10 Crowding distance selection process to fill the last Pareto

Parameters of the utilized optimization solver (NSGA-II) were specified, as shown in Table 7.3. These parameters were selected based on many attempts of trial and error to find the best parameter combination. The remainder of parameters were left as default Matlab options. As the range of two objective functions was significantly different and the option of allowable tolerance for objective functions was applied simultaneously for the two objective functions, the exit gradient objective function value was magnified by a scale factor of 1,000 to provide smooth evaluation for both objectives.

Table 7.3 Utilized NSGA-II parameters for the MOMRO model

Options	Value
Population size	1000
Crossover fraction	0.6
Pareto fraction	0.45
Max generations	200
Function tolerance	1e-3
Constraint tolerance	1e-3
Crossover function	Crossover intermediate
Migration direction	Both

7.7   Formulation of the reliability based MOMRO model

The multi-realization optimization technique was based on formulating stochastic constraints based on the developed ensemble stochastic surrogate models. For each safety factor or condition in the optimization model there was a single or more ensemble stochastic surrogate model/s encompassing 20

surrogate model responses of a specified seepage design variable. Desired reliability level was attained by allowing the optimum solution to satisfy any fraction (n) of the total number (m = 20) of constraints for all stochastic constraints, where n/m value is equivalent to required reliability level. The multi-realization optimization technique reflects uncertainty of seepage quantities due to uncertainty of HHC. For instance, 80% reliability means that the optimum solution satisfies any of 16 stochastic constraints from 20 total constraints.

The multi-realization technique based reliability measure was also incorporated in objective functions in the MOMRO model. The second objective function, which minimized exit gradient value, integrated reliability by incorporating exit gradient stochastic responses in determining the objective function. As exit gradient was minimized, 20 stochastic exit gradient responses based on ensemble stochastic surrogate models were determined and sorted in ascending order. The maximum value of all obtained exit gradient values was selected to be minimized. This is equivalent to 99.9% reliability because the resulting exit gradient value is the safest estimated as all other stochastic values are less than the obtained exit gradient. To attain 80% reliability, for example, the optimization solver is formulated to minimize the fifth maximum value (based on 20 responses) and allow up to four stochastic responses of exit gradient to be higher than the selected one for objective function value.

As there are four locations to determine exit gradient value (ie_1, ie_2, ie_3, ie_4) the maximum value for each location was determined and the average of these values was considered as the second objective function. The same technique was applied to determine the first objective function of minimizing construction cost of HWRS. Construction cost of HWRS is based on upstream and downstream floor width and thicknesses (b, t_1, t_2) and the depths of upstream and downstream cut-offs (d_1, d_2), as shown in Figure 7.1. Floor thicknesses are based on stochastic responses of uplift pressure ensemble surrogate models (pc_1, pe_2). Formulation of the optimization model for MOMRO is as shown below:

$$\text{Find } X = \{x_1,\ x_2,\ x_3,\ x_4,\} = \{d_1,\ d_2,\ b,\ b^*\}$$

Minimize,
$$f_1(X) = c_f\ b\ \frac{\max_{(m-\omega)}(t_1^m) + \max_{(m-\omega)}(t_2^m)}{2} + t_c \sum_{s=1}^{2}\ c_s^c\ d_s \qquad (7.2)$$

Minimize,
$$f_2(X) = \frac{\max_{(m-\omega)}(ie_1^m) + \max_{(m-\omega)}(ie_2^m) + \max_{(m-\omega)}(ie_3^m) + \max_{(m-\omega)}(ie_4^m)}{4} \qquad (7.3)$$

$$ie_i^m = \varepsilon_i^m\ (H, d_1,\ d_2, b, k_m) \qquad \forall\ i, m \qquad (7.4)$$

Subject to:

$$Fs_{fl-us}^m \geq 1.3 \qquad \forall\ m$$

$$Fs_{fl-us}^m = \epsilon^m\ (H, d_1,\ d_2, b, k_m) \qquad \forall\ m \qquad (7.5)$$

$$Fs_{fl-ds}^m \geq 1.3 \qquad \forall\ m$$

$$Fs_{fl-ds}^m = \gamma^m (H, d_1, d_2, b, k_m) \quad \forall \ m \tag{7.6}$$

$$Ecc^m \geq \frac{b}{3} \quad \forall \ m$$

$$Ecc^m \leq \frac{2\,b}{3} \quad \forall \ m$$

$$Ecc^m = \frac{Mpas^m - Mact^m}{Vload^m} \quad \forall \ m \tag{7.7}$$

$$Fs_{over}^m \geq 1.5 \quad \forall \ m$$

$$Fs_{over}^m = \frac{Mpas^m}{Mact^m} \quad \forall \ m \tag{7.8}$$

$$Fs_{slid}^m \geq 1.5 \quad \forall \ m$$

$$Fs_{slid}^m = \frac{C \times b + f \times Vl^m}{Hl} \quad \forall \ m \tag{7.9}$$

$$Mpas^m = f^m(H, b, b^*, t_1^m, t_2^m, k_m, G_c, G_w, pc_1^m, pe_2^m) \quad \forall \ m \tag{7.10}$$

$$Mact^m = f^m(H, b, b^*, t_1^m, t_2^m, k_m, G_c, G_w, pc_1^m, pe_2^m) \quad \forall \ m \tag{7.11}$$

$$Vl^m = f^m(H, b, b^*, t_1^m, t_2^m, k_m, G_c, G_w, pc_1^m, pe_2^m) \quad \forall \ m \tag{7.12}$$

$$Hl = f(H, G_w) \tag{7.13}$$

$$k_m = Lognormal\,(\mu, \sigma) \quad \forall \ m, \quad k_m \in (0, \infty)$$

and reliability constraints are:

$$Z_{q\ logical}^m = Fs_q^m \geq / \leq Fs_{q\ allowable}^m \quad \forall \ q, m$$

$$g(x)_q = \sum^m Z_{logical}^m \leq DR \quad \forall \ q \tag{7.14}$$

Where $\max_{(m-\omega)}$ is a function sorting stochastic responses ascending and returns $(m - \omega)$ th value of the sorted vector. m is the number of stochastic responses (20), ω is based on desired reliability level, e. g., when ω is 0 reliability is 99.9% and for ω is 4 reliability is 80%, etc. t_1^m, t_2^m represents stochastic thickness values of the floor at upstream and downstream sides, respectively. c_f is construction cost of the floor per cubic meter ($400/m³), c_c is construction cost of cut-offs per cubic meter, which is a function of depth of the cut-off (d₁,d₂), as shown in Eq. (7.15)(same to Eq.(3.9) and (3.10)), t_c is thickness of the cut-off and it equals to 1.0 m.

$$c_s^c = d_s^3 + 20\,d_s^2 + 200\,d_s + 400 \quad \forall \ s \tag{7.15}$$

ie_i^m is **m** realizations of exit gradient safety factor determined based on **m** surrogate models $\{\varepsilon_i^m()\}$ and for each location (i) there are **m** realizations of the exit gradient safety factor. Fs_{fl-us}^m, FFs_{fl-ds}^m are stochastic safety factors to impose weight of the upstream and downstream floors of HWRS to safely counterbalance uplift pressure ($Pc_1{}^m$, $Pe_2{}^m$) (Bligh, 1915; U.S. Army Corps of Engineers, 1987).

The computing of Fs_{fl-us}^m, FFs_{fl-ds}^m are mainly based on developed stochastic surrogate models $Pc_1{}^m\{\epsilon^m()\}$, $Pe_2{}^m\{\gamma^m()\}$, respectively. Ecc^m is the design condition to prevent eccentric load condition on the foundation of the HWRS. $Mpas^m$ is passive momentum obtained from all forces increasing stability of the HWRS, $Mact^m$ is active momentum obtained from all forces decreasing stability of the HWRS, $Vload^m$ is resultant of all vertical loads influencing HWRS. $Mpas^m, Mact^m, Vload^m$ are a function to ($H, b, b^*, t_1^m, t_2^m, k_m, G_c, G_w, pc_1^m, pe_2^m$) as shown in Eq. (7.10), Eq. (7.11) and Eq. (7.12). Fs_{over}^m is the overturning stochastic safety factor. Fs_{slid}^m is the stochastic sliding safety factor. C = cohesion resistance soil properties, f= $tan\emptyset$, $\emptyset$ is the internal friction angle (Tanchev, 2014). The values of f and C were assumed as f= $tan\emptyset$=0.7 and C=20 kPa. Hl is the resultant of all horizontal load affecting the HWRS (Eq. (7.13)). k_m are different realizations of HHC based on different values of COV and it implicitly effects prediction of stochastic seepage quantity. $Z_q^m{}_{logical}$ is a logical variable to check violation of stochastic constraints associated with a **q** number safety factors for *m* stochastic realizations. DR is desired reliability for all constraints and objective functions to satisfy a certain reliability level for HWRS design.

Additionally, there are many other logical and boundary constraints utilized to prevent the optimization solver from presenting illogical and negative values. The RBOD using MOMRO model is shown in (flow chart) Figure 7.11.
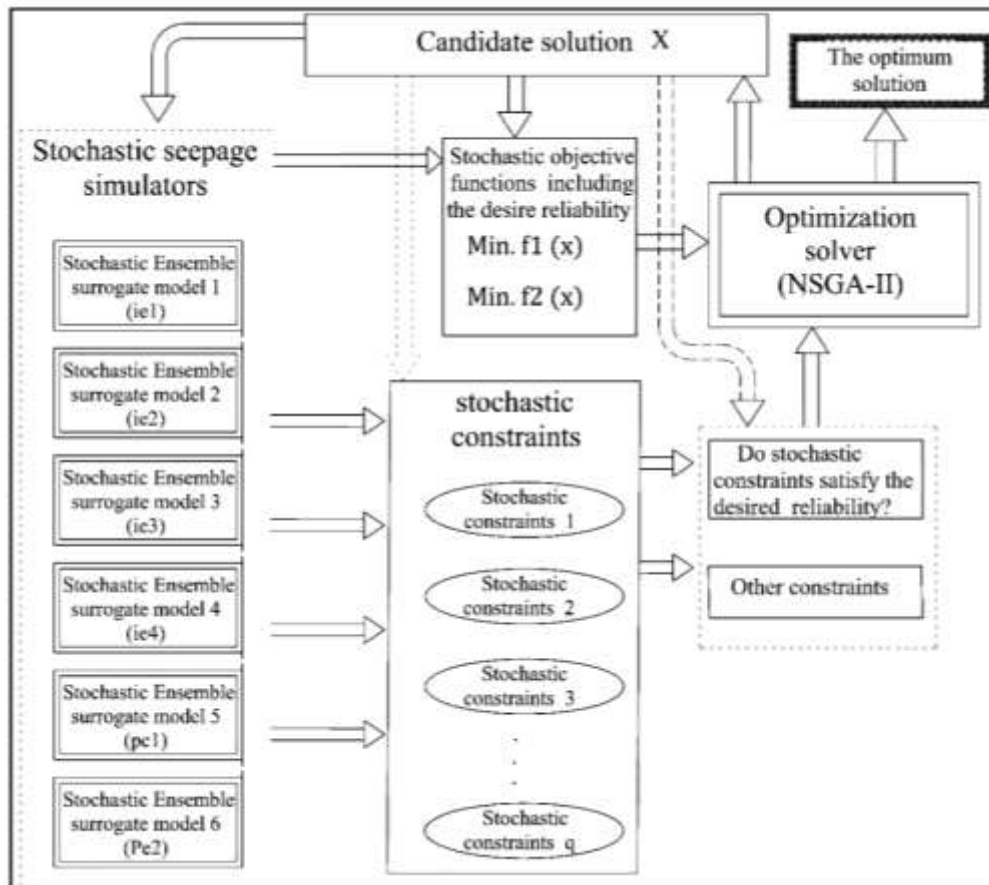
Figure 7.11 Illustrating formulation of reliability based MOMRO stochastic S-O model

7.8 Computing efficiency

The formulation of reliability using the MOMRO model is computationally expensive and a time consuming task, even when surrogate models are used instead of the numerical simulation model. In each iteration of the S-O model, the optimization solver needs to invoke 120 responses of the developed surrogate model twice to evaluate stochastic objective functions and constraints. Furthermore, the NSGA-II is based on a large number of evaluations of a huge size of random populations to attain the global optimum solution. Hence, solving such optimization problem using traditional techniques takes a long time. One roughly selected optimization case was implemented using the traditional computing technique based on 1,000 populations. The time required for the run was 14,100 seconds ($\approx$ 4 hours).

The traditional computing technique is based on writing the constraint code and objective function code in two separate files. Each file calls on the 120 developed surrogate models for each iteration. For each iteration of S-O mode, outcomes of objective functions and constraints codes are passed to the optimization solver after 240 responses are attained based on 120 trained surrogate models.

This procedure is inefficient as many optimization runs must be accomplished to reach the optimum solution.

Alternatively, to increase computing efficiency a nested function technique was utilized (MathWorks, 2015). By using the nested function, both constraint code and objective function code were written in the same (nested function) file. Stochastic surrogate models are uploaded at one time and the resulting objective functions and constraints values computed by the nested function are simultaneously returned as a vector to the optimization solver. The NSGA-II was formulated to adapt the nested function output. This strategy accelerated and doubled computational speed.

More importantly, in evolutionary optimization algorithms based on random population search technique the evaluation process for objective functions and constraints are based on one individual in each iteration and this process continues until all individuals are evaluated. Then, the same procedure is implemented for the second generation, etc. This process takes a longer time compared to the vector-process, which could substantially speed up the optimization evaluation process. By utilizing the vector-process, all individuals are evaluated by the optimization solver at one time to determine the values of stochastic constraints and objective functions. The evaluation outcome for each iteration is a matrix and its length is equal to population size. Each column vector represents a certain value of optimization results, such as a particular constraint or objective function value for all concatenated individuals (population). The optimization solver evaluates the improvement direction for each element in the vector. This means the whole population is evaluated at one time, then the improvement direction determined by selecting high rank individuals in the matrix. This process continues to the next new generations until stopping criteria is satisfied.

Implementing the vector-process combined with nested function for RBOD using the MOMRO model resulted in efficient computation time of around 500 seconds. Although formulating optimization codes based on the vector-process take some time and effort, it was computationally efficient. Also, this strategy provided more flexibility to make systematic iterations to find the best parameter combinations to provide optimum results.

7.9   Results and discussion

The MOMRO technique was applied to hypothetical design scenarios/cases to evaluate RBOD performance based on MOMRO technique. These cases included five different upstream head values (100 m, 80 m, 60 m, 40 m, 20 m) and each combination was subjected to four different reliability levels (99.9%, 80%, 60%, 40%). Reliability levels were incorporated explicitly in stochastic constraints and implicitly in objective functions. Competed objective functions were minimum exit gradient and minimum construction cost of HWRS. The obtained Pareto-optimum fronts for each head value, including different scenarios of reliability level, are presented in Figures 7.12 to 7.16. Each Figure includes wide ranges of optimum solutions for each head value associated with different reliability

levels. To make an appropriate decision, minimum allowable deterministic safe exit gradient (Harr, 2012; Khosla et al., 1936) values were used to locate safe and feasible optimum solutions, as shown in Figures 7.12 to 7.16. There are two horizontal lines, which show locations of safe exit gradient factors 5 and 3, considering the critical gradient value is 1.15. Based on these values, the minimum safe exit gradient could be allocated with different reliability levels. To provide greater safety related to exit gradient, many possible Pareto optimal solutions were available to be considered with ascending construction cost, and the HWRS designer could use one of these solutions as per their preference.

The effects of reliability on optimum design of HWRS were significant. Increasing reliability augmented construction cost. For instance, minimum construction costs for H = 100 m for reliability levels of 40% ,60%, 80% and 100% to satisfy the exit gradient safety factor of 5 were \$112,191,378, \$129,171,757, \$162,166,799 and \$268,206,048, respectively. Similarly, for the same reliability levels, construction costs to satisfy the exit gradient of 3 were \$59,951,442, \$79,158,696, \$106,049,766 and \$160,838,745). This means that to increase reliability of the design from 60% to 100%, construction cost doubles. Consequently, considering reliability in the design of HWRS significantly impacts on optimum design attributes. Moreover, for high reliability levels, only few applicable (feasible) scenarios could be obtained from the Pareto optimal front. For example, for H = 100m and the Reliability level is 99.9% considering the exit gradient safety factor of 5 only a few points were found at higher construction cost (\$268,206,048.88).

The deterministic optimum Pareto front related to the expected hydraulic conductivity (2 m/day) was also considered in this study. In general, the deterministic Pareto optimal was located close to 60% reliability trade-offs. However, some deterministic optimum solutions approached 40% reliability solutions. The 60% or 40% reliability of the deterministic solutions mean that there is high probability to find the exit gradient value approaching the critical exit gradient, which might lead to piping failure. Based on this, we can deduce that the deterministic safety factors of 3 and 5 are insufficient to provide adequate safety for such important projects (HWRS), and they are inappropriate to measure safety of seepage design incorporating a certain degree of uncertainty. This is true if we assume that the prescribed safety factor is used to quantify uncertainty in the HHC only.

For all optimum solutions, slope of the Pareto optimal front became smaller for small exit gradient values (less than 0.4). Consequently, significant cost was required to decrease exit gradient value by a small amount. This is because the most controllable design variable related to exit gradient value is d_2, which must be increased to reduce exit gradient value. As the equation used to determine cut-off construction cost is a function of d_2 (Eq. (7.15)), when d_2 is increased construction cost substantially increases, especially for large d_2 values. Furthermore, because stochastic responses were included in the optimization model, and the maximum value of many stochastic exit gradient values

was minimized, effects of reliability on construction cost were more pronounced when the exit gradient value (the second objective) approached a very small value or zero.
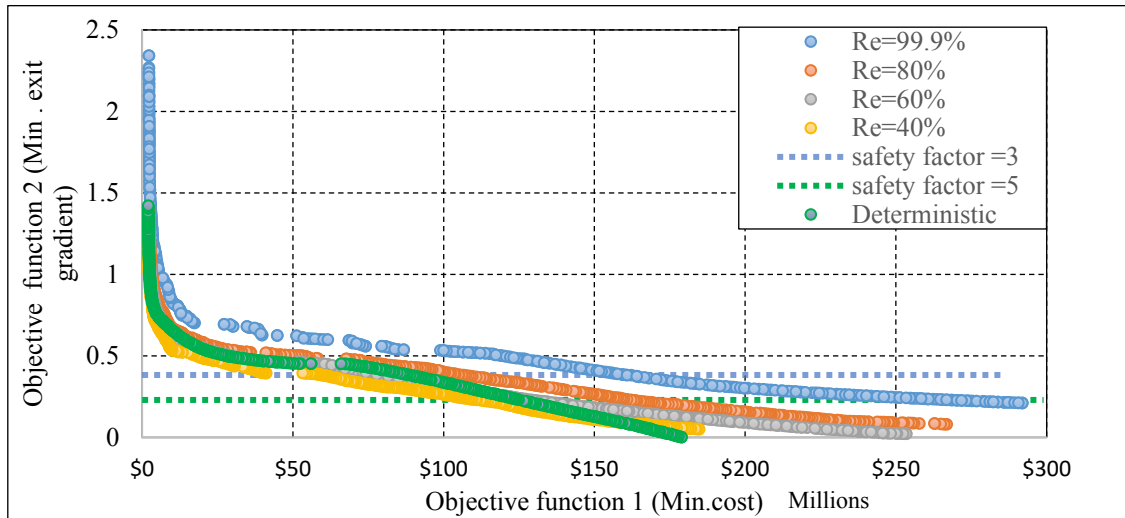
Figure 7.12 Optimum Pareto front for different reliability levels (H=100m)
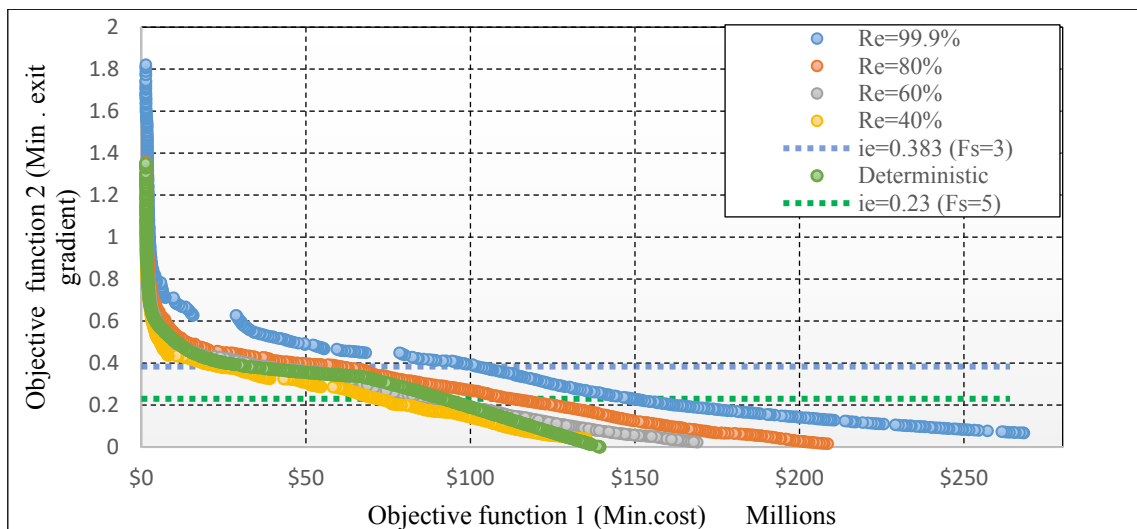
Figure 7.13 Optimum Pareto front for different reliability levels (H=80m)
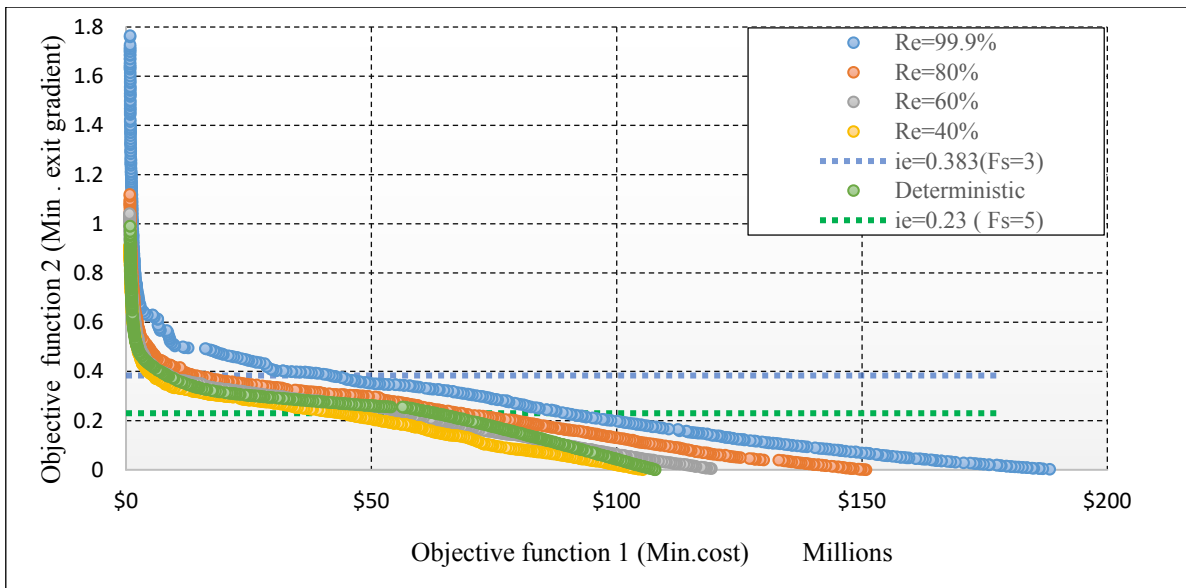
Figure 7.14 Optimum Pareto front for different reliability levels (H=60m)
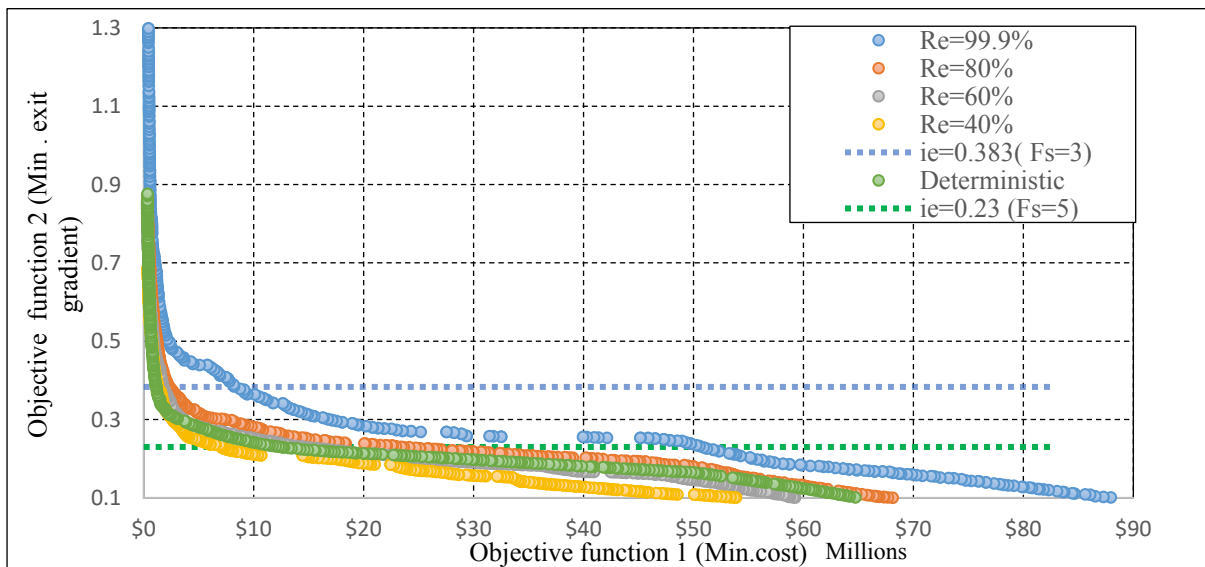
Figure 7.15 Optimum Pareto front for different reliability levels (H=40m)
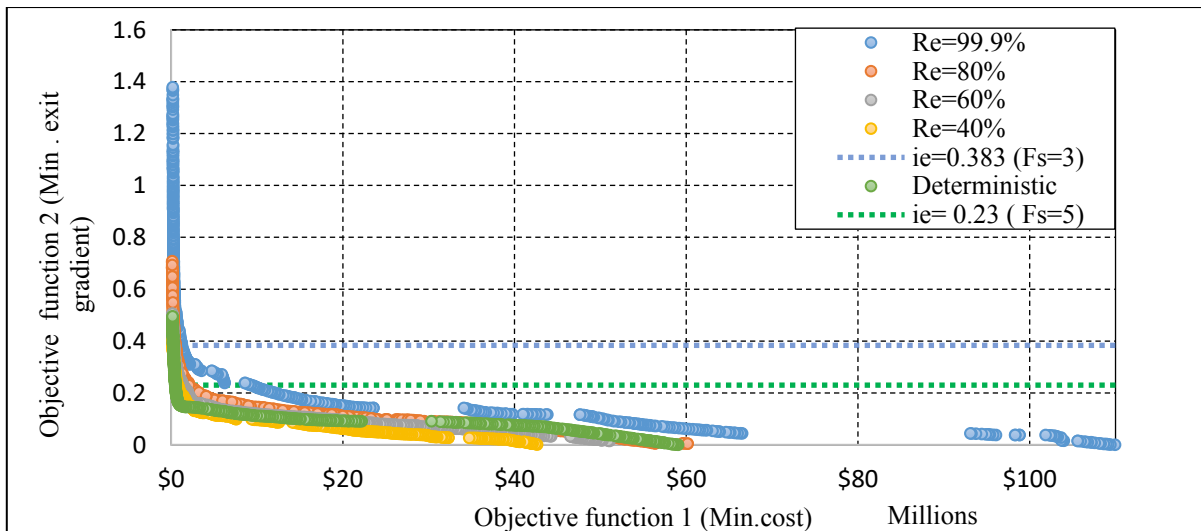
Figure 7.16 Optimum Pareto front for different reliability levels (H=20m)

One important benefit of using multi-objective optimization in RBOM is the diversity of provided optimum solutions. The multi-objective optimization solver provides many optimum solutions for the same objective function values (approximately). These solutions could not be obtained by a single objective optimization model. These solutions provide more flexible options because some optimum solutions are more applicable in terms of design requirements, such as field limitation and construction procedures, etc. Table 7.4 presents a few arbitrarily selected example solutions with the same objective function values including different optimum solution (X) scenarios.

Table 7.4 Different optimum solution values for same objective functions values obtained by NSGA-II

H	Reliability	Construction cost ($)	Exit gradient	d_1	d_2	b	b*
20	40%	39,040,057.6	0.021	3.70	0.50	139.98	39.37
		38,711,633.0	0.021	0.78	3.06	30.93	15.17
40	40%	1,588,280.6	0.365	4.05	5.01	80.29	18.32
		1,544,093.7	0.366	4.16	21.37	46.74	40.80
60	40%	33,765,444.3	0.258	4.48	65.93	179.80	80.40
		33,427,294.7	0.261	61.72	54.47	78.96	49.82
80	40%	28,275,868.8	0.374	58.34	52.27	85.58	77.91
		27,327,404.2	0.374	30.73	65.07	75.37	74.53
20	99.9%	47,623,453.4	0.116	29.58	77.21	28.44	21.01
		43,815,973.8	0.117	45.77	72.83	21.15	19.56
60	99.9%	57,740,766.3	0.342	37.93	80.34	61.05	47.25
		56,752,425.9	0.343	71.71	62.54	86.34	46.50
20	80.0%	40,547,213.5	0.073	34.53	73.33	23.75	12.63
		40,367,765.1	0.074	72.09	41.34	39.87	29.61
80	60.0%	56,079,880.3	0.351	46.49	77.94	76.60	66.26
		55,187,390.3	0.351	26.17	80.08	76.11	68.53
40	60.0%	72,446,076.0	0.072	61.19	79.87	113.16	68.76
		66,394,331.9	0.072	47.71	82.12	68.76	59.16
100	40%	93,811,995.8	0.280	65.02	85.18	158.46	71.76
		93,403,373.0	0.282	56.51	88.54	92.46	91.59

Minimum and maximum feasible optimum solutions (considering exit gradient safety factor) with different reliability levels are listed in Tables 7.5 to 7.9. There was a significant increase in construction cost versus a small decrease in exit gradient values. Also, it can be concluded from these results that the design variable d_2 played a crucial role in reducing exit gradient values.

The main role of the first cut-off depth d_1 was to reduce uplift pressure under the foundation of the HWRS. However, an additional role of d_1 was to reduce exit gradient value because reducing uplift pressure under HWRS leads to reduction in exit gradient values. The optimum width b was necessary for the design to satisfy the requirements for overturning criterion, floatation and sliding safety factors, plus prevent the eccentric load condition. These safety design requirements integrated (b) value directly in their calculation. The variable b* is the part of the floor on the upstream side of HWRS, which might be covered by water (Figure 7.1). This variable made a considerable contribution in safety and stability requirements of HWRS. The water covering b* provided a cheap (costless) weight over the HWRS to counterbalance active momentums and forces which may weaken stability of the HWRS. Some solution values of b* approached the b value, as shown in Tables 7.5 to 7.9. This means that the majority of the

HWRS floor was located on the upstream side. This also reflects the significance of this variable to satisfy safe and minimum cost design.

Table 7.5 Minimum and maximum feasible solutions for different reliability level (H=100 m)

H	Reliability	Construction cost ($)	Exit gradient		d_1	d_2	b	$b*$
100	100%	160,838,745.0	Max.Feasible	0.382	68.998	101.303	94.072	90.217
		291,913,182.3	Min.Feasible	0.211	98.277	110.000	92.960	86.702
	80%	106,049,766.4	Max.Feasible	0.383	64.37	89.62	97.56	96.01
		266,831,321.6	Min.Feasible	0.080	99.65	104.54	97.42	94.04
	60%	79,158,696.9	Max.Feasible	0.378	60.93	82.19	96.90	82.68
		253,417,538.3	Min.Feasible	0.022	95.21	105.57	113.05	83.98
	40%	59,951,442.0	Max.Feasible	0.381	51.30	78.04	93.07	92.66
		184,735,070.3	Min.Feasible	0.050	79.46	101.99	98.36	96.55
	Det.	88,783,399.4	Max.Feasible	0.381	53.53	87.91	92.23	88.42
		177,804,330.1	Min.Feasible	0.006	67.61	104.88	165.85	64.33

Table 7.6 Minimum and maximum feasible solutions for different reliability level (H=80 m)

H	Reliability	Construction cost ($)	Exit gradient		d_1	d_2	b	$b*$
80	100%	102,526,240.8	Max.Feasible	0.382	55.04	91.69	77.43	77.24
		268,199,466.1	Min.Feasible	0.067	93.19	109.63	76.67	69.00
	80%	60,905,832.2	Max.Feasible	0.382	43.84	80.50	75.16	61.32
		208,554,042.6	Min.Feasible	0.016	90.48	100.37	79.83	61.35
	60%	38,552,199.4	Max.Feasible	0.382	57.18	63.58	76.63	69.80
		168,911,916.3	Min.Feasible	0.023	78.94	98.96	102.65	86.93
	40%	23,489,756.5	Max.Feasible	0.383	31.03	62.07	76.17	73.90
		135,258,887.1	Min.Feasible	0.039	68.42	95.94	103.61	66.13
	Det.	32,862,974.7	Max.Feasible	0.383	58.56	57.37	78.18	68.97
		139,701,276.7	Min.Feasible	0.0	57.32	100.20	82.90	49.22

Table 7.7 Minimum and maximum feasible solutions for different reliability level (H=60 m)

H	Reliability	Construction cost ($)	Exit gradient		d_1	d_2	b	$b*$
60	100%	42,075,895.5	Max.Feasible	0.381	39.39	72.99	61.92	46.81
		188,247,133.9	Min.Feasible	0.002	79.94	102.64	67.92	36.71
	80%	14,352,204.0	Max.Feasible	0.383	33.28	52.83	64.91	52.24
		150,815,076.3	Min.Feasible	0.001	77.24	95.84	71.02	37.72
	60%	8,776,368.9	Max.Feasible	0.381	41.81	37.33	62.35	53.75
		119,297,688.9	Min.Feasible	0.005	65.41	93.24	70.85	47.82
	40%	5,634,374.6	Max.Feasible	0.382	29.68	37.36	77.08	53.21
		105,390,868.6	Min.Feasible	0.001	58.99	91.63	66.02	54.75
	Det.	8,474,313.2	Max.Feasible	0.382	27.84	45.39	58.24	49.15
		108,156,829.5	Min.Feasible	0.001	49.83	94.42	63.35	49.13

Table 7.8 Minimum and maximum feasible solutions for different reliability level (H=40 m)

H	Reliability	Construction cost ($)	Exit gradient		d_1	d_2	b	$b*$
40	100%	8,765,797.6	Max.Feasible	0.378	23.70	47.16	60.35	34.15
		151,144,025.4	Min.Feasible	0.001	86.85	89.16	63.35	25.76
	80%	2,406,236.8	Max.Feasible	0.380	22.71	29.43	44.61	36.62
		99,859,421.9	Min.Feasible	0.000	54.83	91.17	93.83	46.15
	60%	1,803,597.6	Max.Feasible	0.383	17.98	27.50	43.99	43.12
		80,204,409.8	Min.Feasible	0.043	64.50	81.31	110.50	64.33
	40%	1,334,875.1	Max.Feasible	0.380	21.88	21.01	48.75	31.61
		67,730,872.9	Min.Feasible	0.027	44.76	83.09	110.75	54.98
	Det.	1,171,848.0	Max.Feasible	0.383	14.15	22.77	52.09	36.74
		84,419,034.7	Min.Feasible	0.001	37.01	89.64	62.92	53.37

Table 7.9 Minimum and maximum feasible solutions for different reliability level (H=20 m)

H	Reliability	Construction cost ($)	Exit gradient		d_1	d_2	b	b^*
20	100%	1,262,284.3	Max.Feasible	0.380	19.86	23.99	27.68	25.03
		109,944,596.0	Min.Feasible	0.000	82.54	79.20	72.16	34.00
	80%	522,344.7	Max.Feasible	0.382	9.28	16.35	57.72	48.64
		60,149,842.6	Min.Feasible	0.004	39.48	81.20	115.27	95.03
	60%	338,708.5	Max.Feasible	0.383	8.88	14.60	30.27	22.13
		51,074,387.8	Min.Feasible	0.015	31.85	78.34	126.82	41.07
	40%	192,408.3	Max.Feasible	0.382	7.37	9.83	28.70	27.41
		42,940,043.9	Min.Feasible	0.000	40.37	73.39	138.01	42.74
	Det.	252,672.2	Max.Feasible	0.382	9.10	11.51	36.87	29.29
		92,965,180.5	Min.Feasible	0.001	90.72	48.89	45.62	17.55

7.10 Evaluation of the methodology

Assessing the accuracy of solutions obtained using the proposed methodology is essential to demonstrate potential applicability and validation of the methodology. Usually, for the deterministic approach, to determine accuracy of S-O model solutions optimum solutions are subsequently processed by the numerical simulation model and each single seepage characteristic obtained by the numerical model is compared with the seepage characteristic predicted as per optimal S-O model solutions. The RBOD model, however, needs a different evaluation technique to quantify accuracy of the developed methodology, especially in terms of reliability quantification. Furthermore, evaluation results for the RBOD do not require measuring the percentage of error for each seepage characteristic individually as in deterministic evaluation. However, quantifying actual reliability of the optimum solution (design) is also based on the multi-realization technique to find the number of scenarios providing safe design of HWRS to the total number of runs based on different realizations of HHC in the numerical model.

Hence, the evaluation method involved implementing numerical seepage simulation for the selected optimum solution for a specified number of times with different realizations of the HHC. The ratio of the number of times allowable limit was satisfied for all safety factors to the total number of iterations equals actual reliability level. Moreover, statistically more accurate actual reliability levels could be achieved by implementing more iterations. In the present study, for the selected optimum solution seepage characteristics were simulated using the numerical model ten times for different realizations of the HHC to measure actual reliability level.

As the seepage design characteristic most impacted by uncertainty of HHC is exit gradient values at the four specified locations, these values were considered to evaluate desired reliability level

of the RBOD model. Other seepage quantities, such as upstream and downstream uplift pressures, were less impacted by uncertainty in HHC.

The evaluation outcomes of four randomly selected optimum solutions demonstrated that the developed methodology provided reasonable indications to measure reliability level. The exit gradient values in Tables 7.10 to 7.13 were obtained from numerical seepage simulations for selected cases. The highlighted exit gradient values are more than the safe allowable exit gradient value (0.382), which was obtained as a second objective function of the optimum solution. The desired reliability level, objective function values and optimum solutions are shown in Tables 7.10 to 7.13. The COV for each implemented case was arbitrarily varied for each case to evaluate performance of the developed methodology with different COV values.

The average actual reliability (as verified by numerical simulation) in some cases, e. g., case A, was slightly less than the desired or specified reliability level (99.9 %). In contrast, in other cases, such as case C, the average of computed actual reliability levels was more than the desired reliability level (60 %). For other cases, average actual reliability almost matched desired reliability levels, such as in cases B and D. Hence, the implemented methodology, which quantifies reliability of seepage predictions under uncertainties, provides acceptable design solutions with potential application to HWRS design problems in real life cases. However, to ensure more accurate results, the number of iterations and number of surrogate models incorporated in the RBOD must be increased.

Table 7.10 Evaluation results for case A (COV=147.5%)

Case A	Rel. =100%	Cost =160838744$		ie=0.382
optimum design	*H* 100.0	d_1 69.00	d_2 101.3	*b* 94.07
Iteration	ie_1	ie_2	ie_3	ie_4
1	0.03	0.26	0.29	0.11
2	0.2	0.22	0.21	**0.67**
3	0.26	0.38	0.33	**0.45**
4	0.21	0.16	0.26	0.08
5	0.01	**0.42**	**0.48**	0.29
6	0.17	0.12	0.17	0.27
7	0.05	0.197	0.19	**1.28**
8	0.31	0.27	0.131	0.175
9	**0.56**	**0.41**	0.17	0.28
10	0.13	**0.58**	**0.54**	0.3
Actual reliability	90%	70%	80%	70%

Table 7.11 Evaluation results for case B (COV=112.5%)

Case B	Rel. =80%	Cost =60905832		ie=0.382
optimum design	*H* 80.0	*d₁* 43.84	*d₂* 80.5	*b* 75.16
Iteration	ie_1	ie_2	ie_3	ie_4
1	**0.62**	0.44	0.18	0.2
2	0.16	0.24	0.26	0.22
3	0.09	**0.56**	**0.53**	0.132
4	**1.08**	**0.59**	0.08	**0.43**
5	0.33	0.198	0.2	0.21
6	0.17	0.24	0.19	**0.44**
7	0.7	0.38	0.15	0.15
8	0.17	**0.48**	0.37	0.25
9	0.12	0.24	**0.56**	**0.54**
10	0.25	0.32	0.37	0.23
Actual reliability	80%	70%	80%	70%

Table 7.12 Evaluation results for case C (COV=182.5%)

Case C	Rel. =60%	Cost =1803597.62		ie=0.383
Optimum design	*H* 40.00	*d₁* 17.98	*d₂* 27.50	*b* 43.99
Iteration	ie_1	ie_2	ie_3	ie_4
1	0.01	0.22	0.28	**0.98**
2	**0.49**	0.33	0.19	0.16
3	0.37	0.37	0.34	0.2
4	0.128	0.32	**0.63**	0.03
5	**0.53**	**0.52**	0.26	0.06
6	0.02	0.21	**0.42**	0.32
7	**0.54**	**0.45**	0.21	0.22
8	0.37	0.219	0.2	0.29
9	0.03	0.18	0.24	0.14
10	0.04	**0.95**	**0.96**	**0.61**
Actual reliability	70%	70%	70%	80%

Table 7.13 Evaluation results for case D (COV=77.5%)

Case D	Rel. =80%	Cost =522344.7	ie=0.382	
Optimum design	*H*	*d₁*	*d₂*	*b*
	20.0	*9.28*	*16.3*	*57.72*
Iteration	ie₁	ie₂	ie₃	ie₄
1	0.34	0.28	0.17	0.29
2	0.1	0.09	**0.388**	**0.449**
3	0.14	0.36	**0.49**	0.33
4	**0.4**	0.31	0.17	**0.45**
5	0.146	0.168	0.24	**0.45**
6	**0.47**	0.27	0.1	**0.4**
7	0.06	0.15	0.26	0.2
8	0.08	0.15	0.2	0.34
9	0.31	0.19	0.2	0.29
10	0.22	0.16	0.27	**0.47**
Actual reliability	80%	100%	80%	60%

7.11 Conclusion

This chapter aimed to finding the safest HWRS design at minimum construction cost, integrating uncertainty in estimation of seepage quantities due to uncertainties in HHC estimates. Although formulation of the RBOD based on responses of a large number of surrogate models is a complex and time consuming task, it was efficiently and successfully implemented based on a new technique (MOMRO). Formulating RBOD problems as an MOMRO model enhances efficiency of population based search solvers, e.g., NSGA-II solver, to find Pareto optimum solutions. In contrast to the single optimization technique, the search process using the MOMRO technique was more efficient in approaching the global optimum solution. This formulation was based on the multi-realization 'staking' technique utilized in constraints and objective functions to incorporate reliability in the RBOD framework. This was achieved by utilizing 120 well trained surrogate models based on the GPR technique to build six stochastic ensemble surrogate models imitating stochastic seepage quantities (Pc_1, Pe_2, ie_1, ie_2, ie_3, ie_4).

Two strategies were adopted in this study to increase computing efficiency of the RBOD. The first was use of nested function formulation and the second was adaptation of the vector-process computing technique. These techniques improved computing efficiency of the MOMRO model to around 35 times faster than the traditional formulation. This procedure simplified the parameter selection process for the NSGA-II related to consequences of optimization performance.

The proposed methodology was applied for four different reliability levels (40%, 60%, 80%, 99.9%) for hypothetical cases, including five different values of upstream head values (100 m, 80 m, 60 m, 40 m, 20 m). Minimizing the stochastic exit gradient value and construction cost were the two objective functions in the MOMRO model. Solution results demonstrated that incorporating reliability

in the optimization model increased safety of HWRS design and strongly affected optimum solutions. Ignoring uncertainty of hydraulic conductivity may negatively impact on HWRS design. Increasing specified reliability levels significantly augmented construction cost due to an increase in required dimensions of cut-offs depths and floor width of HWRS to satisfy the desired reliability level.

The competing trade-offs encompassed numerous alternatives between minimum exit gradient and minimum construction cost objective functions. The optimum solutions in trade-offs may aid HWRS designers to make more reliable and informed decisions. With some experience, and these additional quantified reliability estimates, the rational optimum design can be achieved. Also, safety factors inherent in the specified safe exit gradient level can help decision making to select solutions at optimum reliability levels. Furthermore, the MOMRO technique provided, for the same objective functions values, many different optimum decision vectors (X). These results refer to the robustness of the MOMRO technique to attain diverse optimum solutions, based on the non-dominated population direct search technique, which can lead to the global optimum solution.

Evaluation results show that specified reliability levels agreed with the computed actual reliability levels. Also, the GPR based surrogate models predicted stochastic seepage quantities accurately and efficiently. However, there were some expected errors in the evaluated results. This may be attributed to allowable error of developed surrogate models and inadequate number of iterations used to estimate actual reliability level in the evaluation process.

Finally, historical records (ICOLD, 2016; NPODP, 2015) demonstrate that constructed HWRS had many failures or unsatisfactory performance related to seepage in the underlying porous medium. Hence, the proposed methodology based on the MOMRO technique provides a promising procedure to achieve optimal design considering minimum construction cost and safe exit gradient with quantified reliability of design. For future studies, to achieve more rigorous reliability, it is recommended to incorporate other sources of uncertainty arising from surrogate model predictions, construction cost parameters, upstream water head fluctuations and other related parameters. Also, the deterministic safety factors utilized in specifying permissible exit gradients considered in the evaluation of the stochastic optimum solutions must be integrated into reliability quantification related to design of HWRS.

8   Summary and conclusion

8.1   Summary

This study aimed to develop methodologies for deriving minimum cost safe optimum design of HWRS constructed on permeable soils, incorporating the effect of seepage characteristics, based on the linked simulation-optimization (S-O) technique. With development of numerical methods, such as the finite element method (FEM) which precisely determines seepage quantity for complex flow domains and irregular soil properties, there is motivation to incorporate accurate numerical seepage simulation into optimization models. Hence, the linked S-O model was implemented to identify optimum designs of HWRS based on numerical seepage models. Earlier seepage approximation and analytical methods cannot be utilized to find an accurate solution for complex seepage problems. Usually, direct linking of the S-O model is a challenging task and computationally expensive. Therefore, computational efficiency is enhanced and computational feasibility of the linked S-O model is ensured by replacing the computationally expensive numerical model with adequately and accurately trained and tested surrogate models based on a particular regression machine learning technique. The S-O methodology was applied to different illustrative problems and performance was evaluated for different design scenarios related to design of HWRS.

The S-O model was first applied to a simple conceptual seepage model including homogenous isotropic soil, two end cut-offs and apron. The optimization solver used was the genetic algorithm (GA) and the surrogate model was based on the artificial neural network (ANN) technique. Parameters of the ANN and GA models were systematically selected based on results of many design of experiments using Taguchi method. Consequently, performance of the GA and ANN models was shown to be improved. Seepage characteristics obtained based on S-O model solutions were evaluated by comparing seepage characteristics of the optimum solution obtained based on solving the numerical model to those obtained using the surrogate model linked S-O model. Also, Khosla's method solution was utilized in this comparison. The evaluation was based on many error measurement criteria, such as mean square error (MSE), coefficient of determination (RSQ), SI and bias parameter. Evaluation results demonstrated that the S-O model is potentially applicable to find an optimum design of HWRS based on surrogate models.

The next implementation of the S-O model was to find optimum design of HWRS for comprehensive conceptual seepage scenarios. The comprehensive seepage model included ten varied depth cut-offs with varied location and inclination angle for each cut-off. The model included non-homogenous layers. Hydraulic conductivity and anisotropic hydraulic conductivity for each layer were

different and varied for each numerical simulation. The complexity of the problem and large number of involved variables required an efficient machine learning technique. Hence, the support vector machine (SVM) technique was utilized and linked to the hybrid genetic algorithm (HGA) within the S-O model. The HGA solutions approached global optimum solutions. As there were numerous input design variables, to identify important relevant variables importance analysis of variables was conducted before developing the surrogate model for each seepage characteristic. The resulting optimum solution determined the most important relevant variables, which have a significant contribution compared to other variables, in providing a safe and minimum cost design. Additionally, the effect of hydraulic conductivity and anisotropic ratio on optimum design was considered in this model. An adequate evaluation process was carried out to determine accuracy of the S-O technique.

Furthermore, the S-O methodology was extended to implement reliability based optimum design (RBOD) based on the multi-realization optimization technique. The uncertainty of seepage characteristics due to uncertainty in estimating hydraulic conductivity is incorporated in RBOD framework. Reliability was based on the responses of many surrogate models trained using many different training data sets to reflect uncertainty in estimating hydraulic conductivity. Hydraulic conductivity was incorporated as a random field based on log-normal distribution with a specified standard deviation. The resulting optimum solutions including desired reliability levels were also evaluated based on the multi-realization technique. Evaluation results show that the developed methodology is potentially applicable to incorporate uncertainty of seepage quantitative estimation in optimum design of HWRS. Also, the methodology could be extendable and applicable to different problems and different engineering applications.

As the RBOD is a computationally expensive and demanding task, especially with a large number of stochastic constraints based on the multi-realization technique incorporated in the S-O model, the S-O model based RBOD was formulated based on a different technique - the MOMRO approach. Based on this approach, exit gradient stochastic constraints were transformed into a second objective function to be minimized. The reliability measure was incorporated in the objective function and in the constraints to obtain desired reliability level of minimum cost HWRS design. Evaluation results demonstrated the applicability of the developed methodology in quantifying safe design and reliability of the optimum design.

Generally, many techniques were utilized to increase computational efficiency of linked S-O models. The parallel computing tool available in Matlab can significantly increase computational efficiency by distributing the computation tasks on many cores of the processor unit. Also, using the nested function technique in writing constraints and objective functions codes increased computation efficiency of the S-O model. Moreover, formulating the S-O model in a vectorised system substantially improved computational efficiency.

Performance of optimization solvers was improved using many techniques. The Taguchi design of experiment (DOE) was implemented to select the best parameter combination of the GA to improve the possibility that the GA solution approaches the global optimum solution. Hybridizing the genetic algorithm with a gradient search algorithm, i.e., interior point algorithm(IPA), increased efficiency and speed of the solver to attain global optimum solutions. Additionally, for a complex S-O procedure, such as those including a large number of stochastic constraints, the use of a multi-objective optimization solver (NSGA-II) significantly increased computational efficiency and provided more resilience to the population based direct search technique. Another benefit of using NSGA-II was its ability to provide diverse scenarios of optimum solutions for the same (approximately) objective function values. Additional tables and figures related to the design solutions included in this study are attached as part of the Appendix.

8.2   Conclusion

The S-O model was efficiently and successfully implemented for different optimal design scenarios and objectives to find the optimum design of HWRS. It was shown to be a potentially efficient technique to incorporate different design variables pertaining to seepage related to HWRS and to study the effects of these variables on optimum design of HWRS. The linked S-O model incorporated all expected design requirements and safety factors related to HWRS. These safety factors were implicitly formulated in the optimization model as constraints based on responses of surrogate models. Thus, processing the S-O model with a large number of surrogate models was a challenging task, particularly for large scale problems.

The S-O technique was extended to incorporate the effect of uncertainty in estimating seepage quantities due to uncertainty of hydraulic conductivity. This was achieved by utilizing the multi-realization optimization technique. The reliability of the design was quantified by incorporating different responses of seepage stochastic surrogate models trained based on different scenarios of hydraulic conductivity. The desired reliability level was achieved by allowing the optimum solution to satisfy a specified percentage of all involved probabilistic constraints. This percentage reflects the probability of optimum design of HWRS to attain the desired reliability in terms of safety. However, for a high reliability level, at which all stochastic constraints must be satisfied, attaining a feasible solution was difficult. Hence, the MOMRO formulation was utilized to efficiently quantify reliability of the optimum design based on the multi-objective optimization solver (NSGA-II). The implementation of the MOMRO technique included transforming the exit gradient stochastic constraints to a second objective function to be minimized. Reliability was incorporated in the objective function and constraints based on the multi-realization technique. Evaluation results of the RBOD model based on the S-O model demonstrated the robustness of the developed methodology in quantifying reliability of HWRS design.

Reliability based design results demonstrated that uncertainty in seepage quantity due to uncertainty of hydraulic conductivity substantially influenced safety and design reliability of HWRS. For example, some stochastic exit gradient values resulted in double or more of the deterministic value. This means that the deterministic safety factors (3 to 5) are not sufficient to provide required safety of HWRS design for long life design. Also, construction cost curves show that reliability of the deterministic model was between 60% and 40%. Hence, it is recommended to increase the safety factor for exit gradient value, particularly to provide more safety against piping failure.

The S-O technique is substantially based on accuracy and efficiency of developed surrogate models. Therefore, surrogate models must be critically tested and evaluated independent of training data sets before using them in S-O models. Several error measures were utilized to evaluate all developed surrogate models integrated in the S-O model. However, accuracy and efficiency of developed surrogate models depends also on the type of utilized machine learning techniques.

The ANN model is more affected by noise in training data and tends to overfitting learning, unless sufficient precautions are implemented, such as earlier stopping criteria and using the regularization algorithm. The ANN model is an expeditious technique, but accuracy of the ANN model is deteriorated with augmentation of the number of neurons and size of the ANN model. It is recommended to normalize input and output training data to attain the most efficient surrogate models. Parameters and options of the ANN model should be systematically selected. The most effective parameter in the ANN model was the transfer function of hidden and output layers. The SVM and GPR techniques were more robust than the ANN model, and less impacted by noisy training data. However, prediction speed of SVM and GPR techniques was relatively less than the ANN model. Therefore, for complex problems it is a requirement to increase efficiency of surrogate models responses by reducing involved independent design variables in training surrogate models, or increasing computational efficiency of the S-O model based on many approaches discussed in this study. Performance of the SVM was most affected by the kernel function. The second order polynomial kernel was more suitable for the given training data to build an efficient surrogate model. Similarly, the GPR was most affected by the kernel function. The "squared exponential kernel with a separate length scale per predictor" GPR kernel function provided the most accurate predictions.

In general, from results of all implemented models it was found that exit gradient safety factor was the most important factor in achieving optimum design. The majority of obtained optimum solutions satisfied the minimum permissible values of exit gradient safety factor. Also, eccentric load condition played a crucial role in resulting optimum solutions. The remaining safety factors, such as overturning, sliding and flotation conditions, were satisfied, but had less impact on optimum solutions.

With the prescribed ranges, proposed parameters and boundary conditions of implemented cases, the important conclusion is that optimum design of HWRS should include two ends cut-offs with

an apron between them. However, with high upstream water head, or low hydraulic conductivity anisotropic ratio, or low hydraulic conductivity, more cut-offs and additional aprons may be required to decrease seepage quantities, such as uplift pressure and exit gradient values. The main role of the downstream cut-off was to decrease actual exit gradient value. This role is more effective when inclination angle of the cut-off is toward the downstream (>90 degrees). The main role of the upstream cut-off was to decrease uplift pressure value on the base of the HWRS; consequently, this partially contributed to decreasing exit gradient value. The effect of the upstream cut-off in decreasing uplift pressure was greater inclination angle inclining toward upstream (<90 degrees). The apron (floor) width aided to increase stability of HWRS. Also, this variable provided the required weight to improve HWRS resistance to external hydraulic forces and uplift pressure. Incorporating the weight of water (hydrostatic pressure) at the upstream side in counterbalancing momentum and hydraulic forces corroborated the safety of HWRS. These observations are based only on illustrative design scenarios considered in this study and may not be general in nature.

Finally, applying the S-O model and incorporating uncertainty of involved design variables and parameters can provide more safety for HWRS design at a minimum cost. Furthermore, including all expected uncertainty scenario in hydraulic conductivity in the design of HWRS would provide more reliable design representing real conditions and properties of porous media. This would satisfy high actual reliability level with required safety factors.

8.3 Limitations

All implemented S-O models concentrated only on hydraulic design aspects of HWRS generally mentioned in the literature. However, beyond hydraulic design of HWRS there are many pertaining details that should be considered for real life HWRS design, such as service load conditions, long term effects of generated sediments on the upstream side, uncertainty due to other parameters and upstream water head, and earthquake and ice load impacts. Furthermore, considering foundation design, structural design and bearing capacity requirements may provide more reliable design of HWRS. This may be achieved by combining SEEP/W, SIGMA/W and QUAKE/W components of Geo-Studio software in one model. However, solution of such models may require high speed processors and a significant amount of time and effort in future studies.

By increasing the complexity of seepage modeling scenarios some errors or inaccurate numerical solutions related to seepage characteristics may be observed. This inefficiency is not due to randomness of hydraulic conductivity, but due to convergence criteria of the complex numerical model. This shortcoming may occur for any numerical simulation models. Hence, uncertainty of numerical responses may be addressed by utilizing an adequate number of surrogate models in ensemble models to provide more precise estimations of seepage characteristics. Also, a combination of seepage

numerical responses in the ensemble may be based on different numerical modeling, methods and theories to provide accurate predictions of seepage characteristics.

For evaluation processes, it may be more robust to compare obtained seepage characteristics of optimum design to experimental observations based on a scaled seepage model. However, for complex seepage scenarios more attention, effort and time is required to represent a stratified flow domain based on particular values of hydraulic conductivity with inclined cut-offs, etc.

An obvious challenge of this study was the time required for generating simulated data sets. For each new input data there is a different flow domain that must be drafted in CAD software (AutoCAD/dxf extension) and exported to the seepage numerical simulation model to find the seepage characteristic based on new input data. For an enormous amount of training data sets, generating training data sets requires a long time, especially for complex seepage scenarios. It would be more efficient for the S-O model if a suitable technique is used to acquire numerical solutions in a more expeditious way.

8.4   Recommendations for future studies

It is recommended future studies incorporate unsteady state models and its consequences on optimum design of HWRS, as all scenarios included in this study were implemented for steady state conditions. Additionally, in regards to uncertainty of hydraulic conductivity, using a correlated heterogeneous random field with a predefined hydraulic conductivity value for specific points could be an important aspect to deal with and study different possible scenarios for such cases to determine how it affects optimum design of HWRS. On the other hand, incorporating the effects of dynamic and seismic loads and their consequences on hydrostatic forces and HWRS design could be an interesting direction to consider. This may be achieved by developing many surrogate model responses imitating seismic load for a certain location. Another interesting direction of study is to include structural design requirements of HWRS in addition to hydraulic design to find minimum cost design. Also, different systems of linked S-O models could be developed for improving accuracy and efficiency in modeling based on different machine learning techniques, such as multi-genes genetic programing(MGGP), multi-adaptive regression spline(MARS) and other optimization solvers, such as simulated annealing (SA) or particle swarm optimization (PSO).

9   References

ACI Committee American Concrete Institute & International Organization for Standardization. (2011). *Building code requirements for structural concrete (ACI 318-11m) and commentary*. Framington Hills, MI48331, USA: American Concrete Institute.

Ahmed, A. A. (2012). Stochastic analysis of seepage under hydraulic structures resting on anisotropic heterogeneous soils. *Journal of Geotechnical and Geoenvironmental Engineering, 139*(6), 1001-1004. doi:10.1061/%28ASCE%29GT.1943-5606.0000813

AL-Musawi, W. H., Shukur, A.-H. K., & Al-Delewy, A. A. (2006). Optimum design of control devices for safe seepage under hydraulic structures. *Journal of Engineering and Sustainable Development, 10*(1), 66-87. Retrieved from https://www.iasj.net/iasj?func=fulltext&aId=10146

Al-Suhaili, R. H., & Karim, R. A. (2014). Optimal dimensions of small hydraulic structure cutoffs using coupled genetic algorithm and ANN model. *Journal of Engineering, 20*(2), 1-19. Retrieved from https://www.iasj.net/iasj?func=fulltext&aId=83193

Alpaydin, E. (2014). *Introduction to machine learning*. London, England: MIT press.

Alsenousi, K. F., & Mohamed, H. G. (2008). Effects of inclined cutoffs and soil foundation characteristics on seepage beneath hydraulic structures. *Twelfth international water technology conference* Alexandria, Egypt Retrieved from http://www.iwtc.info/2008_pdf/17-1.PDF

Arman , M., & Ghader, B. (2014). Shape optimization of concrete gravity dams using performance criteria rules *Research Journal of Recent Sciences, 3*(11), 92-97. Retrieved from http://www.isca.in/rjrs/archive/v3/i11/15.%20ISCA-RJRS-2013-909.pdf

Ayvaz, M. T. (2016). A hybrid simulation–optimization approach for solving the areal groundwater pollution source identification problems. *Journal of Hydrology, 538*, 161-176. doi:10.1016/j.jhydrol.2016.04.008

Azamathulla, H. M., Ghani, A. A., Chang, C. K., Hasan, Z. A., & Zakaria, N. A. (2010). Machine learning approach to predict sediment load–a case study. *CLEAN–Soil, Air, Water, 38*(10), 969-976. doi:10.1002/clen.201000068

Azizi, S., Salmasi, F., Abbaspour, A., & Arvanaghi, H. (2012). Weep hole and cut-off effect in decreasing of uplift pressure, case study: Yusefkand Mahabad Diversion Dam. *Journal Civil Engineering Urban, 2*(3), 97-101. Retrieved from http://www.ojceu.ir/main/attachments/article/17/JCEU,%20B19,%20102-107,%202012.pdf

Baecher, G. B., & Christian, J. T. (2005). *Reliability and statistics in geotechnical engineering*. West Sussex PO198SQ, England: John Wiley & Sons.

Bajpai, P., & Kumar, M. (2010). Genetic algorithm–an approach to solve global optimization problems. *Indian Journal of Computer Science and Engineering.* Retrieved from http://citeseerx.ist.psu.edu/viewdoc/download?doi=10.1.1.301.2338&rep=rep1&type=pdf

Baroni, G., Zink, M., Kumar, R., Samaniego, L., & Attinger, S. (2017). Effects of uncertainty in soil properties on simulated hydrological states and fluxes at different spatio-temporal scales. *Hydrology and Earth System Sciences, 21*(5), 2301. doi:10.5194/hess-21-2301-2017

Bashi-Azghadi, S. N., Kerachian, R., Bazargan-Lari, M. R., & Solouki, K. (2010). Characterizing an unknown pollution source in groundwater resources systems using PSVM and PNN. *Expert Systems with Applications, 37*(10), 7154-7161. doi:10.1016/j.eswa.2010.04.019

BAUER Group. (2016). BAUER trench cutter systems. Retrieved from https://www.bauer.de/bauer_group/index.html, http://www.bauerpileco.com/export/shared/documents/pdf/bma/datenblatter/BC_Trench_Cutter_Systems_905-679-2_EN_01-16.pdf

Bayer, P., de Paly, M., & Bürger, C. M. (2010). Optimization of high‐reliability‐based hydrological design problems by robust automatic sampling of critical model realizations. *Water Resources Research, 46*(5). doi:10.1029/2009WR008081

Beckwith, C. W., Baird, A. J., & Heathwaite, A. L. (2003). Anisotropy and depth‐related heterogeneity of hydraulic conductivity in a bog peat. I: laboratory measurements. *Hydrological Processes, 17*(1), 89-101. doi:10.1002/hyp.1116

Behzad, M., Asghari, K., & Coppola Jr, E. A. (2009). Comparative study of SVMs and ANNs in aquifer water level prediction. *Journal of Computing in Civil Engineering, 24*(5), 408-413. doi:10.1061/(ASCE)CP.1943-5487.0000043

Bekele, E. G., & Nicklow, J. W. (2007). Multi-objective automatic calibration of SWAT using NSGA-II. *Journal of Hydrology, 341*(3-4), 165-176. doi:10.1016/j.jhydrol.2007.05.014

Bhagwat, P. P., & Maity, R. (2012). Multistep-ahead river flow prediction using LS-SVR at daily scale. *Journal of Water Resource and Protection, 4*(07), 528. doi: 10.4236/jwarp.2012.47062

Bhattacharjya, R. K., & Datta, B. (2009). ANN-GA-based model for multiple objective management of coastal aquifers. *Journal of Water Resources Planning and Management, 135*(5), 314-322. doi:10.1061/(ASCE)0733-9496(2009)135:5(314)

Bhattacharjya, R. K., Datta, B., & Satish, M. G. (2007). Artificial neural networks approximation of density dependent saltwater intrusion process in coastal aquifers. *Journal of Hydrologic Engineering, 12*(3), 273-282. doi:10.1061/(ASCE)1084-0699(2007)12:3(273)

Bligh, W. G. (1910). *The practical design of irrigation works*. New York: Van Nostrand.

Bligh, W. G. (1915). *Dams and weirs: An analytical and practical treatise on gravity dams and weirs; arch and buttress dams; submerged weirs; and barrages*. Chicago, United States: American Technical Society.

Bornschlegell, A., Pelle, J., Harmand, S., Bekrar, A., Chaabane, S., & Trentesaux, D. (2012). Thermal optimization of a single inlet T-junction. *International Journal of Thermal Sciences, 53*, 108-118. doi:10.1016/j.ijthermalsci.2011.09.016

Breiman, L. (2001). Random forests. *Machine learning, 45*(1), 5-32. doi:10.1023/A:1010933404324

Burger, R. L., & Belitz, K. (1997). Measurement of anisotropic hydraulic conductivity in unconsolidated sands: A case study from a shoreface deposit, Oyster, Virginia. *Water Resources Research, 33*(6), 1515-1522. doi:10.1029/97WR00570

Burke, E. K., & Kendall, G. (2005). *Search methodologies:Introductory tutorials in optimization and decision support techniques*. London: Springer.

Cavazzuti, M. (2012). *Optimization methods: From theory to design scientific and technological aspects in mechanics*. London: Springer Science & Business Media.

Chan, N. (1993). Robustness of the multiple realization method for stochastic hydraulic aquifer management. *Water Resources Research, 29*(9), 3159-3167. doi:10.1029/93WR01410

Chapuis, R. P., Chenaf, D., Bussière, B., Aubertin, M., & Crespo, R. (2001). A user's approach to assess numerical codes for saturated and unsaturated seepage conditions. *Canadian Geotechnical Journal, 38*(5), 1113-1126. doi:10.1139/t01-055

Chen, T., & Ren, J. (2009). Bagging for Gaussian process regression. *Neurocomputing, 72*(7-9), 1605-1610. doi:10.1016/j.neucom.2008.09.002

Chen, Z., Huan, G., & Ma, Y. (2006). *Computational Methods for Multiphase Flows in Porous Media*. Philadelphia, USA: Siam.

Chenaf, D., & Chapuis, R. P. (2007). Seepage face height, water table position, and well efficiency at steady state. *Groundwater, 45*(2), 168-177. doi:10.1111/j.1745-6584.2006.00277.x

Christian, J. T., Ladd, C. C., & Baecher, G. B. (1994). Reliability applied to slope stability analysis. *Journal of Geotechnical Engineering, 120*(12), 2180-2207. doi:10.1061/(ASCE)0733-9410(1994)120:12(2180)

Cimen, M. (2008). Estimation of daily suspended sediments using support vector machines. *Hydrological Sciences Journal, 53*(3), 656-666. doi:10.1623/hysj.53.3.656

Cojocaru, C., Duca, G., & Gonta, M. (2013). Chemical kinetic model for methylurea nitrosation reaction: Computer-aided solutions to inverse and direct problems. *Chemical Engineering Journal, 217*, 385-397. doi:10.1016/j.cej.2012.11.130

Cox, D. R., & Reid, N. (2000). *The theory of the design of experiments*. New York: Chapman and Hall/CRC.

Dao, S. D., Abhary, K., & Marian, R. (2016). Maximising performance of genetic algorithm solver in Matlab. *Engineering Letters, 24*(1), 75-83. Retrieved from http://www.engineeringletters.com/issues_v24/issue_1/EL_24_1_11.pdf

Das, A., & Datta, B. (1999). Development of management models for sustainable use of coastal aquifers. *Journal of Irrigation and Drainage Engineering, 125*(3), 112-121. doi:10.1061/(ASCE)0733-9437(1999)125:3(112)

Das, B. M. (2008). *Advanced Soil Mechanics*. New York, USA: Taylor & Francis.

Datta, B., Chakrabarty, D., & Dhar, A. (2011). Identification of unknown groundwater pollution sources using classical optimization with linked simulation. *Journal of Hydro-Environment Research, 5*(1), 25-36. doi:10.1016/j.jher.2010.08.004

Deb, K. (2001). *Multi-objective optimization using evolutionary algorithms* (Vol. 16). England: John Wiley & Sons.

Delleur, J. W. (2006). *The handbook of groundwater engineering*. USA: CRC press.

Deng, Z.-P., Li, D.-Q., Qi, X.-H., Cao, Z.-J., & Phoon, K.-K. (2017). Reliability evaluation of slope considering geological uncertainty and inherent variability of soil parameters. *Computers and Geotechnics, 92*, 121-131. doi:10.1016/j.compgeo.2017.07.020

Dhar, A., & Datta, B. (2008). Optimal operation of reservoirs for downstream water quality control using linked simulation optimization. *Hydrological processes, 22*(6), 842-853. doi:10.1002/hyp.6651

Dhar, A., & Datta, B. (2009). Saltwater intrusion management of coastal aquifers. I: Linked simulation-optimization. *Journal of Hydrologic Engineering, 14*(12), 1263-1272. doi:10.1061/(ASCE)HE.1943-5584.0000097

Dorsey, R., & Mayer, W. (1995). Genetic algorithms for estimation problems with multiple optima, nondifferentiability, and other irregular features. *Journal of Business & Economic Statistics, 13*(1), 53-66 doi:10.1080/07350015.1995.10524579

Duncan, J. M. (2000). Factors of safety and reliability in geotechnical engineering. *Journal of Geotechnical and Geoenvironmental Engineering, 126*(4), 307-316. doi:10.1061/(ASCE)1090-0241(2000)126:4(307)

El-Jumaily, D. K. K., & AL-Bakry , H. M. J. (2013). Seepage analysis through and under hydraulic structures applying finite volume method. *Engineering and Technology Journal, 31*(9), 1719-1731 Retrieved from http://www.uotechnology.edu.iq/tec_magaz/2013/volum312013/No.09.A.2013/Text%289%29.pdf

Elganainy, M. (1986). Flow underneath a pair of structures with intermediate filters on a drained stratum. *Applied Mathematical Modelling, 10*(6), 394-400. doi:10.1016/0307-904X(86)90017-X

Elganainy , M. A. (1987). Seepage underneath barrages with downstream subsidiary weirs. *Applied Mathematical Modelling, 11*(6), 423-431. doi:10.1016/0307-904X(87)90167-3

Ersayın, D. (2006). *Studying seepage in a body of earth-fill dam by (Artifical Neural Networks) ANNs*. (Master thesis), İzmirİzmir University, Institute of Technology, Turkey. Retrieved from https://core.ac.uk/download/pdf/47253637.pdf

Eslamian, S., Gohari, S., Biabanaki, M., & Malekian, R. (2008). Estimation of monthly pan evaporation using artificial neural networks and support vector machines. *Journal of Applied Sciences, 8*(19), 3497-3502. Retrieved from http://docsdrive.com/pdfs/ansinet/jas/2008/3497-3502.pdf

European Committee For Standardization. (2004). Eurocode 7: Geotechnical design-Part 1: General rules. In. British Standards, UK: CEN.

Farouk, M., & Smith, I. (2000). Design of hydraulic structures with two intermediate filters. *Applied Mathematical Modelling, 24*(11), 779-794. doi:10.1016/S0307-904X(00)00017-2

Feyen, L., & Gorelick, S. M. (2005). Framework to evaluate the worth of hydraulic conductivity data for optimal groundwater resources management in ecologically sensitive areas. *Water Resources Research, 41*(3). doi:10.1029/2003WR002901

Fisher, W. D., Camp, T. K., & Krzhizhanovskaya, V. V. (2016). Anomaly detection in earth dam and levee passive seismic data using support vector machines and automatic feature selection. *Journal of Computational Science, 20*, 143-153. doi:10.1016/j.jocs.2016.11.016

Freeze, R. A. (1975). A stochastic‐conceptual analysis of one‐dimensional groundwater flow in nonuniform homogeneous media. *Water Resources Research, 11*(5), 725-741. doi:10.1029/WR011i005p00725

Gail, M., Krickeberg, K., Samet, J., Tsiatis, A., & Wong, W. (2007). *Statistics for biology and health*. London: Springer.

Garcia, L. A., & Shigidi, A. (2006). Using neural networks for parameter estimation in ground water. *Journal of Hydrology, 318*(1-4), 215-231. doi:10.1016/j.jhydrol.2005.05.028

Garg, N., Bhagat, S., & Asthana, B. (2002). Optimal barrage design based on subsurface flow considerations. *Journal of Irrigation and Drainage Engineering, 128*(4), 253-263. doi:10.1061/(ASCE)0733-9437(2002)128:4(253)

Garg, S. K. (1987). *Irrigation engineering and hydraulic structures*. Nai Sarak Delhi, India: Khanna publishers.

Gen, M., & Cheng, R. (2000). *Genetic algorithms and engineering optimization* (Vol. 7). USA: John Wiley & Sons.

Genuer, R., Poggi, J.-M., & Tuleau-Malot, C. (2010). Variable selection using random forests. *Pattern Recognition Letters, 31*(14), 2225-2236. doi:10.1016/j.patrec.2010.03.014

Gerten, D., Heinke, J., Hoff, H., Biemans, H., Fader, M., & Waha, K. (2011). Global water availability and requirements for future food production. *Journal of Hydrometeorology, 12*(5), 885-899. doi:10.1175/2011JHM1328.1

Goel, A., & Pal, M. (2009). Application of support vector machines in scour prediction on grade-control structures. *Engineering Applications of Artificial Intelligence, 22*(2), 216-223. doi:10.1016/j.engappai.2008.05.008

Gorelick, S. M. (1983). A review of distributed parameter groundwater management modeling methods. *Water Resources Research, 19*(2), 305-319. doi:10.1029/WR019i002p00305

Greenkorn, R., Johnson, C., & Shallenberger, L. (1964). Directional permeability of heterogeneous anisotropic porous media. *Society of Petroleum Engineers Journal, 4*(02), 124-132. doi:10.2118/788-PA

Griffiths, D., & Fenton, G. A. (1997). Three-dimensional seepage through spatially random soil. *Journal of Geotechnical and Geoenvironmental Engineering, 123*(2), 153-160. doi:10.1061/(ASCE)1090-0241(1997)123:2(153)

Griffiths, D., & Fenton, G. A. (2004). Probabilistic slope stability analysis by finite elements. *Journal of Geotechnical and Geoenvironmental Engineering, 130*(5), 507-518. doi:10.1061/(ASCE)1090-0241(2004)130:5(507)

Griffiths, D. V., & Fenton, G. A. (1993). Seepage beneath water retaining structures founded on spatially random soil. *Géotechnique, 43*(4), 577-587. doi:10.1680/geot.1993.43.4.577

Grömping, U. (2009). Variable importance assessment in regression: linear regression versus random forest. *The American Statistician, 63*(4), 308-319. doi:10.1198/tast.2009.08199

Gupta, H. V., Sorooshian, S., & Yapo, P. O. (1999). Status of automatic calibration for hydrologic models: Comparison with multilevel expert calibration. *Journal of Hydrologic Engineering, 4*(2), 135-143. doi:10.1061/(ASCE)1084-0699(1999)4:2(135)

Haines, A., Mills, K., & Filliben, J. (2012). Determining relative importance and best settings for genetic algorithm control parameters. *Evolutionary Computation, 1*, 1-22. Retrieved from https://pdfs.semanticscholar.org/928d/11c638651325d9fde89dabec0cb4c3707c35.pdf

Hamidian, D., & Seyedpoor, S. (2010). Shape optimal design of arch dams using an adaptive neuro-fuzzy inference system and improved particle swarm optimization. *Applied Mathematical Modelling, 34*(6), 1574-1585. doi:10.1016/j.apm.2009.09.001

Hamzaçebi, C. (2008). Improving artificial neural networks' performance in seasonal time series forecasting. *Information Sciences, 178*(23), 4550-4559. doi:10.1016/j.ins.2008.07.024

Han, D., Chan, L., & Zhu, N. (2007). Flood forecasting using support vector machines. *Journal of Hydroinformatics, 9*(4), 267-276. doi:10.2166/hydro.2007.027

Harr, M. E. (1962). *Groundwater and seepage*. New York: McGraw Hill.

Harr, M. E. (2012). *Groundwater and seepage*. New York: McGraw Hill.

Hassan, W. H. (2015). Application of a genetic algorithm for the optimization of a cutoff wall under hydraulic structures. *Journal of Applied Water Engineering and Research*, 1-9. doi:10.1080/23249676.2015.1105161

Haupt, R. L., & Haupt, S. E. (2004). *Practical genetic algorithms*. New Jersey, USA: John Wiley & Sons.

Hazrati-Yadkoori, S., & Datta, B. (2017). Evaluation of unknown groundwater contaminant sources characterization efficiency under hydrogeologic uncertainty in an experimental aquifer site by

utilizing surrogate models. *Journal of Water Resource and Protection, 9*(13), 1612. doi:10.4236/jwarp.2017.913101

He, P., Li, S.-c., Xiao, J., Zhang, Q.-q., Xu, F., & Zhang, J. (2017). Shallow sliding failure prediction model of expansive soil slope based on Gaussian process theory and its engineering application. *KSCE Journal of Civil Engineering, 22*(5), 1-11. doi:10.1007/s12205-017-1934-6

Heydari, F., Saghafian, B., & Delavar, M. (2016). Coupled quantity-quality simulation-optimization model for conjunctive surface-groundwater use. *Water Resources Management, 30*(12), 4381-4397. doi:10.1007/s11269-016-1426-3

Hicks, M. A., Nuttall, J. D., & Chen, J. (2014). Influence of heterogeneity on 3D slope reliability and failure consequence. *Computers and Geotechnics, 61*, 198-208. doi:10.1016/j.compgeo.2014.05.004

Hicks, M. A., & Spencer, W. A. (2010). Influence of heterogeneity on the reliability and failure of a long 3D slope. *Computers and Geotechnics, 37*(7), 948-955. doi:10.1016/j.compgeo.2010.08.001

Hipni, A., El-shafie, A., Najah, A., Karim, O. A., Hussain, A., & Mukhlisin, M. (2013). Daily forecasting of dam water levels: comparing a support vector machine (SVM) model with adaptive neuro fuzzy inference system (ANFIS). *Water Resources Management, 27*(10), 3803-3823. doi:10.1007/s11269-013-0382-4

Housh, M., Ostfeld, A., & Shamir, U. (2012). Box-constrained optimization methodology and its application for a water supply system model. *Journal of Water Resources Planning and Management, 138*(6), 651-659. doi:10.1061/(ASCE)WR.1943-5452.0000229

ICOLD. (2016). International commission on large dams Retrieved from http://www.icold-cigb.org/home.asp

Ijam, A. Z. (2011). Dams with an inclined cutoff. *Electronic Journal of Geotechnical Engineering*. Retrieved from http://www.ejge.com/2011/Ppr11.138/Ppr11.138alr.pdf

Ilyinsky, N., & Kacimov, A. (1991). Problems of seepage under dam. *Proc. Indian Nat. Sci Acad., P. A, 57*, 61. Retrieved from https://www.insa.nic.in/writereaddata/UpLoadedFiles/PINSA/Vol57A_1991_1_Art03.pdf

Ilyinsky, N., Kacimov, A., & Yakimov, N. (1998). Analytical solutions of seepage theory problems. Inverse method, variational theorems, optimization and estimates (a review). *Fluid Dynamics, 33*(2), 157-168. doi:10.1007/BF02698697

Innal, F., Dutuit, Y., & Chebila, M. (2015). Safety and operational integrity evaluation and design optimization of safety instrumented systems. *Reliability Engineering & System Safety, 134*, 32-50. doi:10.1016/j.ress.2014.10.001

Islam, M., Buijk, A., Rais-Rohani, M., & Motoyama, K. (2015). Process parameter optimization of lap joint fillet weld based on FEM–RSM–GA integration technique. *Advances in Engineering Software, 79*, 127-136. doi:10.1016/j.advengsoft.2014.09.007

Jaddi, N. S., Abdullah, S., & Hamdan, A. R. (2013). Taguchi-based parameter designing of genetic algorithm for artificial neural network training. *2013 international conference on informatics and creative multimedia*, 278-281, Kuala Lumpur, Malaysia. doi:10.1109/ICICM.2013.54

Jain, A., & Kumar, A. (2006). An evaluation of artificial neural network technique for the determination of infiltration model parameters. *Applied Soft Computing, 6*(3), 272-282. doi:10.1016/j.asoc.2004.12.007

Jain, A. K. (2011). *Finite depth seepage below flat apron with end cutoffs and a downstream step.* (Doctor of Philosophy), University of Central Florida Orlando, Florida, Florida, USA. Retrieved from http://purl.fcla.edu/fcla/etd/CFE0003898

Jha, M. K., & Datta, B. (2011). Simulated annealing based simulation-optimization approach for identification of unknown contaminant sources in groundwater aquifers. *Desalination and Water Treatment, 32*(1-3), 79-85. doi:10.5004/dwt.2011.2681

Jiang, S.-H., Li, D.-Q., Zhang, L.-M., & Zhou, C.-B. (2014). Slope reliability analysis considering spatially variable shear strength parameters using a non-intrusive stochastic finite element method. *Engineering Geology, 168*, 120-128. doi:10.1016/j.enggeo.2013.11.006

Joorabchi, A., Zhang, H., & Blumenstein, M. (2009). Application of artificial neural networks to groundwater dynamics in coastal aquifers. *Journal of Coastal Research*, 966-970. Retrieved from

https://www.jstor.org/stable/pdf/25737930.pdf?refreqid=excelsior%3Ae17479dc29beb709aaa3cf4a98f0be58

Kang, F., Han, S., Salgado, R., & Li, J. (2015). System probabilistic stability analysis of soil slopes using Gaussian process regression with Latin hypercube sampling. *Computers and Geotechnics, 63*, 13-25. doi:10.1016/j.compgeo.2014.08.010

Kang, F., Xu, B., Li, J., & Zhao, S. (2017). Slope stability evaluation using Gaussian processes with various covariance functions. *Applied Soft Computing, 60*, 387-396. doi:10.1016/j.asoc.2017.07.011

Khan, M. S., & Coulibaly, P. (2006). Application of support vector machine in lake water level prediction. *Journal of Hydrologic Engineering, 11*(3), 199-205. doi:10.1061/(ASCE)1084-0699(2006)11:3(199)

Khaw, J. F., Lim, B., & Lim, L. E. (1995). Optimal design of neural networks using the Taguchi method. *Neurocomputing, 7*(3), 225-245. doi:10.1016/0925-2312(94)00013-I

Khosla, A. N., Bose , N. K., & Taylor, E. M. (1936). *Design of weirs on permeable foundations*. New Delhi: Central Board of Irrigation.

Kim, K., Lee, D., & Essa, I. (2011). Gaussian process regression flow for analysis of motion trajectories. *2011 international conference on computer vision*, 1164-1171, Barcelona, Spain. doi:10.1109/ICCV.2011.6126365

Kim, Y.-S., & Kim, B.-T. (2008). Prediction of relative crest settlement of concrete-faced rockfill dams analyzed using an artificial neural network model. *Computers and Geotechnics, 35*(3), 313-322. doi:10.1016/j.compgeo.2007.09.006

Kolahan, F., & Doughabadi, M. H. (2012). The effects of parameter settings on the performance of genetic algorithm through experimental design and statistical analysis. *Advanced Materials Research, 433*, 5994-5999. doi:10.4028/www.scientific.net/AMR.433-440.5994

Kolda, T. G., Lewis, R. M., & Torczon, V. (2003). Optimization by direct search: New perspectives on some classical and modern methods. *SIAM Review, 45*(3), 385-482. doi:10.1137/S003614450242889

Koljonen, J., & Alander, J. T. (2006). Effects of population size and relative elitism on optimization speed and reliability of genetic algorithms. *Proceedings of the ninth scandinavian conference on artificial intelligence (SCAI 2006)*, 25-27, Vaasa, Finland. Retrieved from http://citeseerx.ist.psu.edu/viewdoc/download?doi=10.1.1.118.6058&rep=rep1&type=pdf

Krahn, J. (2012). *Seepage modeling with SEEP/W: An engineering methodology*. Calgary, Alberta, Canada: GEO-SLOPE International, Ltd.

Kramer, O. (2016). *Machine Learning in Evolution Strategies* (Vol. 20). Switzerland: Springer.

Lambe, T. W., & Whitman, R. V. (1969). *Soil mechanics* New York: John Wiley & Sons.

Lane, E. W. (1935). Security from under-seepage-masonry dams on earth foundations. *Transactions of the American Society of Civil Engineers, 100*(1), 1235-1272.

Le, T. M. H., Gallipoli, D., Sanchez, M., & Wheeler, S. J. (2012). Stochastic analysis of unsaturated seepage through randomly heterogeneous earth embankments. *International Journal for Numerical and Analytical Methods in Geomechanics, 36*(8), 1056-1076. doi:10.1002/nag.1047

Lefebvre, G., Lupien, C., Pare, J. J., & Tournier, J.-P. (1981). Effectiveness of seepage control elements for embankments on semipervious foundations. *Canadian Geotechnical Journal, 18*(4), 572-576. doi:10.1139/t81-067

Lesaja, G. (2009). Introducing interior-point methods for introductory operations research courses and/or linear programming courses. *The Open Operational Research Journal, 3*, 1. doi:10.2174/1874243200903010001

Li, S.-c., He, P., Li, L.-p., Shi, S.-s., Zhang, Q.-q., Zhang, J., & Hu, J. (2017). Gaussian process model of water inflow prediction in tunnel construction and its engineering applications. *Tunnelling and Underground Space Technology, 69*, 155-161. doi:10.1016/j.tust.2017.06.018

Lin, C. D., & Tang, B. (2015). Latin hypercubes and space-filling designs. In *Handbook of Design and analysis of expriments*. Lowa, USA: CRC Press.

Lin, J.-Y., Cheng, C.-T., & Chau, K.-W. (2006). Using support vector machines for long-term discharge prediction. *Hydrological Sciences Journal, 51*(4), 599-612. doi:10.1623/hysj.51.4.599

Liu, J., Chang, J.-x., & Zhang, W.-g. (2009). Groundwater level dynamic prediction based on chaos optimization and support vector machine. *Third international conference on genetic and evolutionary computing*, 39-43, Guilin, China. doi:10.1109/WGEC.2009.25

Liu, M., Tso, S. K., & Cheng, Y. (2002). An extended nonlinear primal-dual interior-point algorithm for reactive-power optimization of large-scale power systems with discrete control variables. *IEEE Transactions on Power Systems, 17*(4), 982-991. doi:10.1109/TPWRS.2002.804922

Loyola, D., Pedergnana, M., & García, S. G. (2016). Smart sampling and incremental function learning for very large high dimensional data. *Neural Networks, 78*, 75-87. doi:10.1016/j.neunet.2015.09.001

Madanayaka, T. A., & Sivakugan, N. (2016). Approximate equations for the method of fragment. *International Journal of Geotechnical Engineering, 10*(3), 297-303. doi:10.1080/19386362.2016.1144338

Mahani, A. S., Shojaee, S., Salajegheh, E., & Khatibinia, M. (2015). Hybridizing two-stage meta-heuristic optimization model with weighted least squares support vector machine for optimal shape of double-arch dams. *Applied Soft Computing, 27*, 205-218. doi:10.1016/j.asoc.2014.11.014

Majumdar, A., & Ghosh, D. (2015). Genetic algorithm parameter optimization using Taguchi Robust design for multi-response optimization of experimental and historical data. *International Journal of Computer Applications, 45*(1), 52-63. Retrieved from http://citeseerx.ist.psu.edu/viewdoc/download?doi=10.1.1.736.561&rep=rep1&type=pdf

Mansuri, B., Salmasi, F., & Oghati, B. (2014). Effect of Location and Angle of Cutoff Wall on Uplift Pressure in Diversion Dam. *Geotechnical and Geological Engineering, 32*(5), 1165-1173. doi:10.1007/s10706-014-9774-3

MathWorks. (2015). *Global Optimization Toolbox User's Guide.* Retrieved from https://www.mathworks.com/help/pdf_doc/gads/gads_tb.pdf

MathWorks. (2018). *Matlab statistics and machine learning toolbox*. Natick, MA, USA. Retrieved from https://au.mathworks.com/help/stats/

Mentaschi, L., Besio, G., Cassola, F., & Mazzino, A. (2013). Problems in RMSE-based wave model validations. *Ocean Modelling, 72*, 53-58. doi:10.1016/j.ocemod.2013.08.003

Misra, D., Oommen, T., Agarwal, A., Mishra, S. K., & Thompson, A. M. (2009). Application and analysis of support vector machine based simulation for runoff and sediment yield. *Biosystems Engineering, 103*(4), 527-535. doi:10.1016/j.biosystemseng.2009.04.017

Moeini, M., & Etemad-Shahidi, A. (2007). Application of two numerical models for wave hindcasting in Lake Erie. *Applied Ocean Research, 29*(3), 137-145. doi:10.1016/j.apor.2007.10.001

Moghaddamnia, A., Ghafari, M., Piri, J., & Han, D. (2009). Evaporation estimation using support vector machines technique. *World Academy of Science, Engineering and Technology 43 2008*, 415-423. Retrieved from http://citeseerx.ist.psu.edu/viewdoc/download?doi=10.1.1.193.3804&rep=rep1&type=pdf

Moharrami, A., Moradi, G., Bonab, M. H., Katebi, J., & Moharrami, G. (2014). Performance of cutoff walls under hydraulic structures against uplift pressure and piping phenomenon. *Geotechnical and Geological Engineering, 33*(1), 95-103. doi:10.1007/s10706-014-9827-7

Mollon, G., Dias, D., & Soubra, A.-H. (2009). Probabilistic analysis of circular tunnels in homogeneous soil using response surface methodology. *Journal of Geotechnical and Geoenvironmental Engineering, 135*(9), 1314-1325. doi:10.1061/(ASCE)GT.1943-5606.0000060

Mollon, G., Dias, D., & Soubra, A.-H. (2010). Probabilistic analysis of pressurized tunnels against face stability using collocation-based stochastic response surface method. *Journal of Geotechnical and Geoenvironmental Engineering, 137*(4), 385-397. doi:10.1061/(ASCE)GT.1943-5606.0000443

Moriasi, D. N., Arnold, J. G., Van Liew, M. W., Bingner, R. L., Harmel, R. D., & Veith, T. L. (2007). Model evaluation guidelines for systematic quantification of accuracy in watershed simulations. *Transactions of the ASABE, 50*(3), 885-900. doi:10.13031/2013.23153

Mulligan, A. E., & Ahlfeld, D. P. (2002). A new interior-point boundary projection method for solving nonlinear groundwater pollution control problems. *Operations Research, 50*(4), 636-644. doi:10.1287/opre.50.4.636.2859

Nourani, V., Sharghi, E., & Aminfar, M. H. (2012). Integrated ANN model for earthfill dams seepage analysis: Sattarkhan Dam in Iran. *Artificial Intelligence Research, 1*(2), 22. doi:10.5430/air.v1n2p22

Novak, P., Moffat, A., Nalluri, C., & Narayanan, R. (2007). *Hydraulic structures*. United Kingdom: CRC Press.

NPODP. (2015). *National Performance of Dams Program*. Retrieved from https://npdp.stanford.edu/

O'Brien, S., Dann, C., Hunter, G., & Schwermer, M. (2005). *Construction of the Plastic Concrete Cut-off Wall at Hinze Dam*. Paper presented at the ANCOLD Proceedings of Technical Groups, Australia https://www.ancold.org.au/

Oh, W. T., & Vanapalli, S. K. (2010). Influence of rain infiltration on the stability of compacted soil slopes. *Computers and Geotechnics, 37*(5), 649-657. doi:10.1016/j.compgeo.2010.04.003

Pal, M., & Deswal, S. (2010). Modelling pile capacity using Gaussian process regression. *Computers and Geotechnics, 37*(7-8), 942-947. doi:10.1016/j.compgeo.2010.07.012

Pallant, J. (2007). *SPSS survival manual: A step by step guide to data analysis using SPSS for windows*. Berkshire, England: McGraw-Hill Open University Press.

Parkinson, A. R., Balling, R., & Hedengren, J. D. (2013). *Optimization methods for engineering design: Applications and theory*. Vol. 5. Brigham Young University. Retrieved from http://flowlab.groups.et.byu.net/me575/textbook/optimization_book.pdf

Parsaie, A., Yonesi, H. A., & Najafian, S. (2015). Predictive modeling of discharge in compound open channel by support vector machine technique. *Modeling Earth Systems and Environment, 1*(1-2), 1-6. doi:10.1007/s40808-015-0002-9

Pavlovsky, N. N. (1935). Principles of hydromechanical computation for senkov-type barrages (In Russian). *Gidrotekhnicheskoe stroitel'stvo*.

Pereira, S. R., Clerc, F., Farrusseng, D., Van der Waal, J. C., Maschmeyer, T., & Mirodatos, C. (2005). Effect of the genetic algorithm parameters on the optimisation of heterogeneous catalysts. *QSAR & Combinatorial Science, 24*(1), 45-57. doi:10.1002/qsar.200420058

Popescu, R., Deodatis, G., & Nobahar, A. (2005). Effects of random heterogeneity of soil properties on bearing capacity. *Probabilistic Engineering Mechanics, 20*(4), 324-341. doi:10.1016/j.probengmech.2005.06.003

Pruett, W. A., & Hester, R. L. (2016). The Creation of Surrogate Models for Fast Estimation of Complex Model Outcomes. *PLOS One, 11*(6), e0156574. doi:10.1371/journal.pone.0156574

Raghavendra.N, S., & Deka, P. C. (2014). Support vector machine applications in the field of hydrology: A review. *Applied Soft Computing, 19*, 372-386. doi:10.1016/j.asoc.2014.02.002

Rajabi-Bahaabadi, M., Shariat-Mohaymany, A., Babaei, M., & Ahn, C. W. (2015). Multi-objective path finding in stochastic time-dependent road networks using non-dominated sorting genetic algorithm. *Expert Systems with Applications, 42*(12), 5056-5064. doi:10.1016/j.eswa.2015.02.046

Rajper, S., & Amin, I. J. (2012). Optimization of wind turbine micrositing: A comparative study. *Renewable and Sustainable Energy Reviews, 16*(8), 5485-5492. doi:10.1016/j.rser.2012.06.014

Rand, W., Riolo, R., & Holland, J. H. (2006). The effect of crossover on the behavior of the GA in dynamic environments: a case study using the shaky ladder hyperplane-defined functions. *Proceedings of the 8th annual conference on genetic and evolutionary computation*, 1289-1296, Seattle, Washington, USA. doi:10.1145/1143997.1144198

Ranković, V., Grujović, N., Divac, D., & Milivojević, N. (2014). Development of support vector regression identification model for prediction of dam structural behaviour. *Structural Safety, 48*, 33-39.

Rao. (2009). *Engineering optimization:Theory and practice* (Fourth Edition). USA: John Wiley & Sons.

Rao. (2013). *The finite element method in engineering*. England: Pergamon Press.

Rasmussen, C. E. (2004). Gaussian processes in machine learning. In *Advanced lectures on machine learning* (pp. 63-71). Berlin, Heidelberg: Springer.

Roberts, S., Osborne, M., Ebden, M., Reece, S., Gibson, N., & Aigrain, S. (2013). Gaussian processes for time-series modelling. *Phil Trans R Soc A 371: 20110550., 371*(1984), 20110550. doi:10.1098/rsta.2011.0550

Ross, S. (2014). *A first course in probability*. Boston, MA , USA: Pearson.

Samui, P. (2011). Application of least square support vector machine (LSSVM) for determination of evaporation losses in reservoirs. *Engineering, 3*(04), 431. doi:10.4236/eng.2011.34049

Samui, P., & Jagan, J. (2013). Determination of effective stress parameter of unsaturated soils: A Gaussian process regression approach. *Frontiers of Structural and Civil Engineering, 7*(2), 133-136. doi:10.1007/s11709-013-0202-1

Santillán, D., Fraile-Ardanuy, J., & Toledo, M. (2013). Dam seepage analysis based on artificial neural networks: The hysteresis phenomenon. *The 2013 international joint conference on neural networks (IJCNN)*, 1-8, Dallas, TX, USA. doi:10.1109/IJCNN.2013.6707110

Schumacker, R. E., & Lomax, R. G. (2004). *A beginner's guide to structural equation modeling*. London: Lawrence Erlbaum Associates, Inc.

Sedghi‐Asl, M., Rahimi, H., & Khaleghi, H. (2012). Laboratory investigation of the seepage control measures under coastal dikes. *Experimental Techniques, 36*(1), 61-71. doi:10.1111/j.1747-1567.2010.00692.x

Seyedpoor, S., Salajegheh, J., & Salajegheh, E. (2010). Shape optimal design of arch dams including dam-water–foundation rock interaction using a grading strategy and approximation concepts. *Applied Mathematical Modelling, 34*(5), 1149-1163. doi:10.1016/j.apm.2009.08.005

Seyedpoor, S., Salajegheh, J., Salajegheh, E., & Gholizadeh, S. (2009). Optimum shape design of arch dams for earthquake loading using a fuzzy inference system and wavelet neural networks. *Engineering optimization, 41*(5), 473-493. doi:10.1080/03052150802596076

Seyedpoor, S., Salajegheh, J., Salajegheh, E., & Gholizadeh, S. (2011). Optimal design of arch dams subjected to earthquake loading by a combination of simultaneous perturbation stochastic approximation and particle swarm algorithms. *Applied Soft Computing, 11*(1), 39-48. doi:10.1016/j.asoc.2009.10.014

Shahrbanozadeh, M., Barani, G.-A., & Shojaee, S. (2015). Simulation of flow through dam foundation by isogeometric method. *Engineering Science and Technology, an International Journal, 18*(2), 185-193. doi:10.1016/j.jestch.2014.11.001

Shi, J. Q., & Choi, T. (2011). *Gaussian process regression analysis for functional data*. New York: Chapman and Hall,CRC Press.

Shourian, M., Mousavi, S. J., Menhaj, M., & Jabbari, E. (2008). Neural-network-based simulation-optimization model for water allocation planning at basin scale. *Journal of Hydroinformatics, 10*(4), 331-343. Retrieved from https://pdfs.semanticscholar.org/a240/4e13feea26ebf0a7821b90745643366a7c95.pdf

Singh, A., & Minsker, B. S. (2008). Uncertainty‐based multiobjective optimization of groundwater remediation design. *Water Resources Research, 44*(2). doi:10.1029/2005WR004436

Singh, R. M. (2010). Design of Barrages with Genetic Algorithm Based Embedded Simulation Optimization Approach. *Water Resources Management, 25*(2), 409-429. doi:10.1007/s11269-010-9706-9

Singh, R. M. (2011). Genetic algorithm based optimal design of hydraulic structures with uncertainty characterization. *International conference on swarm, evolutionary, and memetic computing*, 742-749, Berlin, Heidelberg. doi:10.1007/978-3-642-27172-4_87

Singh, R. M., & Duggal, S. (2015). Optimal design of hydraulic structures with hybrid differential evolution multiple particle swarm optimization. *Canadian Journal of Civil Engineering, 42*(5), 303-310. doi:10.1139/cjce-2014-0441

Sivakugan, N., & Rankine, K. (2011). Three-dimensional method of fragments to study drainage through hydraulic fill stopes. *International Journal of Geomechanics, 12*(5), 612-615. doi:10.1061/(ASCE)GM.1943-5622.0000158

Sivakugan, N., Rankine, K., Lovisa, J., & Hall, W. (2013). Flow rate computations in hydraulic fill mine stopes. *Indian Geotechnical Journal, 43*(3), 195-202. doi:10.1007/s40098-013-0043-9

Sivanandam, S., Sumathi, S., & Deepa, S. (2006). *Introduction to neural networks using Matlab 6.0*. New Delhi: Tata McGraw-Hill.

Sreekanth, J., & Datta, B. (2010). Multi-objective management of saltwater intrusion in coastal aquifers using genetic programming and modular neural network based surrogate models. *Journal of Hydrology, 393*(3-4), 245-256. doi:10.1016/j.jhydrol.2010.08.023

Sreekanth, J., & Datta, B. (2011). Coupled simulation‑optimization model for coastal aquifer management using genetic programming‑based ensemble surrogate models and multiple‑realization optimization. *Water Resources Research, 47*(4). doi:10.1029/2010WR009683

Sreekanth, J., & Datta, B. (2014). Stochastic and robust multi-objective optimal management of pumping from coastal aquifers under parameter uncertainty. *Water Resources Management, 28*(7), 2005-2019. doi:10.1007/s11269-014-0591-5

Sreekanth, J., & Datta, B. (2015a). Review: simulation-optimization models for the management and monitoring of coastal aquifers. *Hydrogeology Journal, 23*(6), 1155-1166. doi:10.1007/s10040-015-1272-z

Sreekanth, J., & Datta, B. (2015b). Simulation-optimization models for the management and monitoring of coastal aquifers. *Hydrogeology Journal, 23*(6). doi:10.1007/s10040-015-1272-z

Strobl, C., Boulesteix, A.-L., Zeileis, A., & Hothorn, T. (2007). Bias in random forest variable importance measures: Illustrations, sources and a solution. *BMC bioinformatics, 8*(1), 25. doi:10.1186/1471-2105-8-25

Su, H., Chen, Z., & Wen, Z. (2016). Performance improvement method of support vector machine‑based model monitoring dam safety. *Structural Control and Health Monitoring, 23*(2), 252-266. doi:10.1002/stc.1767

Sun, A. Y., Wang, D., & Xu, X. (2014). Monthly streamflow forecasting using Gaussian process regression. *Journal of Hydrology, 511*, 72-81. doi:10.1016/j.jhydrol.2014.01.023

Szidarovszky, F., Coppola, E. A., Long, J., Hall, A. D., & Poulton, M. M. (2007). A Hybrid Artificial Neural Network‑Numerical Model for Ground Water Problems. *Groundwater, 45*(5), 590-600. doi:10.1111/j.1745-6584.2007.00330.x

Tanchev, L. (2014). *Dams and appurtenant hydraulic structures*. London: Taylor & Francis, CRC Press.

Tatone, B., Donnelly, C., Protulipac, D., & Clark, C. (2009). Evaluation of the hydraulic efficiency of a newly constructed plastic concrete cut-off wall. *Canadian dam association annual conference*, 3-8, Whistler, Canada.

Tee, K. F., Khan, L. R., Chen, H. P., & Alani, A. M. (2014). Reliability based life cycle cost optimization for underground pipeline networks. *Tunnelling and Underground Space Technology, 43*, 32-40. doi:10.1016/j.tust.2014.04.007

Terzaghi, K., Peck, R. B., & Mesri, G. (1996). *Soil mechanics in engineering practice*. New York: John Wiley & Sons.

Tokaldany, E. A., & Shayan, H. K. (2013). Uplift force, seepage, and exit gradient under diversion dams. *Proceedings of the Institution of Civil Engineers-Water Management*, 452-462. doi:10.1680/wama.11.00084

U.S. Army Corps of Engineers. (1987). *Engineering and design flotation stability criteria for concrete hydraulic structures*. Retrieved from http://www.dtic.mil/dtic/tr/fulltext/u2/a403467.pdf

Vapnik, V. (2013). *The nature of statistical learning theory*. New York: Springer

Vapnik, V. N. (1999). An overview of statistical learning theory. *IEEE Transactions on Neural Networks, 10*(5), 988-999. doi:10.1109/72.788640

Wagner, B. J., & Gorelick, S. M. (1986). A statistical methodology for estimating transport parameters: Theory and applications to one‑dimensional advectivec‑dispersive systems. *Water Resources Research, 22*(8), 1303-1315. doi:10.1029/WR022i008p01303

Wang, H. F., & Anderson, M. P. (1995). *Introduction to groundwater modeling: finite difference and finite element methods*. USA: Academic Press.

White, J., Beaven, R., Powrie, W., & Knox, K. (2011). Leachate recirculation in a landfill: Some insights obtained from the development of a simple 1-D model. *Waste Management, 31*(6), 1210-1221. doi:10.1016/j.wasman.2010.10.022

Willis, R., & Finney, B. A. (1988). Planning model for optimal control of saltwater intrusion. *Journal of Water Resources Planning and Management, 114*(2), 163-178. doi:10.1061/(ASCE)0733-9496(1988)114:2(163)

Xia, W., Luo, B., & Liao, X.-p. (2011). An enhanced optimization approach based on Gaussian process surrogate model for process control in injection molding. *The International Journal of Advanced Manufacturing Technology, 56*(9-12), 929-942. doi:10.1007/s00170-011-3227-4

Xu, J. W., & Suzuki, K. (2011). Massive‐training support vector regression and Gaussian process for false‐positive reduction in computer‐aided detection of polyps in CT colonography. *Medical Physics, 38*(4), 1888-1902. doi:10.1118/1.3562898

Yandamuri, S., Srinivasan, K., & Murty Bhallamudi, S. (2006). Multiobjective optimal waste load allocation models for rivers using nondominated sorting genetic algorithm-II. *Journal of Water Resources Planning and Management, 132*(3), 133-143. doi:10.1061/(ASCE)0733-9496(2006)132:3(133)

Yapo, P. O., Gupta, H. V., & Sorooshian, S. (1998). Multi-objective global optimization for hydrologic models. *Journal of Hydrology, 204*(1-4), 83-97. doi:10.1016/S0022-1694(97)00107-8

Yazd, H. G. H., Arabshahi, S. J., Tavousi, M., & Alvani, A. (2015). Optimal designing of concrete gravity dam using particle swarm optimization algorithm (PSO). *Indian Journal of Science and Technology, 8*(12), 1. doi:10.17485/ijst/2015/v8i12/70714

Yoon, H., Jun, S.-C., Hyun, Y., Bae, G.-O., & Lee, K.-K. (2011). A comparative study of artificial neural networks and support vector machines for predicting groundwater levels in a coastal aquifer. *Journal of Hydrology, 396*(1-2), 128-138. doi:10.1016/j.jhydrol.2010.11.002

Yu, P.-S., Chen, S.-T., & Chang, I.-F. (2006). Support vector regression for real-time flood stage forecasting. *Journal of Hydrology, 328*(3), 704-716. doi:10.1016/j.jhydrol.2006.01.021

Zakaria, M. Z., Jamaluddin, H., Ahmad, R., & Loghmanian, S. M. (2012). Comparison between multi-objective and single-objective optimization for the modeling of dynamic systems. *Journal of Systems and Control Engineering, 226*(7), 994-1005. doi:10.1177/0959651812439969

Zhang, J., Zhang, L., & Tang, W. H. (2011). Reliability-based optimization of geotechnical systems. *Journal of Geotechnical and Geoenvironmental Engineering, 137*(12), 1211-1221. doi:10.1061/(ASCE)GT.1943-5606.0000551

Zhu, X., Wang, X., Li, X., Liu, M., & Cheng, Z. (2017). A new dam reliability analysis considering fluid structure interaction. *Rock Mechanics and Rock Engineering*, 1-12. doi:10.1007/s00603-017-1369-x

10 Appendix A

Example Formulation of ANN equations (ΘE) based on the weights matrix and biases vector

Step1: normalizing the input data (d_1, d_2, 2b, h) using the following formula:

$$Y = (ymax - ymin) * (x - xmin)/(xmax - xmin) + ymin \tag{A3.1}$$

The normalization step is a built in phase of the Matlab training algorithm and a (*mapminmax*) function is used within the training algorithm to provide better training and minimize the error between the ANN response and the target data. Therefore the resulted in weights and biases are corresponded with the normalized data set. Only to use the generated weights and bias correctly (only in this context), the normalized data must be utilized to formulation ANN equations (model). In contrast, the developed ANN models are applied with non-normalized data, because the normalization and de-normalization phases are the interior process within training stage. Also, based on the training process, the weights matrix and bias vector is generated.

Step2: multiplying each variable by the weights matrix, then add a bias vector as shown below:

$$H_s = b_s + \sum_{r=1}^{r=4} X_r \times W_{s \times r} \tag{A3.2}$$

H1 =	-0.124 +	1.406 ×X 1 +	-0.667×X2+	1.559×X3+	-0.721×X4
H2=	1.288+	0.745×X1+	-0.820× X2+	-0.021×X3+	-0.061×X4
H3=	1.131+	0.663×X1+	-0.664× X2+	0.076×X3+	-0.253×X4
H4=	-2.719	-0.951×X1+	-1.064× X2+	0.758×X3+	1.113×X4

Hidden layer

Step 3: substituting the result of the second step (H_s) as the input of the transfer function according to the following equation:

$$As = \frac{1}{(1 + EXP(-Hs))} \tag{A3.3}$$

A1=1/(1+EXP(-H1))

A2=1/(1+EXP(-H2))

A3=1/(1+EXP(-H3))

A4=1/(1+EXP(-H4))

Transfer function

(Logsig)

Step 4: multiplying the outcome vector of last step by the weights matrix of output layer, then add the bias vector as shown below:

$$K_i = b_i + \sum_{s=1}^{s=4} A_s \times W_{i \times s}$$

(A3.4)

| **K=** | 2.525+ | 0.973×A1+ | 15.185×A2+ | -20.160×A3+ | -1.250×A4 | Output layer |

Step 5: de- normalized data to actual data using the following equation

$$x_{actual} = (y - y_{min})(x_{max} - x_{min})/(y_{max} - y_{min}) + x_{min}$$

(A3.5)

Weights and bias tables for the developed ANN models

Table A3.1 Weights and bias factors for the hidden layer of ANN model (ΘC)

Neuron No	Scalar bias for hidden layer (b)	Scalar weight factors for hidden layer			
		W1-1	**W1-2**	**W1-3**	**W1-4**
1	-24.802	5.210	5.050	4.722	2.541
2	14.526	-0.313	8.245	-13.369	15.144
3	0.311	-6.070	-2.623	3.811	-0.256
4	-1.172	-4.241	-0.646	-1.463	1.490
5	3.203	-0.703	1.269	1.776	-0.818
6	-5.044	3.518	1.495	4.518	-1.902
7	4.209	1.180	-3.717	4.303	-4.158
8	-1.352	0.012	0.253	0.456	-1.449
9	7.580	3.958	-13.991	5.042	-8.592
10	1.853	0.976	-0.060	-0.118	-0.860
11	8.975	-1.099	-5.878	5.808	-2.655

Table A3.2 Weights and bias factors for the output layer of ANN model (ΘC)

Neuron No	Scalar bias for output layer (b)	Scalar weight factors for hidden layer										
		W2-1	W2-2	W2-3	W2-4	W2-5	W2-6	W2-7	W2-8	W2-9	W2-10	W2-11
1	2.452	0.074	0.003	-0.073	-0.310	1.340	0.219	-0.137	-1.500	0.014	-3.937	-0.124

Table A3.3 Weights and bias factors for the hidden layer of ANN model (Θ E)

Neuron No	Scalar bias for hidden layer (b)	Scalar weight factors for hidden layer			
		W1-1	W1-2	W1-3	W1-4
1	-0.124	1.406	-0.667	1.559	-0.721
2	1.288	0.745	-0.820	-0.021	-0.061
3	1.131	0.663	-0.664	0.076	-0.253
4	-2.719	-0.951	-1.064	0.758	1.113

Table A3.4 Weights and bias factors for the output layer of ANN model (Θ E)

Neuron No	Scalar bias for output layer (b)	Scalar weight factors for hidden layer			
		W2-1	W2-2	W2-3	W2-4
1	2.525	0.973	15.185	-20.160	-1.250

Table A3.5 Weights and bias factors for the hidden layer of ANN model (Exit gradient)

Neuron No	Scalar bias for hidden layer (b)	Scalar weight factors for hidden layer			
		W1-1	W1-2	W1-3	W1-4
1	-5.716	1.172	-2.300	-4.439	0.518
2	-4.591	0.258	0.465	-0.125	-3.892
3	6.800	-1.678	2.492	4.232	-0.697
4	12.820	0.049	11.040	0.290	-0.518
5	-1.867	-0.297	-0.688	-0.151	0.689

Table A3.6 Weights and bias factors for the output layer of ANN model (Exit gradient)

Neuron No	Scalar bias for output layer (b)	Scalar weight factors for hidden layer				
		W2-1	W2-2	W2-3	W2-4	W2-5
1	1.342	2.201	-4.692	3.929	-6.948	2.552

11 Appendix B

Table B4.1 Variable importance results (PE1)

Variable	Importance	
	SPSS (beta (coefficient)	**Matlab (random forest)**
H	100.00	100.00
b1	0.98	0.72
k_{x1}	0.15	0.04
β1	0.08	0.03
kx 2	0.08	0.06
d1	0.06	0.04
layer depth1	0.04	< 0.01
dd	0.04	< 0.01
layer depth2	0.03	< 0.01
kx_3	0.02	< 0.01

Table B4.2 Variable importance results (PC1)

Variable	Importance	
	SPSS (beta (coefficient)	**Matlab (random forest)**
PE1 m	100.00	100.00
d1	1.27	1.14
$(k_y/k_x)_1$	0.12	0.12
b1	0.11	0.09
dd	0.04	0.01
k_{x1}	0.03	< 0.01
b2	0.03	0.05
kx3	0.02	0.03
b10	0.02	< 0.01
d2	0.01	0.02

Table B4.3 Variable importance results (PE2)

Variable	Importance	
	SPSS (beta (coefficient)	**Matlab (random forest)**
PC1	100.00	100.00
b2	0.22	0.17
d1	0.02	0.01
d2	0.02	0.02
β2	0.02	0.01
$(k_y/k_x)_1$	0.01	< 0.01
β1	0.01	< 0.01
k_{x1}	< 0.01	< 0.01
dd	< 0.01	< 0.01
b1	< 0.01	< 0.01

Table B4.4 Variable importance results (PC2)

Variable	Importance	
	SPSS (beta (coefficient)	**Matlab (random forest)**
PE2	100.00	100.00
d2	1.28	0.85
d1	0.04	0.02
dd	0.03	< 0.01
d10	0.02	0.02
b3	0.01	< 0.01
β1	0.01	< 0.01
$(k_y/k_x)_1$	0.01	< 0.01
b2	0.01	< 0.01
d3	0.01	0.01

Table B4.5 Variable importance results (PE3)

Variable	Importance	
	SPSS (beta (coefficient)	**Matlab (random forest)**
PC2	100.00	100.00
b3	0.24	0.15
β2	0.03	0.02
β3	0.03	0.02
d2	0.02	< 0.01
$(k_y/k_x)1$	0.02	0.03
d3	0.02	< 0.01
b5	< 0.01	< 0.01
layer depth2	< 0.01	< 0.01

Table B4.6 Variable importance results (PC3)

Variable	Importance	
	SPSS (beta (coefficient)	**Matlab (random forest)**
PE3	100.00	100.00
d3	0.61	0.67
d4	0.02	< 0.01
b4	0.01	< 0.01
b3	0.01	< 0.01
d2	0.01	< 0.01
$(k_y/k_x)_1$	0.01	0.01
b10	0.01	< 0.01
β2	< 0.01	< 0.01

Table B4.7 Variable importance results (PE4)

Variable	Importance	
	SPSS (beta (coefficient)	Matlab (random forest)
PC3	100.00	100.00
b4	0.20	0.11
$(k_y/k_x)_1$	0.02	0.01
β4	0.02	0.03
β3	0.02	< 0.01
d4	0.02	0.02
d3	0.02	< 0.01
kx 2	< 0.01	< 0.01
d10	< 0.01	< 0.01

Table B4.8 Variable importance results (PC4)

Variable	Importance	
	SPSS (beta (coefficient)	Matlab (random forest)
PE4	100.00	100.00
d4	0.62	0.58
d3	0.02	0.01
b4	0.01	< 0.01
b10	0.01	< 0.01
b5	0.01	0.01
d5	0.01	0.01
k_{x1}	0.01	< 0.01
d10	0.01	< 0.01

Table B4.9 Variable importance results (PE5)

Variable	Importance	
	SPSS (beta (coefficient)	Matlab (random forest)
PC4	100.00	100.00
b5	0.15	0.11
$(k_y/k_x)_1$	0.02	0.01
d4	0.01	< 0.01
β5	0.01	0.01
d5	0.01	0.01
β4	0.01	0.01
Dd	< 0.01	< 0.01
d10	< 0.01	0.01
b6	< 0.01	< 0.01

Table B4.10 Variable importance results (PC5)

Variable	Importance	
	SPSS (beta (coefficient)	Matlab (random forest)
PE5	100.00	100.00
d5	0.67	0.86
b6	0.03	0.04
d10	0.02	0.01
d6	0.02	0.01
β4	0.01	0.01
d4	0.01	< 0.01
b5	0.01	< 0.01
b11	0.01	< 0.01
β6	0.01	0.01

Table B4.11 Variable importance results (PE6)

Variable	Importance	
	SPSS (beta (coefficient)	Matlab (random forest)
PC5	100.00	100.00
Dd	19.89	17.95
b6	0.25	0.17
$(k_y/k_x)_1$	0.03	< 0.01
β6	0.03	0.02
d6	0.02	< 0.01
β5	0.02	0.01
d5	0.02	0.02
$(k_y/k_x)_2$	< 0.01	0.01
d7	< 0.01	< 0.01

Table B4.12 Variable importance results (PC6)

Variable	Importance	
	SPSS (beta (coefficient)	Matlab (random forest)
PE6	100.00	100.00
d6	1.53	1.73
dd	0.12	0.11
k_{x1}	0.04	0.03
b6	0.04	0.01
b10	0.03	0.05
d5	0.03	0.01
d7	0.02	0.02
d10	0.01	< 0.01
d9	0.01	0.02

Table B4.13 Variable importance results (PE7)

Variable	Importance	
	SPSS (beta (coefficient)	Matlab (random forest)
PC6	100.00	100.00
b7	0.46	0.29
β7	0.05	0.04
$(k_y/k_x)_1$	0.04	0.03
d6	0.04	0.01
β6	0.04	0.01
d7	0.03	0.02
Dd	0.02	0.01
kx 2	0.02	0.01
b10	0.01	< 0.01

Table B4.14 Variable importance results (PC7)

Variable	Importance	
	SPSS (beta (coefficient)	Matlab (random forest)
PE7	100.00	100.00
d7	1.50	1.56
dd	0.09	0.04
d6	0.05	0.03
d8	0.05	0.03
b7	0.02	0.04
β6	0.01	< 0.01
d10	0.01	0.02
b10	0.01	< 0.01
β8	0.01	< 0.01

Table B4.15 Variable importance results (PE8)

Variable	Importance	
	SPSS (beta (coefficient)	**Matlab (random forest)**
PC7	100.00	100.00
b8	0.41	0.29
$\beta 8$	0.05	0.02
d8	0.04	0.03
$\beta 7$	0.03	0.01
$(k_y/k_x)_1$	0.03	0.05
d7	0.03	0.02
Dd	0.02	0.01
d10	< 0.01	< 0.01
$\beta 3$	< 0.01	< 0.01

Table B4.16 Variable importance results (PC8)

Variable	Importance	
	SPSS (beta (coefficient)	**Matlab (random forest)**
PE8	100.00	100.00
d8	2.56	1.82
dd	0.20	0.13
d9	0.10	0.12
k_{x1}	0.09	0.10
$(k_y/k_x)_1$	0.08	< 0.01
d10	0.05	0.06
d7	0.04	0.04
b8	0.04	0.04
b10	0.03	0.04

Table B4.17 Variable importance results (PE9)

Variable	Importance	
	SPSS (beta (coefficient)	**Matlab (random forest)**
PC8	100.00	100.00
b9	0.54	0.49
d8	0.06	0.02
dd	0.06	< 0.01
$\beta 9$	0.03	0.03
d9	0.03	0.03
$\beta 6$	0.02	0.01
$\beta 8$	0.01	0.02
b3	0.01	0.01
$\beta 1$	0.01	< 0.01

Table B4.18 Variable importance results (PC9)

Variable	Importance	
	SPSS (beta (coefficient)	**Matlab (random forest)**
PE9	100.00	100.00
d9	12.13	4.50
d10	2.42	1.31
b11	0.60	0.77
k_{x1}	0.58	0.35
b10	0.53	0.41
kx_2	0.25	0.07
b9	0.24	0.14
kx_3	0.20	0.05
layer depth2	0.18	0.05

Table B4.19 Variable importance results (PE10)

Variable	Importance	
	SPSS (beta (coefficient)	**Matlab (random forest)**
PC9	100.00	100.00
b10	3.60	1.62
d10	2.27	3.50
$(k_y/k_x)_1$	0.81	0.39
$\beta 10$	0.29	0.14
d9	0.23	0.27
b11	0.23	0.18
$\beta 9$	0.18	0.06
layer depth2	0.05	< 0.01
layer depth1	0.04	< 0.01

Table B4.20 Variable importance results (PC10)

Variable	Importance	
	SPSS (beta (coefficient)	**Matlab (random forest)**
b11	100.00	100.00
PE10	22.51	17.06
d10	24.83	9.51
$\beta 10$	11.70	3.94
kx 2	9.17	1.85
k_{x1}	7.84	1.27
dd	3.08	0.88
$(k_y/k_x)_1$	2.61	0.97
kx3	2.13	0.53
layer depth1	1.05	< 0.01

Table B4.21 Variable importance results (Exit gradient)

Variable	Importance	
	SPSS (beta (coefficient)	**Matlab (random forest)**
H	100.00	34.07
$(k_y/k_x)_1$	86.58	100.00
k_{x1}	28.64	8.17
b11	15.30	5.92
d10	9.33	1.72
kx 2	9.05	2.83
kx3	6.16	0.94
layer depth1	5.77	2.93
b10	2.52	0.43

Table B4.22 Training and testing result for the developed SVM models

model	RSQ TRAIN	MSE TRAIN	RSQ TEST	MSE TEST	function
exit model 1	0.96	0.088	0.95	0.086	polynomial 2
exit model 2	0.96	0.08	0.95	0.11	polynomial 2
exit model 3	0.96	0.087	0.954	0.09	polynomial 2
pc10- model 1	0.95	0.92	0.95	1.06	polynomial 2
pc10 model 2	0.959	0.92	0.955	0.93	polynomial 2
pe10- model 1	0.987	1.26	0.988	1.06	polynomial 2
pe10 model 2	0.987	1.27	0.988	1.08	polynomial 2
pc9- model 1	0.981	2	0.983	1.68	polynomial 2
pc9 model 2	0.982	1.97	0.981	1.9	polynomial 2
pe9- model 1	0.997	0.55	0.996	0.65	polynomial 2
pe9 model 2	0.997	0.56	0.997	0.59	polynomial 2
pc8- model 1	0.991	2.02	0.991	1.92	polynomial 2
pc8 model 2	0.991	2.05	0.993	1.65	polynomial 2
pe8- model 1	0.998	0.33	0.998	0.4	polynomial 2
pe8 model 2	0.998	0.339	0.0998	0.308	polynomial 2
pc7- model 1	0.995	1.14	0.997	0.82	polynomial 2
pc7 model 2	0.995	1.09	0.996	1.15	polynomial 2
pe7- model 1	0.996	1.13	0.998	0.66	polynomial 2
pe7 model 2	0.996	1.08	0.996	0.93	polynomial 2
pc6 model 1	0.996	1.15	0.996	1.15	polynomial 2
pc6 model 2	0.996	1.19	0.997	0.91	polynomial 2
pe6 model 1	0.999	0.23	0.999	0.16	polynomial 2
pe6 model 2	0.999	0.22	0.999	0.19	polynomial 2
pc5 model 1	0.998	0.64	0.997	0.66	polynomial 2
pc5 model 2	0.998	0.65	0.997	0.65	polynomial 2
pe5 model 2	0.999	0.199	0.999	0.173	polynomial 2
pc4 model 1	0.998	0.702	0.998	0.702	polynomial 2
pc4 model 2	0.998	0.73	0.998	0.56	polynomial 2
pe4 model 1	0.999	0.25	0.999	0.233	polynomial 2
pe4 model 2	0.999	0.25	0.999	0.25	polynomial 2
pc3 model 1	0.998	0.65	0.998	0.75	polynomial 2
pc3 model 2	0.998	0.66	0.998	0.68	polynomial 2
pe3 model 1	0.999	0.28	0.999	0.407	polynomial 2
pe3 model 2	0.999	0.28	0.999	0.252	polynomial 2
pc2 model 1	0.997	1.18	0.997	1.18	polynomial 2
pc2 model 2	0.997	1.16	0.997	1.33	polynomial 2
pe2 model 1	0.999	0.27	0.999	0.27	polynomial 2
pe2 model 2	0.999	0.26	0.999	0.24	polynomial 2
pc1 model 1	0.996	1.96	0.997	1.8	polynomial 2
pc1model 2	0.996	1.93	0.996	1.89	polynomial 2
pe1 model 1	0.997	1.63	0.998	1.25	Polynomial 2
pe1model 2	0.997	1.61	0.997	1.57	Polynomial 2

Table B4.23 Optimum solution for different value of H

H	20	30	40	50	**60**	70	80	90	100
b1	0.0	0.0	0.0	0.0	0.0	5.9	5.0	6.7	7.0
b2	0.0	0.0	0.0	0.2	1.7	3.0	2.5	3.4	3.5
b3	0.0	0.0	0.0	0.0	0.0	0.0	0.0	0.0	0.0
b4	0.0	0.0	0.0	0.0	0.0	0.0	0.0	0.0	0.0
b5	0.0	0.0	0.0	0.0	0.0	0.0	0.0	0.0	0.0
b6	0.0	0.0	0.0	0.0	0.0	0.0	0.0	0.3	0.0
b7	0.0	0.0	0.0	0.0	0.0	0.0	0.0	0.4	0.0
b8	0.0	6.1	0.0	0.0	0.0	0.0	0.0	0.1	0.0
b9	4.8	7.8	17.2	22.5	28.5	29.1	38.3	39.7	46.1
b10	15.4	34.8	33.0	35.5	36.4	36.6	40.0	43.8	51.6
b11	10.5	10.1	8.0	4.1	0.8	0.0	0.0	0.0	0.0
d1	0.0	0.0	0.0	0.4	3.3	5.9	5.0	6.7	7.0
d2	0.0	0.0	0.0	0.0	0.0	0.0	0.0	0.0	0.0
d3	0.0	0.0	0.0	0.0	0.0	0.0	0.0	0.0	0.0
d4	0.0	0.0	0.0	0.0	0.0	0.0	0.0	0.0	0.0
d5	0.0	0.0	0.0	0.0	0.0	0.0	0.0	0.0	0.0
d6	0.0	0.0	0.0	0.0	0.0	0.0	0.0	0.6	0.0
d7	0.0	0.0	0.0	0.0	0.0	0.0	0.0	0.3	0.0
d8	0.0	0.0	0.0	0.0	0.0	0.0	0.0	0.0	0.0
d9	9.7	15.5	33.6	35.1	34.2	33.3	34.1	38.5	45.0
d10	21.1	20.1	32.5	35.9	38.5	40.0	42.0	38.7	40.8
$\beta1$	30.0	81.8	92.0	102.2	111.9	117.4	125.6	131.9	139.7
$\beta2$	30.0	66.4	68.6	71.2	75.2	76.6	77.5	80.4	82.4
$\beta3$	30.0	107.9	110.1	113.1	116.1	116.1	118.3	120.9	123.2
$\beta4$	30.0	79.2	82.1	86.9	92.3	93.4	97.4	99.8	106.2
$\beta5$	30.0	81.1	77.6	74.4	71.6	69.6	65.3	61.5	59.2
$\beta6$	30.0	118.6	125.7	134.0	140.9	143.3	147.8	150.0	150.0
$\beta7$	30.0	96.3	133.3	137.3	142.8	132.6	125.9	126.4	126.8
$\beta8$	30.0	150.0	30.0	30.0	30.0	30.0	30.0	30.0	30.0
$\beta9$	30.0	30.0	30.0	30.0	30.0	30.0	30.0	30.0	30.0
$\beta10$	139.8	150.0	150.0	150.0	150.0	150.0	150.0	150.0	150.0

Table B4.24 Evaluation results for different values of H

	H=100		H=90		H=80		H=70		H=60		H=50		H=40		H=30		H=20	
	S-O	N. S.*	S-O	N. S.	S-O	N. S.	S-O	N. S.	S-O	N. S.	S-O	N. S.	S-O	N. S.	S-O	N. S.	S-O	N. S.
PE1 m	96.37	91.99	87.00	82.47	77.68	74.22	68.10	64.98	59.10	60.00	49.37	50.00	39.67	40.00	29.92	29.99	20.14	20.00
PC1	88.57	86.18	79.87	76.32	71.51	68.87	62.39	60.74	59.99	55.29	50.41	49.00	40.37	39.75	30.24	29.44	20.22	19.61
PE2	87.85	86.18	79.13	76.28	70.74	68.85	61.63	60.72	59.18	55.41	49.56	48.99	39.54	39.74	29.46	29.42	19.39	19.60
PC2	87.31	86.19	78.59	76.29	70.16	68.84	61.10	60.71	58.58	55.37	48.92	48.90	38.93	39.64	28.89	29.01	19.17	19.40
PE3	85.95	86.19	77.39	76.28	69.10	68.83	60.20	60.71	57.71	55.36	48.21	48.90	38.40	39.63	28.53	28.99	18.83	19.39
PC3	85.42	86.18	76.86	76.28	68.56	68.80	59.66	60.69	57.19	55.33	47.68	48.79	37.87	39.55	28.01	28.67	18.57	19.28
PE4	84.95	86.18	80.25	76.27	68.14	68.79	59.26	60.68	56.79	55.32	47.29	48.80	37.48	39.54	27.62	28.66	19.25	19.27
PC4	86.94	86.17	82.09	76.26	69.66	68.75	60.53	60.67	57.99	55.27	48.24	48.70	38.18	39.48	28.07	28.43	19.84	19.21
PE5	86.37	86.16	81.50	76.25	69.12	68.74	60.04	60.66	57.51	55.26	47.84	48.69	37.88	39.47	27.89	28.42	19.84	19.20
PC5	85.35	86.15	80.54	76.23	68.26	68.69	59.25	60.64	56.74	55.22	47.16	48.61	37.27	39.43	27.35	28.22	19.60	19.18
PE6	86.05	86.14	78.88	76.21	66.96	68.68	59.98	60.63	55.81	55.21	47.88	48.59	37.96	39.41	27.14	28.21	20.57	19.37
PC6	85.88	86.12	80.93	76.09	68.13	68.62	59.79	60.62	56.72	55.16	47.64	48.52	37.68	39.38	27.36	28.12	21.28	19.32
PE7	85.11	86.12	80.20	76.09	67.48	68.62	59.12	60.62	55.96	55.16	47.03	48.52	37.21	39.38	27.19	28.04	21.49	19.32
PC7	84.93	86.10	79.93	76.01	67.25	68.55	58.91	60.58	55.82	55.09	46.83	48.48	36.97	39.33	26.81	27.83	21.38	19.30
PE8	84.69	86.09	79.67	76.01	66.93	68.54	58.60	60.58	55.54	55.09	46.47	48.44	36.54	39.33	25.67	27.18	20.95	19.29
PC8	84.43	86.06	78.70	75.98	66.73	68.47	58.50	60.56	55.45	55.03	46.44	48.38	36.55	39.30	25.65	27.18	20.79	19.28
PE9	82.61	83.95	76.50	74.21	65.44	66.00	57.83	59.98	54.86	54.20	46.21	47.91	36.50	39.11	24.80	27.16	20.36	19.26
PC9	53.23	53.84	51.63	48.92	46.60	45.25	41.28	39.96	38.72	34.31	32.32	28.25	25.77	22.27	20.23	18.92	17.87	13.67
PE10	42.54	39.76	41.20	37.21	37.26	35.67	32.64	31.78	30.38	27.13	24.94	22.16	19.51	17.39	13.55	12.43	13.13	11.39
PC10	2.54	0.00	2.35	0.00	1.50	0.00	1.15	0.00	1.15	0.00	1.15	0.00	1.15	0.05	1.15	0.32	1.15	0.57
Exit gradient	0.23	0.24	0.23	0.22	0.23	0.24	0.23	0.24	0.23	0.22	0.23	0.21	0.23	0.22	0.23	0.27	0.23	0.22

*N.S. is the Numerical Simulation results

Table B4.25 Optimum solutions for different values of k_{x1}

kx	0.1	0.1	0.5	0.9	1.5	4.0	7.0	10.0	13.0	17.0	20.0
b1	0.0	0.0	0.0	0.0	0.0	0.0	4.5	5.4	5.6	5.1	5.4
b2	0.1	0.0	0.0	0.0	0.0	0.0	2.2	3.0	4.5	2.8	3.1
b3	0.5	0.0	0.0	0.0	0.0	0.0	0.0	0.5	0.7	0.4	0.8
b4	0.2	0.0	0.0	0.0	0.0	0.0	0.0	0.4	0.6	0.4	0.7
b5	0.6	0.0	0.0	0.0	0.0	0.0	0.0	0.7	0.7	0.6	0.7
b6	0.1	0.0	0.0	0.0	0.0	0.0	0.0	1.0	3.0	4.6	4.2
b7	0.1	0.0	0.0	0.0	0.0	0.0	1.0	1.5	0.8	0.6	0.5
b8	8.2	0.0	0.0	0.0	0.0	0.0	1.0	12.2	5.2	8.9	8.8
b9	35.7	30.0	29.5	28.7	27.4	23.6	17.9	0.8	7.6	4.5	3.5
b10	133.6	47.3	46.3	45.3	44.1	38.0	21.8	27.2	26.8	29.5	33.0
b11	9.3	0.4	0.1	1.2	1.5	3.9	9.7	4.7	2.6	2.6	2.3
d1	0.0	0.0	0.0	0.0	0.0	0.0	4.5	5.4	5.6	5.1	5.4
d2	0.0	0.0	0.0	0.0	0.0	0.0	0.0	0.5	0.7	0.5	0.8
d3	0.0	0.0	0.0	0.0	0.0	0.0	0.0	0.5	0.6	0.4	0.8
d4	0.1	0.0	0.0	0.0	0.0	0.0	0.0	0.4	0.6	0.4	0.7
d5	0.0	0.0	0.0	0.0	0.0	0.0	0.0	1.0	0.8	0.8	0.7
d6	0.0	0.0	0.0	0.0	0.0	0.0	0.0	1.0	0.6	0.6	0.5
d7	0.0	0.0	0.0	0.0	0.0	0.0	2.0	2.0	1.0	0.6	0.6
d8	0.0	0.0	0.0	0.0	0.0	0.0	0.0	0.2	0.0	0.3	0.5
d9	17.9	60.0	59.1	57.4	54.8	42.0	0.0	1.4	4.0	4.4	4.1
d10	48.4	34.5	33.6	33.2	33.4	34.0	33.2	14.1	7.8	7.8	6.9
dd	0.8	0.0	0.0	0.0	0.0	0.0	0.0	0.0	0.0	0.0	0.0
β1	103.8	101.7	103.5	101.3	101.0	103.0	102.5	99.3	96.1	97.9	98.1
β2	36.9	63.9	64.3	64.9	65.7	69.7	72.8	77.2	81.7	84.6	87.8
β3	38.0	114.5	114.3	114.1	114.1	113.8	109.0	108.1	106.2	104.5	102.6
β4	35.0	83.8	85.4	85.6	84.3	84.1	82.4	82.3	83.3	83.9	87.2
β5	99.9	76.9	76.5	76.1	75.7	75.4	75.6	74.1	71.5	68.6	67.3
β6	81.3	130.6	130.8	130.9	131.2	133.8	126.3	126.1	128.4	129.4	128.0
β7	37.4	150.0	150.0	149.0	145.6	144.7	100.3	66.5	57.4	30.4	30.0
β8	41.0	30.0	30.0	30.0	30.0	30.0	108.0	150.0	150.0	150.0	150.0
β9	30.0	30.0	30.0	30.0	30.0	30.0	30.0	30.0	48.8	54.2	51.8
β10	150.0	150.0	150.0	150.0	150.0	150.0	150.0	150.0	150.0	150.0	150.0

Table B4.26 Optimum thicknesses for different values of k_{x1}

k_{x1}	t1	t2	--	t10	t11	t12	t13	t14	t15	t16	t17	t18	t19	t20
0.1	41.7	42.3	--	40.5	40.0	40.1	39.6	39.9	39.6	39.8	40.9	23.3	18.3	1.0
0.5	43.0	42.5	--	40.6	40.1	40.2	39.7	40.0	39.6	39.8	40.9	23.3	18.4	1.0
0.9	41.9	42.6	--	40.7	40.2	40.2	39.8	40.0	39.6	39.8	40.9	23.6	17.7	1.0
1.5	42.1	42.8	--	40.9	40.3	40.4	39.9	40.0	39.7	39.8	41.0	24.1	18.2	1.0
4	42.6	43.5	--	41.5	40.9	40.8	40.2	40.1	39.8	39.9	40.9	25.4	19.3	1.0
7	42.0	34.4	--	32.5	32.2	31.8	31.6	30.9	30.2	29.7	29.5	27.4	21.5	1.0
10	43.1	35.3	--	33.5	33.1	32.6	32.4	31.6	29.8	29.6	29.8	26.1	17.8	1.3
13	43.3	35.4	--	33.9	33.5	32.9	32.7	31.8	30.3	27.1	27.3	22.4	13.4	1.1
17	43.2	33.3	--	32.6	32.1	31.5	31.3	30.5	28.7	28.7	26.3	22.6	13.5	1.1
20	42.1	32.3	--	30.1	29.8	29.2	29.0	28.3	26.6	26.8	24.6	20.0	12.8	1.0

Table B.27 Optimum solutions for different values of $(k_y/k_x)_1$

$(k_y/k_x)_1$	0.1	0.3	0.5	0.7	0.9	1.1	1.3	1.5
b1	0.01	0.01	0.01	0.01	0.01	0.39	0.01	0.36
b2	7.13	3.97	0.01	0.01	0.78	1.55	0.97	0.19
b3	0.01	0.01	0.01	0.01	0.01	0.01	0.01	0.01
b4	0.01	0.01	0.01	0.01	0.01	0.01	0.01	0.01
b5	0.01	0.01	0.01	0.01	0.01	0.01	0.01	0.01
b6	0.01	0.01	0.01	0.01	0.01	0.01	0.01	0.01
b7	0.01	0.01	0.01	0.01	0.01	0.01	0.01	0.01
b8	0.01	0.01	1.51	0.01	0.01	0.01	0.01	0.01
b9	77.80	47.37	31.50	27.67	24.65	22.81	22.52	21.97
b10	150.00	140.79	92.12	42.22	38.30	36.27	37.14	41.60
b11	0.01	0.01	0.01	1.10	4.27	5.72	5.59	7.01
d1	14.25	7.92	0.01	0.01	1.56	3.09	1.93	0.36
d2	0.01	0.01	0.01	0.01	0.01	0.01	0.01	0.01
d3	0.01	0.01	0.01	0.01	0.01	0.01	0.01	0.01
d4	0.01	0.01	0.01	0.01	0.01	0.01	0.01	0.01
d5	0.01	0.01	0.01	0.01	0.01	0.01	0.01	0.01
d6	0.01	0.01	0.01	0.01	0.01	0.01	0.01	0.01
d7	0.01	0.01	0.01	0.01	0.01	0.01	0.01	0.01
d8	0.01	0.01	3.01	0.01	0.01	0.01	0.01	0.01
d9	60.00	60.00	60.00	55.32	41.76	35.64	35.52	42.83
d10	14.19	15.94	21.90	29.13	34.84	36.89	38.77	40.36
β1	119.70	113.95	109.83	104.60	103.99	101.50	100.08	102.05
β2	67.99	67.84	65.04	67.41	70.77	74.00	76.23	80.96
β3	100.38	103.38	107.28	109.40	111.58	114.17	118.16	124.31
β4	53.77	68.23	67.15	80.61	84.63	90.65	96.28	150.00
β5	48.48	52.91	58.40	64.29	71.56	78.57	87.91	150.00
β6	140.02	140.66	138.96	135.67	133.58	132.02	139.56	30.00
β7	73.13	78.65	85.41	117.07	132.16	149.40	150.00	30.00
β8	150.00	150.00	133.20	30.00	30.00	30.00	30.00	30.00
β9	30.00	30.00	30.00	30.00	30.00	30.00	30.00	30.00
β10	150.00	150.00	150.00	150.00	150.00	150.00	150.00	150.00

Table B4.28 Optimum thicknesses for different values of $(k_y/k_x)_1$

$(k_y/k_x)_1$	t1	t2	--	t11	t12	t13	t14	t15	t16	t17	t18	t19	t20
0.1	42.8	35.7	--	36.2	37.4	37.8	37.3	36.9	36.8	36.4	21.4	11.1	1
0.3	42.7	41.2	--	38.4	38.4	38.6	38.2	37.5	37.8	37.2	23.0	12.1	1
0.5	42.6	41.7	--	40.8	42.0	42.1	41.8	40.9	40.1	40.1	22.4	14.6	1
0.7	42.7	43.3	--	39.4	39.3	39.1	38.8	38.5	38.5	38.0	22.6	17.3	1
0.9	42.8	43.4	--	39.4	39.2	38.8	38.6	38.2	38.2	37.0	25.8	20.0	1
1.1	42.9	43.4	--	39.3	39.1	38.5	38.3	38.1	38.0	36.7	27.0	20.6	1
1.3	42.9	43.6	--	41.1	40.8	40.1	39.9	39.8	39.4	38.7	27.0	21.6	1
1.5	42.9	42.5	--	41.1	41.2	41.2	41.1	40.3	40.0	39.4	25.9	20.3	1
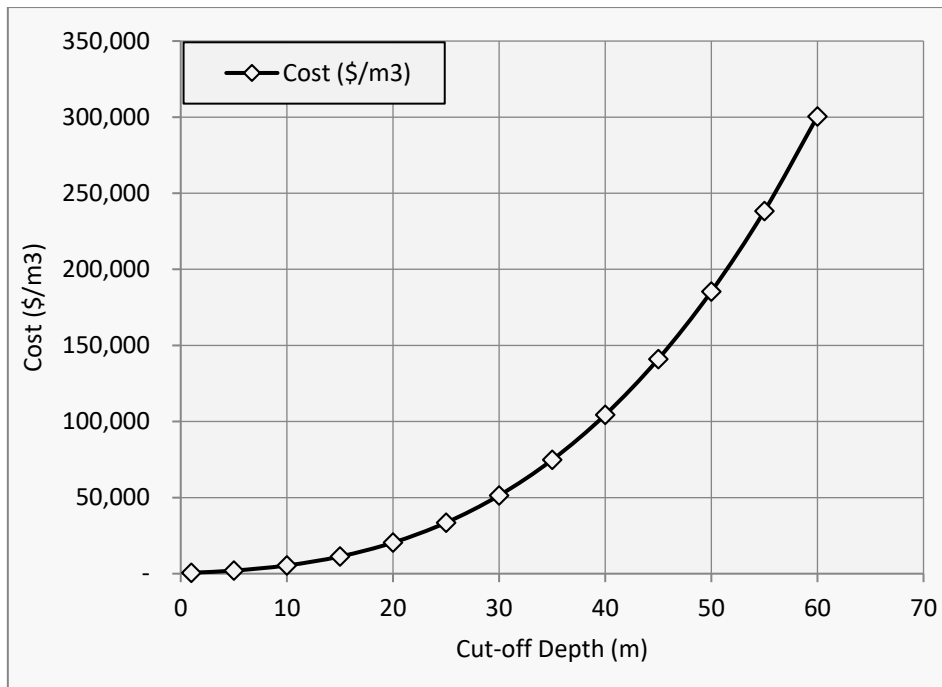
Figure B3.1   Cost variation (function) with cut-off depth